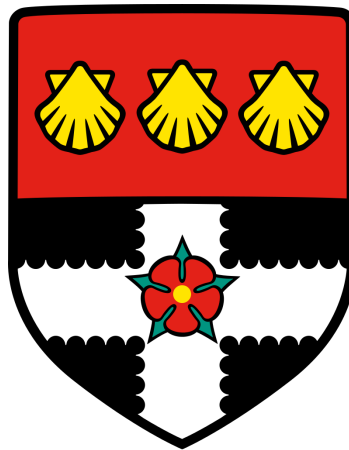


Modelling and Control of Position and Velocity Drives Subject to Friction



Anthony Chidolue Nnaji

School of Systems Engineering
University of Reading

Thesis submitted for the award of the degree of
Doctor of Philosophy

November 2017

To my dear wife Miriam, and children Mmesoma, Chizaram and Kamsi, the very best any
man can ever ask for ...!!!

Declaration

I hereby confirm that this is my own work and the use any material from other sources has been properly and fully acknowledged.

Signature:

Anthony Chidolue Nnaji
November 2017

Acknowledgements

I humbly express profound gratitude first and foremost to God who alone is wise and the infinite source of wisdom for guiding me this far. I am what I am only because of His grace. I sincerely thank my supervisors Professor William Holderbaum and Professor Victor Becerra for their support, encouragement and advice which have enabled me go through the drills and thrills. You guys are truly amazing and God sent.

I would also like to acknowledge Stefano Pietrosanti for all the support rendered in so many ways. Dear friend and colleague thank you so very much.

Dr. Ian Harrison, Dr. Loannis and Tani Obamo, I thank you guys for your support both emotionally and physically.

Pastors Andy & Hephzibah Abraham and all the members of The Everlasting Arms Ministries (TEAM), Reading branch, thank you for providing such a healthy spiritual atmosphere for the pursuit of excellence.

I would not fail to thank my spiritual father pastor Chinedu Uzoma for the spiritual covering and his timeless prayers.

I thank the family of Ike and Roseline Harmony and also Obioma Onuoha, you guys did ensure that I lacked no good thing during this period.

I thank also my mother Catherine, and sisters; Amaka, Nneka, Ebere, Chinelo, and Chinyere its an honour to have you for support and encouragement. I also appreciate my colleagues at the Enugu State University of Science and Technology and the Nigerian government for financial support. My special appreciation goes to my family; my wife whose fervent prayers, love and commitment to me has been changeless, Nne. . . I love you. To my children, the very gift from heaven; Mmesoma, Chizaram, and Kamsi, thank you all for the sacrifices, support and putting up with my inadequacies. To all who contributed in one way or the other during this period, may God bless you in Jesus name, Amen.

Now unto the King eternal, the Lord of all flesh, be the glory, honour and unending praise for great things He has done!!

Abstract

Performance degradation in most mechanical systems with friction which are not easily eliminated through design mechanisms can be greatly reduced within acceptable limits through the process of friction compensation. Generally friction compensators are used to improve system performance in terms of error reduction, transient response, thereby countering the effects of friction. Model-based techniques for friction compensation require an accurate model of the system friction. This is very important for high precision mechanical systems where excellent positioning and motion tracking, especially in the low velocities, is critical. This thesis proposes a new integrated friction model structure capable of modelling known friction dynamics. The new friction model incorporates a pre-sliding friction function with non-local hysteretic features. Analysis of the model shows the model to possess dissipative, boundedness, passivity and uniqueness properties. Results of sensitivity and robustness analysis indicate the new friction model is robust to parameter variations. A friction characterisation test-bed was designed and constructed for the purposes of friction identification, compensation and control. A set of experiments were designed and implemented on the test rig/bed to demonstrate friction dynamics. The input- output results of the experiments were used for parameter estimation of the proposed new friction model and some other relevant friction model structures. The performance of the new friction model for position and velocity control was studied using the experimental friction test-bed and simulations. The result of such analysis underscores the advantage of integrating a friction observer in the system control loop. The new friction model provided better position and velocity control of the experimental friction test-rig when compared with other well known models of friction.

Table of contents

List of figures	xv
List of tables	xxv
1 Introduction	1
1.1 Background of research	1
1.2 Friction Identification Paradox	3
1.3 Research Objectives	5
1.4 Thesis outline	5
1.5 Chapter summary	7
2 Literature Review	9
2.1 Introduction	9
2.2 The friction phenomena	10
2.2.1 Stick-slip motion	10
2.2.2 Hysteresis with non-local memory	12
2.2.3 Frictional lag	13
2.2.4 Breakaway and varying breakaway friction	15
2.2.5 Stribeck effect	15
2.3 Friction models	16
2.3.1 Static friction model structures	17
2.3.2 Dynamic friction model structures	22
2.4 Friction parameter estimation	30
2.4.1 System identification techniques	31
2.4.2 Non-linear systems structure	33
2.4.3 The system identification process	34
2.5 Friction compensation in control systems	35
2.5.1 Friction compensation techniques	35

2.5.2	Adaptive friction compensation	40
2.6	Chapter summary	41
3	A new friction model for low velocities	43
3.1	Introduction	43
3.2	A new model structure for friction	44
3.2.1	Model behaviour	46
3.2.2	Similarities with some existing models	49
3.3	Properties of the proposed new model	52
3.3.1	Boundedness of states	52
3.3.2	Existence/ uniqueness	53
3.3.3	Dissipativity	54
3.3.4	Passivity	56
3.4	Describing function analysis	57
3.4.1	The describing function concept	58
3.4.2	Limit cycle prediction for the proposed non-drift dynamic friction model hysteresis	60
3.5	Sensitivity analysis	68
3.5.1	Stick-slip motion	69
3.5.2	Discussion of stick-slip simulation results	71
3.5.3	Models sensitivity to parameters variations	74
3.5.4	Discussion of sensitivity analysis results	83
3.6	Pre-sliding performance analysis	95
3.6.1	Non-drift features	95
3.6.2	Hysteresis with non-local memory	101
3.7	Chapter summary	108
4	Friction Characterization and Identification	113
4.1	Introduction	113
4.2	Materials and Methods	114
4.2.1	Set-up for characterisation experiments	116
4.3	Model structure of the experimental test-rig	117
4.4	General procedure for identification of friction models	121
4.5	Friction characterisation	123
4.5.1	Experiment 1	123
4.5.2	Experiment 2	124
4.5.3	Experiment 3	126

4.5.4	Experiment 4	127
4.5.5	Analysis of results of characterisation experiments	129
4.6	Parameter estimation of friction models	132
4.6.1	Parameter estimation under constant velocity	133
4.6.2	Parameter estimation under pre-sliding	136
4.6.3	Computation of the micro-damping parameters	143
4.6.4	Parameter estimation under frictional-lag	147
4.6.5	Friction model validation	149
4.6.6	Analysis of parameter estimates	155
4.7	Chapter summary	159
5	Friction Compensation and Control	163
5.1	Introduction	163
5.2	Linear controller design for the experimental test-bed	164
5.2.1	Design of a lag compensator for velocity control	164
5.2.2	Design of a PID controller for position control	165
5.3	Friction observer design	166
5.3.1	Design concept	166
5.3.2	Observer design for velocity control	171
5.3.3	Observer design for position control	174
5.4	Observer based friction compensation implementation	177
5.4.1	Velocity control example	178
5.4.2	Position control example	186
5.5	Analysis of simulation results	186
5.5.1	Velocity control	193
5.5.2	Position control	194
5.5.3	Comments on results	195
5.6	Chapter summary	196
6	Friction Compensation Experiments and Analysis	199
6.1	Introduction	199
6.2	Friction compensation implementation on the test-bed	200
6.2.1	Experimental set-up	200
6.3	Velocity control experiments	202
6.3.1	Tracking experiment	203
6.3.2	Regulation experiment	203
6.3.3	Analysis of results	209

6.4	Position control experiment	215
6.4.1	Tracking experiment	215
6.4.2	Analysis of results	216
6.5	Velocity and position control simulations	222
6.5.1	Velocity tracking simulation	223
6.5.2	Velocity regulation simulation	226
6.5.3	Position control simulation	226
6.6	Comparing the experimental and simulation results	231
6.6.1	Discussion	231
6.7	Chapter summary	232
7	Conclusion and Recommendations	233
7.1	Introduction	233
7.2	Summary	233
7.3	Original contributions to knowledge	235
7.4	Limitations of the work	235
7.5	Recommendations for further research	236
	References	239
	Appendix A Linear Controller Design	249
	Appendix B Simulations, Simulink diagrams and Matlab codes	255
B.1	Introduction	255
B.2	In chapter 3	255
B.2.1	The proposed non-drift friction model algorithm and Matlab codes .	255
B.2.2	The stick-slip effect	262
B.3	In chapter 4	263
B.4	In chapter 5 and 6	267

List of figures

2.1	A simple block of mass-spring system subjected to a constant low velocity in the direction shown by the arrow used to demonstrate the stick slip motion	11
2.2	The motion of the mass as a function of time for the mass-spring system above showing the stick-slip oscillatory nature. The blue shows the sticking regime and the red the sliding regime	11
2.3	Friction force as a function of time for the system of figure(2.1). The maximum force is the static friction force and the flattened stage the kinetic (coulomb) friction force	12
2.4	Non-local memory pre-sliding hysteresis; (a) the reference force input for the pre-sliding hysteretic function investigation, and (b) the pre-sliding hysteresis friction characteristic with non-local memory	14
2.5	Frictional lag; friction as a function of unidirectional periodic velocity input; the right arrow indicates increasing velocities (acceleration) and the left arrow decreasing velocities (deceleration). More details are provided in chapter 4	15
2.6	Friction force variation with: (a) displacement, (b) rate of change of force, and (c) total time sticking or dwell time	16
2.7	Variations of the classical friction model: (a) Coulomb friction, (b) Coulomb+Viscous friction, (c) Stiction+Coulomb+Viscous friction, and (d) Stribeck+Viscous friction	20
2.8	The general bristle representation of contact surfaces showing their deflections. Here the upper face bristles are assumed rigid while the lower face bristles are flexible: (a) the random nature of bristle distribution, (b) the single bristle showing the deflection from initial value of y to a value of x	23
2.9	The stress-strain curve for various kinds of materials showing their rupture points 'a' for brittle and 'b' for ductile materials	24
2.10	Representation of the Generalised Maxwell Slip (GMS) friction model	29

2.11	Model-based feedforward friction compensation approach	39
2.12	Model-based feedback friction compensation approach	39
3.1	The frictional lag as feature with the Proposed model for different frequencies	45
3.2	Describing function analysis approach to non-linear systems; (a) Feedback control of a system with hard non-linearity, (b) A Describing Function equivalent scheme	58
3.3	Hysteresis friction for the condition that the signal input amplitude A is greater than the breakaway displacement Z_b ; top-left ; friction hysteresis, bottom-left ; signal input and top-right ; friction hysteresis and the signal input against time	65
3.4	Hysteresis friction for the condition that the signal input amplitude A is less than the breakaway displacement Z_b ; top-left ; friction hysteresis, bottom-left ; signal input and top-right ; friction hysteresis and the signal input against time	66
3.5	Limit cycle oscillation prediction using the describing function approach showing the intersection of the Nyquist plot $G(\omega)$ and the $-\frac{1}{N(A)}$ plot	67
3.6	Limit cycle oscillation prediction using a simulation approach	68
3.7	A simple mass-spring system for friction simulations	69
3.8	The friction and spring forces as captured by the: (a) the Coulomb+Stiction, (b) the LuGre, (c) the E-P, (d) the Proposed, (e) the Xiong, and (f) the GMS, models of friction	72
3.9	The stick-slip motion velocity as captured by the various friction models considered: (a) the Coulomb+Stiction, (b) the LuGre, (c) the E-P, (d) the Proposed, (e) the Xiong, and (f) the GMS friction models	73
3.10	The friction force against (a) displacement, and (b) velocity, for the LuGre model for various values of the parameter σ_0	75
3.11	The friction force against (a) displacement, and (b) velocity, for the LuGre model for various values of the parameter σ_1	76
3.12	The friction force against (a) displacement, and (b) velocity, for the LuGre model for various values of the Stribeck parameter v_s	77
3.13	The friction force against (a) displacement, and (b) velocity, for the proposed non-drift dynamic friction model for various values of the parameter σ	79
3.14	The friction force against (a) displacement, and (b) velocity, for the proposed non-drift dynamic friction model for various values of the Stribeck parameter v_s	80
3.15	The friction force against (a) displacement, and (b) velocity, for the proposed non-drift dynamic friction model for various values of the parameter Z_b	81

3.16	The friction force against (a) displacement, and (b) velocity, for the proposed non-drift dynamic friction model for various values of the parameter τ	82
3.17	The friction force against (a) displacement, and (b) velocity, for the GMS model for various values of the parameter α_i	84
3.18	The friction force against (a) displacement, and (b) velocity, for the GMS model for various values of the parameter C_i	85
3.19	The friction force against (a) displacement, and (b) velocity, for the GMS model for various values of the parameter σ_{0i}	86
3.20	The friction force against (a) displacement, and (b) velocity, for the GMS model for various values of the parameter σ_{1i}	87
3.21	The friction force against (a) displacement, and (b) velocity, for the GMS model for various values of the parameter v_s	88
3.22	The friction force against (a) displacement, and (b) velocity, for the Xiong model for various values of the parameter K_i	89
3.23	The friction force against (a) displacement, and (b) velocity, for the Xiong model for various values of the parameter σ_{1i}	90
3.24	The friction force against (a) displacement, and (b) velocity, for the Xiong model for various values of the Stribeck parameter v_s	91
3.25	The friction force against (a) displacement, and (b) velocity, for the Xiong model for various values of the parameter λ_i	92
3.26	The friction force against (a) displacement, and (b) velocity, for the Xiong model for various values of the parameter τ	93
3.27	Non-drift characteristic of friction test	96
3.28	The friction force against (a) Time, and (b) Displacement; showing the non drift property of real friction for the Proposed model.	97
3.29	The friction force against (a) Time, and (b) Displacement; showing drift for the LuGre model, contrary to the non-drift property of real friction	98
3.30	The friction force against (a) Time, and (b) Displacement; showing the non drift property of real friction for the E-P model	99
3.31	The friction force against (a) Time, and (b) Displacement; showing the non drift property of real friction for the GMS model	100
3.32	(a) The friction force against time, and (b) The displacement against time showing drift, contrary to non-drift property of real friction for the Xiong model	102
3.33	The reference force input for testing the hysteresis (with non-local memory) capabilities of the various friction models	103

3.34	The friction hysteresis (friction force against displacement) for the Proposed model	103
3.35	The friction hysteresis (friction force against displacement) for: (a) the LuGre model, (b) the E-P model, (c) the Xiong model and (d) the GMS model	104
3.36	Friction force for: (a) Velocity transitions including zero velocity and reversal, and (b) The steady state friction force against velocity for constant velocities	106
3.37	The breakaway friction force for varying force rates	107
3.38	Sensitivity of the breakaway friction for different values of the micro-damping parameter (σ_1): (a) Force-displacement plot, and (b) Force-velocity plot	109
3.39	Sensitivity of the breakaway friction for different values of the Stribeck parameter (v_s) (a) Force-displacement plot, and (b) Force-velocity plot . . .	110
3.40	Sensitivity of the breakaway friction for different values of the τ parameter; (a) Force-displacement plot, and (b) Force-velocity plot	111
3.41	Sensitivity of the breakaway friction for different values of the breakaway displacement parameter (Z_b): (a) Force-displacement plot, and (b) Force-velocity plot	112
4.1	A picture of the friction test rig	117
4.2	The schematic representation of the DC-servo motor system	118
4.3	The schematic representation of the system test-bed showing the arrangement of gears, friction discs and sensor positions	119
4.4	The friction torque measured against velocity for the constant velocity friction experiments	125
4.5	The Frictional-Lag experiment: (a) Torque output against-time, and (b) The lag plot average showing friction torque variations the acceleration and deceleration velocity regimes of the unidirectional signal	126
4.6	The Pre-sliding Hysteresis with non-local memory (a) Reference input signal, and (b) Measured hysteretic friction-torque output showing quantisation . .	128
4.7	Friction torque against velocity showing friction dependence on the rate of application of force	130
4.8	The modelling of constant-velocity friction-torque relationship with the proposed model (a) Estimation result, and (b) Validation result	137
4.9	The modelling of constant-velocity friction-torque relationship with the Xiong model (a) Estimation result, and (b) Validation result	138

4.10	The modelling of pre-sliding hysteresis friction-torque displacement relationship with the proposed model (a) Estimation result, and (b) Torque-displacement result	140
4.11	The modelling of pre-sliding hysteresis friction-torque displacement relationship with the LuGre model (a) Estimation result, and (b) Torque-displacement result	141
4.12	The modelling of pre-sliding hysteresis friction-torque displacement relationship with the GMS model (a) Estimation result, and (b) Torque-displacement result	144
4.13	The modelling of pre-sliding hysteresis friction-torque displacement relationship with the Xiong model (a) Estimation result, and (b) Torque-displacement result	145
4.14	The modelling of frictional-lag with the proposed model (a) estimation result, and (b) validation result, for unidirectional motion	150
4.15	The modelling of frictional-lag with the LuGre model (a) estimation result, and (b) validation result, for unidirectional motion	151
4.16	The modelling of frictional-lag with the GMS model (a) estimation result, and (b) validation result, for unidirectional motion	152
4.17	The modelling of frictional-lag with the Xiong model (a) Estimation result, and (b) Torque-displacement result, for unidirectional motion	153
4.18	The frictional-lag: obtained by plotting the predicted friction torque for varying velocities against velocity	156
4.19	Pre-sliding hysteresis validation results for: (a) The proposed model, and (b) The LuGre model	157
4.20	Pre-sliding hysteresis validation results for: (a) The GMS model, and (b) The Xiong model	158
5.1	The general structure for feedback model-based observer for friction control experiments	167
5.2	The structure of an observer based friction compensation for velocity control simulations	172
5.3	The structure of an observer based friction compensation for position control simulations where F and \hat{F} are torque variables that depend on the angular velocity of the plant	175
5.4	A disturbance signal used for the velocity control simulations	179
5.5	Block diagram of the observer-based friction compensator for the velocity control simulation example	179

5.6	Linear controller performance in the absence of friction: top- Disturbance (red), and output (blue) velocities, middle- The control error signal, and bottom- The PI control signal	180
5.7	Linear controller performance in the presence of friction: top- Disturbance (red), and output (blue) velocities, mid-upper- The error signal showing increased error due to friction, mid-lower- The system friction, and bottom- The PI control signal	181
5.8	Observer based velocity control of a system subject to friction using the proposed model: top- Disturbance 'red', and output 'blue' velocities, mid-upper- The error signal showing increased error due to friction, mid-lower- The system friction 'red' and estimate friction 'blue', and bottom- The linear control signal 'blue' and the modified control law 'red'	182
5.9	Observer based velocity control of a system subject to friction using the LuGre model: top- Disturbance 'red', and output 'blue' velocities, mid-upper- The error signal showing increased error due to friction, mid-lower- The system friction 'red' and estimate friction 'blue', and bottom- The linear control signal 'blue' and the modified control law 'red'	183
5.10	Observer based velocity control of a system subject to friction using the GMS model: top- Disturbance 'red', and output 'blue' velocities, mid-upper- The error signal showing increased error due to friction, mid-lower- The system friction 'red' and estimate friction 'blue', and bottom- The linear control signal 'blue' and the modified control law 'red'	184
5.11	Observer based velocity control of a system subject to friction using the Xiong model: top- Disturbance 'red', and output 'blue' velocities, mid-upper- The error signal showing increased error due to friction, mid-lower- The system friction 'red' and estimate friction 'blue', and bottom- The linear control signal 'blue' and the modified control law 'red'	185
5.12	Block diagram of the observer-based friction compensator for the position control simulation example	187
5.13	Linear controller position control performance in the absence of friction: top- Reference input 'red', and output response 'blue' positions, middle- The velocity signal, and bottom- The PID control signal	187
5.14	Linear controller position control performance in the presence of friction: top- Reference input (green), and output response (red) positions, mid-upper- The velocity signal showing limit cycle prediction, mid-lower- The friction predicted and bottom- The PID control signal	188

5.15	Position control of a system subject to friction using the proposed model as observer: top- Reference input 'green', and output response 'red' positions, mid-upper- The velocity signal, mid-lower- The friction forces (both estimated and predicted and bottom- The PID 'blue' and modified 'red' control signals	189
5.16	Position control of a system subject to friction using the LuGre model as observer: top- Reference input 'green', and output response 'red' positions, mid-upper- The velocity signal, mid-lower- The friction forces (both estimated and predicted and bottom- The PID 'blue' and modified 'red' control signals	190
5.17	Position control of a system subject to friction using the GMS model as observer: top- Reference input 'green', and output response 'red' positions, mid-upper- The velocity signal, mid-lower- The friction forces (both estimated and predicted and bottom- The PID 'blue' and modified 'red' control signals	191
5.18	Position control of a system subject to friction using the Xiong model as observer: top- Reference input 'green', and output response 'red' positions, mid-upper- The velocity signal, mid-lower- The friction forces (both estimated and predicted and bottom- The PID 'blue' and modified 'red' control signals	192
6.1	The SIMULINK-hardware-in-the-loop of the friction test bed for real time control	201
6.2	Velocity control implementation experiments for the laboratory test-bed . .	202
6.3	A linear controller implementation result for velocity tracking of the test-bed showing: top- The input (red) and output (green) velocities in (rad/sec), mid-upper- The velocity error signal, mid-lower- The control signal input to the plant, and bottom- The friction torque in (N-m)	204
6.4	A velocity tracking and control experiment with a model-based friction observer for the test-bed with: top- The output 'green' and reference 'red' velocities, mid-upper- The error signal, mid-lower- The control signal and bottom- The friction torques of the system rig 'green' and estimated by the observer 'red'	205

6.5	A velocity tracking and control experiment with a model-based friction observer for the test-bed with: top- The output 'green' and reference 'red' velocities, mid-upper- The error signal, mid-lower- The control signal and bottom- The friction torques of the system 'green' and estimated by the observer 'red'	206
6.6	A velocity tracking and control experiment with a model-based friction observer for the test-bed with: top- The output 'green' and reference 'red' velocities, mid-upper- The error signal, mid-lower- the control signal and bottom- The friction torques of the system 'red' and estimated by the observer 'green'	207
6.7	A velocity tracking and control experiment with a model-based friction observer for the test-bed with: top- The output 'green' and reference 'red' velocities, mid-upper- The error signal, mid-lower- the control signal and bottom- The friction torques of the system 'green' and estimated by the observer 'red'	208
6.8	A linear controller implementation result for velocity regulation of the test-bed showing: top- The input (red) and output (green) velocities in (rad/sec), mid-upper- The velocity error signal, mid-lower- The control signal input to the plant, and bottom- The friction torque in (N-m)	210
6.9	A velocity regulation and control experiment with a model-based friction observer for the test-bed with: top- Output 'red', input 'green', mid-upper- Error, mid-lower- The control law and bottom- The friction torques; system 'green', observer 'red'	211
6.10	A regulation tracking and control experiment with a model-based friction observer for the test-bed with: top- Output 'red', input 'green', mid-upper- Error, mid-lower- The control law and bottom- The friction torques; system 'green', observer 'red'	212
6.11	A velocity regulation and control experiment with a model-based friction observer for the test-bed with: top- Output 'red', input 'green', mid-upper- Error, mid-lower- The control law and bottom- The friction torques; system 'green', observer 'red'	213
6.12	A velocity regulation and control experiment with a model-based friction observer for the test-bed with: top- Output 'red', input 'green', mid-upper- Error, mid-lower- The control law and bottom- The friction torques; system 'green', observer 'red'	214
6.13	Position control implementation experiment for the laboratory test-bed . . .	215

6.14	A linear controller implementation result for position tracking of the test-bed showing: top- The input (green) and output (red) positions in (radians), mid-upper- The position error signal, mid-lower- The control signal input to the plant, and bottom- the friction torque in (N-m)	217
6.15	A position tracking and control experiment with a model-based friction observer for the test-bed with: top- Output 'red' input 'green', mid-upper- Error, mid-lower- The control law and bottom- The friction torques; system 'green', observer 'red'	218
6.16	A position tracking and control experiment with a model-based friction observer for the test-bed with: top- The output 'red' and reference 'green' velocities, mid-upper- The error signal, mid-lower- the control signal and bottom- The friction torques of the system 'red' and estimated by the observer 'green'	219
6.17	A position tracking and control experiment with a model-based friction observer for the test-bed with: top- Output 'red' input 'green', mid-upper- Error, mid-lower- The control law and bottom- The friction torques; system 'green', observer 'red'	220
6.18	A position tracking and control experiment with a model-based friction observer for the test-bed with: top- Output 'green', input 'red', mid-upper- Error, mid-lower- The control signal and bottom- The friction torques; system 'green', observer 'red'	221
6.19	Block diagram for velocity control simulations of the experimental test-bed	222
6.20	Block diagram for position control simulations of the experimental test-bed	223
6.21	Linear controller simulation result for velocity tracking of the test-bed showing: top- The input (green) and output (red) velocities in (rad/sec), mid-upper- The velocity error signal, mid-lower- The control signal input to the plant, and bottom- The friction torque in (N-m)	224
6.22	A velocity tracking and control simulation with a model-based friction observer for the test-bed with: top- Output 'green', input 'red', mid-upper- Error, mid-lower- Control and bottom- The friction torques; system 'green', observer 'red'	225
6.23	Linear controller simulation result for velocity regulation of the test-bed showing: top- The input (red) and output (green) velocities in (rad/sec), mid-upper- The velocity error signal, mid-lower- The control signal input to the plant, and bottom- the friction torque in (N-m)	227

6.24	A velocity regulation and control simulation with a model-based friction observer for the test-bed model with top- Output 'red', input 'green', mid-upper- Error, mid-lower- Control and bottom The friction torques; system 'green', observer 'red'	228
6.25	A linear controller implementation for position tracking of the test-bed . . .	229
6.26	A position tracking and control simulation with a model-based friction observer for the test-bed with top- Output 'red' input 'green', mid-upper- Error, mid-lower- Control and bottom The friction torques; system 'green', observer 'red'	230
A.1	Test-rig response and Bode diagram of the open loop transfer function . . .	251
A.2	Test-rig response and open loop Bode diagram of the transfer function showing too high cross-over frequency	252
A.3	Test-rig response to input step, and Bode diagram showing error difference	252
A.4	Integrating the compensator network to improve system performance	253
A.5	PID controller design	254
B.1	Proposed non-drift dynamic friction model structure representation with Simulink block diagram	256
B.2	Block diagram for the simulation of stick-slip effect of friction using the proposed friction model	263
B.3	Simulink block diagram for the friction characterisation experiments using the test-bed	264
B.4	Simulink block diagram for the estimation of parameters of the proposed friction model	264
B.5	Block diagram for the position control simulations of the test-bed using the proposed friction model	268
B.6	Block diagram for the velocity control experiments on the test-bed using the proposed friction model	268

List of tables

4.1	Friction discs and their coefficients of friction for dry surfaces	116
4.2	Estimated static parameters for constant-velocity motion using the proposed/LuGre models	136
4.3	Predicted (static) parameters for constant-velocity using the GMS/Xiong models	136
4.4	Estimated parameters under pre-sliding for the proposed model	139
4.5	Predicted parameters for friction hysteresis with LuGre model	142
4.6	Estimated parameters under pre-sliding for th GMS model	143
4.7	Estimated parameters under pre-sliding for the Xiong model	143
4.8	Estimated parameters under frictional lag for the proposed model	149
4.9	Estimated parameters under frictional lag for the LuGre model	149
4.10	Estimated parameters under frictional lag for the GMS model	154
4.11	Estimated parameters under frictional lag for the Xiong model	155
4.12	Predicted parameters for frictional lag using the Xiong model	160
4.13	Harmonised parameter values for the proposed friction model	161
4.14	Harmonised parameter values for the LuGre friction model	161
4.15	Harmonised parameter values for the GMS friction model	161
4.16	Harmonised parameter values for the Xiong friction model	161
5.1	Performance indices for the various control schemes studied under velocity control	180
5.2	Performance indices for the various control schemes studied under position control	193
6.1	The adjusted parameter values for the friction control experiments	201
6.2	Index for velocity tracking experiment	203
6.3	Index for the velocity regulation experiment	209
6.4	Index for position tracking experiment	216

6.5	Index for velocity tracking simulation	223
6.6	Index for velocity regulation simulation	226
6.7	Index for position tracking and control simulation	226
A.1	Parameters of the friction test-bed	250
A.2	Parameters effect on the closed loop response	254
B.1	Description of symbols used in the thesis with their SI units	269

Chapter 1

Introduction

1.1 Background of research

Industrial mechanical and/or electromechanical systems experiencing relative motions are often actuator driven. Servo actuators are one of the most frequently used actuating mechanisms in industry and there are many kinds depending on the underlying operational mechanisms. Some of the more popular servos are pneumatic, hydraulic, electrical servos. Of these the electrical (dc type) servos have gained wide acceptability mainly due to; the ease with which its output speed and/ or position can be controlled, its simplicity of design, and low cost [1], [2], [3], [4].

One feature of mechanical systems with a relative motion between the surfaces in contact is the presence of non-linear friction [5], [6], [7]. Friction is the tangential force between two surfaces in contact experiencing relative motion. Friction phenomena have been studied and positively utilised for many centuries now. Da Vinci made the first recorded attempt to study the phenomena but Coulomb was able to formulate a relationship between friction and the load which became the well known Coulomb friction and the base for many classical friction models. Friction has received attention in control engineering because of the increasing need for precision control in certain systems [8], [9], [10], tracking systems with little error tolerance, and the availability of more tools of analysis, modelling and design. Friction plays a significant role in automobile braking systems, tyre design technology [11]. However, friction often has a negative impact on mechanical systems. Some of these effects include tracking errors in velocity and position, limit circles, wear, oscillations [12], [13], [14]. Friction may cause limitations on the precision of position and tracking systems and can lead to undesired oscillations. From studies on friction two distinct regimes can be observed: the pre-sliding and the gross sliding regimes. The pre-sliding regime is the friction experienced in a system from the time of the application of an external force up until the

parts are about to slide relative to each other. Here the friction is primarily a function of the displacement. In this regime the friction undergoes elastic and plastic deformation under the application of an external force. If the applied force is large enough, then gross sliding is initiated. The gross-sliding friction is the friction existing when the parts are in relative sliding (rolling) motion. It is mainly a function of the relative velocity between the two surfaces in contact [15], [16]. Friction can also be classed as either dry or lubricated friction. In lubricated friction there are four lubrication phases observed with varying degrees of the friction dynamic. These phases are:

1. Solid to solid phase; in this phase the applied force is not enough to break the adherence force between the surfaces to initiate motion and as such there is no lubrication between the contacts since there is no motion
2. Boundary lubrication phase; in this phase the surfaces are at the edge of sliding relative to each other, little displacements are experienced but no gross-sliding. This is much similar to the solid to solid phase. The lubricant is scarcely introduced between the surfaces. Stick-slip motion could be experienced in this phase.
3. Partial lubrication phase; in this phase there is relative motion between the surfaces though very low, this forces the lubricants into the surfaces at a low rate and thus lowers the friction between the surfaces. The lubricant in the surfaces is not large enough to separate fully the surfaces. Stick-slip motions and Stribeck effects are possible in this phase.
4. Full lubrication phase; in this phase the friction influence is governed hydro dynamically and the friction force increases with increasing velocity because there is full separation of the surfaces.

Some key features of the friction phenomenon are:

Stribeck effect: In [17], it was shown from experimental studies that friction decreases as a function of the velocity at very low values of the velocity while at high values it increases as a function of increasing velocity. This is called the Stribeck effect, and the curve of friction against velocity capturing this feature is called the Stribeck curve.

Pre-sliding Hysteresis: This is the friction feature arising from the adhesion and deformation of the surface asperities when subjected to an external force that is less than the breakaway value. These interactions give rise to a friction force that is dependent of the relative displacement of the asperities rather than the relative velocities of the contacting bodies [18].

Frictional lag: This is also known as velocity dependent hysteresis and is the variation of the friction force as a function of the increasing or decreasing velocity. This acceleration or

deceleration in velocity leads to different friction values [19].

Breakaway and varying breakaway forces; The breakaway force is the minimum force required to initiate a relative motion between two surfaces in contact. The varying breakaway is the observed effect the rate of change of the applied external force and the dwell time have on the breakaway force of the body at rest [20].

Stick-slip phenomenon: This is the spring-like behaviour of the friction surfaces when subjected to a steady velocity characterised by periodic phases of sticking and slipping thereby making the system oscillatory. These features, explained in greater detail in chapter 2, clearly capture the dynamics of the friction phenomena and show that it not only depends on the relative motion between the parts involved but also on the internal states of the parts, properties of the materials involved, operating temperature, surface finish, presence or absence of lubrication, etc. Thus research results and experimental data indicate that friction exhibits non-linearity, dynamism and dependency on environmental parameters as well as materials properties. These characteristics make accurate models of friction difficult to obtain [21], [22].

1.2 Friction Identification Paradox

The performance of control systems subject to friction using model based friction compensation approaches is dependent on the availability of an adequate model representative of friction [23]. In obtaining an accurate model of friction or any physical model, it is important to have a good understanding of the system characteristics. Accurate friction model formulation is constrained by the following conditions as noted in [24]: First, the friction force at steady state velocities is only a function of the relative velocity, and second, the friction force in the pre-sliding regime (small displacements) is essentially a hysteretic function of the position and exhibits non-local memory characteristics. Thus a good model of friction therefore should possess some basic qualities such as:

1. Complexity; should be complex enough to capture closely the various observed features of the friction phenomenon.
2. Simplicity; should be simple enough for implementation and simulation purposes and ease of integration into real-time control systems.
3. Efficiency; the model should be computationally efficient in time and resource consumption.

4. Accuracy; the difference between the friction features predicted by the model and those observed experimentally should be small according to an appropriate measure.

The paradox is in finding a friction model that is both accurate (complex enough to capture friction features) and yet simple and efficient for implementation.

The study of friction cuts across many disciplines including tribology, control systems, materials physics, mechanics and geology. Because of the vast influence of friction many models have been developed in these fields capturing the essence of friction as it relates to those application areas. Two broad approaches for modelling friction are the black-box and the white-box approaches depending on the level of the physics involved. Black-box friction modelling based on experimental input-output measurements is common [25], neural network, (NN) (GA, AI) based modelling approach [26]. Other approaches that are purely physics motivated are called the white-box models. Combinations of both the black-box and the white-box methods known as the grey-box models have found wider application in modelling frictional systems since it involves part physics-based knowledge of the system and part empirical input-output data. Most existing friction models can be classed as either static or dynamic. Static models of friction relate in a static manner the friction directly to velocity and/or displacement. Examples are the classical (Coulomb model and its modifications), Karnopp [27], Lorinc [5], and the Armstrong models [28], [29]. Essentially there is a direct mapping of these parameters in the static models. On the other hand, dynamic models capture friction as a function of velocity and/or displacement through its internal states. These internal state variables are usually difficult to measure so they are usually estimated. Some of the more popular dynamic friction models are: Dahl [30], LuGre [31], [32], Bristle [33], Leuven [34], and GMS models [35], [31].

The Friction Problem: From a Control Perspective

Friction modelling can be very useful for control purposes especially in high precision systems. Friction compensation in control systems has been carried out in various ways each having its merits and demerits. Some of the techniques adopted in friction compensation and control are; the use of a dither signal, acceleration feedback, and model based friction compensation. The dynamic nature of friction makes it necessary to track the parameter variations in the system model to be able to accurately capture at all times friction effects. According to [36], [37], these adaptive techniques are often applied since it is not always possible to obtain accurate models of friction with constant parameters.

1.3 Research Objectives

Most of the existing friction models are application dependent and as such need adjustments for different applications. Characterising friction phenomena especially in the pre-sliding and low velocity regimes is difficult due to the highly non-linear and dynamic nature of friction [5]. However, as shown in [38], [39], many friction models have been proposed in the field of control and tribology, some of which are static and thus suffer from the challenges facing static models. And the dynamic models of which the LuGre friction model is the most popular due mainly to its simplicity though it does not adequately exhibit true hysteresis with non-local memory and suffers from frictional drift when subject to force vibration less than the stiction value.

The objectives of this thesis are:

1. Investigate the performance of friction models suitable for use in friction compensation and propose a new model structure to address identified deficiencies.
2. Performance of a sensitivity and robustness analysis of the proposed friction model in comparison to other models of friction
3. To characterise of the phenomenon of friction on an experimental test-bed and use this facility to test the performance of the proposed friction model.
4. Design and implement a model based observer using the new friction model, and use this observer for model based friction compensation of the experimental test-bed.

1.4 Thesis outline

The outline of the rest of the thesis is such that a review of the literature with respect to friction models and the various control methods adopted for systems with friction were presented in chapter 2, while chapters 3-6 report how the research objectives were pursued and achieved with chapter 7 providing conclusions and areas for future research. The contents of these chapters are briefly described below.

Chapter 2: Literature Review. Chapter layout; a review of relevant areas pertaining to the research such as friction features and friction model structures, parameter identification, compensation and control were carried out, with section 2.1 providing general review background. Section 2.2 dealt with the characteristic features of friction, while section 2.3 laid down the various models of friction relevant for control starting with the simple static model structures to the complex dynamic models. In section 2.4 some aspects of system parameter

identification relevant for the thesis are reviewed, the compensation and control of systems with non-linear friction was investigated in section 2.5. Finally in section 2.6 a summary was provided.

Chapter 3: A New Model Structure for Friction. The layout of the chapter is as follows: general background information is provided in 3.2. In section 3.2 a new friction model capable of predicting relevant features of friction was proposed, while section 3.3 looked at the properties of the proposed friction model such as stability, dissipativity, passivity and uniqueness. In section 3.4, a describing functions analysis of the hysteretic properties of the proposed model was studied and empirical values derived. The ability of the model to predict stick-slip friction phenomenon and sensitivity analysis of the proposed model with some relevant models were discussed in sections 3.5. Section 3.6 looked at pre-sliding performance analysis of some of the friction models in chapter 2 in comparison with the new friction model. In section 3.7, summary of the main results was articulated.

Chapter 4: Friction Characterization and Identification. Chapter layout; general background information was provided in section 4.1. A brief description of the test-bed and the various equipments used for the experiments formed part of section 4.2, and description of the experimental set-up for the characterization of the friction non-linearities. In section 4.3, a general model of the dc servo-motor based experimental test-bed used to perform the experiments was derived. Section 4.4 described the experiments performed for the determination of various friction characteristics. In section 4.6 the task of system identification, dealing with the parameters estimation for the various models studied was carried out. A more general discussion on the observations noted during the various experiments and identification were elaborated upon also. The chapter ended with a summary section 4.7.

Chapter 5: Friction Compensation and Control. Chapter layout; general background information was provided in section 5.1. Section 5.2 dealt with the design of the linear part of the compensator called the feedback controller, while section 5.3 with the design of the friction observer for velocity and position control purposes. In section 5.4 the simulation implementation examples of the velocity and position observer-based compensators were performed, while analysis of the results of simulations discussed in section 5.5. The chapter ends with a summary, section 5.6.

Chapter 6: Friction Compensation Experiments and Analysis. Chapter layout; general background information was provided in section 6.1. In section 6.2 set-up of the experiment, model parameters used for the experimental implementation of friction compensation and control of the test-bed were discussed while velocity control experiments were performed on the test-bed and subsequent analysis of the experimental results in section 6.3. Position control experiments and analysis of the results were discussed separately in section 6.4.

Section 6.5 presented the velocity and position control simulation for the experimental test-bed. A comparative analysis of both simulation and experimental results for velocity and position control and discussion were carried out in section 6.6. Chapter summary articulated in section 6.7.

Chapter 7: Conclusion and Recommendations. Chapter layout; general background information was provided in section 7.1. Section 7.2 contains main conclusions drawn from the research while the original contributions of the research to the general body of knowledge were discussed in section 7.3. The limitations and constraints encountered in the course of the research discussed in section 7.4. Section 7.5, offering recommendations for future research in this area concluded the thesis report.

1.5 Chapter summary

A general background description of friction and the friction phenomena has been provided as relates to most mechanical system with surface contacts in relative motion. A brief description of the research reported in this thesis has been given setting out the research objectives and some key areas to be developed in the main body of the thesis. The trade off between the model accuracy and its simplicity in terms of implementation and simulation explained. The thesis outline given above would be built upon in the subsequent chapters that follow.

Chapter 2

Literature Review

2.1 Introduction

Understanding the characteristics and physics of friction is relevant for modelling and control of high performance mechanical systems with relative motions. Tribological research findings contributed much to the current status of friction modelling and control. Tribology is the study of the science of contacting surfaces subjected to relative motion [26], especially as it relates to friction, wear, and lubrication. Friction has received much research attention as a result of its relevance not just in the field of control engineering, but also in many other fields such as meteorology and geology. This is partly because of the many adverse effects of its presence in any system but also because of advances in technological tools needed to study, determine and analyse its complex nature.

As illustrated in the previous chapter, the various features of the friction phenomena; stick-slip, breakaway and varying breakaway forces, frictional lag, pre-sliding hysteresis, and the Stribeck effect, many of which are not captured by the static friction models have led to extensive researches leading to many dynamic models which capture some of these dynamics of friction. However these dynamic models are not without their own demerits such as increasing system complexities and implementation issues. This thus makes it imperative that a trade off exists between the complexity of the model and its implementation efficiency.

The mechanical surfaces in contact can be viewed from a microscopic point as contacting at a large number of points called bristles or asperities which are randomly distributed over the entire surface. The cumulative interactions of these bristles give rise to friction. The presence of friction thus influences the overall behaviour of the surfaces under the effect of an external force [40]. The theory of contacting surfaces gives rise to the distinction between the apparent surface area and the real surface area of contact.

In this chapter a review of relevant areas necessary for adequate understanding of the en-

the thesis is set out. These areas are; Friction model structures, system identification of model parameters, and compensation and control of friction which serve as broad sub-divisions of the chapter. However, before this, some relevant features of the friction phenomenon are first discussed thereby providing needed basis for the comparison of the different models to be reviewed afterwards. Section 2.2 deals with the characteristic features of friction, while section 2.3 lays down the various models of friction relevant for control starting with the simple static model structures to the complex dynamic ones. The merits and demerits of such models are also discussed in context. In section 2.4 some aspects of system parameter identification relevant for the thesis are reviewed, and the compensation and control of non-linear friction in systems is investigated in section 2.5. A general summary of the entire chapter highlighting main points, concludes the chapter in section 2.6.

2.2 The friction phenomena

A good understanding of the characteristic features of friction is paramount to understanding and analysing existing models of friction as this will be the basis to gauge the adequateness of the models under review. Friction features are varied and non-linear in nature, and any good friction model is determined by its ability to replicate these observed phenomena closely. Some of the more pronounced characteristics of friction to be discussed here are; stick-slip motion, the pre-sliding hysteresis, break-away and varying breakaway forces, frictional lag, and the Stribeck effect.

2.2.1 Stick-slip motion

Motions at velocities much less than the Stribeck velocity often involve phases of slipping and sticking which can be traced to the stick-slip phenomenon of friction. As an illustration consider a simple mechanical system consisting of a mass, spring system under the influence of friction as shown in figure 2.1. The application of a steady velocity $v(t)$ in the direction indicated on the slider-belt will first cause the spring to extend while the mass is motionless relative to the slider-belt (stick-regime). The force transmitted to the spring is a function of the elongation of the spring (x), and the spring stiffness K . The mass remains motionless until the spring-force (Kx) is large enough to cause the attached mass to move backwards (slip-regime) towards the fixed end of spring. Thus the mass experiences motion (slip) when the spring force (Kx) is greater than or equal to its static friction (F_s), at which point the mass begins to move and accelerates as a result of a fall from static friction to kinetic friction. This acceleration is in the direction opposite the applied force, and hence reduces the stress

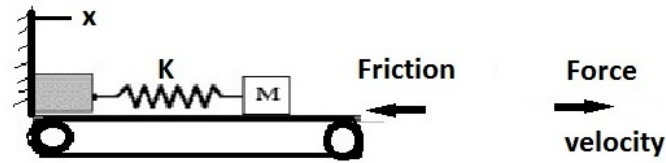


Fig. 2.1 A simple block of mass-spring system subjected to a constant low velocity in the direction shown by the arrow used to demonstrate the stick slip motion

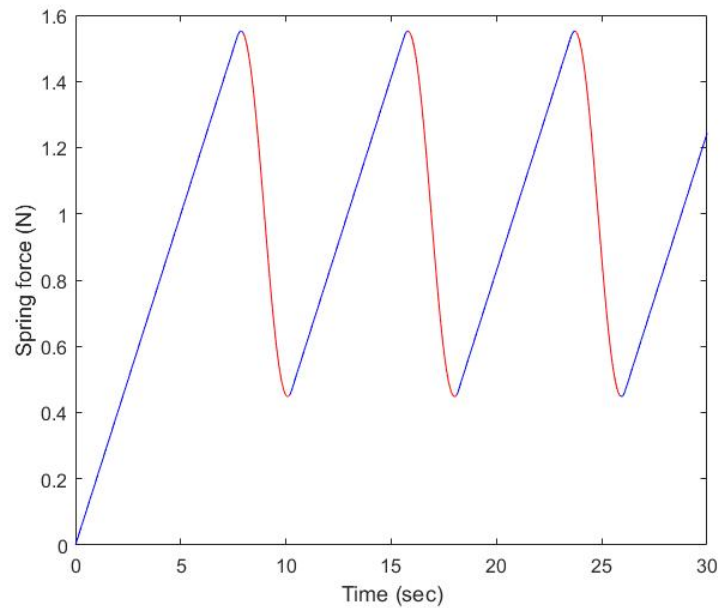


Fig. 2.2 The motion of the mass as a function of time for the mass-spring system above showing the stick-slip oscillatory nature. The blue shows the sticking regime and the red the sliding regime

in the spring. This causes the amount of force on the mass to decrease. The reduction of this force below a certain level causes the motion of the mass to stop and stick again on the slider-belt. Therefore, spring force begins to build up again to the static value replicating the whole process again, hence the name stick-slip motion. Figures 2.2 and 2.3 respectively capture the position of the mass as a function of time and the friction force as a function of time. This kind of motion is a feature of friction as observed experimentally and reported in some papers [20], [41], [42]. Some examples are; the creaking sound of a door slowly closed or opened, motion of a wiper on a dry windscreen.

This type of motion is cyclic with periods of sticking and slipping as shown in figure 2.2 and the cause of many undesirable effects in mechanical systems like squeal noise and

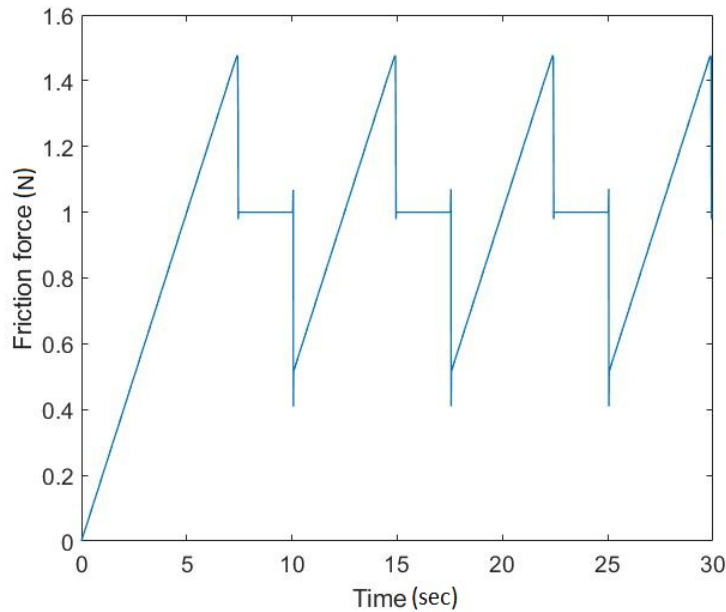


Fig. 2.3 Friction force as a function of time for the system of figure(2.1). The maximum force is the static friction force and the flattened stage the kinetic (coulomb) friction force

limit cycles. It is clear that this effect will disappear if the stiction friction and the coulomb (kinetic) friction are to be equal. For the system shown the equation of the motion during stick as the body moves from rest is given by Newton's second law of motion

$$m\ddot{x} = F_s - Kx \quad (2.1)$$

And that during slipping is

$$m\ddot{x} = F_c - Kx \quad (2.2)$$

with $\dot{x} = v$, as the velocity, F_s and F_c are the static and kinetic friction forces respectively, K is the spring constant and x its extension as a function of time and m the mass of the body.

2.2.2 Hysteresis with non-local memory

This is the non-linear spring like behaviour of the asperities surface due to the adhesive and deformation forces of interaction between the surfaces leading to the elasto-plastic deformation of these asperity junctions. This phenomenon has been shown to be a function of the displacement at micro-level rather than the velocity dependence of friction at macro-level. This rate independent friction also exhibits a non-local memory feature. The relative displacement of the asperities is a function of the external force and increases to saturation beyond

which the asperities slide (gross-sliding) as a function of force until velocity reversal. As such the friction force increases in relation to this displacement until breakaway displacement beyond which the friction force becomes a function of velocity. Hysteresis losses occur at every closed cycle of operation as the stored energy is dissipated. This phenomenon is illustrated in figure 2.4 for a system subjected to a reference force input.

As an illustration of the non-local memory consider a simple system as shown in figure 2.1, if the applied external force figure 2.4a then no motion is experienced between the mass and slider surface. This is possible when the applied force is less than the force necessary to break the adhesion forces of the asperities. Given the applied force $(a - b - c - d - e - f - g)$, the asperities deform tracing first a virgin curve $(a' - b')$ as shown in figure 2.4b, as the reference force changes direction moving from $(b - c)$ the friction force traces $(b' - c')$ curve. Reversal of the direction of applied force $(c - d)$, the friction also traces the loop $(c' - d')$ and as the force reverses direction tracing $(d - e)$, the friction force subsequently traces $(d' - e')$ loop. For the branch direction $(e - f - g)$ of the applied force, the friction force traces the loop $(e' - f' - g')$, however as the friction force reaches the point f' coinciding with point d' on the outer loop $(c' - d')$, there is a closing of the inner loop $(d' - e' - f')$ given that points d' and f' coincide. This thus makes the path $(e' - f' - g')$ appear to trace the outer loop of $c' - d'$ extrapolated, thus wiping out (or forgetting of) the inner loop $(d' - e' - f')$.

This phenomenon of friction is termed non-local memory. Many models of friction are not able to predict this complex friction feature as would be shown in the sections following.

2.2.3 Frictional lag

In [19], it was observed that the friction force and the velocity have a dynamic relationship especially at low velocities. The research showed that a periodic time varying unidirectional low velocity produces a corresponding friction force which lags the velocity in time. This friction force behaviour exhibits hysteretic features though a function of velocity as against that of the pre-sliding hysteresis which is a function of displacement. Observations showed that the friction forces are higher for increasing time varying velocities (acceleration) than for decreasing time varying velocities (deceleration). Increasing the velocity time rate widens the hysteretic loop as in figure 2.5 for 2 rad/sec, 5 rad/sec, and 10 rad/sec sinusoidal reference velocities with constant amplitude. The figure is a result of frictional-lag experiments carried out on the test-bed designed for this research, see chapter 4 for more details.

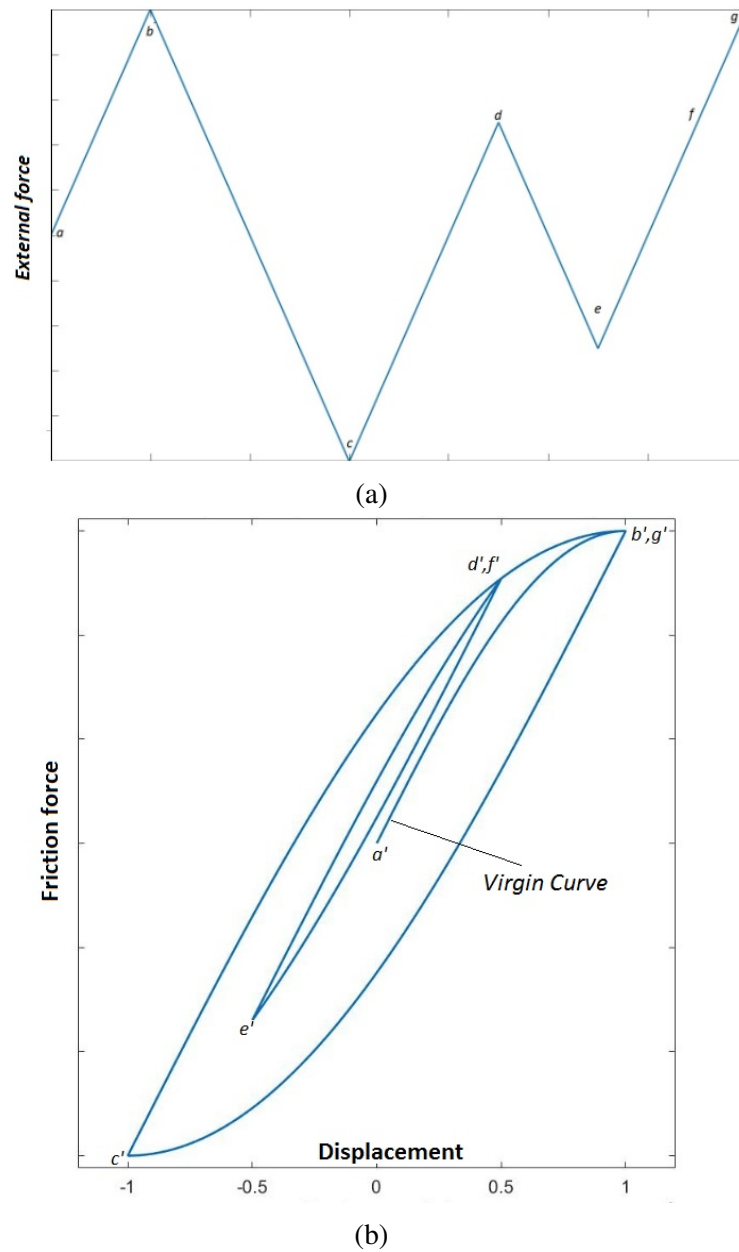


Fig. 2.4 Non-local memory pre-sliding hysteresis; (a) the reference force input for the pre-sliding hysteretic function investigation, and (b) the pre-sliding hysteresis friction characteristic with non-local memory

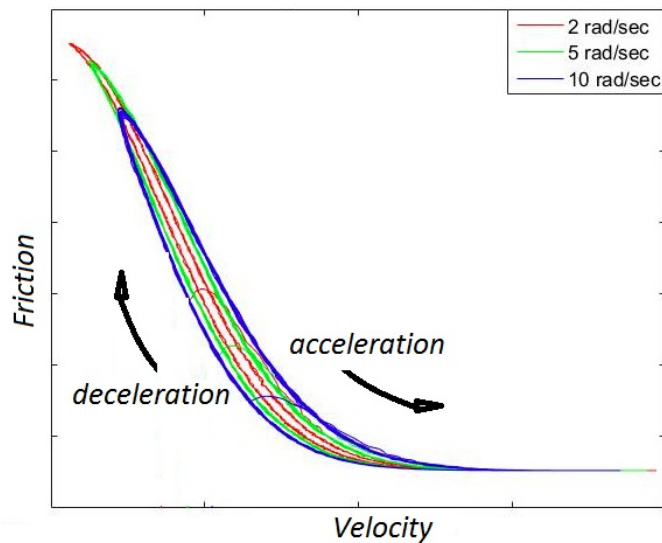


Fig. 2.5 Frictional lag; friction as a function of unidirectional periodic velocity input; the right arrow indicates increasing velocities (acceleration) and the left arrow decreasing velocities (deceleration). More details are provided in chapter 4

2.2.4 Breakaway and varying breakaway friction

The breakaway force is the minimum force required to initiate motion between two surfaces in contact. This force must be able to overcome the static forces of adhesion for relative motion to begin. The transition from the pre-sliding (stick) to gross-sliding (slip) regime is dynamic and continuous. In his inclined plane block-ball experiments [20], Rabinowicz noted that the maximum friction force occurs at a small displacement as shown in figure 2.6 and not at zero displacement indicating friction to be function of the displacement between the surfaces. The time of stick was also seen to affect the stiction or the force required to initiate motion. The breakaway force is also found to be dependent on the rate at which the external force is changing [43]. In other words, increasing the rate of application of force lowers the breakaway force and vice versa. Figures 2.6a, b, and c respectively show break-away friction force, the breakaway friction force as a function of the rate of change of external force, and the breakaway friction force variation with total time of stick.

2.2.5 Stribeck effect

Prior to the experimental investigations carried out by Stribeck, friction has been thought of and modelled as a static function proportional to velocity. In his paper [17] and contrary to

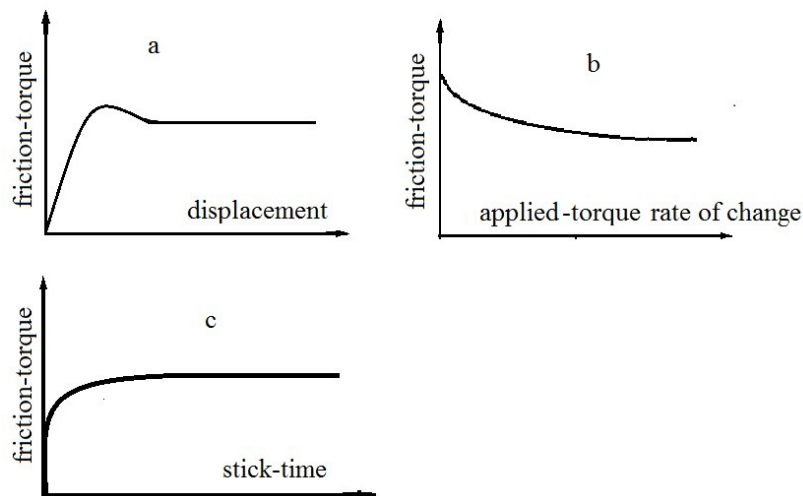


Fig. 2.6 Friction force variation with: (a) displacement, (b) rate of change of force, and (c) total time sticking or dwell time

generally perceived notion, friction was captured to be decreasing as velocity increased in the low velocity range while it increases in function of velocity beyond a certain level of the velocity. The transition velocity between the decreasing and increasing friction is called the Stribeck velocity. The friction-velocity relation is the Stribeck curve shown in figure 2.7d. The decreasing and subsequent increasing friction force as a function of the velocity increase is often referred to as velocity weakening and strengthening respectively. The weakening is attributable to Stribeck effect and the strengthening to the viscous friction effect. Thus the Stribeck friction is an exponentially decreasing function of the velocity bounded by the stiction force (upper bound) and the coulomb force (lower bound) [44].

The aforementioned friction characteristics will be experimentally investigated on an experimental test-bed designed for the purpose of friction characterisation and control.

2.3 Friction models

Having looked at the various characteristics of friction, this section presents a review of some of the relevant friction models in the field of control engineering. These friction model structures are generally grouped as either static or dynamic models depending on whether the model is able to capture and replicate the dynamisms of friction. The section is presented in such a manner that the simple static friction models are presented first then followed by the more complex dynamic friction models in each sub-section.

2.3.1 Static friction model structures

Static models of friction capture friction as a function of the velocity relative to both surfaces. Under the static friction the following models will be reviewed: Classical, Karnopp, model proposed by Lorinc, exponential, and neural network based models.

Classical model variations

This friction model is made up different component which individually capture different aspects of the friction phenomena. The component make-up of the classical model are: coulomb, viscous, static, and Stribeck friction.

Coulomb friction

This model simply states that the friction force is directly proportional to the normal loading between the surfaces and acts in such a way as to oppose the motion of these bodies. It is not dependent on the relative velocity. Mathematically the friction force is

$$F_f = \mu_k N \text{sgn}(v) \quad (2.3)$$

and with $F_c = \mu_k N$ then

$$F_f = F_c \text{sgn}(v) \quad (2.4)$$

where F_f is the friction force, μ_k is the coefficient of kinetic friction, N is normal loading and v is relative velocity, F_c is the Coulomb friction force. sgn is a signum function.

The coulomb force takes on either of two values of equal magnitude, but of opposite direction depending on the direction of the motion as shown in Fig 2.7a. This model finds application in many engineering systems because of its simplicity, and yields approximate values of the friction force mostly at increasing velocities. Because of this it has been used in friction modelling and compensation [40], [41], [42]. However it does not capture the dynamics of the friction phenomena especially in the zero velocity regions.

Viscous friction

The viscous friction force is proportional to the velocity of relative motion, hence as velocity increases or decreases this friction force increases or decreases in proportion. This is friction as a result of contact lubrication. However, the viscous friction coefficient is quite small such that friction due to viscosity is very small for low velocities. The friction force as a result of viscosity is often modelled as linear function of the velocity as

$$F_f = f_v v \quad (2.5)$$

with f_v being the coefficient of viscous friction and other terms as previously defined.

The viscous friction is usually incorporated into the coulomb model yielding the Coulomb+viscous model as in eqn. 2.6 to account for the fact that friction actually is dependent on the relative velocity of motion. This is represented as in [45], mathematically .

$$F_f = \mu N \text{sgn}(v) + f_v v \quad (2.6)$$

This implies that during sliding the friction force is the sum of the coulomb and viscous forces, figure 2.7b.

Static friction

The friction force in the pre-sliding and the gross-sliding regimes are different, it is shown that for most materials the sliding friction is lower than the friction at no sliding. The static friction (or stiction) is the amount of force required to initiate motion. The stiction value is dependent on the applied external force and not on the velocity. It increases with this force till a threshold is reached beyond which there is sliding. This force threshold is called the breakaway or Stiction force. The underlying concept is that the friction force is independent of the contact area and the relative velocity of motion and it opposes motion. So the stiction force is modelled thus

$$F_f = \begin{cases} F_e & \text{if } v = 0, |F_e| < F_s \\ F_s \text{sgn}(F_e) & \text{if } v = 0, |F_e| \geq F_s \end{cases} \quad (2.7)$$

where F_s is the static friction, v relative velocity, F_e the applied external force. The static friction is related to the normal force through

$$F_s = \mu_s N$$

where μ_s is the coefficient of static friction.

In order to reflect this in the coulomb base model the friction at no sliding is depicted as static friction while that during sliding is called the Coulomb (kinetic) friction as in figure 2.7c. The modified classical structure is then of the form

$$F_f = \begin{cases} F_c \text{sgn}(v) + f_v v & \text{if } v \neq 0 \\ F_e & \text{if } v = 0, |F_e| < F_s \\ F_s \text{sgn}(F_e) & \text{if } v = 0, |F_e| \geq F_s \end{cases} \quad (2.8)$$

Stribeck friction

From experiments it was observed that the transition of friction from the static to the kinetic regime is not sudden but gradual with a continuous drop in the friction value from the static value towards the coulomb friction value, as relative velocity is increased from zero. This effect is called the Stribeck effect, and the friction-velocity relation is called the Stribeck curve [17], see figure 2.7d.

The Stribeck curve is usually modelled by exponential functions of the form

$$F_f = F_c \text{sgn}(v) + (F_s - F_c) e^{-\left(\frac{v}{v_s}\right)^\delta} \quad (2.9)$$

where v_s is the transition velocity called the Stribeck velocity and the δ a curve shaping parameter.

Hence the combination of eqn. 2.8 with the exponential Stribeck friction eqn. 2.9 gives rise to a more complex but better representation of the friction features of (2.10). Mathematically it is represented as [46].

$$F_f = \begin{cases} F(v) & \text{if } v \neq 0 \\ F_e & \text{if } v = 0, |F_e| < F_s \\ F_s \text{sgn}(F_e) & \text{if } v = 0, |F_e| \geq F_s \end{cases} \quad (2.10)$$

with $F(v)$ being the friction force as a function of the velocity.

$$F(v) = F_c \text{sgn}(v) + (F_s - F_c) e^{-\left(\frac{v}{v_s}\right)^\delta} + f_v v \quad (2.11)$$

The eqn. 2.11, which is a Gaussian variant of the exponential models [5], is often useful for the steady state identification of friction model parameters as will be shown in subsequent chapters.

The classical model of friction takes on a continuum of values bounded by the stiction at the upper and lower bounds, and is discontinuous at zero velocity. This discontinuity poses simulation and implementation challenges.

In the paper [47], a modification of the stiction force was proposed to reflect its dependence on the rate of change of the applied force (section 2.2). This modification closely captures observed features of the friction phenomena before gross sliding begins as the velocity varies as suggested in the paper. In the paper the stiction is replaced by a function

$$\Phi_s(\dot{\tau}) = F_c + (F_s - F_c) e^{-\left|\frac{\dot{\tau}}{v_s}\right|^\delta} \quad (2.12)$$

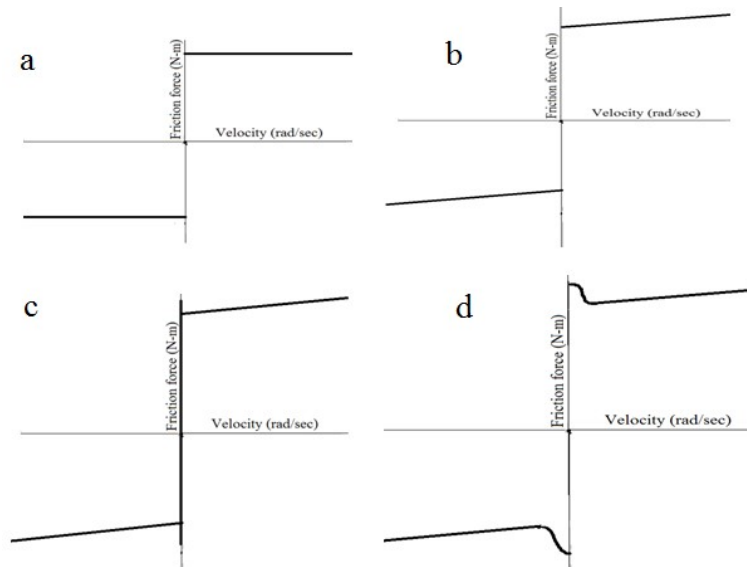


Fig. 2.7 Variations of the classical friction model: **(a)** Coulomb friction, **(b)** Coulomb+Viscous friction, **(c)** Stiction+Coulomb+Viscous friction, and **(d)** Stribeck+Viscous friction

where $\Phi_s(\dot{\tau})$ is the static friction force as a function of the applied torque rate of change, $\dot{\tau}$ the rate of change of applied torque, t_s is the torque rate coefficient, δ a curve fitting parameter. This exponential function is bounded between the stiction F_s and the Coulomb friction F_c forces.

Karnopp model

The variations of the classical friction model discussed above are not capable of handling friction dynamics resulting in the pre-sliding regime. The Karnopp model [reference], was developed to address some of the shortcomings of the classical models namely the friction force at zero velocity. To achieve this, Karnopp introduced a low velocity range D_v such that if $|v| \leq |D_v|$ then the system is assumed to be in stick mode. The friction force within this band is equivalent to the static friction F_s or the applied external force F_e . As the applied external force exceeds the stiction, the body experiences an increasing velocity from the rest position beyond D_v . Beyond D_v the model switches to the slip mode. This model is easy to simulate since it does not have to detect zero velocities. The can be depicted as in equation

2.13 by

$$F_f = \begin{cases} F_c \operatorname{sgn}(v) + f_v v & \text{if } |v| \geq |D_v| \\ \min(F_e, F_s) & \text{if } F_e \geq 0 \\ \max(F_e, -F_s) & \text{if } F_e \leq 0, |v| < |D_v| \end{cases} \quad (2.13)$$

Some of the limitations of the Karnopp friction model are;

1. It is application specific; the model is bespoke for every configuration so one cannot use the same model for different applications, [46].
2. System coupling; the model forms part of the system configuration.
3. Zero velocity deviation; there is no cohesion between the model output and the output of observed real systems.
4. It's complexity; the model complexity increases with system complexity geometrically and this possess strong limitation to its applicability, [33].

Lorinc model

In his paper [5], Lorinc presents a static model for friction non-linearity. The model is essentially a linearised version of the exponential model (Tustin variation) of the friction force. The formulation assumes a static mapping of the friction force as a function of velocity and is subject to implementation problems at zero velocities. For Positive velocities the friction force (F_f) representation is

$$F_f = \Phi_f^T \xi_f(\omega) \quad (2.14)$$

where the parameter vector is Φ_f , and $\xi_f(\omega)$ the regressor vector, The Lorinc friction model has been applied in control systems problems as in [7], [39]. Model realisation uses two different linear equations of the Tustin model to reproduce the low and high velocity regimes and a switching function capable of detecting the Stribeck switch velocity. Other dynamic features of friction like frictional lag, pre-sliding hysteresis are difficult to reproduce using this model. Being an approximate linear model though simple, it does not reflect true friction at low velocities.

Neural network based models

Soft approaches based on the neural networks (NN) are increasingly being explored in the modelling of system friction, [10]. This is driven by the ease by which the networks can

easily approximate any continuous function to a high degree of accuracy so long as the network is large enough. This approximation property is used in generating non-linear mapping of the inputs and outputs data obtained from experiments, on the basis of the Stone-Weierstrass theorem [48], with the use of activation functions. Various options for these function activators are; Radial Basis Function (RBF), the hyperbolic tangent and the sigmoid. It should be noted however that though neural networks are easy to train and use, and simple structured with high approximation properties, it is not without its own issues some of which are: lack of network dynamism since it is a static approximator, it yields opaque models often without mathematical interpretation, difficulties in model analysis, isolation of cause and effect, and determination of dynamic characteristics of the system from the model. Friction modelling and compensation using this approach has been proposed in many articles [49], [50]. In [25] application to dc model parameter identification using compound evolution techniques was investigated.

2.3.2 Dynamic friction model structures

Static friction models generally suffer from detection of friction force and the attendant rich friction dynamics in the pre-sliding regime. This is because they are often a static mapping of the force as a function of velocity and not position. For high precision mechatronic systems, effects of friction non-linearities especially in the pre-sliding regime often lead to errors that cannot be neglected, underscoring the need for more accurate models exhibiting some dynamism. Friction models capable of reproducing friction features in this regime are usually modelled as a function of not only the velocity but also of the internal state of the contact surfaces. Naturally this leads to more complex models called dynamic friction model structures. Many dynamic models exist in literature (as will be shown below) however, we investigate some of the more popular dynamic models such as; Bristle, Dahl, LuGre, Leuven, GMS, and the Xiong models. These models have some similarities with the model proposed in the next chapter.

Bristle model

In their paper [33], Haessig and Friedland presented the bristle and the reset integrator friction models. In the bristle model friction originated from interactions of the bristle like surfaces in which the macroscopic friction effect is taken to be the sum of the spring forces experienced by each of these bristles (microscopic friction), when subjected to an external force. The friction on each bristle pair is proportional to the strain experienced by the bristles figure 2.8a. These bristles are randomly distributed over the entire surface of interaction. There

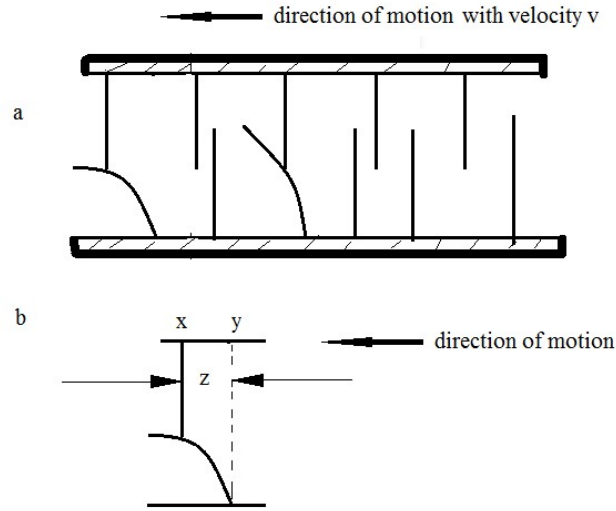


Fig. 2.8 The general bristle representation of contact surfaces showing their deflections. Here the upper face bristles are assumed rigid while the lower face bristles are flexible: **(a)** the random nature of bristle distribution, **(b)** the single bristle showing the deflection from initial value of y to a value of x

is a continual breaking and formation of new bonds as the bristles slip on each other. For simplicity of analysis the bristles on one surface are assumed rigid while the other surface has flexible bristles. Under external loading, the bristle deflects in proportion to the load. On reaching a maximum (breakaway) displacement it snaps to form a new bond with another bristle figure 2.8a. These bond interactions are assumed massless and pliable. The friction force on a single bristle figure 2.8b is given as

$$F_f = Kz \quad (2.15)$$

with $z = (x - y)$ as the bristle deflection, and K bristle stiffness. If the number of bristle elements is N , then the total friction force is given as the sum of individual forces as

$$F_f = \sum_{i=1}^N K_i z_i \quad (2.16)$$

$$i = 1, 2, \dots, N$$

where x is the point of formation of bristle and y the bristle position at any given time. This model accurately captures friction forces as a function of displacement explicitly and implicitly as a function of the relative velocity since N the total number of bonding bristles at any instant is a function of this velocity. It should be noted that this model does not capture

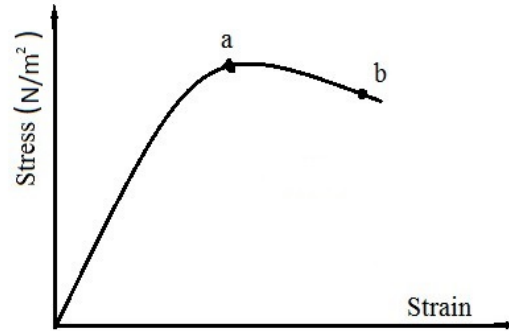


Fig. 2.9 The stress-strain curve for various kinds of materials showing their rupture points 'a' for brittle and 'b' for ductile materials

the Stribeck effect, the frictional lag and varying breakaway. However inefficiency often arises due to snapping discontinuities of the bonds resulting in unusually short integration steps. Also the fact of no damping imposes a great limitation to the system implementation. As a result, this model though good does not easily lend itself for control purposes in a real system. The second model called the reset integrator was an attempt to resolve the simulation and implementation problems of the bristle model and still preserve its accuracy to model friction.

Dahl model

In [30], the Dahl model was proposed to capture the friction effect mainly the pre-sliding features. The Dahl model was based on the assumption that the origin of friction is in the quasi-static contact bonds that are continuously being formed and subsequently broken between material surfaces in contact. This stress-strain relationship at micro level gives rise to the macro friction force experience shown in figure 2.9. At small displacements the material tends to regain its original position when stress is removed but with large displacements permanent displacements occur as a result of plastic deformation. The strain caused by the applied force leads to pre-sliding displacements until it is large enough to initiate gross-sliding. For a ductile material as illustrated in figure 2.9, the force for gross sliding is smaller than that before rupture due to the ductility of the material while for brittle materials it is observed that the breakaway force and the force of sliding are virtually the same connoting the absence of stiction. The mathematical formulation of the Dahl concept is as given below

$$\frac{dF_f}{dt} = \sigma \left(1 - \frac{F_f}{F_c} \text{sgn}(\dot{z}) \right)^\delta \quad (2.17)$$

given that

$$\frac{dF_f}{dt} = \frac{dF_f}{dz} \frac{dz}{dt}$$

then

$$\dot{z} = v - \sigma \frac{|v|}{F_c} z$$

and

$$F_f = \sigma z$$

where F_f is the friction force, z the deflection of the bristles, σ is the stiffness of the bristles, F_c the coulomb friction, and δ a curve shaping parameter. This model exhibits pre-sliding hysteresis without the non-local memory features, however it is unable to capture some other features like Stribeck effect, stiction and frictional lag, [32], [51]. Because of its simplicity and implementation ease this model has been used for friction compensation in some applications, [52], [53].

LuGre model

A model of friction that captures many of the friction phenomena was proposed in [32], as a result of the joint research efforts between the Lund university and the Grenoble lab in France. This model of friction captures the input-output relations and is easy to implement with good computational efficiency. It also exhibits many of the prominent features of friction like the stick-slip motion, Stribeck effect, varying breakaway force, pre-sliding hysteresis, and frictional lag. It evolved from the Dahl model by incorporating some other features that make it to be rate dependent rather than the rate independent Dahl model. It is an integrated model since it uses a single formulation to portray the pre-sliding and gross-sliding friction properties. It is easily adopted for simulation and controller synthesis. The approach adopted was the bristle technique where the friction is captured at microscopic level as the interaction between bristles when subjected to a shearing force between the surfaces that leads to the elasto-plastic deformation of these asperities. The LuGre model is formulated thus

$$F_f = \sigma_0 z + \sigma_1(v) \dot{z} + f_v(v) \quad (2.18)$$

$$\dot{z} = v - \frac{|v|}{g(v)} z \quad (2.19)$$

$$g(v) = \frac{1}{\sigma_0} \left(F_c + (F_s - F_c) e^{-\left(\frac{v}{v_s}\right)^2} \right) \quad (2.20)$$

where F_f is the friction force, f_v is the viscous damping coefficient, z is the micro displacement between the surfaces (or bristle deflection), σ_0 is the stiffness of the material, σ_1 is the

material damping coefficient, $g(v)$ is the non-linear term modelling the Stribeck effect at low velocities, v is the relative velocity between the surfaces in contact. v_s is the Stribeck velocity. The LuGre friction model gained much popularity because of its low number of parameters and the integration of both regimes of friction in one state equation. Worth noting though, the improvement on the Dahl model by the LuGre is the result of the following:

1. Insertion of the non-linear rate dependent function $g(v)$ to capture the low velocity Stribeck effect.
2. Inclusion of a velocity dependent micro-displacement damping function σ_1

LuGre model has found wide applications (in pneumatics, robotics and mechanical) for the control and compensation of systems with friction, [54], [31], [55], [56]. Despite this popularity it has been observed that the model has some limitations [31], such as:

1. Inability to reproduce experimentally observed reversal point with non-local memory at small pre-sliding displacements [34], [57], [51].
2. It is subject to the drifting effect (zero drift displacement) and some other implementation related issues [58], [55], [59]
3. Presence of discontinuity in the mathematical formulation [60], [61]

To address these shortcomings of the LuGre model, many other variants which are simple modifications of the LuGre were proposed. Some of these are briefly reviewed. In trying to overcome the discontinuity of the LuGre model a continuous approximation of the model was proposed in [60]. However, passivity and stability properties of the model was not established. The drift feature of the LuGre was addressed by an extended LuGre model known as the Elasto-Plastic (E-P) model presented in [62]. The state and friction force equations of the E-P model similar to the LuGre are given by

$$F_f = \sigma_0 z + \sigma_1(v) \dot{z} + f_v(v) \quad (2.21)$$

$$\dot{z} = v - \alpha(z, v) \sigma_0 \frac{|v|}{g(v)} z \quad (2.22)$$

with

$$\alpha(z, v) = \begin{cases} 0 & \text{for } |z| < Z_b, \text{sgn}(v) = \text{sgn}(z) \\ \frac{1}{2} \sin \left(\pi \frac{z - (\frac{z_{max} + Z_b}{2})}{z_{max} - Z_b} \right) + \frac{1}{2} & \text{for } Z_b \leq |z| < z_{max}, \text{sgn}(v) = \text{sgn}(z) \\ 1 & \text{for } |z| \geq z_{max}, \text{sgn}(v) = \text{sgn}(z) \\ 0 & \text{for } \text{sgn}(v) \neq \text{sgn}(z) \end{cases} \quad (2.23)$$

z_{max} is the maximum bristle deflection, Z_b the breakaway friction displacement, and z the bristle deflection. Thus from equation 2.22, when $\alpha(z, v) = 1$, the model is equivalent to the LuGre model. The breakaway deflection often chosen less than the maximum deflection given as $g(v)/\sigma_0$. This model is simple to implement as the LuGre but with the added advantage of non-drift. However the elasto-plastic friction model does not capture the pre-sliding hysteresis with non-local memory.

Leuven model

An integrated friction model aimed at resolving the hysteresis with non-local memory problem of the LuGre model was proposed in [34]. Non-local memory implies that in the force-position (hysteresis) plane every point for velocity reversal can be recovered, see section 2.2. The Leuven model consists of the state equation

$$\dot{z} = v \left(1 - \text{sgn} \left(\frac{F_d(z)}{g(v) - F_b} \right) \left| \frac{F_d(z)}{g(v) - F_b} \right|^n \right) \quad (2.24)$$

and the friction force equation expressed as

$$F_f = F_h(z) + \sigma_1 \dot{z} + f_v(v) \quad (2.25)$$

with the hysteresis function $F_h(z)$ modelled as

$$F_h(z) = F_b + F_d(z) \quad (2.26)$$

where $F_h(z)$ is used to capture the hysteretic friction behaviour with two parameters depending on the transitions. $F_d(z)$ is a displacement dependent function modelling the friction for each branch transition, F_b the friction force at the beginning of each branch or reversal point, $g(v)$ is the Stribeck function. In depth description of this model can be found in [34]. Some challenges posed by this model are related to how the hysteresis function is implemented, and possible discontinuity in the friction force predicted. The requirement for memory

stacking leads to possible stack overflow [35], and continued detection of velocity reversals, setting and resetting of the memory at every transition from pre-sliding to gross-sliding lead to possible errors in the calculations and detection [51], thus making implementation of this model complex. In [35], a solution was proposed to tackle some of the problems with the Leuven model. To overcome this, a physics motivated model capable of modelling most known dynamics of friction was proposed [24]. The model being very complex for implementation and control purposes led to further modifications resulted in the Maxwell and Generalised Maxwell-slip (GMS) models.

GMS model

In [63] a multi-state friction model, the result of a simplification of the model proposed in [24], and called the Generalised Maxwell Slip model by the authors, [58] was proposed. It is a generalisation of the Maxwell slip model formulated by the introduction of a rate-state law in place of the Coulomb slip concept of [35]. The model contains two state equations representing the stick and the slip phases of motion. For sticking the state equation is

$$\dot{z}_i = v \quad (2.27)$$

and for slipping

$$\dot{z}_i = \text{sgn}(v)C_i \left(1 - \sigma_{0i} \frac{z_i}{g_i(v)} \right) \quad (2.28)$$

$$i = 1, 2, \dots, N$$

During stick, the elements remain stuck till the deflection $z_i = \frac{1}{\sigma_{0i}}g_i(v)$, and also during slip, the element continues to move until the velocity v goes through zero (reversal). The friction force is thus given as;

$$F_t = \sum_{i=1}^N (\sigma_{0i}z_i + \sigma_{1i}\dot{z}_i) + f_v \quad (2.29)$$

with $z \in \mathbb{R}^N$ where z_i is the deflection of the i th element, $g_i(v)$ is the velocity weakening Stribeck function, C_i is an attraction parameter showing how rapidly the z_i tracks changes in $g_i(v)$, σ_{0i} is the stiffness of the i th element and N is the number of massless bristle elements. This model replicates most features of friction though the qualitative prediction of the stick-slip motion differs from that of most popular models like the LuGre, Leuven. Moreover the computation of the force being dependent on the number of elements makes the number of model parameters increase thereby increasing model's complexity. It also suffers continuity related problems, and does not capture qualitatively the stick-slip and the pre-sliding hysteresis effects according to [58], [64]. The GMS model has also been shown

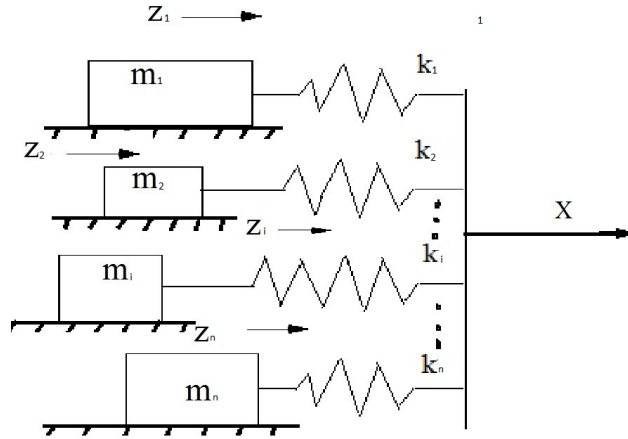


Fig. 2.10 Representation of the Generalised Maxwell Slip (GMS) friction model

to exhibit some rate-dependence hysteresis in the pre-sliding regime, [65]. This model has found applications in control schemes and a comparative performance of the model with other models was carried out in [63], [66]. The GMS model structure is quite complex especially with increasing number of bristle elements, it also exhibits difficulties due to its switching function implementation as the system moves from the stick regime to slip regime. This on-line implementation difficulties and also possible discontinuity of the \dot{z} motivated further modifications of the model structure [67], [68], [64].

Xiong model

This is also a multi-state friction model structure (called the 'Xiong' model in this thesis) presented in [69], to capture friction characteristics both in the pre-sliding and gross-sliding friction regimes. The model developed from a differential algebraic friction models [70], [69]. This model structure, like the GMS model is multi-bristle-element based and could get very complex to implement as the number of bristle elements increases. The structure is of the form

$$\dot{\gamma} = \frac{g(v) - \gamma}{\tau} \quad (2.30)$$

$$\dot{z}_i = \frac{\text{sat}(\lambda_i \gamma, K_i z_i + \sigma_i v) - K_i z_i}{\sigma_i} \quad (2.31)$$

$$F_f = \sum_{i=1}^N \text{sat}(\lambda_i \gamma, K_i z_i + \sigma_i v) \quad (2.32)$$

$i = 1, 2, \dots, N$

where γ is a state variable representation of lagged $g(v)$, λ is such that $\sum_{i=1}^N \lambda_i = 1$, K

stiffness of the bristle element, σ is the micro-damping parameter, τ Xiong's equivalent of GMS model's C showing the convergence rate of γ to $g(v)$, and N is the number of elements. This model was shown by simulations to be able to capture the non-drift property of friction, stick-slip motion, frictional lag, pre-sliding hysteresis with non-local memory. However due to the multi-element nature there is implementation challenges as N is increased.

As stated earlier, this review is definitely not intended to be exhaustive given that some other models of friction exist such as the seven parameter model by Armstrong et al, [38], the Bengisu and Akay friction model [71], Wojewoda et al's static model [72] and the family of models developed by Bliman and Sorine [73], [74]. However the motivation for this review has been based on their relevance to the present research in relation to systems control. From the various friction model structures investigated, the difficulty in choosing a model for control satisfying the criteria of simplicity and fidelity is apparent especially in the pre-sliding low velocity friction regime. As a result of this a new dynamic model structure for modelling friction phenomena for control purposes that is both simple and efficient would be presented in the next chapter.

2.4 Friction parameter estimation

Modelling of systems is focused on approaches adopted for the determination of the mathematical relationships existing between the input and output of any given system whether linear or non-linear, single-input single-output, or multi-input multi-output systems. Such a model adequate for control purposes is usually a compromise arising from many factors, thus a perfect model of a system is only an idealisation as a result of practical exigencies. A system model is often regarded as the mathematical formulation which relates the system output to its past input(s), and/or past output(s). A good system model often makes it possible to infer peculiarities, nature and properties of the system it represents, and also to predict future output(s). Hence it is a pre-condition for system analysis and controller designs. System modelling is thus the process of determining the best mathematical structure representative of the system in question. This area of research which is a subset of the control theory has evolved over the second half of the last century and attracted much research attention [75], [76]. Linear systems modelling is therefore a mature research area with established techniques and algorithms unlike non-linear systems even though almost all real life scenarios are non-linear. In this section an attempt is made to discuss some of the general trends in the modelling of systems with a view to understanding their strengths and weaknesses and tools which can be modified and/or adopted in the present research. As such, modelling of systems and the

various approaches adopted in recent years are studied as they relate to friction. In system modelling one pertinent question that must be answered a priori is the purpose to which the model would be deployed. This is very important due to the fact that research indicates that there exists no "perfect" model of any real system since most systems are inherently non-linear. Rather models which are useful for specific purposes can be obtained usually as a compromise among many variables where the increased accuracy in determination of one variable leads to increase in the uncertainty of another, [77]. Most modelling activities and dynamic model applications have been greatly motivated and influenced by some underlying pre-cursors, which are;

1. Satisfaction of scientific curiosity
2. Explanation of system behaviour
3. Simulation and validation (optimization)
4. Prediction and control
5. Fault detection and diagnosis

2.4.1 System identification techniques

Some approaches have been adopted over the years in the modelling of systems in general and some of these techniques are discussed next. Most of the techniques adopted in system modelling can be grouped into three main categories depending on the level of physical knowledge of the system taken into account. These techniques are;

1. The white-box,
2. The black-box, and
3. The grey-box.

The white box and the black box identification techniques to modelling are the two extremes adopted in system modelling while more practical models often are with shades of grey in between these extremes.

White-box approach

In white box method, a model of the system is derived from first principles considering the physical, biological, chemical parameters and components influencing the system and their

interactions. Because of the many considerations this phenomenological method often gives rise to very complex models which often are computationally impossible or expensive at the best. Sometimes adequate model structures of complex systems may even prove impossible to obtain in reasonable time frame owing to complexities in the systems, processes and their interactions. This may be feasible for some very simple systems and processes, however as the system increases in complexity it becomes nearly impossible to adopt this identification approach. The main appeal of this method is the fact that the entire model reflects the true nature of the system and the corresponding parameters are of real physical interpretation. As a result of this difficulty in modelling complex systems, the black box and grey box modelling are better alternatives for modelling complex systems, [77], [78]. An example of such modelling approach adopted for friction is illustrated in [24].

Black-box approach

Another approach is to deduce system models based on the input-output data set obtained by measurements without any attribution or emphasis on the exact nature and physics of the system itself. This makes the black box method empirical and reduces the modelling problem to that of identification of the existing relationship between input-output data from which future output could be inferred. This pre-supposes the possibility of obtaining input and output data through measurement procedures. The downside to this approach is in the fact that it entirely relies on the authenticity of the data used, thus the model can at best be as good as the data used for modelling. Relying on this data makes the method dependent on some factors like the type of devices used for data acquisition, and analysis, this process could thus become subjective. other demerits of this approach are; it yields opaque models often without mathematical interpretation, difficulties in model analysis and the isolation of cause and effect is not easy. This method without a priori knowledge of the system is termed the black box approach, [79], [80]. Typical examples of friction model structures obtain through this technique are the machine based models of section 2.2

Grey-box approach

Often-times a good or partial understanding of the system under study is of immense help in determining the structure of system's model. A combination of this part knowledge of the system (phenomenological) and input-output identification (empirical) process often leads to models that are somewhat in-between these extremes of black and white. These models are therefore called Grey models, and different shades of grey depicts the extent of physical insight involved. They consider some properties and physical nature of the system

in deducing the model structure [77], [81]. A typical example is when a model structure has been deduced for a given system based on the white-box approach and its parameters are estimated through identification (black-box) method.

2.4.2 Non-linear systems structure

Many variations of non-linear systems such as friction have been studied and reported as indicated by the volume of publications in this regard. However, for the present research interest we categorise them into four main groups.

The Volterra series model representation; In this representation a functional called the Volterra functional comprising a convolution integral and Taylor series is adopted for the model structure. The convolution integral represents the linear part of the system while the static non-linearity is captured by the Taylor series. Parameters estimation are often computationally involving because of the exponential relation between the number of parameter and the degree of the kernel. This and the fact that it cannot be used to model some non-linearities such as saturation, backlash, dead zone and hysteresis are the major drawbacks of this model which resulted in the Wiener series model. A tensor based approach has been proposed to reduce the effect of complexities associated with parameter estimation such as the Volterra-Parafac model and the Volterra-Laguerre model, [82], [83].

Block oriented model representation; It has been possible to formulate models of systems in block formation relating the inputs and outputs, these blocks can be combinations of linear dynamic and non-linear static blocks interconnected in cascade or in parallel. Typical examples of this formulation are the Hammerstein and Wiener block models. In the former the linear block is after the static non-linear block in a series connection while the reverse is the case for the later. The Wiener formulation is better able to handle non-linearities resulting from input amplitude induced dynamics. The main appeal of the block diagram approach is its simplicity, however, the requirement of some level of a priori system knowledge and restriction on the nature of excitation used place great limitations to the structure, [84], [81].

Neural Network model representation; Neural Networks have drawn a lot of research attention in system modelling mainly due to their excellent approximation property. The radial basis function (RBF) and the multi-layer perceptions (MLP) are the most widely used feed-forward Neural Networks for modelling many industrial processes [79], [85].

NARMAX model representation; In Non-linear Auto-Regressive Moving Average with exogenous input (NARMAX) model representation, an extension of the ARMAX model for linear systems is a form of system representation with non-linear difference equations or polynomials. This form has generated much interest as a result of these qualities;

1. No restrictions to the nature of signal inputs unlike the others previously studied
2. Its model parameters are linear thus rendering analysis simpler
3. Physical interpretations of the models are possible under certain conditions
4. It allows for integration of other formulations like the block oriented, and Volterra series model structures

The NARMAX model structure has successfully been applied to systems modelling and identification problems as illustrated in the following.

Piece-wise linear models; These are representations of approximations of the system non-linearities localized at various regions of operation. This technique has also been used often where it is nearly impossible to obtain a single model representation of the system capturing most of the system characteristics. One major issue with this model is the determination of the regions of model validity.

2.4.3 The system identification process

The basic motivation in system identification is; given a model structure of a system to obtain the estimation of model parameters adequate for replication of the system from the input-output data set. The models obtained could therefore be;

1. Linear or non-linear
2. Static or dynamic
3. Continuous-time or discrete-time
4. Deterministic or stochastic
5. Parametric (lumped or distributed) or non-parametric
6. Phenomenological or representative

Insight and prior knowledge of a system are often helpful in the determination of an adequate model structure for the system and estimation of its parameters to fit the data to a given model structure. Many a time identification problems reduce to curve fitting optimisation problems, minimizing the difference between the measured output data and the model structure often in a square-error-sense. Minimization of a cost function subject to some constraints can often take any of the many forms in the previous section depending on the purpose and the level of physical insight employed.

In chapter 4, a carefully designed set of experiments would be performed for the purpose of using the input-output data from such experiments to identify the parameters of the proposed model structure and some other model of friction. In the next section a review of friction compensation and control schemes adopted for frictional systems is undertaken since one of the research objectives is to identify models adequate for the purposes of control.

2.5 Friction compensation in control systems

Performance degradations in systems which may not easily be eliminated through design mechanisms are greatly reduced within acceptable limits through the process of compensation. Generally, compensators are used to improve system performance in terms of error reduction, transient response improvement, increased settling time. Friction compensation and control has been an area of active research in the control systems community because of the desire to minimize the problems of friction in mechanical systems. This is attested to by the catalogue of research publications regarding the subject. Compensation of friction has been carried out in various ways each having its merits and demerits. In this section we explore some of the relevant schemes that have been adopted to compensate the friction phenomena. It should be noted however owing to its complex nature complete elimination of friction in any system is difficult. Compensation and control effort are therefore performed to reduce to acceptable limits the adverse effects resulting from friction.

2.5.1 Friction compensation techniques

The very first step in friction control is to design mechanical systems for control, which is a problem (friction) avoidance approach, adopted to minimise friction effects. For example stick-slip minimization in a system by mass reduction, or increased system damping was investigated in [36]. Other design choices such as actuator type, bearing design, surface finish and material type can be designed such that friction is reduced [95]. Lubricants have been used in many mechanical systems to reduce the effects of friction and wear in contacting surfaces experiencing relative motion. Application of lubricants tends to reduce the friction-velocity slope. These lubricants are usually in the form of fluids such as grease, paraffin, oil and even water sometimes. Dry lubricants such as polytetrafluoroethylene (Teflon) have also been used for the same purpose. The scheme is however not a compensation scheme in the strict sense but rather friction avoidance, or elimination approach.

Friction compensation techniques adopted in systems control can be categorized into two main groups namely:

1. Non-model based friction compensation schemes under which are;
 - (a) Use of a dither,
 - (b) Impulsive signal,
 - (c) Classical Proportional, Integral, Derivative, (P.I.D) based feedback controllers
 - (d) Acceleration feedback, and
 - (e) Soft computing.

2. Model-based compensation schemes under which are;
 - (a) Feedforward
 - (b) Feedbackand combinations of both

Non-model based friction compensation

The technique does not explicitly require a friction model for its compensation in any system and because of simplicity and choice, it has found applicability in many platforms as discussed in [38]. This approach can take on many forms some of which are discussed further below.

Dither driven compensation

This is a high frequency signal often used to reduce especially static friction in a mechanical system. This signal when added to the control signal induces a mechanical vibration effect between the surfaces in contact thereby lowering the static friction level and the stick-slip motion reduction. It has been used to control servo valves of hydraulic actuators. Research indicates that this approach has been used to reduce friction and related effects in many control systems, [86], [87]. However, wear related issues make it not too often used in many mechanical systems subject to friction.

Impulse driven compensation

Impulse signal which introduces small-duration impacts on the system has been used to reduce friction effects. The impulse signal drives the system unlike the dither in which it is introduced along-side the driving signal. In [88], a high gain torque controller was implemented for the purposes of friction control. Impulse signals are used to reduce friction due to its high gain, short duration nature which lowers the static friction between the surfaces. Successful use of these methods in compensating friction is highly dependent on some aspects of machine design like surface finish, contact loading, material properties etc.

Classical P(I/D/ID) compensation

Performance characteristics of a system such as the transient response can often be improved by the use of any of/or combinations of Proportional, Integral, and/or Derivative, (P.I.D) controllers in a feedback control scheme. The proportional controllers improve the transient response while increasing the peak overshoot, the integral controllers improve the steady state tracking by minimizing the steady state error with the possibility of introducing limit circle in the system and problems associated with zero, low or reversal velocities [89]. High gain PD control is equivalent to increased system damping which as stated previously minimizes stick-slip effect. This approach to control is often used in conjunction with other forms of compensation since it is not very effective for non-linear systems control, [90], [91]. Generally this approach finds more appeal for linear controller design, as such it handles friction as a disturbance non-linearity. At medium and high velocities it could perform well since friction in these ranges is seen to be more linear than non-linear. However for very low velocities and reversals this scheme is often helpless and grossly ineffective for friction control [92]. It should be stated here that PID controllers are usually used in combination with a friction compensator since they do not compensate the system friction. This will be illustrated in chapters 5 and 6.

Acceleration feedback compensation

A robust way of reducing friction effects in a system is by use of acceleration feedback. When a feedback loop is closed around an accelerometer, it is possible to derive a high gain loop which could be used for the control of the acceleration of any given mass (inertia) directly [93], [94]. This scheme is simple in concept but increases cost as a result of the acceleration sensors incorporated in the control. Acceleration observers can be used to estimate the acceleration rather than obtaining a second order derivative of the position from an encoder output as this introduces noise in the system.

Compensation based on machine-learning

Artificial intelligence-based systems such as Fuzzy, Neural Network (NN), and Genetic Algorithms (GA), have been used in reconstructing (modelling) the friction torques to be compensated or for self-tuning of the system controller gains. These soft computing techniques are gaining grounds due to availability of powerful computers capable of complex computations at reduced time. The technique has been applied for the control of some mechanical systems as in [95], where the neural networks were used in parallel to a linear observer for an electromechanical positioning system. A hybrid compensation method, comprising ANN and parameterized coulomb model was adopted in [96], while a support vector approach was used in [10], for compensation. Neural Networks are easy to train and use, and simple structured with high approximation properties. However, it is not without its

own issues some of which are: lack of network dynamism, difficulty in relating to physical properties of friction.

Friction estimators such as the Kalman-based filter and predictive filters are also some other forms of non-model based techniques to friction compensation and control.

Model-based friction compensation

Model-based compensation, involves the use of a model of the system friction to eliminate friction by means of introducing the friction model in the control loop, [97]. The concept thus generates adequate signal which compensates the system friction when added to the control signal. Many models of friction have been proposed, however, only a handful of them are actually used for experimental identification and compensation of the friction phenomena. This is due to the fact that a great difference exists between simulation and modelling of friction, experimental identification and compensation challenges in real systems as a result of the nature, complexity and implementation ease of the models for control purposes. Research indicates that the use of this technique when possible, for friction compensation purposes has led to design of good friction compensators adequate for control. This approach thus has increased as a result of developmental progress made in the last few decades in modelling the friction phenomena [98], [55]. The efficacy of this method is however, heavily dependent on the model used for control. Many static models have been successfully applied for the purposes of friction compensation and control, [57], [99], despite its limitations as shown earlier due to their simplicity. On the other hand, among the dynamic models, the LuGre model has gained the most popularity owing to it's simplicity, ease of implementation and ability to model most friction phenomena as against the GMS, Leuven and Xiong models, [55], [31]. Some of the more approaches in implementation of the model-based technique are further illustrated under feedforward and feedback compensation strategies.

Feedforward approach

Figure 2.11 depicts the approach adopted in this method whereby the friction estimate from an observer is obtained using the reference trajectory needless of any closed loop calculations. In this way the closed loop stability as determined by the linear controller will be unaffected. It's merit lies in the usage of reference signal for friction computations. From the figure, the linear feedback controller helps ensure stability and disturbance rejection while the friction feedforward compensator injects pre-calculated friction into the system to eliminate friction inherent in the system. This method has been used to compensate friction in [12], [100].

In the figure 2.11, F is the friction in the plant, \hat{F} is the friction predicted by the model, $A(s)$ the transfer function of the PID linear controller, $Y_r(s)$ the reference input expressed in Laplace, and the $Y_0(s)$ Laplace transform of the system output.

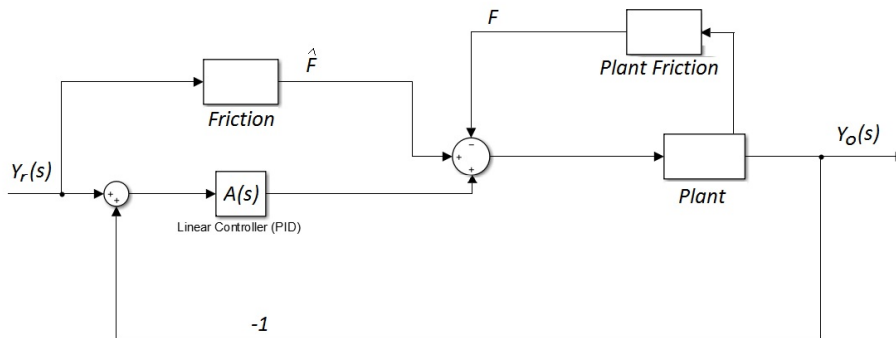


Fig. 2.11 Model-based feedforward friction compensation approach

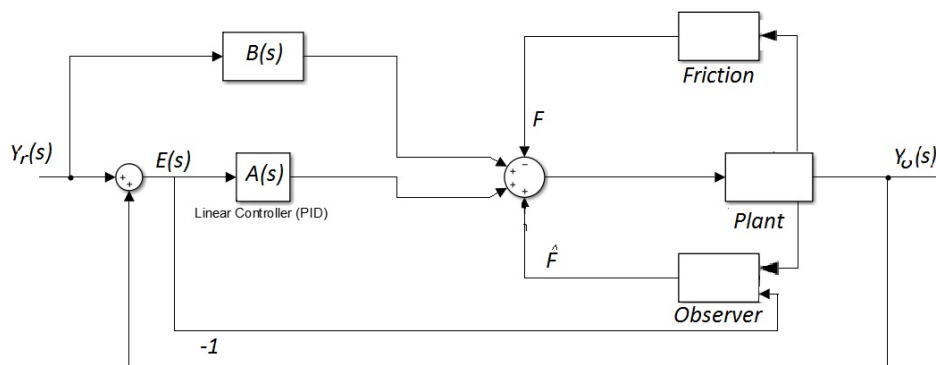


Fig. 2.12 Model-based feedback friction compensation approach

Feedback approach

In the model based feedback approach the friction observer is as shown in figure 2.12 with observer input being the system output rather than the reference as in the feedforward above. In this manner the friction estimate is dependent on the output and because the states are difficult to measure an estimate is sought via the observer. Moreover, a closed loop stability analysis of the system must be carried out to ensure system stability before the compensation loop is incorporated. It's merit lies in the usage of the actual output signal rather than the reference for friction estimations. This method has been adopted for real time compensation of systems such as in [101], [102]. Worthy of note are:

1. The linear feedback controller appears in both the feedforward and feedback compensation approaches since it enhances stability and disturbance rejection.

2. Sometimes a combination of the feedback and feedforward compensation scheme is adopted to further improve system performance.
3. An inverse of the process (plant) could also be integrated into the control to enhance error reduction as represented by the gain $B(s)$.

In the figure F is the friction in the plant, \hat{F} is the friction predicted by the model, $A(s)$ the transfer function of the PID linear controller, $B(s)$ the Laplace transform of an inverse model of plant, $E(s)$ is the error signal expressed in Laplace. $Y_r(s)$ the reference input expressed in Laplace, and the $Y_0(s)$ laplace transform of the system output.

Some of the problems associated with the model based compensation are issues of over-compensation and under-compensation of the friction non-linearity in a system and parameter mis-match. These would be explained later in the report.

2.5.2 Adaptive friction compensation

Parametric changes in models are unavoidable given that friction is dependent on the system operating conditions like temperature, lubrication, time, humidity etc. This implies that a given model might be more accurate at some operating conditions than at others. This error can be costly where high precision is needed hence necessitating parametric models whose parameters change in accordance to changes in the system friction and operating conditions. Such control systems that change so as to reflect changes in system conditions are called adaptive control systems. Friction force parameters can be made adaptive to reflect parametric changes resulting in operational variations of the system like temperature, humidity, time, degree of dryness rather than being static. Online and offline parameters identification are often used for system identification of model parameters. Offline approach often leads to models of friction with static parameters while online approach yields adaptive models capable of tracking changes in model parameters as a result of changes in the system. These adaptive systems can be made robust to handle uncertainties in the modelling [103], [37]. In [56], a modified LuGre model was used for design of an adaptive robust friction compensator for linear motors. Adaptive friction compensation could be model-based or not based on a model of the system friction [104]. Model-based compensators use a friction model structure for estimating the friction effect, while non model-based have no such requirements for friction estimation. An estimation of the non-linear friction model parameter based on recursive least square method was presented in [105]. Support vector regression method with neural network was presented for adaptive friction identification and compensation in [106]. Significant improvement was observed in the tracking performance of a hard disk drive actuator by means of the neural network based compensator.

Sometimes more than one strategy may be adopted in a given situation for improved system modelling, tracking and control. Such composite compensation approach was adopted in [107], the control system comprised of the sliding mode controller, a recurrent fuzzy-neural network, a friction state observer. A fuzzy logic based adaptive compensator was proposed for stick-slip friction, and backlash compensation, [108].

2.6 Chapter summary

A deeper understanding of the underlying friction dynamics characterizing friction has been investigated. From the foregoing it is apparent that friction behaviour is most problematic in the pre sliding and low velocity regimes. This is because of the rich dynamism characterizing friction in these regions. Most existing models of friction are actually application and regime dependent. Application dependent in the sense that certain models perform better than others in robotic systems while in systems with rolling friction they may not give optimal results. Regime dependent in the sense that one model out-performs others in pre-sliding regime while another performs better in the gross-sliding regime. In this thesis the main thrust is thus developing a dynamic model that will be rich enough to replicate relevant observed friction features and yet simple enough for implementation, compensation and control purposes. Model-based compensation and control of such systems under friction have also been reviewed and the prevailing methods adopted investigated. While this is not exhaustive, it gives a review of the current state of the friction model formulations that have dominated the control community and the various approaches adopted in parameter identification, compensation and control of this feature of most mechanical systems.

Chapter 3

A new friction model for low velocities

3.1 Introduction

In the previous chapter, general features of many existing friction models were reviewed. The result of the review suggests that the simple friction models such as the classical models are not able to capture some of the important friction dynamics and may not be adequate for high precision control systems design. On the other hand, dynamic friction models though able to capture many of these dynamics are generally more complex and this complexity increases with increasing dynamics of these models of friction. This scenario results in the trade of between model fidelity and simplicity which are key objectives in system modelling and control as discussed in chapter 1. Thus a good model is not necessarily judged by its ability to replicate friction features but also in the ease with which such models could be used for their desired objectives such as control.

In this chapter therefore the motivation is to present a dynamic friction model that is simple enough for implementation, simulation and yet appropriately captures most friction dynamics. The interest is in identifying a model structure capable of predicting known friction features and yet simple enough for identification. Such a model should be appropriate for control purposes. The modelling approach adopted is such that is both heuristic and empirical; such hybrid grey-box technique (see 2.4) whereby the structure of the model is not only physics based but also based on empirical results from identification data. In this way the model structure easily renders itself to physical interpretation. Results from the laboratory test rig designed especially for this purpose are used for system model's parameter identification, to be carried out in the next chapter.

The layout of the chapter is thus as follows: In section 3.2 a new friction model capable of predicting relevant features of friction is proposed, while section 3.3 looks at the properties of the proposed non-drift dynamic friction model such as stability, dissipativity, passivity and

uniqueness of the new model. In section 3.4, a describing functions analysis of the hysteretic properties of the proposed non-drift dynamic friction model was studied and empirical values derived. The ability of the model to predict stick-slip friction phenomenon and sensitivity analysis of the proposed non-drift dynamic friction model with some relevant models are discussed in sections 3.5. Section 3.6 looked at Pre-sliding performance analysis of some of these model with the new model. In section 3.7, a summary of the main results was articulated.

3.2 A new model structure for friction

In this section a new friction model capable of predicting major friction phenomena such as Stribeck effect, pre-sliding hysteresis with non-local memory, limit cycle oscillations, stick-slip motion, is presented. This friction model structure is dynamic and able to meet the control objectives of simplicity and fidelity and easy for implementation as set out in chapter 1. Most models describing the friction phenomena as shown in chapter 2 either over simplify the friction phenomenon thereby not being able to capture some of the essential features of friction or are too complex for implementation and control purposes. To achieve this objectives, the macroscopic and microscopic behaviour of friction is put in perspective.

Consider a microscopic representation of contacting surfaces, the friction surface shown in figure 3.1a, where the bristles represent the microscopic view of the contacting surfaces for a given force applied. Therefore, the model proposed in this chapter is based on the cumulative behaviour of the bristles using a single bristle to capture this friction behaviour figure 3.1b. Bristle analysis was earlier discussed in chapter 2 and have been the basis for many models of friction (LUGre and Dahl models) as seen in the previous chapter. The friction phenomena is such that the pre-sliding and gross sliding friction features differ and hence need different model features to capture these behaviours. Here an attempt is made to obtain a unified structure for this complex friction behaviour.

Friction has been noted to exhibit a non-local memory hysteresis in the pre-sliding regime of motion which is rather a function of the displacement in the pre-sliding range. Thus a model structure proposed for pre-sliding friction regime is

$$f_b(z) = \sin\left(\frac{z - z_r}{|z_t - z_r|} \frac{\pi}{2}\right) \quad (3.1)$$

and

$$F_{hyst}(z) = f_b(z)|f_t - f_r| + f_r \quad (3.2)$$

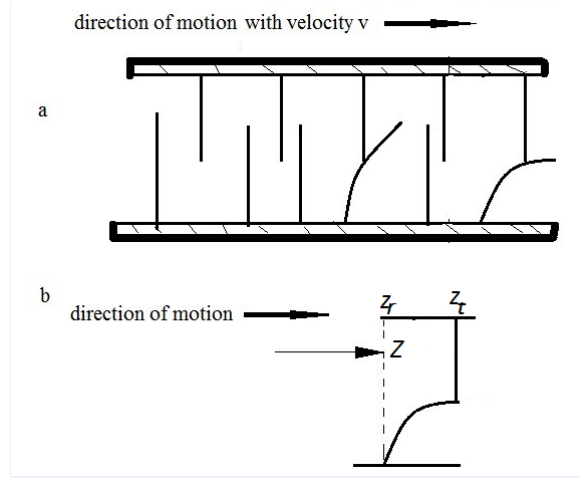


Fig. 3.1 The frictional lag as feature with the Proposed model for different frequencies

with $z_t, z_r, \in z \in \mathbb{R}$, where $f_b(z)$ is the pre-slide function for any given branch deflection, $F_{hyst}(z)$ is the total friction force in the pre-slide regime at any given time, z the bristle displacement, z_r the bristle displacement at the beginning of a branch, z_t is the target displacement (which is a function of the reversal displacement z_r and the breakaway displacement Z_b), f_b the current branch friction force, f_r is the friction force at the beginning of a branch (takes into account the stressed state of the bristles), f_t target friction force (also a function of the reversal point force f_r and the stiction force).

The first equation is a function of the bristle deflection with a monotonically increasing characteristics. Other non-linear elements such as the hyperbolic tangent and some cumulative distribution functions with similar features as the sine function used here could also be used. However the sine function was used due to the ease of integrating relevant parameters of interest and attaining saturation in finite time as would be illustrated in the next chapter. The second equation is the pre-sliding friction force equation with the first term capturing the frictional force for any branch and the second term the friction force value prior to external force application. Thus the second term is a description of the current state of the bristle before the external force influence. In the gross-sliding friction regime, two distinct friction features appear in the low velocity region namely; the Stribeck and the frictional lag effects. The Stribeck effect has been effectively modelled as shown earlier in chapter 2 but lacks the capacity to capture the lag effect. In order to capture the fact that friction force states for acceleration and deceleration at low velocities are different a new state equation in the Stribeck region is defined thus

$$\dot{\gamma} = \frac{g(v) - \gamma}{\tau} \quad (3.3)$$

where γ is a state variable representation of the lagged version of the Stribeck function $g(v)$, introduced to improve the frictional-lag prediction capability of the model [70], and τ is the time constant determining how fast the new friction force state variable γ tracks $g(v)$. The function

$$g(v) = F_c + (F_s - F_c)e^{-(v/v_s)^2}$$

is the Stribeck function (always a positive value), $v_s \neq 0$ is the Stribeck velocity. A second state equation relating the bristle deflection is given by

$$\dot{z} = \frac{1}{\sigma}(\text{sat}(\gamma, F_{hyst}(z) + \sigma v) - F_{hyst}(z)) \quad (3.4)$$

indicating that the deflection behaviour in the pre-sliding and gross-sliding friction regimes vary. In the light of equations 3.4 and 3.3, as z implies deflection or position measure so also the term γ indicates friction force measure due to the external force influence. The friction force is then defined by the following equation

$$F_f = F_{hyst}(z) + \sigma \dot{z} + f_v v \quad (3.5)$$

where $F_{hyst}(x)$ the pre-sliding friction force, σ is the micro-viscous damping parameter, v is the relative velocity of the bodies in contact, f_v is the macro-viscous friction component, and F_f is the overall friction force.

3.2.1 Model behaviour

In this section a discussion on the characteristic features of the model both in the pre-sliding and gross sliding regimes of friction is presented. Thus highlighting the peculiarities of the new model and its similarities to some existing models.

Mechanism of the pre-sliding friction function

In the pre-sliding regime friction exhibits a non-local memory characteristic effect as described previously in chapter 2, section 2.2. This hysteresis is captured by the function in equations 3.1, and 3.2. Figure 2.4 of chapter 2 is also used for the analysis here. Prior to application of force at point a in figure 2.4a, the values of the z_r and f_r reflect respectively the initial displacement and force the bristle is subjected to. For surface under tension this is often non-zero while for non-tensed surfaces it is regarded as zero. For the analysis the initial values of these two variables are 0. z_t is the target displacement at which maximum force is expected to result which for this is the breakaway displacement (Z_b) for the virgin curve

(see section 2.2), and the target force is the stiction force F_s . Thus the virgin curve could be said to be the path the friction force traced from rest position towards the saturation force against the displacement. Hence, as the applied force rises from $a - b$, the branch friction force given as $f_b(z)$ starts from zero and rises non-linearly with the externally applied force until either there is a reversal of the direction of motion (as is the case here) or saturation of the friction force. The friction force then traces $(a' - b')$.

Direction reversal:

When the external force changes direction at b resulting in direction change from $b - c$ before saturation, an inner loop results. For this new branch $b - c$ the variable z_r assumes the value of the displacement at the beginning of this new branch, that is the value of displacement at b , while the displacement variable z takes on the displacement value at point b also, hence the function $f_b(z)$ starts again from zero rising as the path $(b' - c')$ is traced. The value of f_r is given as the force of the $(a' - b')$ branch at point b' . The new target displacement z_t and the new target force f_t are recalculated by an algorithm. Internal or inner loops result when several direction reversals occur without the saturation of the friction force or when the displacement is less than the breakaway value which is the case here. As the force reverses direction again at c , $f_b(z)$ restarts again from zero, while the value of the variables z_r and f_r are updated to the respective values of the displacement and force at the reversal point. The values of the target displacement (z_t) and force (f_t) recalculated again reflecting current scenarios. The same happens for the path $c - d$ and $d - e$. Inner loop are never closed unless the current loop displacement z is larger or equal to the any previous loops. However when such conditions exist inner loops are closed from inside towards outside with inner ones closing before the outer ones. In such a scenario which results in this case as the applied force traces the path $(e' - f' - g')$, on reaching f' towards (g') , the displacement z for the current branch becomes larger than the previous immediate displacement in the same direction thus the loop $(d' - e' - f')$ will be closed since d' and f' are of the same displacement value. The current branch takes the trajectory of the previous branch in the same direction, branch $(c' - d')$ for this case and this action wipes out the inner loop. It achieves this by taking on the values of z_t and f_t of the previous branch and thus extending the branch as if it never reversed. This behaviour is known as non-local memory hysteresis.

Friction force saturation:

At any time when the displacement z reaches the breakaway value Z_b , the friction force becomes a maximum value and saturates (reaches breakaway value), it therefore becomes independent of the displacement, however dependent on the direction of the motion, this is represented as the stiction force F_s since z being the deflection of bristles is assumed to have reached a maximum value of Z_b . Beyond this breakaway displacement the system is in

gross-sliding.

The pre-sliding friction force at any point in the process is always given as the sum of $f_b(z)$ and f_r represented as $F_{hyst}(z) = f_b(z) + f_r$.

Motion dynamics

Pre-slide and gross-slide features:

In general consider the model representation of equations (3.4), (3.5);

During the pre-sliding regime

$$|F_{hyst}(z) + \sigma v| \leq |\gamma| \quad (3.6)$$

the deflection rate of the bristle is the same as the pre-slide velocity, that is

$$\dot{z} = v \quad (3.7)$$

and the friction force becomes

$$F_f = F_{hyst}(z) + \sigma \dot{z} + f_v v \quad (3.8)$$

putting (3.7) into (3.8)

$$F_f = F_{hyst}(z) + (\sigma + f_v)v \quad (3.9)$$

Given that the micro-damping parameter (σ) is often chosen much greater than viscous damping coefficient (f_v), implies the micro damping dominates the viscous damping in the pre-sliding regime. One can also approximate this pre-sliding force as

$$F_f = F_{hyst}(z) + \sigma v \quad (3.10)$$

since $\sigma \gg f_v$

During the gross-sliding regime

$$\dot{z} = \frac{\gamma - F_{hyst}(z)}{\sigma} \quad (3.11)$$

and

$$F_f = \gamma + f_v v \quad (3.12)$$

Thus (3.12) shows that the micro-damping parameter does not appear in this regime but the macro damping parameter f_v . So during gross-sliding the macro-damping dominates.

Steady state features:

The steady state features of the proposed non-drift dynamic friction model is investigated considering the constant zero velocity (pre-sliding case) and the constant non-zero velocity

(gross-sliding case):

The first case with $\dot{z} = 0, v = 0$

$$F_{hyst}(z) = \text{sat}(\gamma, F_{hyst}(z) + \sigma v) \quad (3.13)$$

so that

$$F_{hyst}(z) = F_{hyst}(z) \quad (3.14)$$

and

$$F_f = F_{hyst}(z) \quad (3.15)$$

This shows that during pre-sliding regime the slowly varying displacement is $\dot{z} \approx 0$ the friction force is described by the pre-sliding friction force.

For the second case with $\dot{z} = 0$, and $v \neq 0$

$$0 = \text{sat}(\gamma, F_{hyst}(z) + \sigma v) - F_{hyst}(z) \quad (3.16)$$

which implies

$$\gamma = F_{hyst}(z) \quad (3.17)$$

and

$$F_f = \gamma + f_v v \quad (3.18)$$

This also shows that during the constant velocity regime (gross-sliding) the friction force is simply a lagged version of the Stribeck function and the viscous force. Note the equivalence of equations 3.18 and 3.12 suggesting that the influence of the micro-damping is limited to the pre-sliding regime.

3.2.2 Similarities with some existing models

The new model presented has some similarities with some existing models. These model structures serve as motivation for the structure of the new model. Some of the similarities and differences with other models are now considered in the light of pre-sliding and gross-sliding friction regimes.

With the LuGre model:

In the pre-sliding regime the integrated LuGre friction model does not have explicit expression, however given that in this regime,

$$\dot{z} \approx v$$

since

$$\frac{\sigma_0 z |v|}{g(v)} \approx 0$$

This then gives a friction force equivalent to

$$F_f = \sigma_0 z + \sigma_1 v$$

For the new model during pre-sliding regime the friction model reduces to

$$F_f = F_{hyst}(z) + \sigma \dot{z}$$

with

$$\dot{z} = v$$

in this region thus in comparison both model structures have the same micro-damping expression, while the pre-slide friction force term of the LuGre model

$$\sigma_0 z$$

exhibits hysteresis without the non-local memory and the new model term $F_{hyst}(z)$ exhibits hysteresis with non-local memory features as shown earlier.

During gross-sliding regime, for constant velocities the LuGre model

$$F_f = g(v) \text{sgn}(v) + f_v v$$

and the new model given as

$$F_f = g(v) \text{sgn}(v) + f_v v$$

are clearly the same. However, for varying velocities the LuGre is given as equations 2.18 and 2.19, and the new model from equations 3.3, 3.5 is

$$F_f = \gamma + f_v v$$

this difference makes the new model not subject to the negative impact the micro damping term $\sigma \dot{z}$ often have in the low velocity friction regime.

With the GMS model:

The GMS model structure in the pre-sliding regime is given by equations 2.27 and 2.29 for $N = 1$ is

$$F_f = \sigma_0 z + \sigma_1 \dot{z} + f_v v$$

similar to the LuGre model, here one sees the GMS model to be a multi-element version of the LuGre model. The ability of this model to exhibit hysteresis with non-local memory is connected to its multi-element nature hence the more the number of elements, the better the hysteresis predicted. The steady state friction force also is same as the LuGre for $N = 1$ which is also similar to the new model. Varying velocity model of GMS could be subjected to instability due to the presence of the $\sigma_1 \dot{z}$ equation 2.28, unlike the new model.

With the Xiong model:

The integration of another state model in the new model defining the frictional lag is inspired by the Xiong model which demonstrated this possibility as seen in section 2.3. As such in the pre-sliding regime the Xiong model and the GMS model both being multi-state models are similar and by extension similar to the LuGre when $N = 1$. In the same way the proposed new model also differs from the Xiong model in this regime of friction. For constant velocities, the Xiong model, the friction force is given as

$$F_f = g(v)\text{sgn}(v) + f_v v$$

which also is similar to the LuGre and the new models. For velocity variations, the Xiong model is given as equations 2.30 and 2.32 for $N = 1$, is

$$F_f = \gamma + f_v v$$

with

$$\dot{\gamma} = \frac{g(v) - \gamma}{\tau}$$

this model is therefore equivalent to the new model for $N = 1$ in the sliding regime.

With the Leuven model:

The pre-sliding hysteretic function $F_{hyst}(z)$ of the new model is rooted in the Leuven model though the operations of the mechanism of the pre-sliding function differs for both models. The new model does not have a reset mechanism for the reversal points but uses some conditions to update the variables as previously described. Both models also exhibit similar characteristics for constant velocity with

$$F_f = g(v)\text{sgn}(v)$$

The presence of the micro-damping term for varying velocities differentiates the Leuven model from the new model in gross-sliding.

From the above, the new model with low number of parameters is able to model friction features both in the pre-sliding and gross-sliding regimes and it's parameter identification is

quite easy and uncomplicated contrary to the more sophisticated models of GMS, Xiong and Leuven.

3.3 Properties of the proposed new model

In this section we explore the mathematical properties of the proposed friction model. Properties such as boundedness, dissipativity, passivity and uniqueness of the model structure are studied. The study is not a mere academic exercise but gives credence to the behaviour of the model in real implementation scenarios. Properties such as boundedness are relevant for stability proofs of adaptive control laws, [57]. In the discussions that follow the focus is on the positive displacement, velocity excursions as the same argument can easily be extended to the negative displacement, velocity excursions. For the friction model defined by the following state equations 3.4 and 3.5

$$\dot{\gamma} = \frac{g(v) - \gamma}{\tau} \quad (3.19)$$

$$\dot{z} = \frac{1}{\sigma} (\text{sat}(\gamma, F_{hyst}(z) + \sigma v) - F_{hyst}(z)) \quad (3.20)$$

And the friction (output) equation

$$F_f = F_{hyst}(z) + \sigma \dot{z} + f_v v \quad (3.21)$$

where $F_{hyst}(z)$ is described by equations 3.1 and 3.2. How well behaved the model is could be ascertained by some of these properties and may prove useful in the design of adequate compensation schemes. Some of these properties like dissipativity and passivity become handy during the design of adequate controls for the new model.

3.3.1 Boundedness of states

Assuming a piece-wise continuous and bounded velocity range v , from the state equation 3.20, the average rate of change of the deflection is also bounded.

Proof

During the stick (pre-sliding) regime the state equation given by

$$\dot{z} = v \quad (3.22)$$

is bounded since the velocity v is bounded and continuous (piece-wise) during the pre-sliding regime, then the average deflection of the bristles is bounded and also piece-wise continuous given that \dot{z} is bounded.

For the slip (gross-sliding) regime, the average rate of change of deflection

$$\dot{z} = \frac{1}{\sigma} \gamma - F_{hyst}(z) \quad (3.23)$$

Consider a positive definite Lyapunov function given as

$$V = \frac{1}{2} z^2 \quad (3.24)$$

whose derivative in the z direction is

$$\dot{V} = z\dot{z} \quad (3.25)$$

thus

$$\dot{V} = \frac{z}{\sigma} (\gamma - F_{hyst}(z)) \quad (3.26)$$

But $|F_{hyst}(z)| \leq |F_s|$ and $\gamma : F_c \leq \gamma \leq F_s$ is bounded and continuous for all $v \geq 0$ Then $|F_{hyst}(z)| \geq |\gamma|$ for all $v \geq 0$.

The average deflection of the bristles is bounded given that (3.26) is negative semi-definite so that the set $\omega = \{z : |z| \leq F_s\}$ is an invariant set implying that all z values starting within F_s always remains within $F_s \forall t \geq 0$. Thus equations (3.20) and (3.21) satisfy the condition that if v is bounded, then z and \dot{z} are always bounded. The implication of this is that the boundedness of both z and \dot{z} , also ensures that the friction force is bounded for any bounded velocity input, following similar arguments in [109].

The boundedness of the second state γ can also be established given a non-negative function $V = \frac{\gamma^2}{2}$ whose derivative in the trajectory of the state is

$$\dot{V} = \frac{g(v) - \gamma}{\tau} \gamma$$

Given $F_s \geq g(v) \geq F_c$ then $|\gamma| \leq F_s$ is always satisfied so long as the initial value of γ satisfies the condition $|\gamma| \leq F_s$. Therefore, from (3.5) the friction force is bounded in the gross-sliding regime.

3.3.2 Existence/ uniqueness

For a non-linear system

$$\dot{x}(t) = f(x(t), u(t)) \quad (3.27)$$

with $x \in X \in \mathbb{R}$ and $u \in \mathbb{R}$ being the state and input variables respectively. Considering the free dynamics of the system where the input variable is thus assumed to be zero then

$$f^*(x) = f(x, 0) \quad (3.28)$$

If $f^*(x)$, an n dimensional vector whose components satisfy the following Lipschitz condition of $\|f^*(x_1) - f^*(x_2)\| \leq L\|x_1 - x_2\| \forall (x_1, x_2)$ in the neighbourhood of x_0 . with $x_1, x_2 \in X \in \mathbb{R}$ where L is the positive (Lipschitz) constant, then $\dot{x} = f^*(x)$ has a unique solution with an initial condition $x(0) = x_0$.

Given the velocity v is continuous and differentiable, and in the pre-sliding regime $\dot{z} = v$ then the state equation in the pre-sliding regime is locally Lipschitz since every continuously differentiable function is locally Lipschitz. This condition thus guarantees the existence of a unique solution of the state equation. Also for the gross sliding regime $\sigma\dot{z} = \gamma - F_{hyst}(z)$ since γ is upper bounded and continuously differentiable within the bounds, and $F_{hyst}(z)$ is lower bounded by F_s ensure that the gross sliding regime representation of the state equation satisfies the Lipschitz condition thus ensuring the existence of unique solution to the state equation in this regime.

3.3.3 Dissipativity

Assume that the input velocity signal v is bounded and positive and that the friction force is in the pre-sliding regime as equation 3.21, with the state equation 3.22, then such a system is said to be dissipative if it obeys the dissipativity inequality given as

$$\int_0^t F(\tau)v(\tau)d\tau > C \quad (3.29)$$

with $v(t)$ being the input velocity signal, $F(\tau)$ the output of the system and C a non-negative constant (though this can be relaxed to include negative, corresponding to the limit of energy that can be stored in the non-linear spring during this regime). The variable τ is such that $\tau \in [0, t]$. Thus within this time bound $0 \leq \tau \leq t$ the system is said to be dissipative. The product of the input and the output $F(t)v(t)$ is known as the energy flow (supply) rate i.e. power.

In the pre-sliding regime of friction

$$\dot{z} = v$$

and the friction force is given by

$$F(t) = F_{hyst} + \sigma \dot{z}(t)$$

Thus

$$F(t)v(t) = F_{hyst}(z)v + \sigma \dot{z}v \quad (3.30)$$

$$\forall t \geq 0$$

Noting that if the individual terms that make up the function of (3.30) is dissipative then the entire expression is dissipative. Therefore we proceed to establish dissipativity for each term

1. The hysteretic term: $F_{hyst}(z)v$: The function derivative of $F_{hyst}(z)$ with respect to the state variable z is seen to be a decreasing function for positive values of the state and increasing for decreasing values of the state. Thus for increasing positive values of velocity this derivative is decreasing and vice versa. The implication of this is energy dissipation.
2. The micro-damping term $\sigma \dot{z}v$: In the pre-sliding regime, the terms \dot{z} and v are always of the same sign and thus implies energy is dissipated by this term during pre-sliding.

Therefore, the dissipativity inequality is satisfied and the model exhibits this property in pre-sliding. The above intuitive reasoning can be formalised by means of the following theorem.

THEOREM 3.1: A system is said to be dissipative if it is possible to obtain a non-negative function (Lyapunov) of the state variables such that the dissipativity inequality holds

$$\dot{V} \leq y^T u - g(t) \quad (3.31)$$

where V is a non-negative Lyapunov function, y the system output, u system input and $g(t)$ is the power generated or dissipated by the system.

Proof

If we chose $V = \int_0^z F_{hyst}(\tau) d\tau$ then $\dot{V} = F_{hyst}(z)\dot{z}$, and $y = F(t)$ as the output and $u = v$ as the input, then from (3.31)

$$y^T u \geq \dot{V} + g(t) \quad (3.32)$$

substituting the various values we have

$$F(t)v(t) = F_{hyst}(z)\dot{z} + \sigma(\dot{z})^2 + f_v v^2 \quad (3.33)$$

the term $f_v v^2$ is obviously a dissipative function, removing it from the equation therefore

$$F(t)v(t) \geq \dot{V} \quad (3.34)$$

is satisfied since $\sigma(\dot{z})^2 \geq 0$.

In the gross sliding regime of friction with

$$\dot{z}(t) = \frac{1}{\sigma}(\gamma - F_{hyst})$$

and the friction force given as $F_f(t) = F_{hyst}(z) + \sigma\dot{z}(t)$

yielding

$$F_f(t) = \gamma \quad (3.35)$$

then the flow rate in the gross-sliding regime is given as

$$F(t)v(t) = \gamma v(t) \quad (3.36)$$

but $\gamma v(t)$ is non-negative indicative of the fact that $f(t) \geq C$ since γ is upper and lower bounded by F_s^+ and F_c^+ for positive v , this thus shows that the friction force is dissipative in the whole region of gross-sliding.

One should observe that the micro-damping term $\sigma\dot{z}(t)$ interestingly does not appear in the gross sliding regime noting that in this regime it is non-dissipative and could lead to possible destabilisation due to energy generation, [32].

3.3.4 Passivity

Systems which generate energy are regarded as active systems while those which do not generate but rather dissipate energy are called passive systems. Friction phenomenon is often seen as energy dissipating often through heat. Thus a passive system can be defined in the following manner.

Definition 3:1 A system is passive if it is dissipative with respect to the supply rate of the type $u^T y$, it is strictly input passive if there is such a positive constant $\delta > 0$, so that the system is dissipative with respect to $u^T y - \delta \|u\|^2$ it is strictly output passive if there is a non-negative value $\epsilon > 0$ so that the system is dissipative with respect to $u^T y - \delta \|y\|^2$, [110].

Given that $u^T y = uy$ for single input single output (SISO) systems which our system belong to. In the light of the previous section we were able to show that the relation $u^T y - \delta \|u\|^2$ holds true for the model under study, then the state variable z is also passive.

An illustrative example of the passivity property of the model is considered

Given a second order mass-spring system shown below with F_f being the friction force, the

relation exists:

$$m\ddot{x} + kx + F_f = u \quad (3.37)$$

with m being the mass, k spring constant, and u the control input. Rearranging the equation of motion yields

$$m\ddot{x} + kx = u - F_f \quad (3.38)$$

Defining a storage (positive definite) function as

$$V(x, \dot{x}) = \frac{1}{2}(m\dot{x}^2 + kx^2) \quad (3.39)$$

whose derivative in the trajectory of x is

$$\dot{V}(x, \dot{x}) = \dot{x}(m\ddot{x} + kx) \quad (3.40)$$

Given that $x(0) = x_0 = 0$, and $\dot{x}(0) = \dot{x}_0$, and the output $y = \dot{x}$ then

$$V[x(t), \dot{x}(t)] = V[x(0), \dot{x}(0)] + \int_0^t u(\tau)\dot{x}(\tau)d\tau - \int_0^t F_f(\tau)\dot{x}(\tau)d\tau \quad (3.41)$$

The free dynamics (assuming $u = 0$) of the system shows that

$$V[x(t), \dot{x}(t)] = V[x(0), \dot{x}(0)] - \int_0^t F_f(\tau)\dot{x}(\tau)d\tau \quad (3.42)$$

Thus energy stored in the spring is dissipated by the friction term between $t_0 = 0$ and t . $F_f\dot{x}$ given as (3.3), (3.4), and (3.5) for both the pre-sliding and gross-sliding regimes is strictly positive thus ensuring that the system is dissipative at all times. This dissipativity with respect to the supply rate $u^T y$ thus indicates the passivity property of the model.

3.4 Describing function analysis

One of the main features of systems with non-linearities is the possible existence of limit cycles oscillation. In this section an approach for the prediction of the hysteretic features of the proposed new model was formulated. This approach was then used for the prediction of the existence of limit cycles for a particular system and the results compared with that obtained from simulations. Given that a closed form analytical solution of a non-linear differential equation is not easily obtained, an approximate method is often adopted as a useful alternative. One of the popular approximate methods is the describing functions approach. In this approach a linear approximation of the non-linearity is sought using an

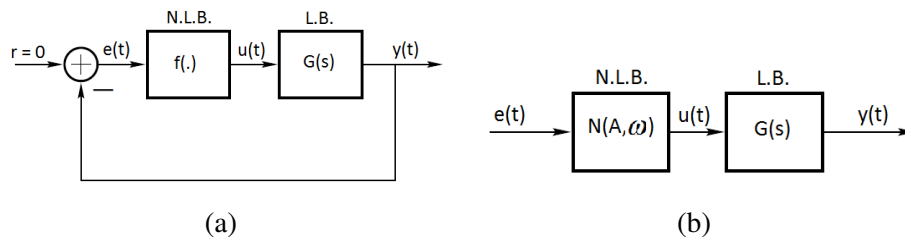


Fig. 3.2 Describing function analysis approach to non-linear systems; **(a)** Feedback control of a system with hard non-linearity, **(b)** A Describing Function equivalent scheme

extended version of the frequency response technique. Thus this linear time invariant system so obtained captures the heart of the non-linearity it represents and can be used for the prediction of non-linear behaviours. The conventional describing function originated by Kochenburger expands the output of the non-linearity in a Fourier series and uses the first Fourier harmonic as the equivalent sinusoidal output. One main application of the describing functions technique is in the prediction and determination of the existence of limit cycles, [111].

3.4.1 The describing function concept

Consider a system whose non-linear and linear parts can be separated as shown in the figure 3.2a. If it is possible to represent the linearity by a low pass filter and the non-linearity lumped as shown, then it might be possible to use the describing functions method to analyse such a system. The spirit of the describing function technique is in replacing the non-linear element by an equivalent quasi-linear element as shown in the figure 3.2b, such that the output of the non-linear block and that of describing function (represented by its transfer function) are approximately the same. For sustained oscillations, and the output feedback to the system (assuming no external input) to the non-linear block, the output of the non-linear block assumed to be periodic can thus be represented using Fourier series. Feeding this non-linear block output as input to the linear block (serving as a low pass filter) ensures that only the fundamental frequency components of the Fourier series remain. Hence one can represent the output of the non-linear block approximately by the equivalent Fourier series representation of the first order. This is justified given that the output of the linear block being low pass would invariably cut off higher order frequency signals. So if the input signal is given as

$$e(t) = A \sin \omega t \quad (3.43)$$

and the output of the non-linear block is

$$u(t) = \frac{a_0}{2} + \sum_{n=1}^{\infty} (a_n \cos(n\omega t) + b_n \sin(n\omega t)) \quad (3.44)$$

with

$$a_n = \frac{2}{T} \int_0^T (u(t) \cos(n\omega t)) d\omega t$$

$$b_n = \frac{2}{T} \int_0^T (u(t) \sin(n\omega t)) d\omega t$$

ω is the angular velocity, and n the n th term of the series. Assuming that the function is independent of frequency term ω then the output is given as, (treating ω as a constant). From figure 3.2

$$u(t) = a_1 \cos(\omega t) + b_1 \sin(\omega t) \quad (3.45)$$

the output of the linear block LB is

$$y(t) = G(s)u(t) \quad (3.46)$$

and the output of the non-linear block expressed using describing function is

$$u(t) = N(A, \omega)e(t) \quad (3.47)$$

where $N(A, \omega)e(t)$ is the describing function term. However the objective is the output of the non-linear block to a sinusoidal input of the form (3.43) to be of the form (3.44). For $n = 1$, therefore

$$u(t) = a_1 \cos(\omega t) + b_1 \sin(\omega t) = M \sin(\omega t + \theta)$$

which can also be expressed as

$$u(t) = M \sin(\omega t + \theta)$$

with

$$M(A, \omega) = \sqrt{a_1^2 + b_1^2}$$

and

$$\theta(A, \omega) = \arctan(a_1/b_1)$$

Thus using complex number notation

$$u(t) = (b_1 + ja_1)e^{j(\omega t + \theta)} \quad (3.48)$$

Defining the describing function $N(A, \omega)$ as the ratio of the fundamental output of the non-linear block and the input signal, we obtain

$$N(A, \omega) = \frac{u(t)}{e(t)} = \frac{a_1 \cos \omega t + b_1 \sin \omega t}{A \sin \omega t} \quad (3.49)$$

Expressing this in complex notation yields

$$N(A, \omega) = \frac{(b_1 + ja_1)e^{j(\omega t + \theta)}}{Ae^{j\omega t}} = \frac{b_1 + ja_1}{A} \quad (3.50)$$

The Describing function for the Hysteretic function is independent of the frequency and so the describing function of the hysteretic friction model under study is thus $N(A)$.

Therefore, the transfer function of the system $T(s)$, figure 3.2b replacing the non-linearity with the describing function equivalent $N(A)$ as in figure 3.2a is

$$T(s) = \frac{Y(s)}{E(s)} = \frac{G(s)N(A)}{1 + G(s)N(A)} \quad (3.51)$$

s is the Laplacian variable

Replacing s by $j\omega$ the frequency domain, the characteristic equation becomes

$$1 + G(s)N(A) = 0$$

and

$$G(j\omega) = \frac{-1}{N(A)} \quad (3.52)$$

Equation 3.52 is thus used for the prediction of the existence or otherwise of limit cycles in the given system as follows: The intersection of the plots of the Nyquist $G(j\omega)$ and the $\frac{-1}{N(A)}$ indicates the existence of a limit cycle and yield possible approximate values of amplitude and frequency of the limit cycle predicted. If there is no such intersection then there is no limit cycle predicted.

3.4.2 Limit cycle prediction for the proposed non-drift dynamic friction model hysteresis

One of the main applications of the describing function technique is in the prediction of the existence of limit cycles in non-linear systems. Limit cycles are simply sustained oscillations which persist even after system input is removed and are peculiar to non-linear systems behaviour. They can thus be represented by sinusoidal signals. In studying the limit cycle

prediction capability of the proposed friction model the interest is in the hysteresis friction function representing the pre-sliding regimes of friction. The friction force in this regime is dependent only on the displacement and not the relative velocity of the moving surfaces. The hysteresis friction force exhibits non local memory characteristics. It is also a multivalued function and as such its DF will be expressed as a complex function of the amplitude only given that the hysteresis feature is rate (frequency) independent. The pre-sliding friction force for the proposed non-drift dynamic friction model from equations 3.1 and 3.2 is

$$F_f = F_{hyst}(z)$$

and

$$F_{hyst}(z) = \sin\left(\frac{e - z_r}{|z_t - z_r|} \frac{\pi}{2}\right) |f_t - f_r| + f_r$$

with $z = e$ the input displacement and the rest as previously defined. For simplicity

$$|f_t - f_r| = 2F_s$$

and

$$|z_t - z_r| = 2Z_b$$

with F_s and Z_b being respectively the stiction force and the breakaway displacement

Therefore

$$F_{hyst}(z) = 2F_s \sin\left(\frac{e - z_r}{2Z_b} \frac{\pi}{2}\right) + f_r \quad (3.53)$$

Given a sinusoidal input signal

$$e(t) = A \sin(\omega t)$$

to the non-linear function of equation 3.53, the output is

$$F_{hyst}(z) = 2F_s \sin\left(\frac{A \sin(\omega t) - z_r}{2Z_b} \frac{\pi}{2}\right) + f_r \quad (3.54)$$

where $z_r = \pm A$, and f_r the values of $F_{hyst}(z)$ at $\pm A$ the reversal point, A is the amplitude of the input signal.

thus

$$f_r = F_s \sin\left(\frac{\pm A}{Z_b} \frac{\pi}{2}\right) \quad (3.55)$$

and equation 3.54 becomes

$$F_{hyst}(e) = 2F_s \sin\left(\frac{A \sin(\omega t) \pm A}{2Z_b} \frac{\pi}{2}\right) + F_s \sin\left(\frac{\pm A}{Z_b} \frac{\pi}{2}\right) \quad (3.56)$$

Clearly 3 situations may arise due to the value of the input signal $e(t)$ over a complete cycle in relation to the breakaway displacement Z_b

1. When the input signal $e(t)$ becomes greater than the breakaway displacement Z_b
2. When the input signal $e(t)$ is less than or equal to the breakaway displacement Z_b , and
3. When the input signal $e(t)$ is less than the negative breakaway displacement $-Z_b$

This thus gives rise to the following

$$F_{hyst}(e) = \begin{cases} F_s & \text{if } e(t) > Z_b \\ F_{hyst} & \text{if } -Z_b \leq e(t) \leq Z_b \\ -F_s & \text{if } e(t) < -Z_b \end{cases} \quad (3.57)$$

Equation 3.56 is then analysed for the variations in the input signal $e(t)$. To simplify this, we investigate 2 instances of the amplitude A in relation to the breakaway displacement Z_b

Instance 1: $|A| > Z_b$ refer to figure 3.3

The input signal is

$$e(t) = A \sin(\omega t)$$

defining an angle ϕ_T such that

$$A \sin(\phi_T) = Z_b$$

and

$$\phi_T = \sin^{-1}\left(\frac{Z_b}{A}\right)$$

with

$$f_r = \pm F_s$$

as the force at reversal, then

$$a_1 = \frac{2}{T} \int_0^T u(\tau) \cos(\omega \tau) d\tau \quad (3.58)$$

with $u(\tau)$ replaced by $F_{hyst}(e)$ as represented in equation 3.57 for a complete period. Taking advantage of the symmetry over the two halves of the period and simplifying we obtain

$$a_1 = j \frac{4F_s}{A\pi} \left(\sqrt{1 - \frac{Z_b^2}{A^2}} - \frac{4\sqrt{2}Z_b \sin\left(\frac{A\pi\sqrt{1 - \frac{Z_b^2}{A^2}}}{4Z_b}\right)}{A\pi} \right) \quad (3.59)$$

In the same token

$$b_1 = \frac{2}{T} \int_0^T u(\tau) \sin(\omega\tau) d\tau \quad (3.60)$$

and

$$b_1 = \frac{4F_s Z_b}{A\pi} \quad (3.61)$$

Thus the describing function is

$$N(A) = \frac{b_1 + ja_1}{A} \quad (3.62)$$

yielding

$$N(A) = \frac{4F_s Z_b}{A^2 \pi} - j \frac{4F_s}{A\pi} \left(\sqrt{1 - \frac{Z_b^2}{A^2}} - \frac{4\sqrt{2}Z_b \sin\left(\frac{A\pi\sqrt{1 - \frac{Z_b^2}{A^2}}}{4Z_b}\right)}{A\pi} \right) \quad (3.63)$$

As expected the describing function is a complex variable which is independent of the frequency of oscillation, and in agreement with fact that hysteretic functions with memory usually have a complex describing function.

The reciprocal the describing function is therefore obtained by

$$\frac{1}{N(A)} = \frac{\alpha + j\beta X}{\alpha^2 + (\beta X)^2} \quad (3.64)$$

where

$$\alpha = \frac{4F_s Z_b}{A^2 \pi}$$

$$\beta = \frac{4F_s}{A^2 \pi^2}$$

$$X = \left(\pi \sqrt{1 - \frac{Z_b^2}{A^2}} - \sqrt{32} Z_b \sin \left(\frac{\pi \sqrt{A^2 - Z_b^2}}{4Z_b} \right) \right)$$

Obtaining the intersection of $-1/N(A)$ as A varies from zero towards infinity, and the Nyquist curve of $G(j\omega)$ as the frequency changes from zero, if it exists predicts the amplitude and frequency of the limit cycle in approximate terms.

Instance 2: $|A| \leq Z_b$ refer to figure 3.4

For the situation where the amplitude A of the input signal $e = A \sin(\omega t)$ is less than the breakaway displacement Z_b , this implies that the entire system motion dynamics is contained in the pre-slide regime of friction and saturation never occurs. This shows that for the entire cycle the signal is bounded between the positive and negative breakaway ($\pm Z_b$) as is true with the figure 3.4.

An application example for limit cycle prediction:

To illustrate the applicability of the above DF for the proposed non-drift dynamic friction model consider a certain system with the following motion equation;

$$m\ddot{x} + F_f = u \quad (3.65)$$

If a PID position controller with a control law u given as

$$u(t) = -K_v \dot{x}(t) + K_p x(t) + K_i \int_0^t (x(\tau) - x_{ref}(\tau)) \quad (3.66)$$

where K_v is the derivative gain, K_p the proportional gain and K_i integral gain of the controller while x_{ref} is the reference input to the system. The closed loop performance of the control system when a reference position of 1 m/s is passed to the system, with a unit mass was appropriate within design specifications when there is no frictional influence. However, in the presence of friction, the performance deteriorates and limit cycle oscillations are observed as shown in figure 3.6. Assuming that $K_p = 3$, $K_v = 6$, $K_i = 4$, and $m = 1$. Using the proposed friction model as the friction force F_f present in the system, the result of position control using the linear controller u above yields a position reference that oscillates around the reference position. Parameter values of the model used are $Z_b = 0.001$, $F_s = 1$, $F_c = 0.6$, $v_s = 0.01$, $\sigma = 100$, $\tau = 0.002$. The predicted amplitude using the describing functions method is $A = 0.0787$, and the limit cycle frequency of oscillation $\omega = 2.35$ rad/sec, see figure 3.5 while the amplitude A from the simulation is $A = 0.0930$ and the corresponding frequency $\omega = 0.3927$ rad/sec, see figure 3.6. By this the capability of the proposed new friction model to predict limit cycle oscillations is demonstrated. From figure 3.5, it is observed that the predicted limit cycle is stable given that as A the amplitude increases, the value of $-\frac{1}{N(A)}$

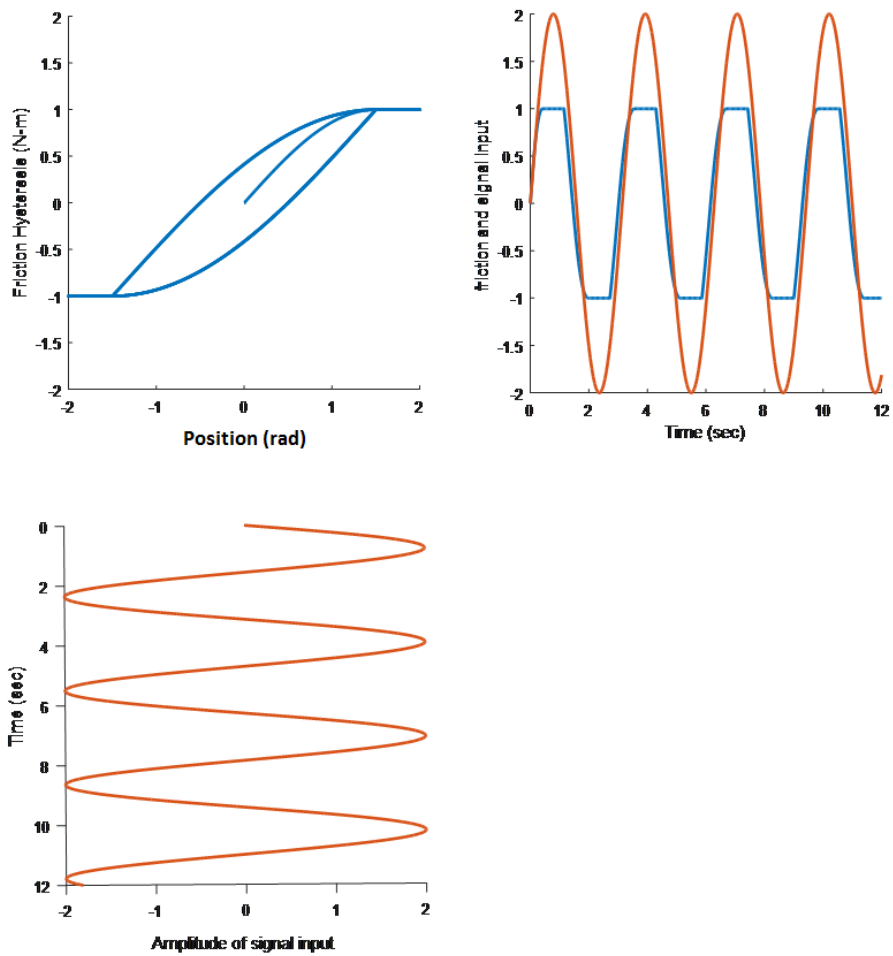


Fig. 3.3 Hysteresis friction for the condition that the signal input amplitude A is greater than the breakaway displacement Z_b ; **top-left**; friction hysteresis, **bottom-left**; signal input and **top-right**; friction hysteresis and the signal input against time

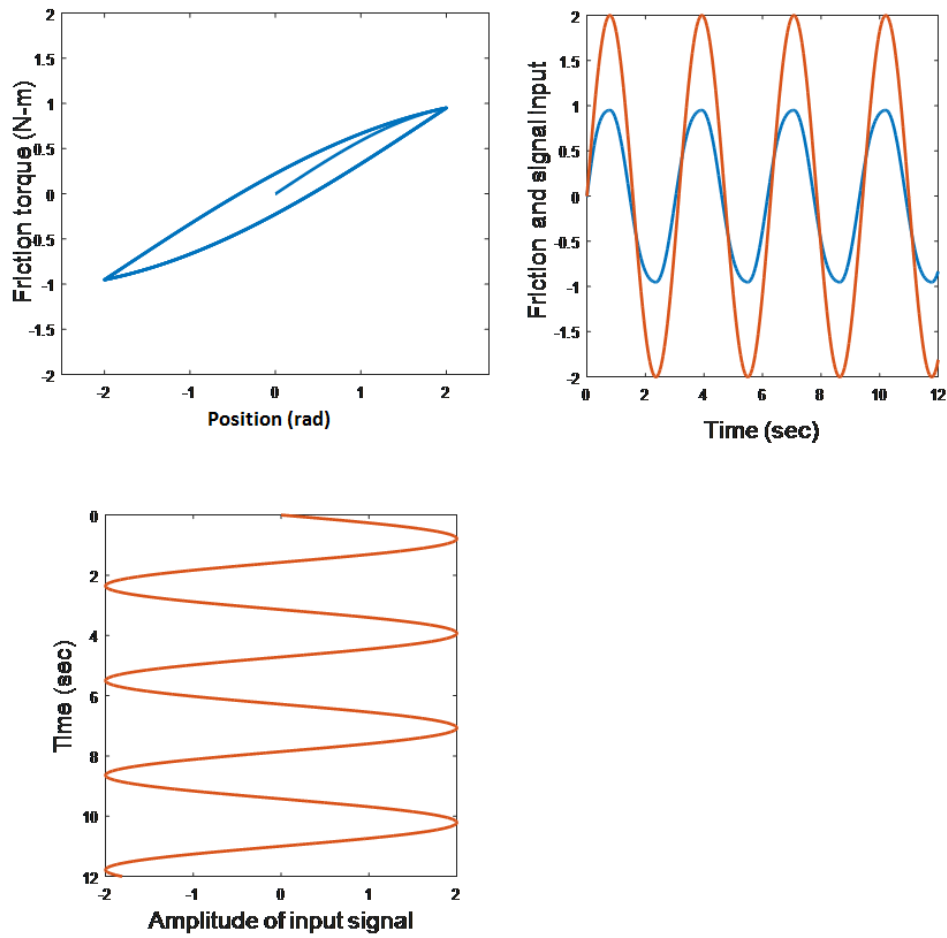


Fig. 3.4 Hysteresis friction for the condition that the signal input amplitude A is less than the breakaway displacement Z_b ; **top-left**; friction hysteresis, **bottom-left**; signal input and **top-right**; friction hysteresis and the signal input against time

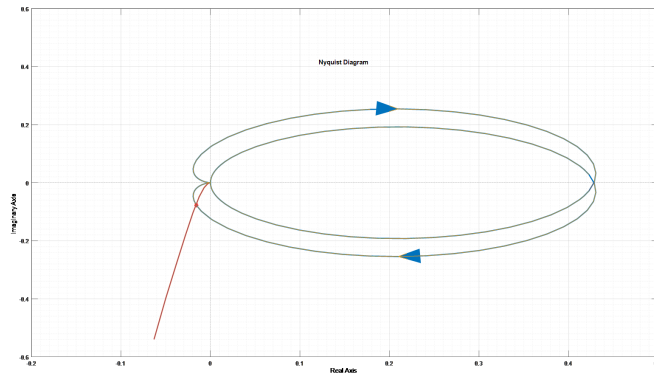


Fig. 3.5 Limit cycle oscillation prediction using the describing function approach showing the intersection of the Nyquist plot $G(j\omega)$ and the $-\frac{1}{N(A)}$ plot

increases further away from the portion encircled by the $G(j\omega)$ curve in figure 3.6. The variations in the values of the predicted and actual values of the limit cycle oscillations is attributable to the fact that the describing functions method is an approximation technique and shows the effect of limiting the output only to the first (fundamental) harmonics.

Describing functions limitations

The describing function approach for the prediction of limit cycles is limited due to the assumptions upon which the method was developed. Some of these assumptions are:

1. Single non-linear element in the system; implying that even if there are more than one non-linear element in the system the most pronounced non-linearity is considered while the others are neglected, or better still where possible the non-linearities are lumped into a single equivalent.
2. The non-linearity is odd; ensuring symmetric characteristics between the output-input relationships of the non-linear block about the origin.
3. The system is unforced (autonomous) and time invariant; meaning there are no external inputs to the system and system parameters do not vary with time during operation.
4. The linear part of the system provides sufficient low-pass filtering characteristics such that only the fundamental components (first harmonics) of the Fourier based output (of the non-linear block) for any sinusoidal input (to the non-linear block) is taken into account. This is the filtering hypothesis since the filter-like linear block will ensure that higher order components are eliminated.

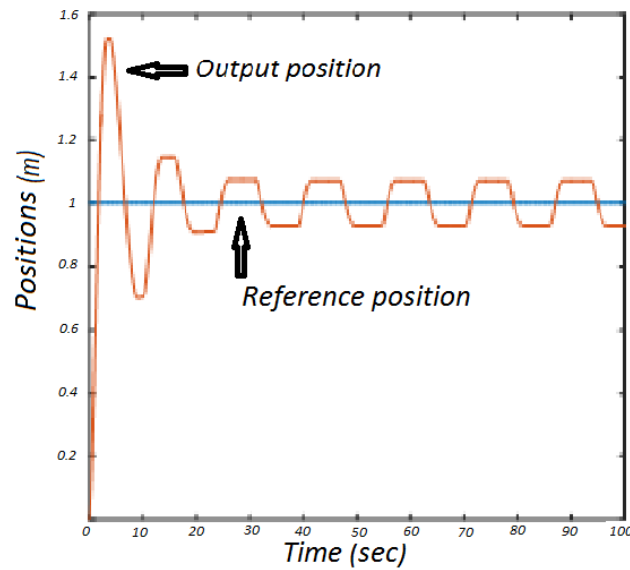


Fig. 3.6 Limit cycle oscillation prediction using a simulation approach

Because of these limitations, DF methods may yield unrealistic results in that it could predict limit cycles where there are none or, it may also not be able to predict limit cycle existence when in reality the system is subject to limit cycle oscillations.

3.5 Sensitivity analysis

Here the objective is to study the individual effects the variation of some parameters might have on the models and their robustness to such parameter variations. It should be noted that many of the friction models share some common parameters, their influence on the models are sometimes very different as observed in the following analysis, [112]. A mass-spring system of figure 3.7 was used and the friction as a function of the pre-sliding displacement and friction as a function of velocity graphs are obtained and analysed for the different values of the parameters and their variations. However to do this the stick-slip features of the various models under study was first demonstrated and a comparative deduction of the model performance against some of the most popular friction models made. To this, consider the simple mass-spring system figure 3.7, whose mathematical equation is

$$m\ddot{x} = F_e + F_f \quad (3.67)$$

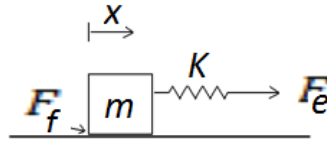


Fig. 3.7 A simple mass-spring system for friction simulations

where m is mass, x position, F_e the external force applied to the system and F_f the friction force, this system is subjected to a constant velocity $v(\dot{x})$. Given that the mass $m = 1$ kg, $F_c = 1$ N, $F_s = 1.5$ N, $v = 0.1$ m/s and the spring stiffness $K = 2$ N/m. The simulations are performed at low velocity variations. The following friction models were used for the tests: Coulomb+Stiction, LuGre, Xiong, E-P, GMS and the proposed new model

For frictional features in the low velocities the following were investigated; stick-slip motion and the Stribeck effects.

In generating the simulation results in this section and the rest of the chapter, a non stiff solver for ODEs (ordinary differential equations) namely ode4 (Runge-Kutta 4th order) solver with a tolerance of 10^{-5} was used.

3.5.1 Stick-slip motion

As illustrated in previous chapter stick-slip effect is one of the negative effects due to the friction non-linearity affecting the low velocity regimes. This causes systems experiencing stick-slip to have periods of motion (slip) followed by periods where the relative motion becomes zero (stick).

The Coulomb+Stiction model

With the model as given by eqn. 2.10, without the viscous friction force; the following parameters were used for the simulation of the system $F_c=1$ N, $F_s=1.5$ N and the results are shown in the figures 3.8 and 3.9. From figure 3.8a it can be observed that the model is not capable of predicting friction around the sticking or near zero velocity regimes and at velocity reversals. The velocity plot of figure 3.9a suggests stick regime to last for a while and the system becomes more or less oscillatory. So essentially stick-slip phenomenon is not well predicted by the model.

The LuGre model

With the model as given by eqns. 2.18, 2.19 and 2.20; the parameters for the simulation were chosen as; $F_c=1$ N, $F_s=1.5$ N, $\sigma_0=100000$, $\sigma_1 = \sqrt{100000}$, $v_s=0.01$ m/s, $\delta=2$. From the figure 3.8b, the LuGre model was able to predict stick-slip motion of friction, that is it predicts friction dynamics in the near zero and regions of velocity reversals unlike the

Coulomb+Stiction model. The velocity graph of figure 3.9b captured clearly the stick and slip regimes of friction.

The Elasto-Plastic model

Since it is essentially a modified version of the LuGre model as shown by equations 2.21, 2.22, and 2.23, with the same parameters plus an extra parameter z_b . The figures show same resemblance with the LuGre model, capturing the friction dynamics at near zero velocities and velocity reversals figures 3.8c and 3.9c. Also the velocity graph resembles that of the LuGre model. The parameters for the simulation are $F_c=1$ N, $F_s=1.5$ N, $\sigma_0=100000$, $\sigma_1 = \sqrt{100000}$, $v_s=0.01$ m/s, $\delta=2$, $Z_b=0.7z_{max}$.

The Proposed model

With the proposed new model as given by eqns. 3.3, 3.4, 3.5, the new model has one parameter more than the LuGre and the parameters used for the simulation chosen as; $F_c = 1$, $F_s=1.5$, $\sigma_1 = \sqrt{100000}$, $v_s=0.01$, $Z_b=0.001$, $\tau=0.002$. The friction force modelled by the proposed non-drift dynamic friction model captures the friction at low, zero and velocity reversals as in figure 3.8d. The velocity plot in figure 3.9d indicates obvious stick-slip regimes of motion correctly.

The GMS model

With the model as given by eqns. 2.27, 2.28, and 2.29; the parameters for the model with number of elements $N=10$ are; $F_s=1.5$, $F_c=1$, $v_s=0.01$ $\sigma_{0i}= 10, 18, 26, 34, 42, 50, 58, 66, 74, 82$, $\sigma_{1i}= 10, 15, 20, 25, 30, 35, 40, 45, 50, 55$, $\alpha_i= 0.0955, 0.0965, 0.0975, 0.0985, 0.0995, 0.1005, 0.1015, 0.1025, 0.1035, 0.1045$, $C_i= 0.00955, 0.00965, 0.00975, 0.00985, 0.00995, 0.01005, 0.01015, 0.01025, 0.01035, 0.01045$.

The features of friction as captured by this model are shown in figures 3.8e and 3.9e. From figure 3.8e one observed that the stick-slip friction feature captured by the GMS model is more in agreement with that of the Xiong model and both differ qualitatively from the other models in some ways. The velocity graphs show clearly regimes of stick and slip, see figure 3.9e.

The Xiong model

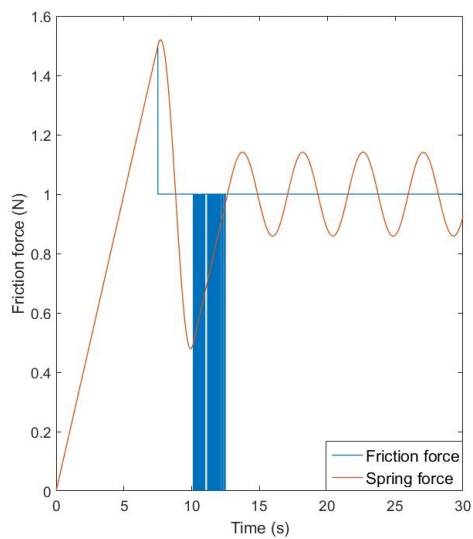
With the model as given by eqns. 2.30, 2.31, and 2.32; For the parameters of the model with 10 elements are $F_s=1.5$, $F_c=1$, $v_s=0.01$, $K_i=1000, 1800, 2600, 3400, 4200, 5000, 5800, 6600, 7400, 8002$, $\sigma_i= 5, 7.5, 10, 12.5, 15, 17.5, 20, 22.5, 25, 27.5$, $\tau=0.002$, $\lambda_i= 0.0955, 0.0965, 0.0975, 0.0985, 0.0995, 0.1005, 0.1015, 0.1025, 0.1035, 0.1045$.

This model captures essential friction features at low and zero velocity excursions like the previous models mentioned. From this plot of figure 3.8f, it is also observed that the friction model response shows some oscillation in the stick regime like the GMS model. The velocity

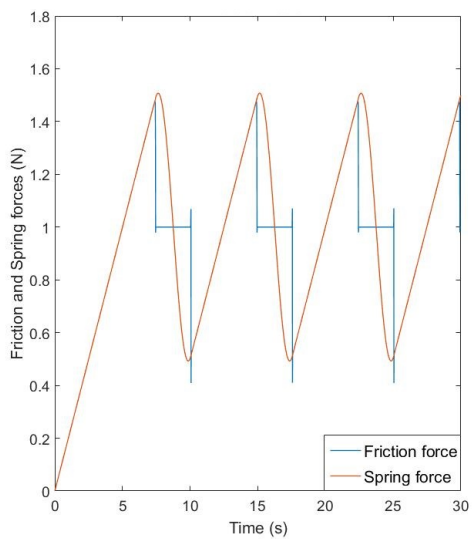
plot figure 3.9f shows clearly the stick-slip regimes of friction.

3.5.2 Discussion of stick-slip simulation results

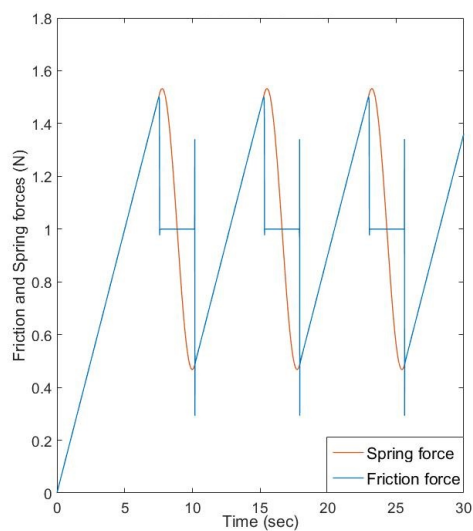
For the stick-slip motion as shown in the friction and spring forces figure 3.8 and the velocity figure 3.9 some observations are made. From figure 3.8a and figure 3.9a, the inability of the Coulomb+Stiction model to capture this important friction feature is evident and rather the system after stiction showed a region of instability depicted by spikes in the friction force value until the system came out of this region as indicated by the spring force rising above the coulomb force. Beyond this region the system moved with a constant friction force equivalent to the coulomb friction force. The velocity plot suggest the absence of true stiction so no true stick-slip exists. The LuGre model behaviour figure 3.8b and figure 3.9b, and the E-P model figure 3.8c and figure 3.9c exhibit great similarity with small deviations in the degree to which the friction force rises above the coulomb level as the system moved from stick to slip, this could be the result of the added parameter to ensure the LuGre model does not drift. It was seen that the spring and friction forces are proportional in the stick regime while the friction force experience a sharp transition from the stiction to kinetic motion the spring transition was rather gradual. The velocity plots indicates the existence of true stick-slip motion. Analysis of the spring and friction force figure 3.8d and the velocity plot figure 3.9d for the proposed new model showed that the friction force and spring force closely resemble each other in the stick regime, like the LuGre model, however the transition from slip motion to stick is smoother than the LuGre and E-P models. The velocity plot also suggests the prediction of true stick-slip motion. The GMS and Xiong models showed close resemblance in predicting the stick-slip motion as shown in their respective spring and friction forces figures 3.8d, 3.8e and the velocity plots figure 3.9d and 3.9e and qualitatively differ from the previous models predictions. These friction force figures indicate variations in the stiction for the different slip regimes. The predicted friction force by these multi-element models (GMS and Xiong) exhibit oscillatory transitions from slip-to-stick unlike the single element models like the LuGre, elasto-plastic models. Some researchers, [113], [70], [24], have argued that this oscillatory feature is closer to the friction reality in these regions. It is observed that the proposed non-drift dynamic friction model being a single element model is able to exhibit very smooth transitions from stick to slip regimes better than the other models with little to no oscillations.



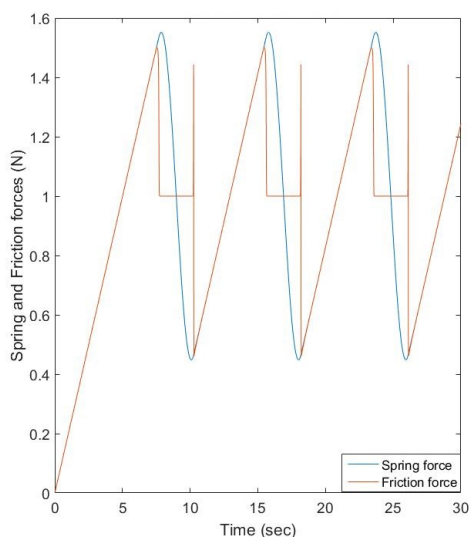
(a)



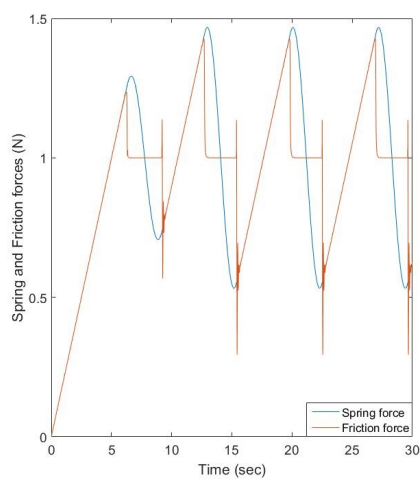
(b)



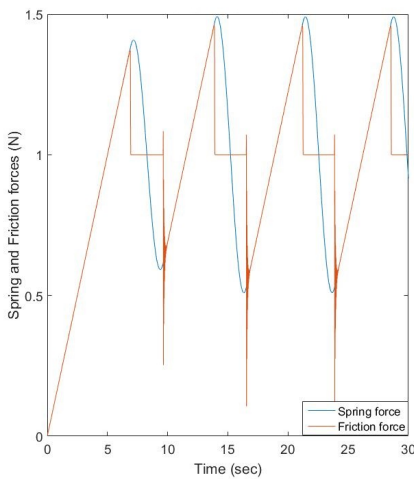
(c)



(d)



(e)



(f)

Fig. 3.8 The friction and spring forces as captured by the: (a) the Coulomb+Stiction, (b) the LuGre, (c) the E-P, (d) the Proposed, (e) the Xiong, and (f) the GMS, models of friction

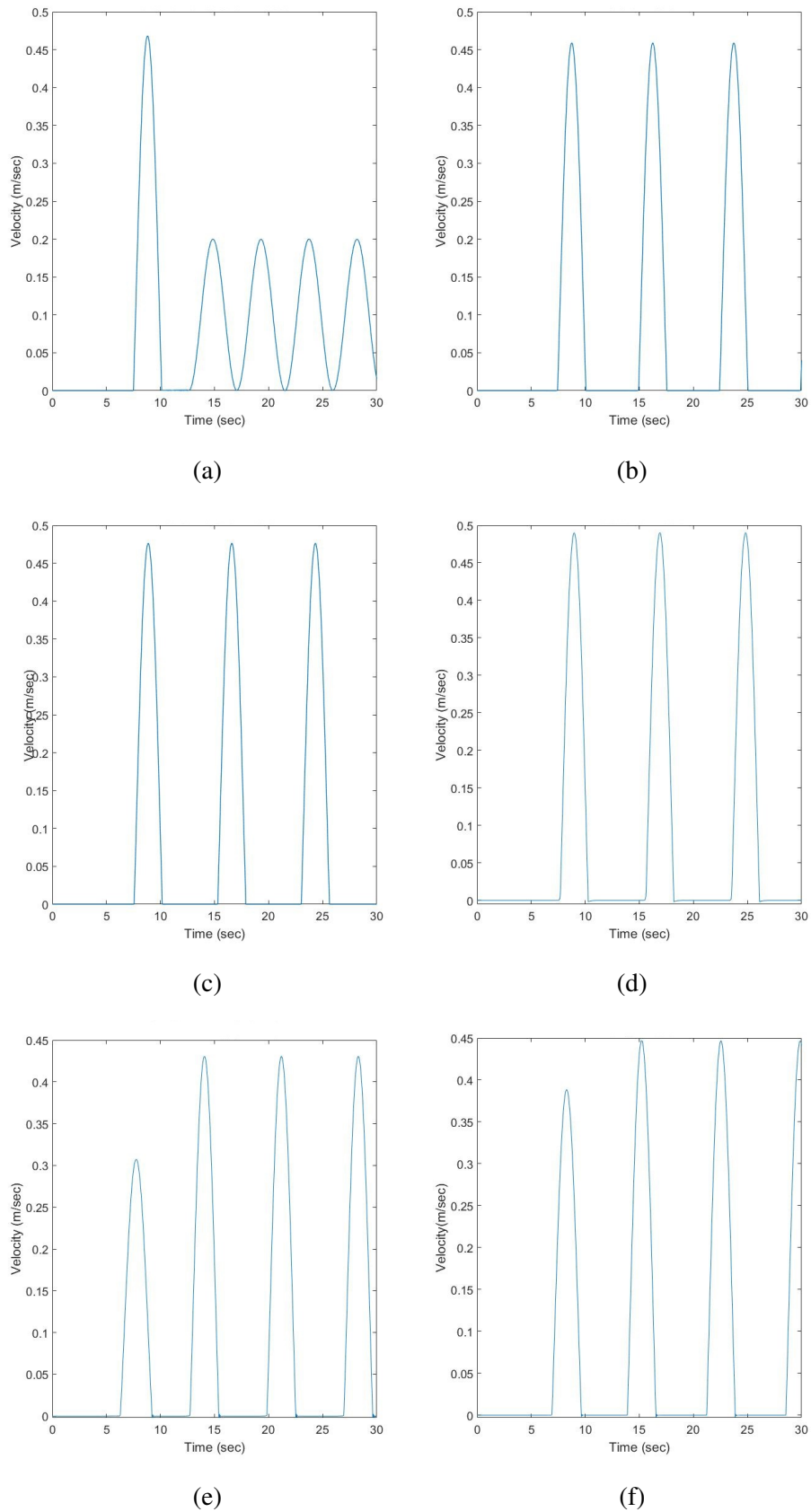


Fig. 3.9 The stick-slip motion velocity as captured by the various friction models considered: (a) the Coulomb+Stiction, (b) the LuGre, (c) the E-P, (d) the Proposed, (e) the Xiong, and (f) the GMS friction models

3.5.3 Models sensitivity to parameters variations

For the sensitivity analysis a simplified approach is sought by using three different values of each parameter of interest to capture these variation trends. These are; the default, half, and double the default values. The analysis are based on the pre-sliding and low velocity sliding simulations performed.

The LuGre model:

For the LuGre model the parameters of interest are; σ_0 , σ_1 , v_s . The Stribeck curve shaping parameter δ is chosen to be 2 for all the simulations. The plots of figures 3.10, 3.11, and 3.12 capture the friction-displacement and friction-velocity variations for varying σ_0 , σ_1 , and v_s respectively. From figure 3.10a, the stiffness parameter σ_0 affects the friction-displacement slope during the pre-sliding regime beyond which it exerts little or no differing effect. Thus it tends to increase the pre-sliding regime (breakaway displacement) and this caused the friction to fall below the coulomb value before rising again to it during sliding. In figure 3.10b, a slight reduction in the frictional-lag width due to the increased value in the friction force for velocities approaching zero is observed as this parameter increases.

The friction-displacement and friction-velocity relation as micro-viscous damping parameter σ_1 is varied are shown in figure 3.11. From 3.11a one notes that the smaller the parameter, the smoother the transition from stick to slip and vice versa, while larger parameters values introduce overshoot to the system dynamics as transition from pre-sliding to sliding regime sets in. Figure 3.11b shows that the parameter's influence on the size of the oscillations near the zero velocity. At low velocities the frictional-lag curve is seen also to intersect each other as this parameter value increases and this could lead to undesirable effects, [109].

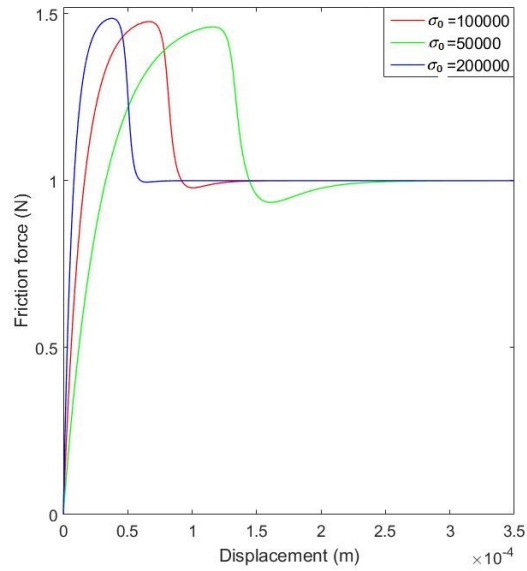
In figure 3.12, the Stribeck velocity parameter v_s variations is shown to affect the pre-sliding displacement, and the smoothness or otherwise of the transition from stick to slip. The stiction is observed to increase as Stribeck is increased, figure 3.12a. Friction is observed to increase as the Stribeck velocity decreases towards zero in the sliding regime and also increased oscillations in the stick region is noticed, figure 3.12b. Similar effects were observed for the elasto-plastic model bearing in mind their resemblance to the LuGre, so it was not recorded here.

The proposed non-drift dynamic friction model:

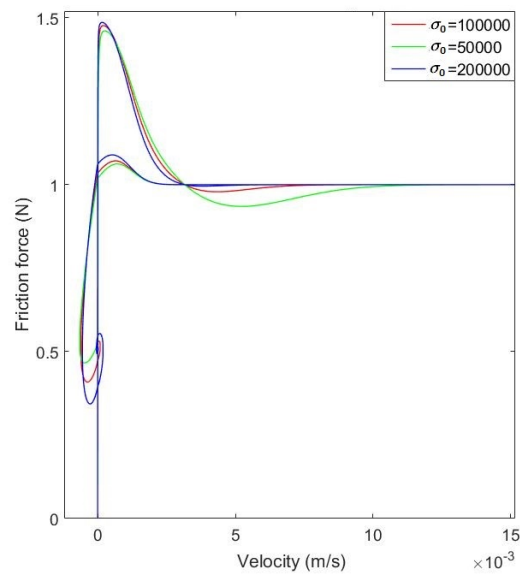
The model parameters investigated are: σ , v_s , Z_b and τ .

Figures 3.13, 3.14, 3.15, and 3.16 capture the friction-displacement and friction-velocity variations for varying σ_1 , v_s , Z_b and τ respectively.

As seen from the graphs of figure 3.13 the parameter σ_1 affects the pre-sliding displacement minutely with an increase in the slope as the micro-damping is increased figure 3.13a,

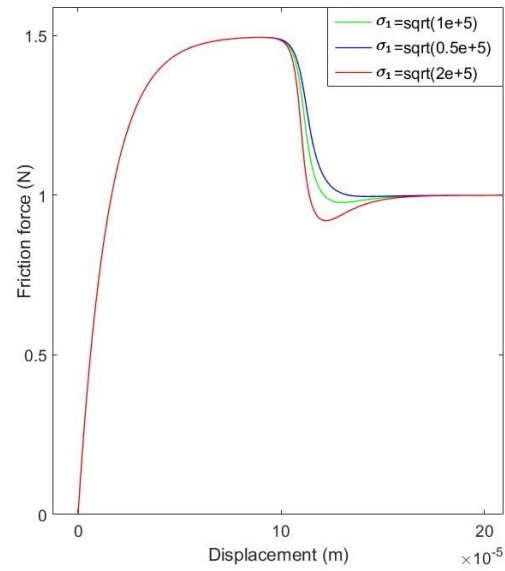


(a)

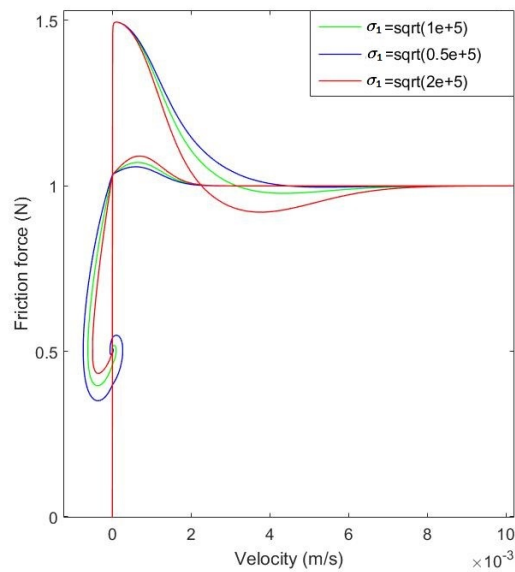


(b)

Fig. 3.10 The friction force against (a) displacement, and (b) velocity, for the LuGre model for various values of the parameter σ_0

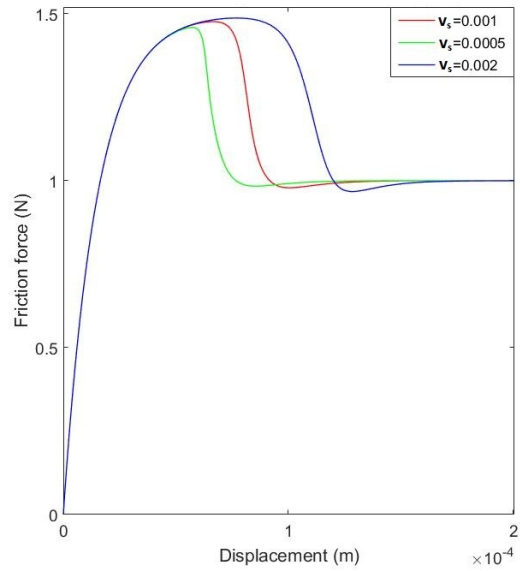


(a)

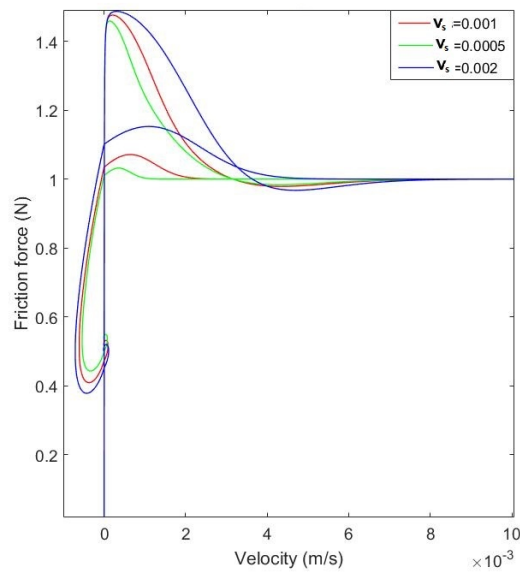


(b)

Fig. 3.11 The friction force against **(a)** displacement, and **(b)** velocity, for the LuGre model for various values of the parameter σ_1



(a)



(b)

Fig. 3.12 The friction force against (a) displacement, and (b) velocity, for the LuGre model for various values of the Striebeck parameter v_s

thus increasing the breakaway displacement slightly unlike the LuGre model which increases the range of deformation range. There is always a smooth transition from stick to slip regimes. However the effect of this parameter in the sticking regime as shown in figure 3.13b, has no noticeable effect during gross sliding unlike the LuGre.

The Stribeck velocity parameter v_s is seen to exert the reversed effect of the micro-damping parameter in the pre-sliding regime, incrementing this parameter is thus seen to increase the stiction and the displacement before sliding figure 3.14a, while in the friction-velocity plot figure 3.14b, it appears to show little or no effect in the stick (pre-slide) regime but increases the friction force towards the zero velocity as it increases as with the LuGre. Generally keeping the width of the frictional lag to be same.

The breakaway displacement parameter Z_b variations are seen to exert some effects such as a reduction in the breakaway (stiction) force as it increases and thereby increasing the pre-sliding displacement (which is what it is) figure 3.15a. Figure 3.15b suggests the effect of this parameter in the gross sliding regime to be negligible except only in the pre-slide region where incrementing it reduces the oscillations.

The influence of the τ parameter changes on the model, has little or no effect on the friction-displacement plot, figure 3.16a. In figure 3.16b, the plot suggests that incrementing the τ parameter widens the friction-lag effect (which in effect is the motivation for its introduction into the model).

The GMS model:

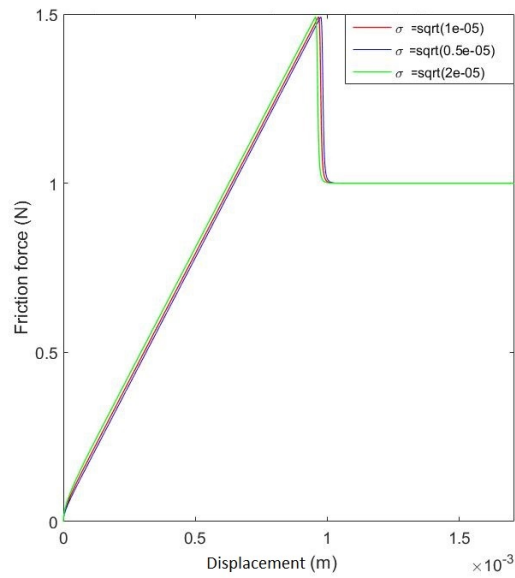
The model parameters to be investigated are α_i , C_i , σ_{0i} , σ_{1i} , and v_s . As a multi-state multi element model like Xiong model, analysis of the various effects of the model parameters was simplified and performed with 10 elements.

Figure 3.17 depicts the variations in the pre-slide, and gross-slide regimes respectively as the parameter α_i is varied. From figure 3.17a varying this parameter α_i has the same effect as λ parameter on the Xiong model, that is it increases or lowers the Coulomb value proportionately in the stick regime while in figure 3.17b the frictional lag is enlarged or reduced depending on the whether the parameter was increased or reduced in the slip regime.

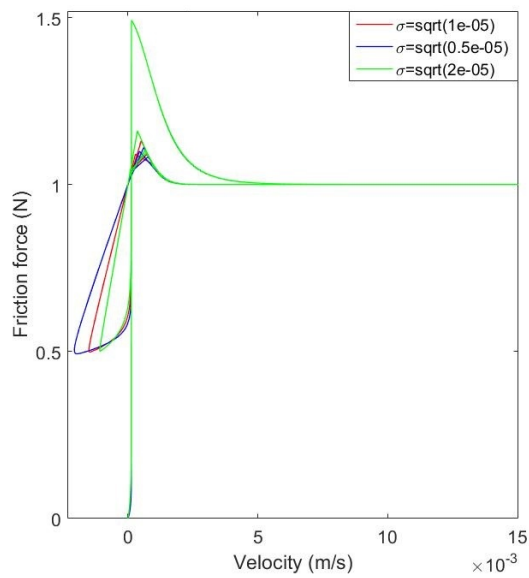
The parameter C_i the shape of the frictional lag is decreased by increments in this parameter figure 3.18a while in the pre-slide regime incrementing it caused a reduction in the stiction and possible oscillations figure 3.18b.

The parameter σ_{0i} figure 3.19a increased the stiction as it increased and also showed a reduction in the lag width of the gross-sliding regime much like the effect it had on the LuGre model, figure 3.19b.

For the micro-damping parameter σ_{1i} figure 3.20, it is noticed that increasing this parameter showed little effect on the stiction, with possible oscillations, figure 3.20a. The

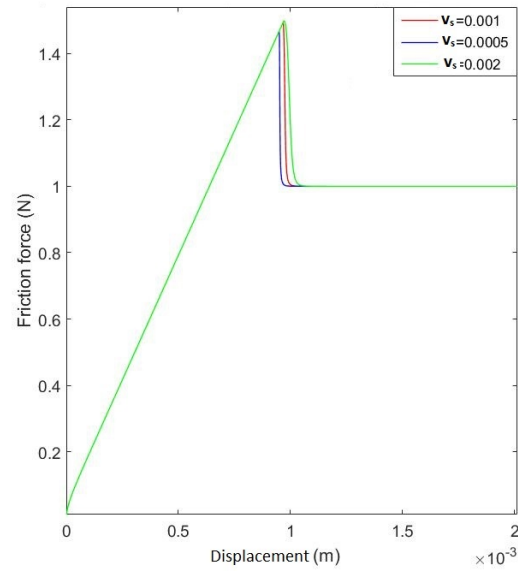


(a)

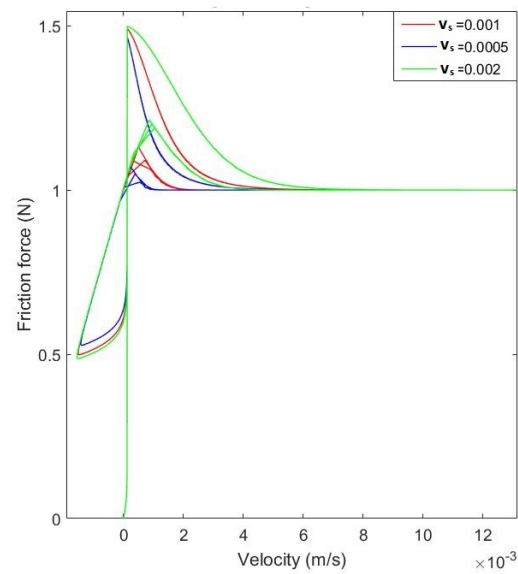


(b)

Fig. 3.13 The friction force against (a) displacement, and (b) velocity, for the proposed non-drift dynamic friction model for various values of the parameter σ

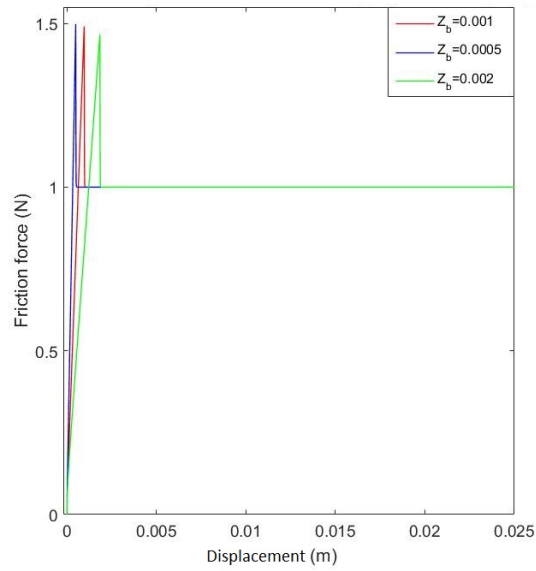


(a)

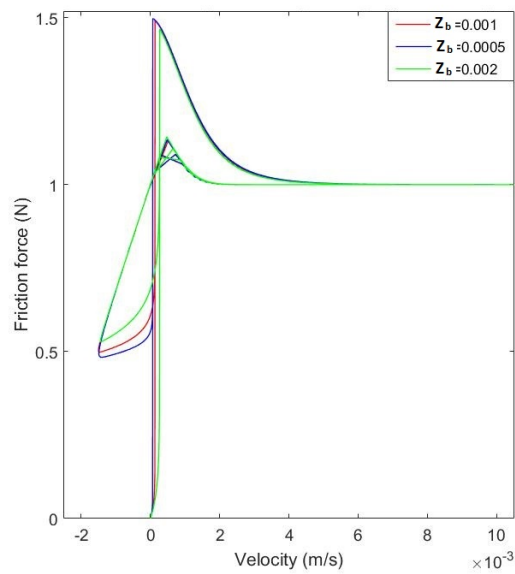


(b)

Fig. 3.14 The friction force against (a) displacement, and (b) velocity, for the proposed non-drift dynamic friction model for various values of the Stribeck parameter v_s

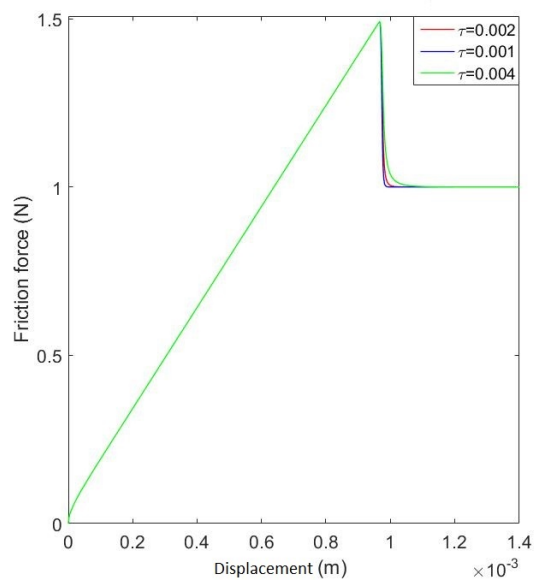


(a)

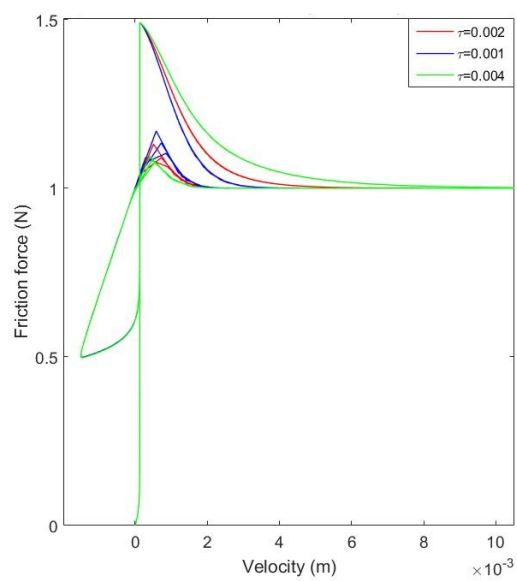


(b)

Fig. 3.15 The friction force against (a) displacement, and (b) velocity, for the proposed non-drift dynamic friction model for various values of the parameter Z_b



(a)



(b)

Fig. 3.16 The friction force against (a) displacement, and (b) velocity, for the proposed non-drift dynamic friction model for various values of the parameter τ

frictional-lag features of figure 3.20b is seen to shrink a bit as it increased like the LuGre.

The Stribeck velocity parameter v_s is shown to increase the stiction and pre-sliding displacement as it increased figure 3.21a, while figure 3.21b showed the general rise in the friction as Stribeck parameter incremented.

The Xiong model:

The model parameters investigated are K_i , σ_{1i} , v_s , λ_i and τ . The multi-state multi element Xiong model analysis for various parameter changes was performed and some observations made.

Figure 3.22 depicts the variations in the pre-slide (a), and gross-slide (b) regimes as the parameter K_i is varied. From figure 3.22a, the variations in the element's stiffness K_i extends the displacement in the stick regime before breakaway and thus stiction increased as stiffness was increased. Figure 3.22b captures the frictional lag with the friction value decreasing as the stiffness is reduced and the increased oscillation. The sensitivity of this parameter has close resemblance to σ_0 of the LuGre model of figure 3.10.

For the micro-damping parameter σ_{1i} figure 3.23, it is noticed that increasing this parameter has little effect on the pre-sliding displacement figure 3.23a, and also little effect is noticed on the gross sliding regime figure 3.23b. Thus the influence of σ_1 parameter seemed to be same for both the Proposed model and the Xiong model and differs with that of the LuGre model.

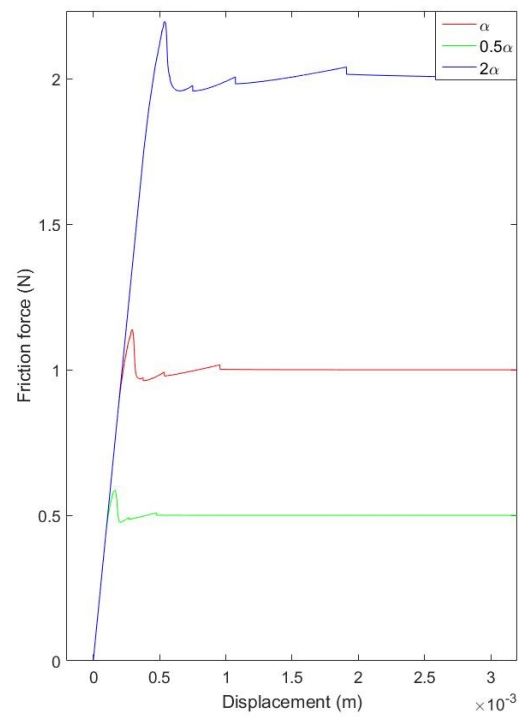
The Stribeck velocity parameter v_s is shown to increase the stiction and pre-sliding displacement during sticking as it increases in value figure 3.24a, while figure 3.24b showed the general rise in the friction as Stribeck parameter is incremented while maintaining the lag width.

The need for the parameter λ_i to sum to a unit value is shown in figure 3.25 where it affects the steady state values of the friction. The shape of the frictional-lag remains the same generally as in figure 3.25b with the possibility of oscillations increasing as the parameter value increases.

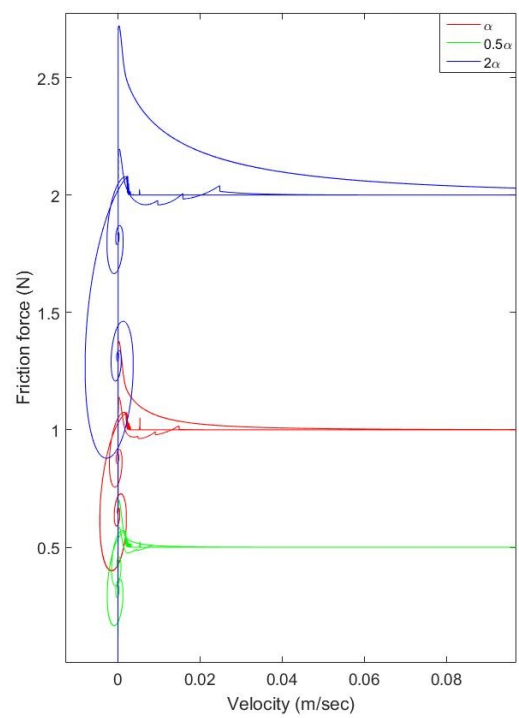
In figure 3.26, the parameter τ affects mainly the shape of the frictional lag by widening the same, figure 3.26b, while it exerts negligible effect on the slope and displacement of the pre-slide region figure 3.26a as seen in the proposed non-drift dynamic friction model 3.16a.

3.5.4 Discussion of sensitivity analysis results

From the results focus is on how these parameters and their variations affect the overall performance of the individual models both for the pre-sliding and gross-sliding friction

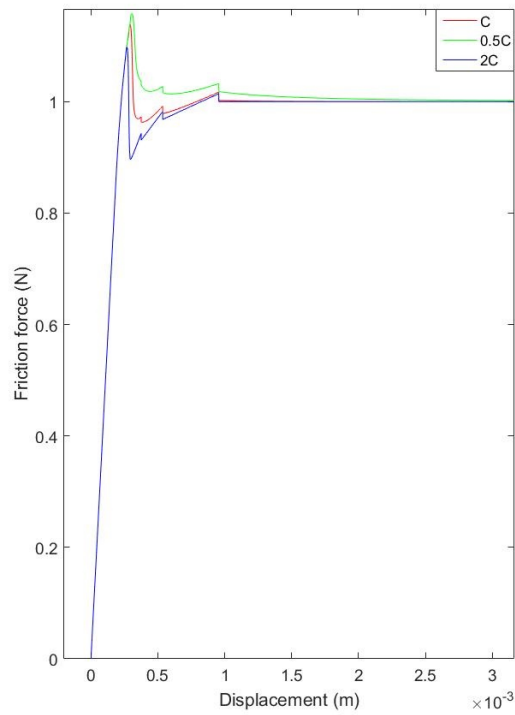


(a)

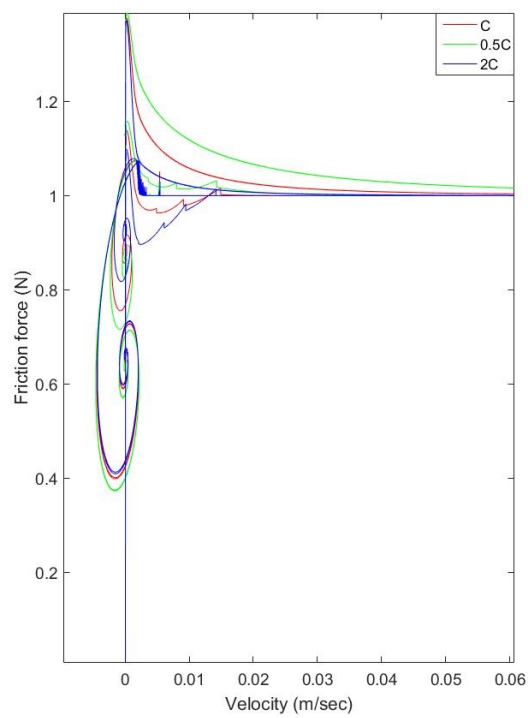


(b)

Fig. 3.17 The friction force against (a) displacement, and (b) velocity, for the GMS model for various values of the parameter α_i

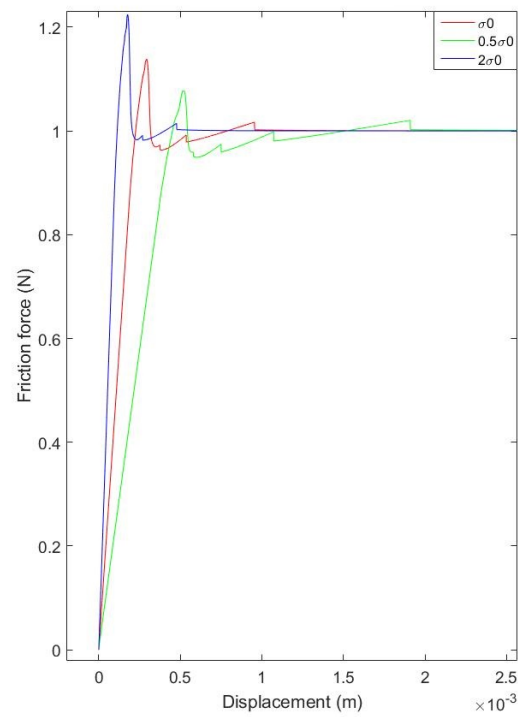


(a)

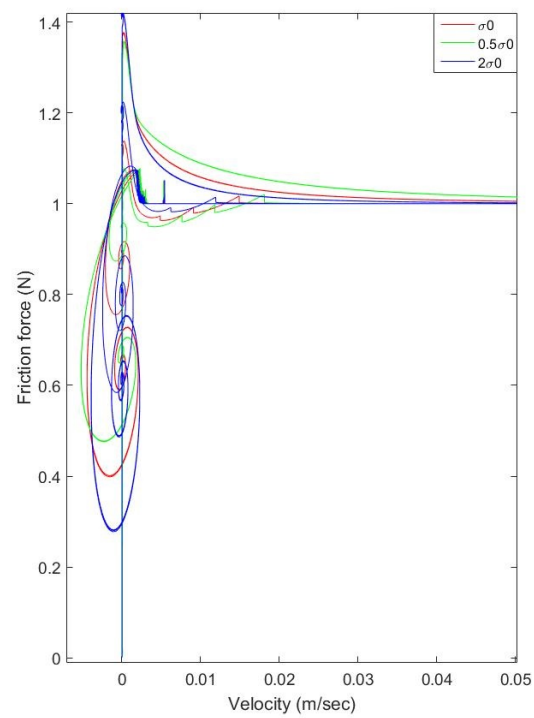


(b)

Fig. 3.18 The friction force against (a) displacement, and (b) velocity, for the GMS model for various values of the parameter C_i

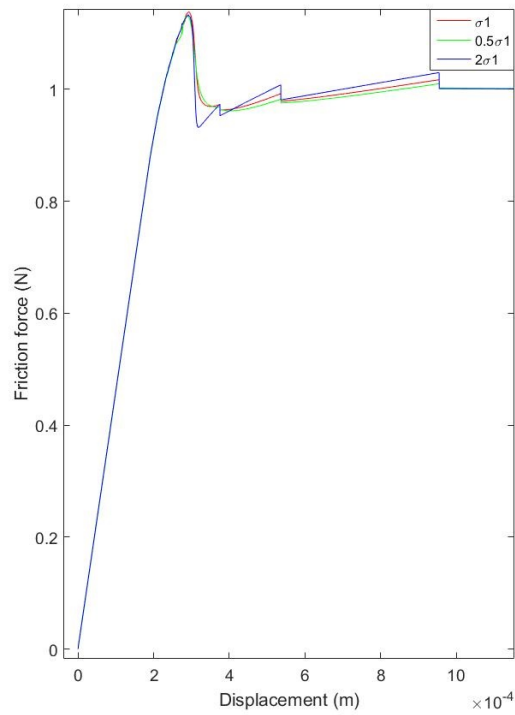


(a)

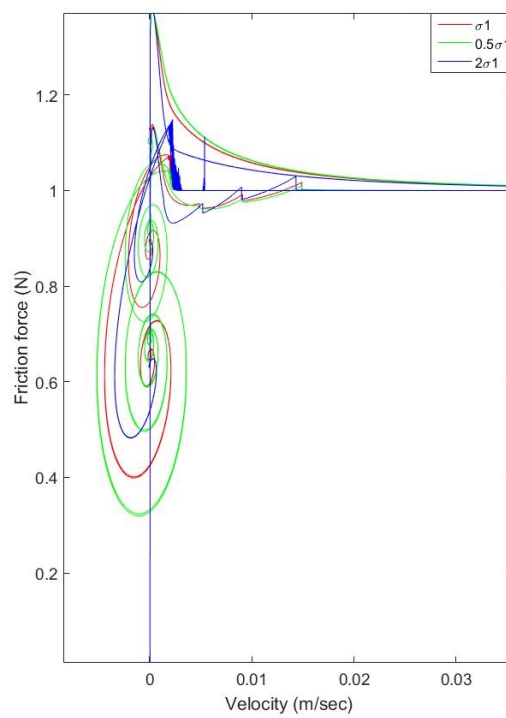


(b)

Fig. 3.19 The friction force against (a) displacement, and (b) velocity, for the GMS model for various values of the parameter σ_0

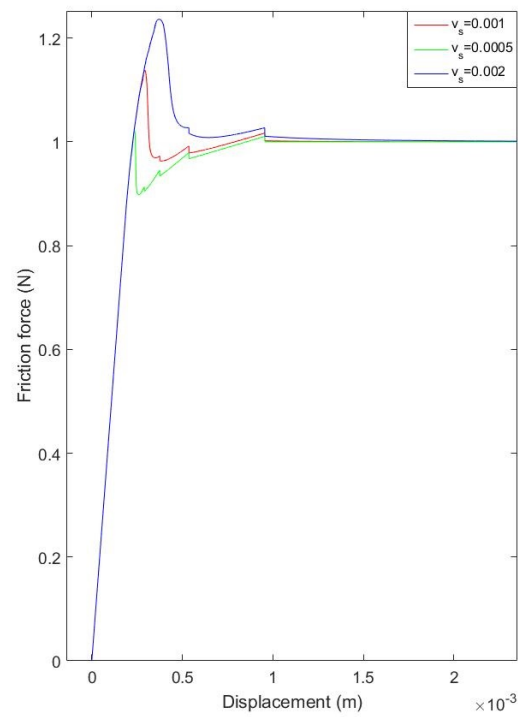


(a)

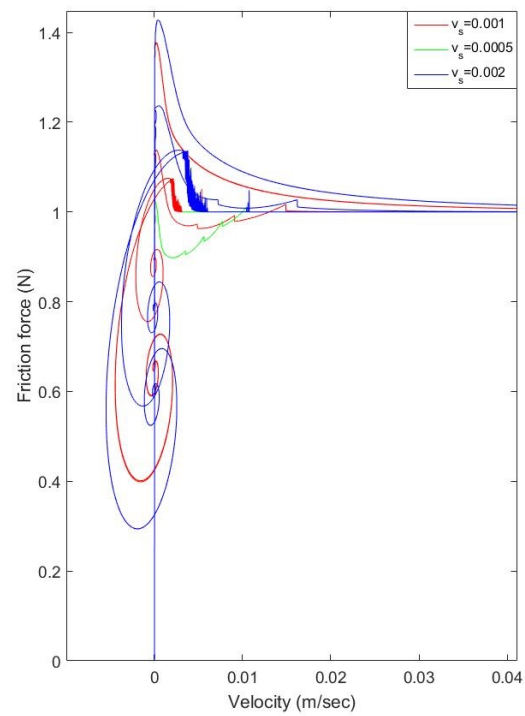


(b)

Fig. 3.20 The friction force against (a) displacement, and (b) velocity, for the GMS model for various values of the parameter σ_{1i}

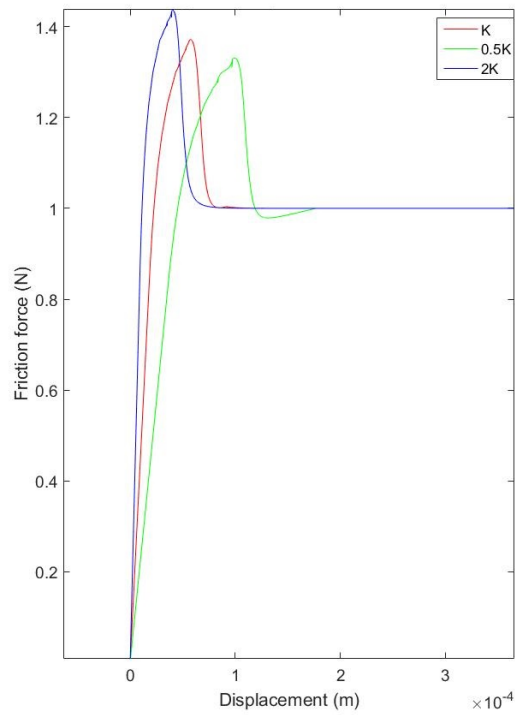


(a)

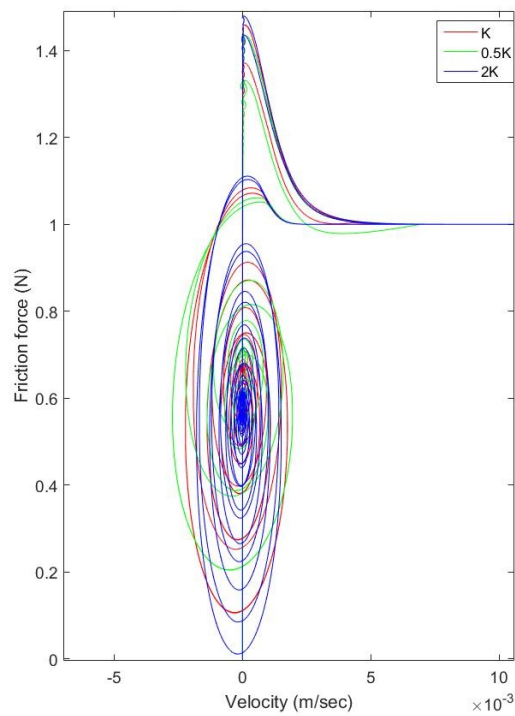


(b)

Fig. 3.21 The friction force against (a) displacement, and (b) velocity, for the GMS model for various values of the parameter v_s

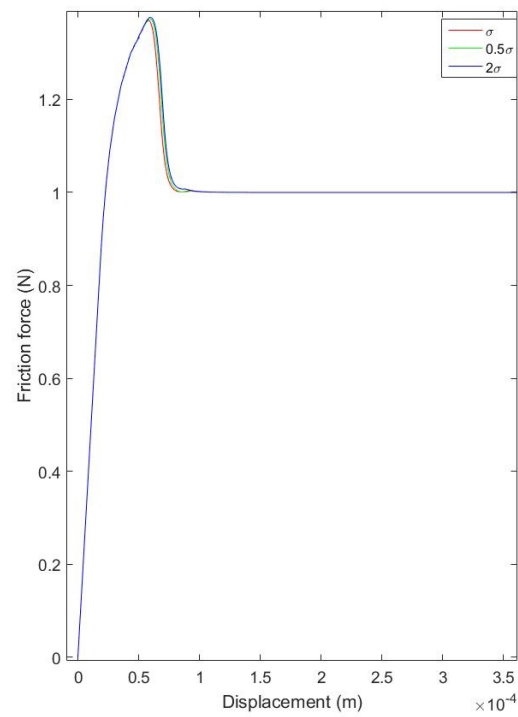


(a)

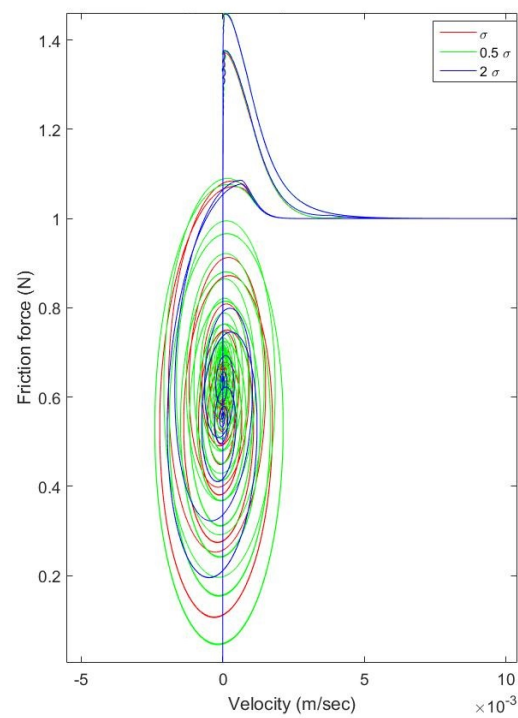


(b)

Fig. 3.22 The friction force against (a) displacement, and (b) velocity, for the Xiong model for various values of the parameter K_i

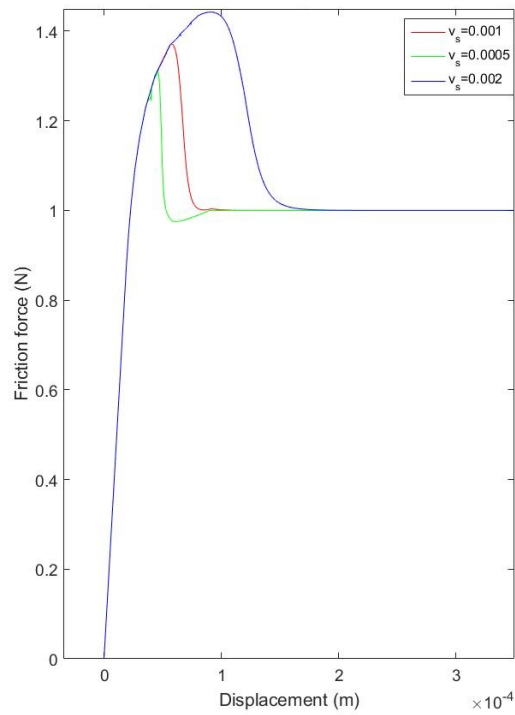


(a)

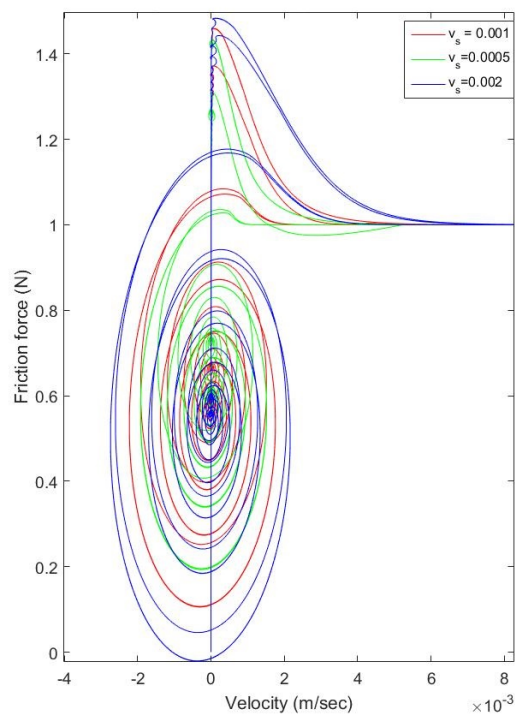


(b)

Fig. 3.23 The friction force against (a) displacement, and (b) velocity, for the Xiong model for various values of the parameter σ_{1i}

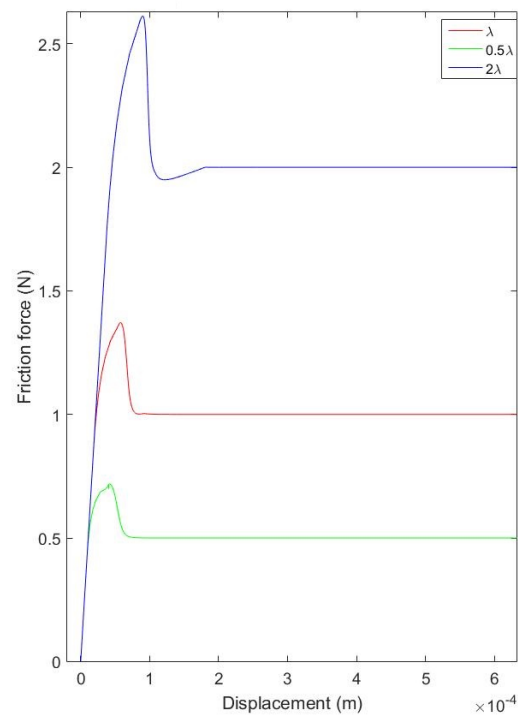


(a)

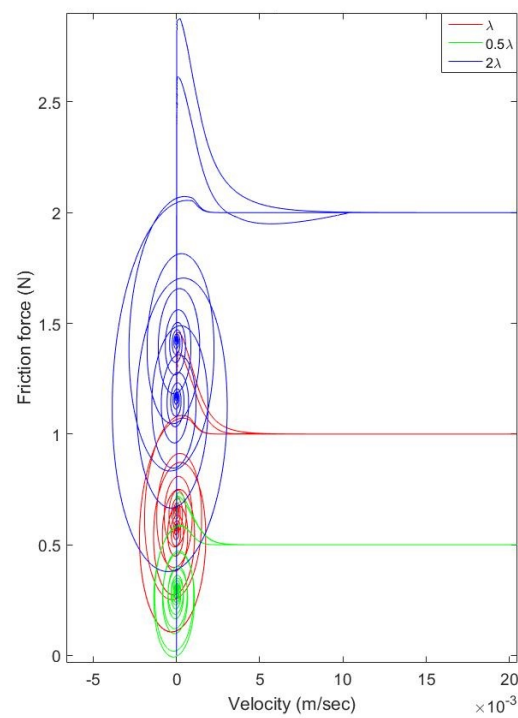


(b)

Fig. 3.24 The friction force against (a) displacement, and (b) velocity, for the Xiong model for various values of the Stribeck parameter v_s

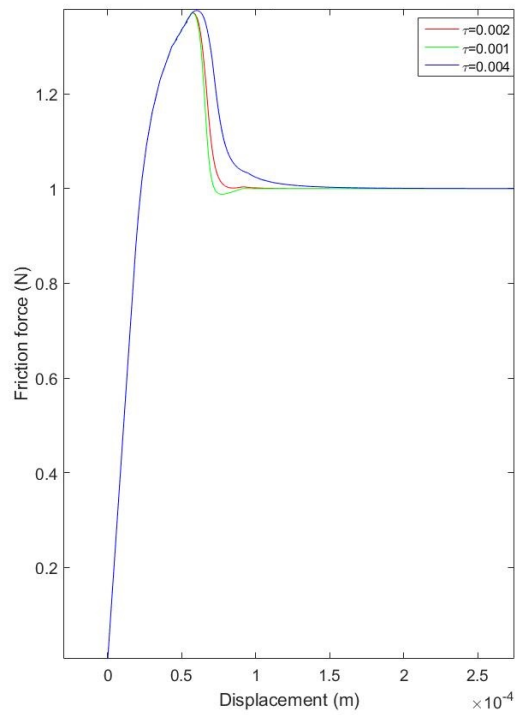


(a)

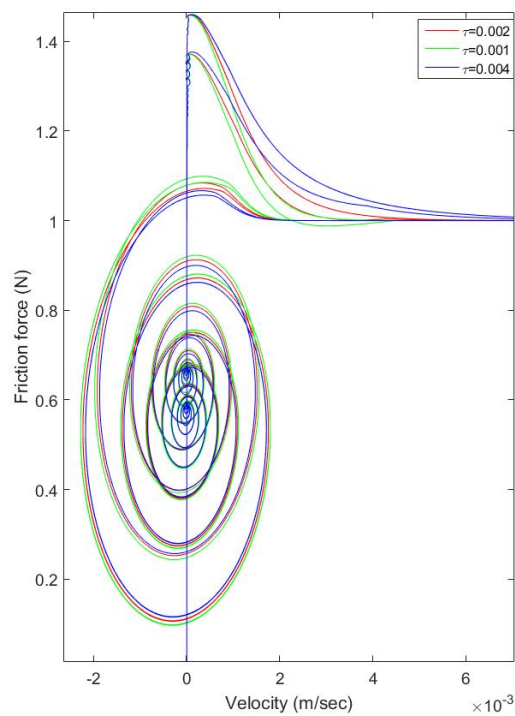


(b)

Fig. 3.25 The friction force against (a) displacement, and (b) velocity, for the Xiong model for various values of the parameter λ_i



(a)



(b)

Fig. 3.26 The friction force against (a) displacement, and (b) velocity, for the Xiong model for various values of the parameter τ

regimes and their transitions.

LuGre model:

Increasing the stiffness increased the stiction slightly, and reduced the pre-sliding displacement with smoother transition to gross-sliding, while in the gross sliding regime increments in the stiffness parameter shrink the frictional lag loop and reduced the possibility of loop crossing. Loop crossing simply means a situation whereby the acceleration friction force is lower than the deceleration value at some point as the velocity goes through periodic motion, see figure 2.5. The micro-damping parameter introduced possible undershoot as its value is increased in the pre-sliding regime and decreased the frictional lag loop with the possibility of overlap as it is increased in the gross-sliding regime. This behaviour is why it may not be wise to arbitrarily increase this parameter in the LuGre model. A preferred approach adopted by the authors to model this parameter was to make it a decreasing function of the relative velocity. Increasing the Stribeck parameter also increased the stiction and displacement in the pre-sliding regime with undershoot and loop crossing in the gross-sliding for increments in the parameter. Thus from the above, the LuGre model exhibits appreciable sensitivity to parameter variations.

Proposed model:

The micro-damping parameter increments resulted in the increase of the stiction and reduction of the pre-sliding displacement in the pre-sliding regime while this did not affect the frictional lag shape in any way in the gross-sliding regime. The stiction force and the pre-sliding displacement were seen to increase in response to increased Stribeck velocity during pre-sliding and increased the frictional lag while preserving the loop shape (loop shift). For the pre-sliding displacement parameter increments resulted in the lowering of the stiction, and no effect on the frictional lag in the gross sliding-regime. The parameter τ did not affect the pre-sliding regime, but was seen to increase the loop shape of the frictional lag. It should be noted that the introduction of this parameter was to improve the frictional lag feature of the new model. From the observations the proposed new model exhibits a degree of robustness to parameter changes and for most variations the general shape and features of the friction phenomenon is preserved both for the pre-sliding and gross-sliding regimes. From the above, the proposed new model was shown to exhibit higher degree of robustness to parameter variations for the simulation tests performed and parameters values used.

GMS model:

Increasing the stiffness led to increase in the stiction and breakaway displacement reduction in the pre-sliding while in the gross-sliding regime, the frictional lag shape was reduced. The micro-damping had little to no effect on the stiction and breakaway displacement values as it increased during pre-sliding and general reduction in the frictional lag shape in the gross

sliding regime was observed. The static friction and breakaway displacement increased as the Stribeck velocity increased for the pre-slide regime, while for the gross-slide regime the frictional lag shape increased also. Parameter C increments resulted in decreasing stiction while breakaway displacement remain unchanged, and a reduction in the frictional lag in gross-sliding. The parameter α increased the stiction and breakaway displacement in the pre-slide regime, it also increased the frictional lag shape in the gross-slide regime as it was increased. From these one sees that the GMS model is sensitive to parameter variations though to a less degree compared to the LuGre model.

Xiong model:

Incrementing the stiffness increased the stiction while lowering the breakaway displacement, improving transitions from pre-sliding to gross-sliding. It increased the frictional lag shape in the sliding regime. The micro-damping had little effect on the static friction and none on the breakaway displacement and frictional lag. The Stribeck velocity increased the stiction and breakaway displacement as it increased, while in the gross sliding it increased the frictional lag shape (loop shift). As the scaling parameter increased the stiction, breakaway displacement, and the frictional lag were shown to increase. Increasing the τ value smooths transition from pre-slide to gross-slide, it also increased the breakaway displacement while in the gross-sliding the frictional lag shape increased. Note as in the proposed new model the τ parameter functions in similar manner to improve the frictional lag prediction of the model. The Xiong model is thus sensitive to variations to its parameters except for the micro-damping with least effect on the model.

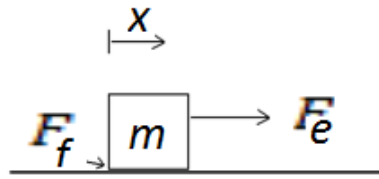
Hence from the above simulations and results, the proposed new model of friction exhibited more robustness to variations in it's parameters more than the other friction models investigated.

3.6 Pre-sliding performance analysis

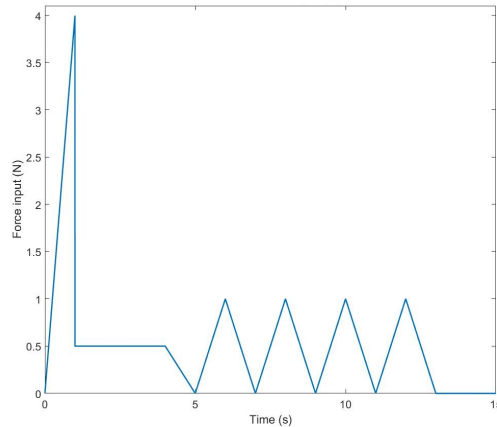
In performing these simulations the aim is to determine the capability of the various models to predict frictional behaviour for friction forces of less value than the stiction, and the non-drifting feature of actual friction behaviour in real systems. The different models and their ability to model friction forces in these regimes are therefore compared.

3.6.1 Non-drift features

For the simulations, the force input used is as shown, figure 3.27b, and the system is a simple mass with friction subjected to an external force figure 3.27a. The force input initially ramps



(a) A simple system for non-drift test



(b) Reference force input

Fig. 3.27 Non-drift characteristic of friction test

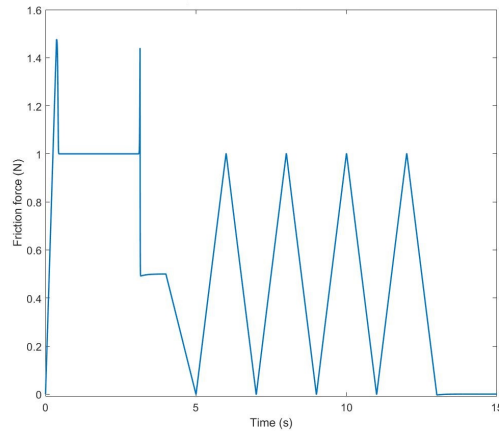
to a value much greater than the stiction and then suddenly falls well below this value and remains within same while moving in a zigzag manner. Interests are on the ability of the models to show stiction and then the non-drift feature of real frictions in contact surfaces.

Proposed model:

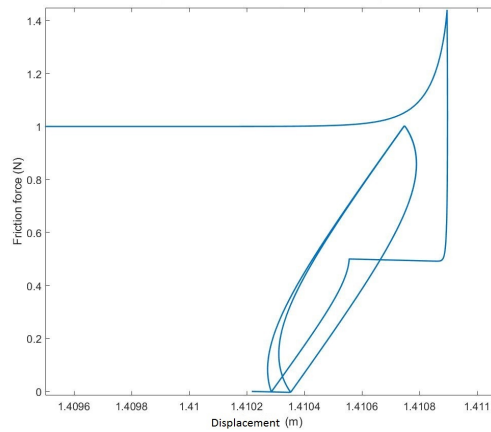
Parameters for the proposed non-drift dynamic friction model are chosen as: $F_s=1.5$, $F_c=1$, $v_s=0.01$, $Z_b=0.001$, $\tau=0.002$, $\sigma = \sqrt{100000}$. On simulation, the new model captured the stiction force and subsequent motion till the force falls below the coulomb level. In the region less than the coulomb force, friction is virtually equal to the applied external force as shown in the plot of figure 3.28a. The non-drifting property of the model is also observed to be exhibited by the new model as shown in figure 3.28b. One easily notices the hysteresis loop in the friction position plot also.

LuGre model:

Parameters for the LuGre friction model are: $F_s=1.5$, $F_c=1$, $v_s=0.01$, $\sigma_1 = \sqrt{100000}$, $\sigma_0=100000$. Figure 3.29a shows that LuGre captured the friction force as expected. However, it also shows in figure 3.29b that the model exhibits the drift phenomenon which is unlike actual friction in real systems suggesting forces less than the friction (say vibrations) are



(a)



(b)

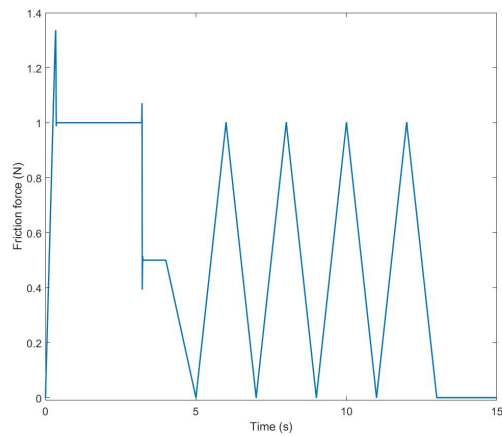
Fig. 3.28 The friction force against (a) Time, and (b) Displacement; showing the non drift property of real friction for the Proposed model.

capable of initiating observable relative displacement between such surfaces in contact.

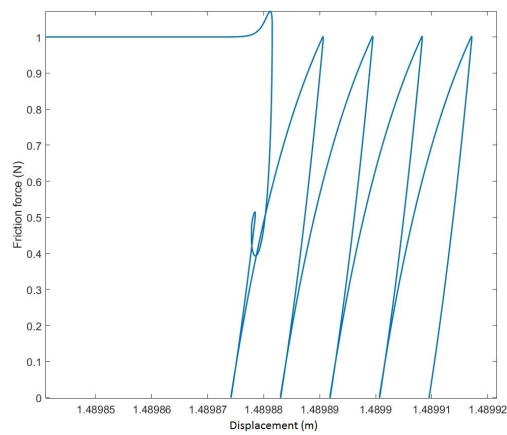
Elasto-Plastic model:

The following parameters were used to capture pre-sliding non-drift feature of the E-P friction model are $F_s=1.5$, $F_c=1$, $v_s=0.01$, $\sigma_1 = \sqrt{100000}$, $\sigma_0=100000$, $Z_{ba}=0.69Z_{ss}$. This model was able to exhibit the non drift property of friction though it seems to be strongly dependent on the choice of some parameters like the Z_{ba} , it has been shown that the non-drift feature of the elasto-plastic model is limited by the value of the breakaway displacement parameter Z_{ba} . The friction force prediction and the non-drift property are very well captured as shown in figure 3.30.

GMS model:

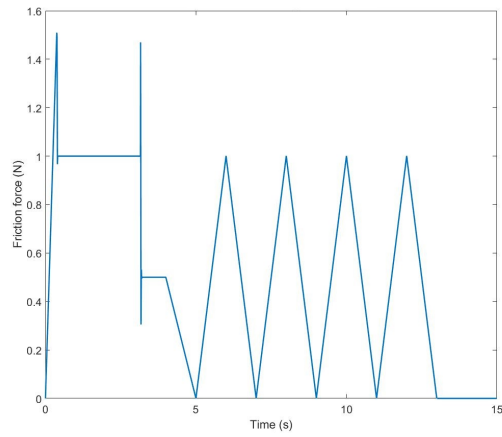


(a)

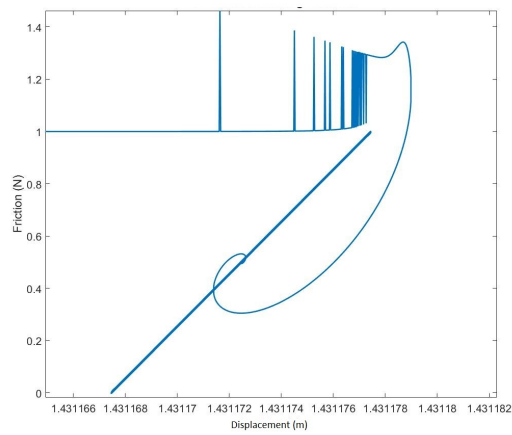


(b)

Fig. 3.29 The friction force against (a) Time, and (b) Displacement; showing drift for the LuGre model, contrary to the non-drift property of real friction

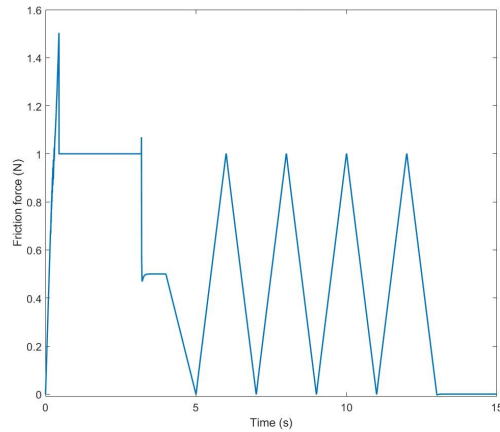


(a)

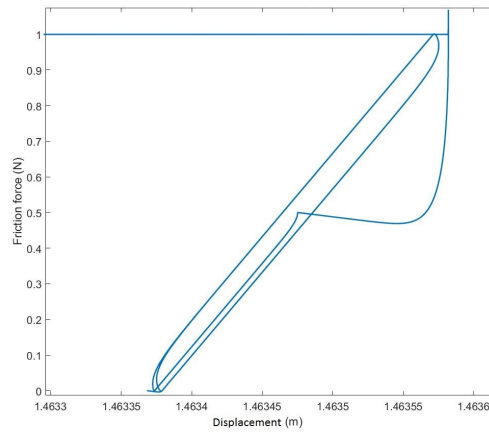


(b)

Fig. 3.30 The friction force against (a) Time, and (b) Displacement; showing the non drift property of real friction for the E-P model



(a)



(b)

Fig. 3.31 The friction force against (a) Time, and (b) Displacement; showing the non drift property of real friction for the GMS model

The GMS model was able to predict stiction and exhibit the non-drift property of real friction as shown in figure 3.31. The following parameters were used to capture pre-sliding non-drift feature of the GMS model $F_s=1.5$, $F_c=1$, $v_s=0.01$, $\sigma_{0i}=10, 18, 26, 34, 42, 5, 58, 66, 74, 82$, $\sigma_{1i}=10, 15, 20, 25, 30, 35, 40, 45, 50, 55$, $\tau=0.002$, $\alpha_i=0.0955, 0.0965, 0.0975, 0.0985, 0.0995, 0.1005, 0.1015, 0.1025, 0.1035, 0.1045$, $C_i=0.00955, 0.00965, 0.00975, 0.00985, 0.00995, 0.01005, 0.01015, 0.01025, 0.01035, 0.01045$.

Xiong model:

The following parameters were used to capture pre-sliding features of the Xiong model $F_s=1.5$, $F_c=1$, $v_s=0.01$, $K_i=1000, 1800, 2600, 3400, 4200, 5000, 5800, 6600, 7400, 8200$, $\sigma_i=5, 7.5, 10, 12.5, 15, 17.5, 20, 22.5, 25, 27.5$, $\tau=0.002$, $\lambda_i=0.0955, 0.0965, 0.0975, 0.0985$,

0.0995, 0.1005, 0.1015, 0.1025, 0.1035, 0.1045.

Unlike LuGre model, Xiong model exhibits the stiction friction feature and it also demonstrates the non-drift property figure 3.32, like real friction.

3.6.2 Hysteresis with non-local memory

In this subsection an attempt is made to show the capability of the proposed friction model, and some other models to capture the pre-sliding hysteresis feature with non-local memory and a comparison is made amongst the five chosen models. As in the previous section the system of interest is a simple mass system under external force application. For external force inputs less than the stiction, the actual friction force has been shown to follow a hysteresis curve with non-local memory. The term non-local memory was earlier explained in chapter 2. Thus a good model of friction would be able to model this non-local hysteresis phenomenon as a function of displacement only. The reference force input used for the simulations is as shown figure 3.33.

Proposed model:

Applying this reference force input signal to the system the following observations were made: A pre-sliding hysteresis function as shown in figure 3.33 with non-local memory was exhibited by the proposed non-drift dynamic friction model. Parameters used for the simulation are: $F_s = 1.5$, $F_c = 1$, $v_s = 0.001$, $\tau = 0.002$, $\sigma = \sqrt{100000}$, $Z_b = 0.001$.

LuGre model:

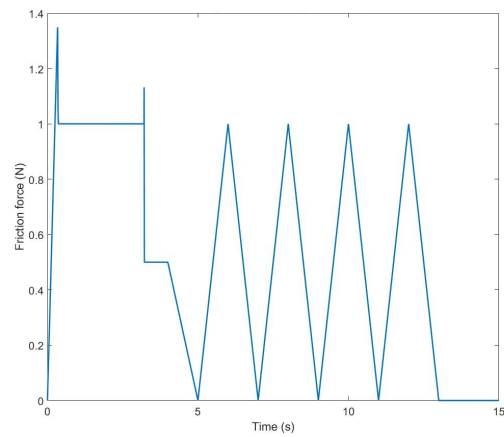
For the LuGre model a pre-sliding hysteresis function was also obtained, however this does not seem to exhibit the non-local nature of the true hysteresis in the pre-sliding regime of friction as shown in figure 3.35a as supported by other researchers, [101]. The model parameters used are: $\sigma_0 = 100000$, $v_s = 0.001$, $F_s = 1.5$, $F_c = 1$, $\sigma_1 = \sqrt{100000}$.

E-P model:

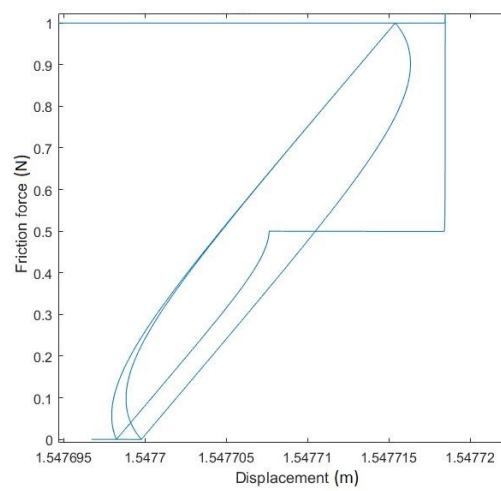
A hysteresis plot, figure 3.35b was predicted using the elasto-plastic model that is similar to that of the LuGre model. The model parameters used are: $\sigma_0 = 100000$, $v_s = 0.001$, $F_s = 1.5$, $F_c = 1$, $\sigma_1 = \sqrt{100000}$, $Z_{ba} = 0.69Z_{ss}$.

GMS model:

It was shown that the GMS model was able to predict true pre-sliding hysteresis with non-local memory qualitatively with a close resemblance to the proposed non-drift dynamic friction model, figure 3.35d. The following parameters were used for the simulation $\sigma_{1i} = 10, 15, 20, 25, 30, 35, 40, 45, 50, 55$, $F_c = 1$, $F_s = 1.5$, $v_s = 0.00001$, $C_i = 0.00955, 0.00965, 0.00975, 0.00985, 0.00995, 0.01005, 0.01015, 0.01025, 0.01035, 0.01045$, $\sigma_0 = 10, 18, 26, 34, 42, 50, 58, 66, 74, 82$, $\alpha_i = 0.0955, 0.0965, 0.0975, 0.0985, 0.0995, 0.1005, 0.1015$,



(a)



(b)

Fig. 3.32 (a) The friction force against time, and (b) The displacement against time showing drift, contrary to non-drift property of real friction for the Xiong model

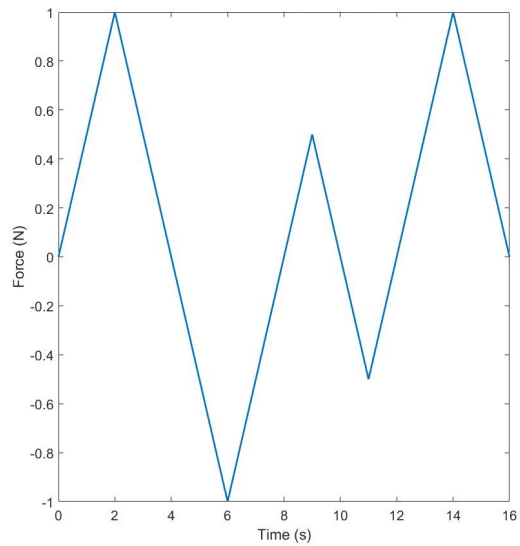


Fig. 3.33 The reference force input for testing the hysteresis (with non-local memory) capabilities of the various friction models

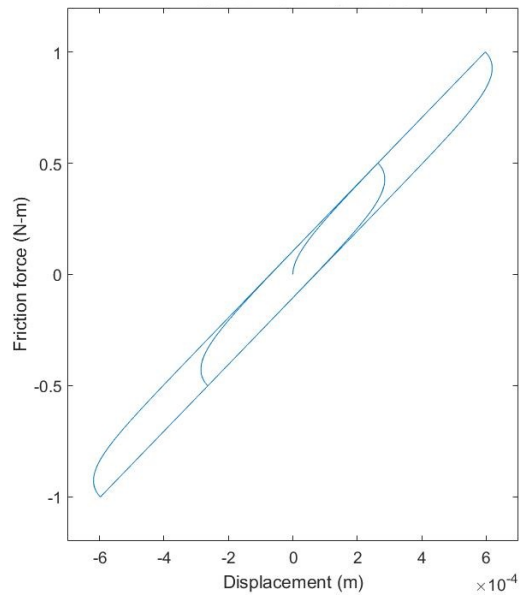
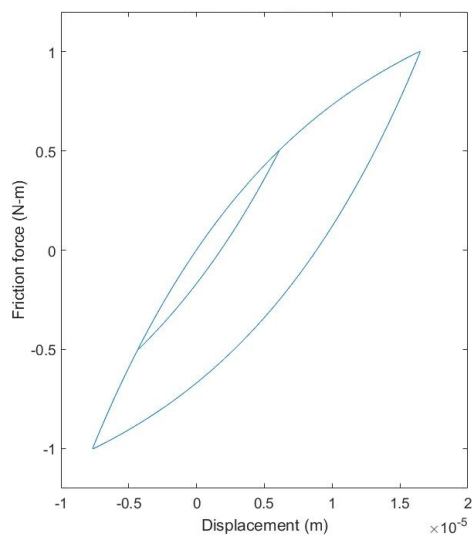
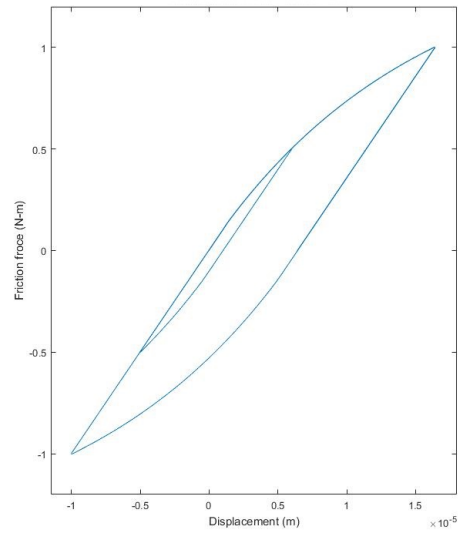


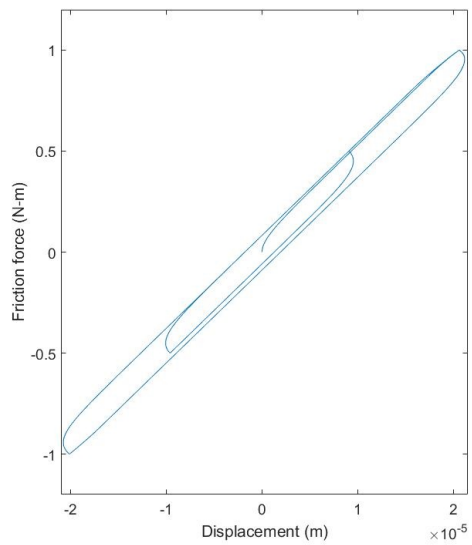
Fig. 3.34 The friction hysteresis (friction force against displacement) for the Proposed model



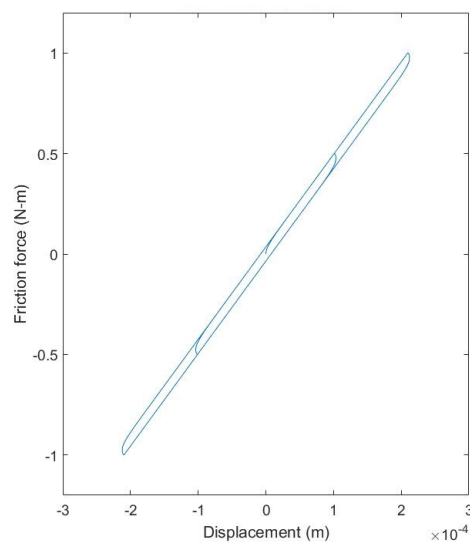
(a)



(b)



(c)



(d)

Fig. 3.35 The friction hysteresis (friction force against displacement) for: (a) the LuGre model, (b) the E-P model, (c) the Xiong model and (d) the GMS model

0.1025, 0.1035, 0.1045.

Xiong model:

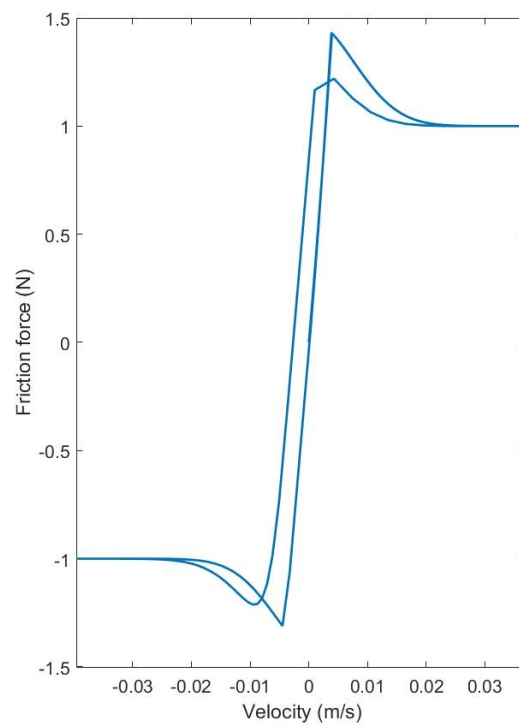
The simulation result for the pre-sliding hysteresis with non-local memory prediction using the Xiong model of friction is shown in figure 3.35c. The simulation results showed that this model is able to predict the hysteretic feature with similarities with the proposed and GMS models. The parameters used for the simulations are: $F_s = 1.5$, $F_c = 1$, $v_s = 0.0001$, $\tau = 0.002$, $K_i = 1000, 1800, 2600, 3400, 4200, 5000, 5800, 6600, 7400, 8200$, $\lambda_i = 0.0955, 0.0965, 0.0975, 0.0985, 0.0995, 0.1005, 0.1015, 0.1025, 0.1035, 0.1045$, $\sigma_i = 5, 7.5, 10, 12.5, 15, 17.5, 20, 22.5, 25, 27.5$

Transition from stick to slip and vice versa and the constant velocity prediction

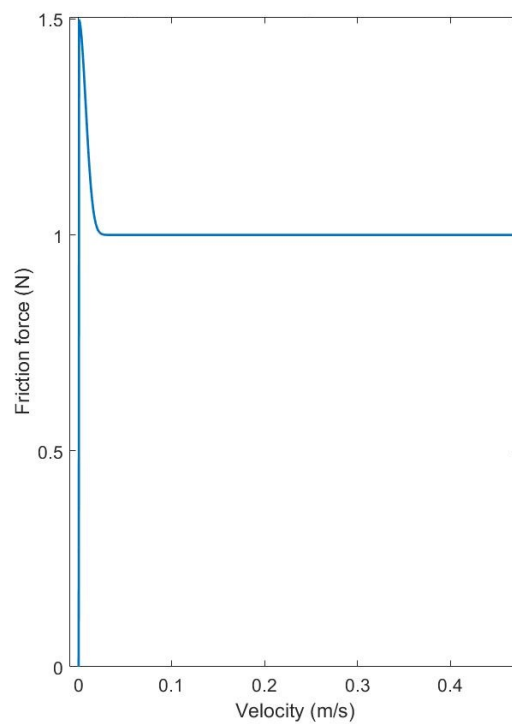
Next we investigate how the proposed non-drift dynamic friction model is able to model friction for varying velocities, especially transiting from sticking to sliding, going through velocity reversals to negative velocities. Followed by the friction force as a function of steady velocities. The first feature is obviously a dynamic phenomenon while the latter depicts a static relation between friction force and velocity. Many researchers have documented these features as predicted by some relevant models of friction like the LuGre, GMS, E-P and Leuven models [114], [58]. The attention is thus on how the proposed non-drift dynamic friction model is able to predict this dynamic feature. In carrying out the simulations the default parameters values were used. A sinusoidal velocity was applied to the system (a simple mass-spring system) and the resulting friction force predictions obtained. From the result the model is capable of predicting transitions from stick to slip and vice versa showing its behaviour around zero velocities as shown in figure 3.36a. Figure 3.36b portrays the friction force in relation to constant velocities. This feature captures the Stribeck effect at low velocities as friction decreases towards its minimum kinetic value (F_c) for increasing velocities from its stiction value.

Breakaway friction and varying breakaway friction prediction

The application of an external linearly increasing force to the system will lead to a friction force build up, this build up will continue proportionately with the externally applied force until it is able to break the forces of adhesion between the surfaces to initiate a relative motion between the two bodies. The friction force value beyond which the bodies slide relative to each other is termed the stiction and it has been experimentally found that this



(a)



(b)

Fig. 3.36 Friction force for: **(a)** Velocity transitions including zero velocity and reversal, and **(b)** The steady state friction force against velocity for constant velocities

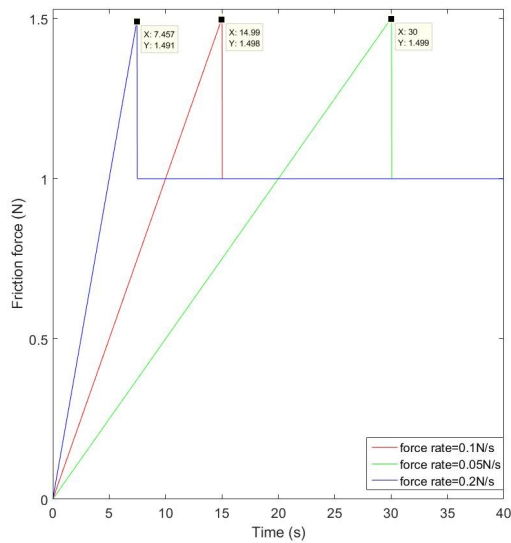


Fig. 3.37 The breakaway friction force for varying force rates

value is dependent on the rate at which the force is being applied, [20]. For the varying breakaway force a ramp signal was used varying the slope (rate) as follows: 0.1 N/s, 0.05 N/s, and 0.2 N/s. Two separate set of simulations were performed: First to determine the effect of force rate on the breakaway friction force, and second to determine the influence of parameter variations on the breakaway friction force predicted by the proposed non-drift dynamic friction model. The model parameter values used are the default values $F_s=1.5$, $F_c=1$, $\sigma = \sqrt{1000000}$, $v_s=0.001$, $\tau=0.002$, $Z_b=0.001$, and the results are as shown in the respective figures.

Force-rate effect

This is otherwise known as the varying breakaway feature and the model was able to predict this variation showing that as the rate of application of the external force is increased, the breakaway friction force predicted also increased as in figure 3.37.

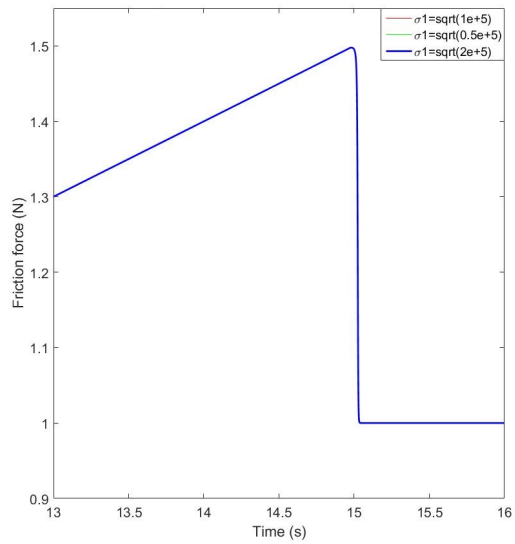
Parameter variations on the breakaway

Next we study the impact of varying the model parameters on the breakaway friction as predicted by the model. In doing this the parameters of the model are chosen as the default and their variations are half and double the default values. The effect of the micro-damping parameter (σ) was first examined and some observations made as seen in the figure 3.38 below. From the figure it is observed that the micro-damping parameter variation has little or no effect on the value of the breakaway friction force predicted figure 3.38a, thus the velocity at breakaway for the various values of the damping remain about the same figure 3.38b. This thus corroborates what was earlier indicated in figure 3.13. In figure 3.41a, it is observed

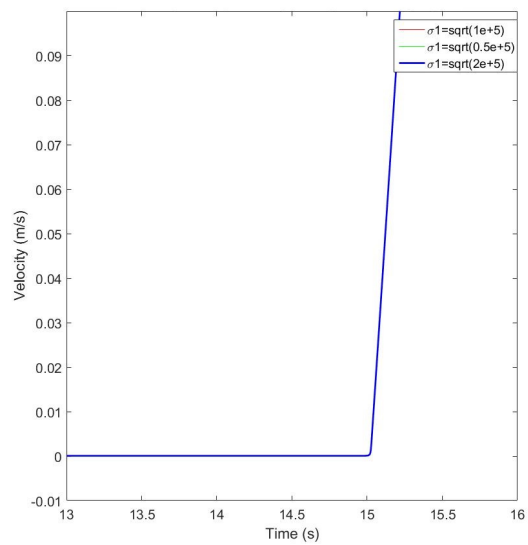
that the breakaway friction force seems to be lowered in response to increasing values of the breakaway (Z_b) parameter this indicates the possibility of gross sliding to be initiated faster as the parameter decreases as in figure 3.41b. This also appears to validate the observed behaviour in figure 3.15. The Stribeck parameter (v_s) variation as it affects the breakaway friction is illustrated in figure 3.39. Figure 3.39a shows the breakaway force to increase as the Stribeck value increased and also the velocity corresponding to such values increase thus indicating that the higher the Stribeck value the longer it will take for true sliding to be initiated, figure 3.39b. Variations of the τ parameter is shown to have little effect on the breakaway friction force, however on close examination one sees that this parameter seem to enhance the transition from stick to slip thus reducing the steepness of the slope as seen in figure 3.40a below and corresponded by the velocity time plot of figure 3.40b.

3.7 Chapter summary

A new dynamic model of friction capable of modelling most relevant friction features such as the pre-sliding hysteresis with non-local memory, Stribeck effect, stick-slip motion, frictional lag, non-drift property has been presented. The model was shown also to exhibit some properties such as uniqueness, boundedness, stability and dissipativity. A describing function equivalent for the hysteretic friction function was also obtained and used for limit cycle prediction. A comparative analysis of the proposed non-drift dynamic friction model and some of the more relevant models of friction such as the LuGre, Elasto-Plastic, GMS, and Xiong models was performed to demonstrate their ability to capture relevant feature of the friction phenomena. The proposed non-drift dynamic friction model showed a higher level of robustness to parameter variations from the sensitivity analysis performed, especially in the low velocity (below the Stribeck). It will be illustrated in the next chapter the ease of identification of the pre-sliding parameters of the model which renders the model more appealing than the multi-element models.

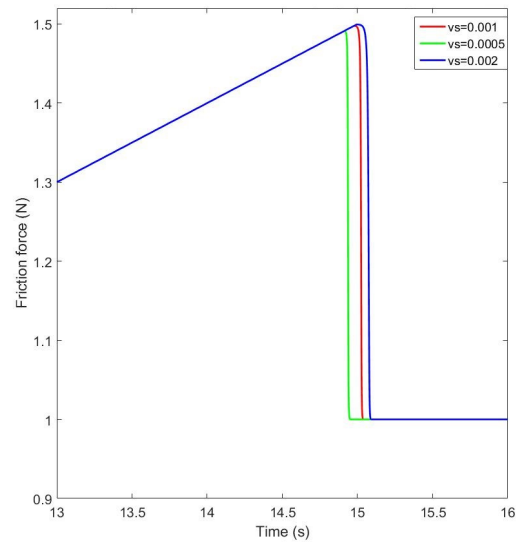


(a)

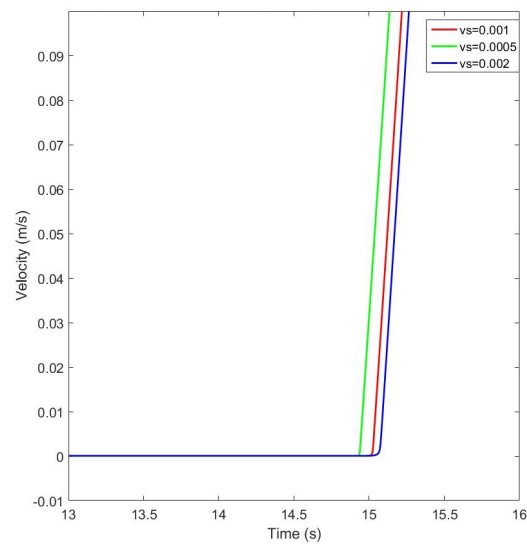


(b)

Fig. 3.38 Sensitivity of the breakaway friction for different values of the micro-damping parameter (σ_1): (a) Force-displacement plot, and (b) Force-velocity plot

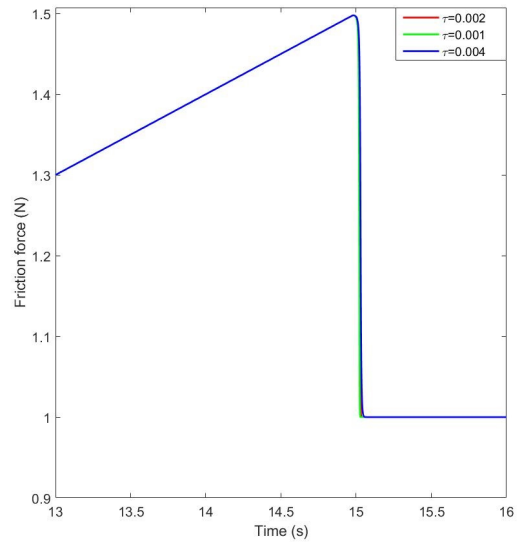


(a)

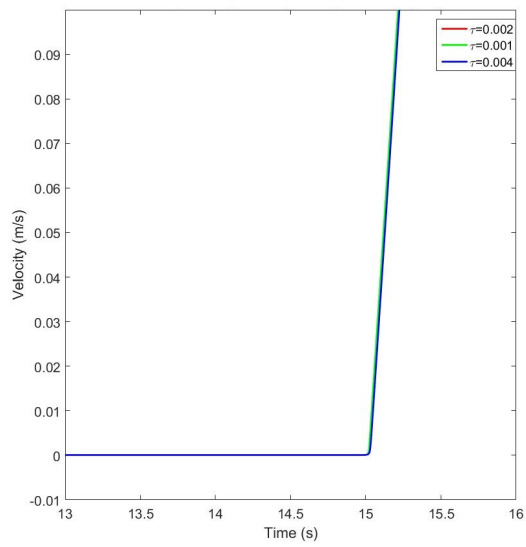


(b)

Fig. 3.39 Sensitivity of the breakaway friction for different values of the Striebeck parameter (v_s) (a) Force-displacement plot, and (b) Force-velocity plot

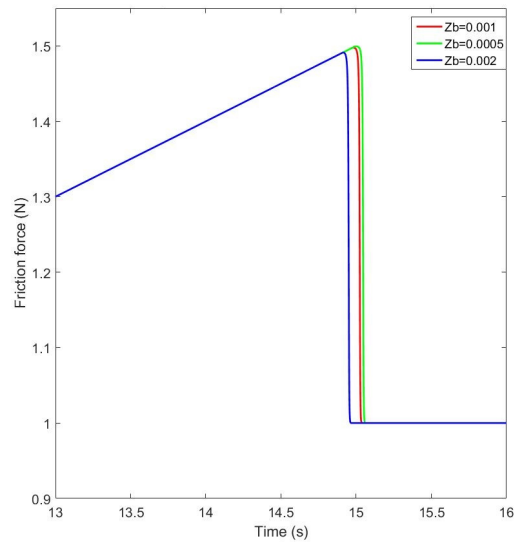


(a)

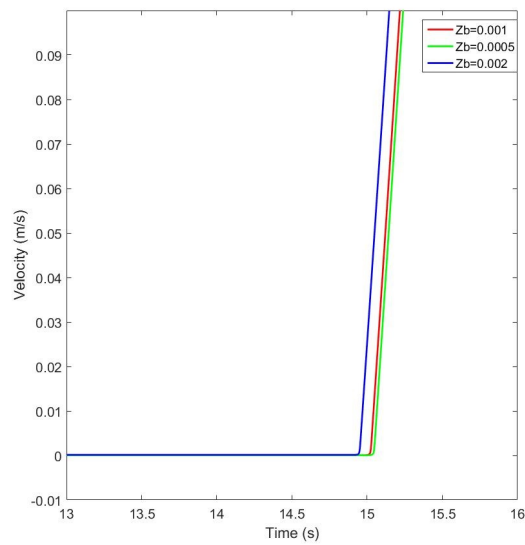


(b)

Fig. 3.40 Sensitivity of the breakaway friction for different values of the τ parameter; (a) Force-displacement plot, and (b) Force-velocity plot



(a)



(b)

Fig. 3.41 Sensitivity of the breakaway friction for different values of the breakaway displacement parameter (Z_b): (a) Force-displacement plot, and (b) Force-velocity plot

Chapter 4

Friction Characterization and Identification

4.1 Introduction

Features of friction such as the pre-sliding hysteresis, frictional-lag, breakaway variations, and the Stribeck effect; which are largely non-linear in nature make modelling and control of friction a challenging task for the control engineer. Most of the existing models of friction are grouped as either static or dynamic depending on whether they are able to model friction dynamics as exhibited by real systems experiencing friction. Some of these models show greater representation of friction than others though generally at the expense of some other relevant factors such as computation complexity, simulation efficiency. The purpose in this chapter is two-fold;

1. To investigate relevant friction features/ characteristics on an experimental test-bed designed for the purpose, and
2. To estimate parameter values of the various friction models such as the proposed, LuGre, GMS and Xiong models that adequately capture these friction characteristics for control purposes.

To achieve these, experiments were designed and performed using an experimental friction test-rig specifically designed and constructed to test and determine friction characteristics of surfaces subjected to relative motion. The experiments reflect the various features of friction as it is impractical to design a single experiment capable of demonstrating all relevant phenomena of friction. Constant-velocity experiments were performed to capture the Stribeck effect which is an important characteristic of the friction phenomena. The second experiment

was the frictional-lag experiment designed to show the time-lag between the friction-torque and the corresponding velocity for non-constant velocity signals. Friction-displacement experiment was performed in the pre-sliding regime to obtain the hysteretic features of friction with non-local memory characteristics against the previously held opinion of non-memory based hysteresis. Optimization methods were then used to obtain suitable model parameter values which yield best fit results for the various models used for the identification.

Thus a brief description of the test rig and the various equipments used for the experiments form part of section 4.2, and describes the experimental set-up for the characterization of the friction non-linearities. In section 4.3, a general model of the dc motor servo-based system used to perform the experiments is derived. Section 4.4 sets out the experiments performed for the determination of various friction characteristics. In section 4.6 the task of system identification, dealing with the parameters estimation for the various models studied was carried out. A more general discussion on the observations noted during the various experiments and identification were elaborated upon also. The chapter ends with a summary, section 4.7.

4.2 Materials and Methods

An experimental test-bed for friction characterisation and control was developed in the control laboratory with the SRV-02 as the base plant. The experimental test-bed is made up of the following:

1. A Quanser universal power supply module: This is a power amplifier for driving the servo-plant and has the following specifications:
 - (a) A single +/- 12 Volt DC Power Supply
 - (b) 4 Analogue sensor (for bias and measurement) inputs
 - (c) A single sensor output port (To A/D) feeding all the sensor inputs to the DAC
 - (d) An amplified analogue power output to drive the servomotor.
 - (e) The reference input to be amplified is fed from the D/A output of the CAD to the servo-motor load via the 'To load' of the UPM.
 - (f) Test ports for external signal monitoring.
2. A Quanser servo-plant (SRV-02) with the following components:
 - (a) DC servo-motor: Single coreless motor as the actuator, a product of Faulhaber, with model number 2338006S with specifications; nominal operating voltage

of 6 Volts DC, maximum power output of 3.23Watts, terminal resistance of 2.6 Ohms, efficiency 0.69, stall torque 2.42 oz-in, torque constant 1.088 oz-in/A, rotor inductance 180 micro Henry, back emf constant 0.804mV/rpm, maximum (no load) velocity 7,200 rpm. An internal gear box (gain of 5) driving external gears in a high torque delivery mode with a gain of 14. Thus making the output torque 70 times greater than that at the motor shaft. The input to the motor is from the 'To load' of the UPM.

- (b) A model 132 potentiometer from Vishay Spectrol: This measures the absolute angular position of the load gears. It consists of a single turn wire-wound sensor of 10 kilo-Ohm resistance, an output voltage range of ± 5 volts over its degree range of 352 continuous electrical degrees. A power rating of 2.75 watts.
 - (c) An optical encoder (from US Digital S1) is a single ended encoder for measuring the relative angular position of the load shaft. This incremental encoder has a voltage output of 5VDC with high resolution of 4096 counts per revolution in the quadrature mode or 1024 lines per revolution usually operated in the quadrature mode. The encoder output is connected to the DAC without first routing it through the UPM.
 - (d) A model series 2251U006S1.5G tachometer TACH, used to measure the angular velocity of the motor shaft has an EMF constant of 1.5mV/rpm and continuous operating speed of less 5,000 rpm. The tachometer is connected directly to the actuator motor to ensure accuracy in the measurements and timing latencies in the response are eliminated. The output of the TACH is connected to the UPM from which it is fed to one of the DAC A/D input channels.
3. A torque sensor from FUTEK: MBA500 model and item no FSH00752. It is multi component dual sensor measuring Thrust and Torque, has an output sensitivity of 2mV/V rating and maximum output torque of 23Nm. Input excitation is a maximum of 18 volts (ac or dc) 10 volts DC used in the experiment, the bridge resistance is 350 Ohms, it weighs 184g.
 4. A CSG110 amplifier from FUTEK: This amplifier supplies the excitation voltage of 10 volts dc to the torque sensor, has the following settings: Input voltage range: 14-26V (15 volts Dc used in the experiment), desired output range: 5-10 VDC. For the experiment the input gain is set to 2mV/V for excitation of 10vdc and 4mV/V for an excitation of 5vdc.

5. Q2-USB Data Acquisition Card (DAC): This is a compact Hardware-In-the-Loop (HIL) control board from Quanser, some of its relevant features are: a 2 ADC input channels(0,1), 2 DAC output channels (0,1), 8 digital input/ output pins which can be configured to user need, 2 single-ended encoder input channels with 4X quadrature decoding, a power/ watchdog LED, 2 Pulse Width Modulated (PWM) digital outputs. Also real time target support for Quanser QUARC windows target and API. A USB 2.0 cable for connection to a PC. The DAC is driven by quarc software interfaced with MATLAB/SIMULINK for real time acquisition and processing of data.

4.2.1 Set-up for characterisation experiments

The diagram representing a picture of the experimental test-bed set-up is presented in figure (4.1), and it consists of many components such as the torque sensor, friction load discs, the SRV-02 rotary servo system (housing the motor, tachometer and the encoder), and power supply source. The SRV-02 rotary servo from Quanser is powered by a dc power supply providing needed dc to drive the motor, the angular speed of the motor shaft is measured by the tachometer attached to the motor shaft, and the encoder measures the angular position of the load disc in a quadrature mode, see figure 4.3. The friction load discs are made from mild-steel, Aluminium and copper with coefficients of friction given in table 4.1 below. The

Table 4.1 Friction discs and their coefficients of friction for dry surfaces

Disc material type	static friction coefficient	kinetic friction coefficient
Mild-steel/Aluminium	0.61	0.47
Mild-steel/mild-steel	0.74	0.57
Aluminium/Aluminium	1.05-1.35	1.4
Copper/Aluminium		
Copper/Copper	1.21	-

friction torque between the static and moving discs are measured using the torque sensor coupled to the static disc. A data acquisition card was used to interface the hardware (SRV-02) with the Quanser Quarc software running on a PC. This software is accessed using the MATLAB/SIMULINK software tool to run the real time experiment.

The friction discs, torque sensor and the motor shaft are aligned properly to ensure a uniform distribution of normal load over the entire surface.

Friction is a result of the relative motion of the motor shaft and the static load disc and is measured by a torque sensor connected to the load disc. The torque sensor is also powered through a 14v dc power supply and amplified by the CSG110 amplifier to provide the right

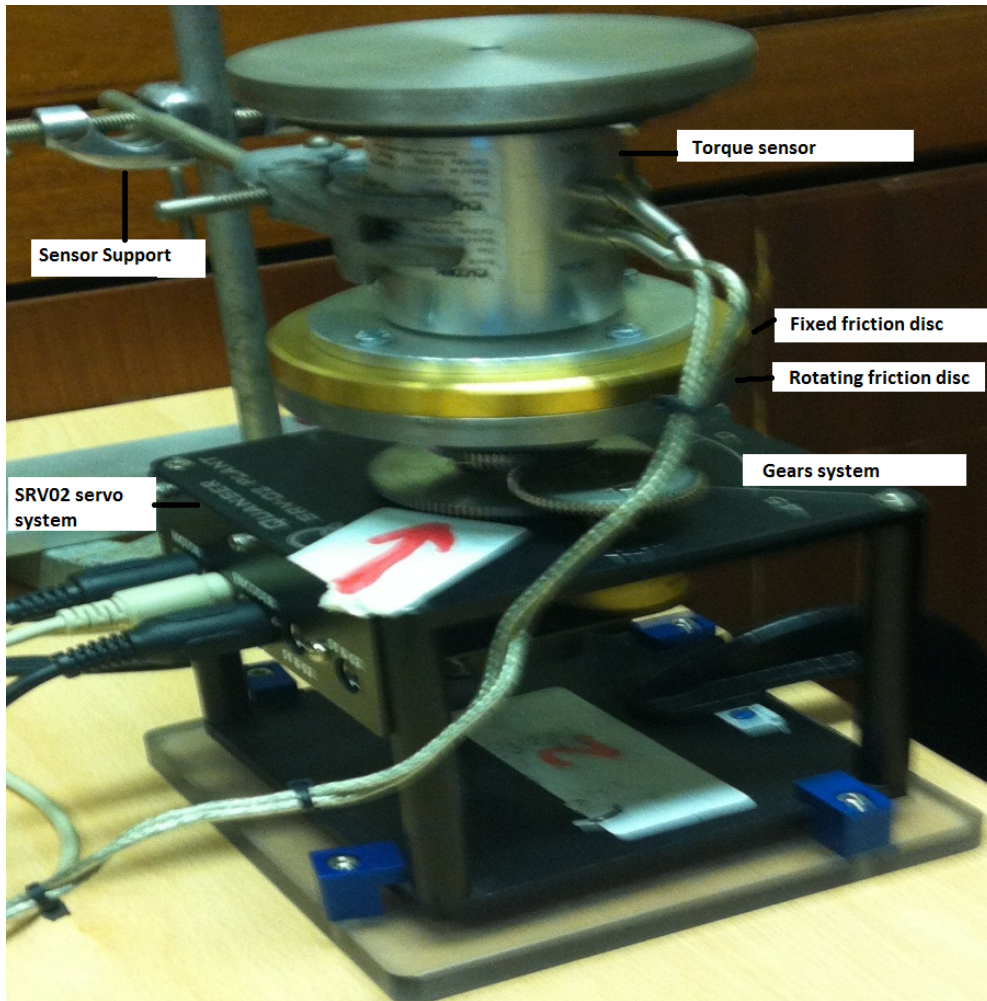


Fig. 4.1 A picture of the friction test rig

excitation to the torque sensor. Various experiments were then carried out using different input references in the SIMULINK environment as would be described in later sections.

4.3 Model structure of the experimental test-rig

Friction in the DC motor actuated test-bed used can occur at the motor shaft, brushes, in the gear transmission systems, and in the disc load surfaces. For the control of motor driven systems the need to model friction phenomena in the motor and the entire system set-up is very important since the linear model derivation for the motor friction is not adequate to account for the non-linear nature of friction especially for high precision tracking and control. The general model of the electric motor (Permanent Magnet DC type) driven system can be obtained from the schematic shown in figure 4.2. Splitting the figure into its electrical and

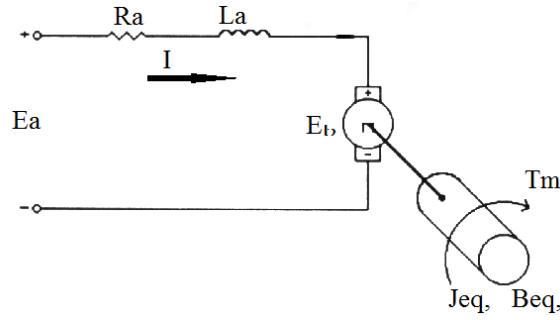


Fig. 4.2 The schematic representation of the DC-servo motor system

mechanical sides for easy analysis. For the electrical side the governing equation is

$$E_a = E_b + IR_a + L_a \frac{dI}{dt} \quad (4.1)$$

where E_a is the motor armature voltage of the motor, E_b motor induced back EMF, R_a the armature resistance, and I is the armature motor current, and L_a the motor inductance.

The induced back EMF causes the rotation of the motor shaft with an angular velocity, ω_m . The back EMF is related to this angular velocity by a constant called the back EMF constant K_b by the following

$$E_b = K_b \omega_m \quad (4.2)$$

The mechanical torque transmitted to the motor shaft T_m as a result is related to the armature current I by

$$T_m = IK_t \quad (4.3)$$

where K_t is called the motor torque constant.

The mechanical torque K_t constant has been shown to be equivalent to the emf torque constant K_b and as such are represented as the constant K_m . For an ideal motor the total power generated at the back emf equals the total power transmitted to the motor shaft in form of torque so that equations (4.2) and (4.3) are equal. The motor shaft is connected to the load via a set of gears as shown in the figure 4.3 for the transformation of the torque or angular velocity (position). Given that the gear transmission ratio A is given as

$$A = \frac{n_l}{n_m}$$

with n_m as the number of teeth on the motor side gears and n_l number of teeth on the load side gears. Thus A relates the motor angular velocity (position) to the gear-box output shaft

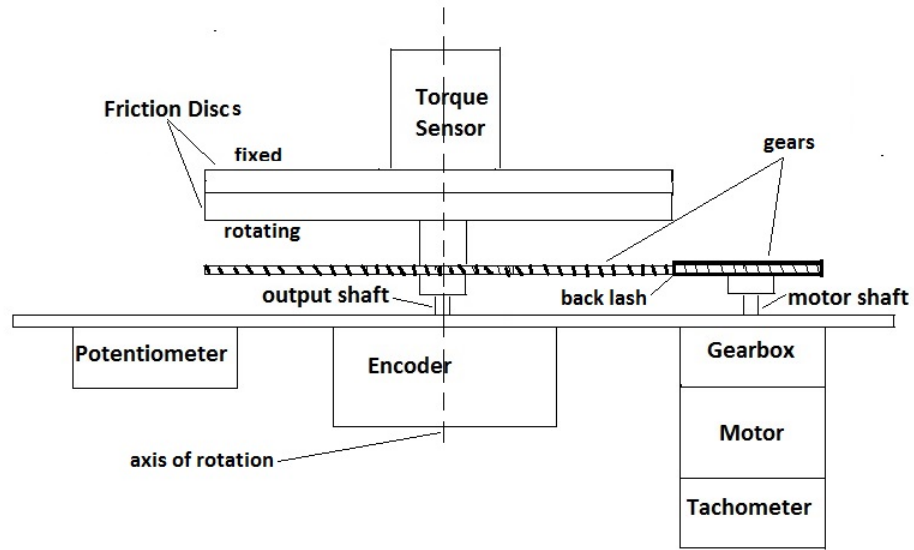


Fig. 4.3 The schematic representation of the system test-bed showing the arrangement of gears, friction discs and sensor positions

angular velocity (position) by this

$$A = \frac{\omega_m}{\omega_l}$$

for velocity relation, and

$$A = \frac{\theta_m}{\theta_l}$$

for position relation.

The torque produced at the motor shaft is

$$T_m = J_m \dot{\omega}_m + J_l \frac{\dot{\omega}_l}{A} + b_m \omega_m + b_l \frac{\omega_l}{A} \quad (4.4)$$

where $J_l \frac{\dot{\omega}_l}{A}$ is the load torque (due to load inertia J_l) reflected to the motor shaft, and $b_l \frac{\omega_l}{A}$ the load frictional torque reflected to the motor shaft.

But $\omega_m = A \omega_l$

thus

$$AT_m = (A^2 J_m + J_l) \dot{\omega}_l + (A^2 b_m + b_l) \omega_l \quad (4.5)$$

If

$$J_{eq} = (A^2 J_m + J_l)$$

is the equivalent inertia and

$$B_{eq} = A^2 b_m + b_l$$

the equivalent frictional damping. But the load (or output) torque $T_l = AT_m$ therefore, the torque output of the gear box is

$$T_l = AT_m = J_{eq} \dot{\omega}_l + b_{eq} \omega_l \quad (4.6)$$

Substituting the Laplace transform of eqns. 4.3, 4.2 and 4.1 into the above equation 4.6 expressed in Laplace, with E_a the armature voltage as input, and ω_l as the output of the test-bed leads to

$$AK_m E_a(s) = (J_{eq}s + B_{eq})(R_a + L_a s) + (AK_m)^2 \omega_l \quad (4.7)$$

whose transfer function becomes

$$\frac{\omega_l}{E_a(s)} = \frac{AK_m}{(J_{eq}s + B_{eq})(R_a + L_a s) + (AK_m)^2} \quad (4.8)$$

For most dc motors the value of the electrical time constant represented by the armature inductance L_a is often much less than the mechanical time constant represented by the armature resistance R_a . Thus the fast dynamics of the electrical time constant with fast decay implies that the resulting transient response could be ignored. Therefore, the armature inductance L_a could be removed in the above expression without introducing much error. This approximation simplifies the equation by reducing the order of the transfer function by 1, [115], [116].

$$\frac{\omega_l}{E_a(s)} = \frac{AK_m}{(J_{eq}s + B_{eq})R_a + (AK_m)^2} \quad (4.9)$$

which is a first order system.

Given that the output of interest is the position θ_l and using the relation

$$\theta_l = \frac{1}{s} \omega_l$$

then

$$\frac{\theta_l(s)}{E_a(s)} = \frac{AK_m}{s((J_{eq}s + B_{eq})R_a + (AK_m)^2)} \quad (4.10)$$

Equations 4.9 and 4.10 are the transfer functions for velocity and position outputs respectively. The frictional damping term B_{eq} comprising the frictions in the motor, gear and load is here modelled as a linear function of the output velocity though in reality this linear function is non-linear and not only a function of the velocity but also of the displacement (in the pre-sliding regime). In the previous chapter a model of this friction non-linearity was presented

and will later be used for identification purposes. One major objective in this chapter is the characterisation of this friction and to obtain various representations of its features. Equations 4.9 and 4.10 are the general velocity, position model structures for the friction test-bed used for the experiment. To obtain a simplified linear model from the above models the friction term represented by the B_{eq} is thus removed and the equations reduce to the following linear models for the velocity and position respectively

$$\frac{\omega_l}{E_a(s)} = \frac{AK_m}{J_{eq}sR_a + (AK_m)^2} \quad (4.11)$$

and

$$\frac{\theta_l(s)}{E_a(s)} = \frac{AK_m}{s(J_{eq}sR_a + (AK_m)^2)} \quad (4.12)$$

these two equations would be used for the simulations in chapter 6 to compare the performance of the simulated model with friction effect modelled by the proposed new model presented in the previous chapter. The parameters of the friction test-rig are contained in the specification sheet as supplied by the manufacturer, however relevant values are as presented later in this chapter.

4.4 General procedure for identification of friction models

As seen from the equations and the relevant block diagrams, the identification aim is the determination of the overall friction effect in the system comprising the actuator friction, the gear friction, and the friction as a result of the disc surfaces and there from through optimisation techniques obtain the parameters for the model earlier proposed in chapter 3. This friction effect in the system was modelled by the viscous equivalent B_{eq} . The aim is thus to find a non-linear model to characterize true friction since the linear representation does not effectively capture the low velocity and reversal velocity dynamics associated with friction. In other to achieve this objective some steps were taken, these are typically categorised as;

1. Set-up of adequate experiments; once the motivation for the determination of the system's model has been established, optimal design of experiment from which the data set will be generated follows. It is here that what to be identified, nature of the input excitation signals appropriate for the experiments, outputs, and how to measure (acquire) them, and other necessary assumptions are made. Also decisions on whether the experiments be carried out under open or closed loop conditions. In the experiments that follow the nature the various inputs used to capture the different friction features

are explained in the respective experiments. Unless stated otherwise most of the experiments performed were carried out in closed-loop.

2. Acquisition of data set; here the required data sets (say input and output data set) are often acquired via data acquisition cards like the USB-Q2 card from Quanser used in this research. Most instruments for measurements are of the digital type therefore issues like sampling rate are relevant so as to avoid errors resulting from aliasing and the likes. These data acquired often includes some level of noise either introduced by the set-up, measuring instruments, or the environment, thus may need to be "treated". Removing the effects of noise and quantisation due to the torque sensor sensitivity and capacity used was necessary. To do this a filtering algorithm in matlab environment was used namely 'sgolayfilt (torque-data,3,31)', which is a Savitzky-Golay filtering algorithm. In particular this was useful to remove the noise embedded in the measured velocity and the quantisation effect of the torque sensor on the measured friction torque.
3. Model structure selection; as mentioned earlier, insight into the physical system and available knowledge are useful in choosing a model structure. Information from the observed data set is also relevant in this process. Sometimes a trials and error approach or application of some statistical tools could yield adequate model structures for a set objectives.
4. Model parameters estimation; unknown parameters of the model structure are determined by an estimation process which usually leads to a problem of minimizing a cost function. This process yields estimated values of the parameters of the system model used for the identification such as the proposed friction model.
5. Validation of identified model; finally the parameters of the model and its structure pass through a validation process to ascertain how true it represents the real system. Sometimes a series of models and model parameters are generated and the one yielding a parsimonious results in a generalised sense is then chosen.

Generally, 1 and 2 above suggest some series of experiments be performed on the friction experimental test-bed designed for the purpose. More detailed discussion on this is grouped under friction characterisation experiment in the next section 4.5 (discussing items 1 and 2), and friction identification task section 4.6 (discussing items 3, 4, and 5) above.

4.5 Friction characterisation

In this section experiments were designed and performed to accomplish tasks 1 and 2 above. These series of experiments performed on the friction experimental test-bed were designed to target the various relevant friction phenomena such as the Stribeck effect, the lag phenomenon, and the pre-sliding friction hysteresis with non-local memory. The nature of the input-output data set was determined prior to the experiments so as to capture the characteristics of interest. Also discussed in this section are the results obtained from the experiments and how they agree or otherwise with other similar experiments as performed by other researchers.

Characterisation experiments

The following experiments have been designed to capture the friction non-linearities as observed in physical systems;

1. Experiment 1: Friction-constant velocities characterization; To determine the steady state friction torque-velocity relationship.
2. Experiment 2: Friction-varying velocities characterisation; To determine the frictional torque as a function of time varying velocities.
3. Experiment 3: Pre-sliding hysteresis characterisation; To determine the friction torque-displacement relationship in the pre-sliding regime. This is the friction-hysteresis effect with non-local memory.
4. Experiment 4: Friction-varying velocity rate characterisation; To determine the static friction (stiction) and the varying breakaway characteristics

4.5.1 Experiment 1

Friction-constant velocities characterization:

Objective: Determination of friction torque-velocity relationship for a range of constant velocities.

Background: Previous researches as pointed out earlier in this report (see chapter 2) indicates that at very low velocity ranges the friction curve has a negative slope for velocity increments. However, beyond a velocity threshold called the Stribeck velocity (v_s), the friction torque-velocity relation becomes more linear and positively sloped. This behaviour is thus termed the Stribeck effect. There have been many model representations of the friction-velocity feature. A closed loop (velocity feedback) is adopted in the series of constant-velocity experiments to take advantage of its appeal and merits over the open loop. Some of these merits are:

Reduction in the system's sensitivity to disturbance, reduction in the time constant thus making the system track input changes faster, and stability features. To ensure appropriate tracking of the reference velocity, a proportional controller in series with a lag-compensator was used for the system.

Procedure: For each reference velocity input the system was run for 15 seconds and the load side velocity measured using the tachometer at a rate of 1ms obtaining a total 15000 data points. The first 3,000 and the last 1,500 of these measured data were discarded and the average of the remaining obtained as. This was done to ensure the elimination of transient behaviours thus allowing the system settle to its true value since for this experiment the interest is the steady state values. The value of the friction torque was also measured by the torque sensor and recorded for the same data points as for the measured velocity. For each velocity reference, the experiment was performed 10 times and the mean value recorded as the final friction torque, velocity data point. This was done to eliminate errors and thus increase the accuracy of the data in the light of its true value and it was observed that 10 runs were adequate for the purpose. The reference velocities for the steady-state experiment range from very low values of 0.03 rad/sec-to-4. rad/sec since lower values does not show any form of motion whatsoever. Thus a total of 80 friction torque-velocity data points was obtained and two different sets of experiments performed the results of which would be used for the identification and validation of the models in the next section. Figure 4.4 captures the results.

4.5.2 Experiment 2

Friction-varying velocity characterization:

Objective: To determine the frictional torque variation as a function of varying unidirectional velocities.

Background: There is a relative time-lag between the friction torque and the corresponding velocity, in the sense that the system-friction does not respond instantaneously to system inputs. This lag gives rise to a hysteresis effect in the velocity regime similar to the hysteresis effect in the pre-sliding displacement regime. Research shows that the frictional torque is larger for increasing velocities (acceleration) than for decreasing velocities (deceleration), the loop of the frictional lag encloses the Stribeck low velocity curve indicative of the vanishing of the former for increasing velocities. Thus the constant velocity-friction torque curve at low velocity acts as an attractor to both the acceleration and deceleration friction torques.

Procedure: In designing the experiments, a time varying periodic and unidirectional reference signal was applied. To obtain this a pure sinusoidal signal was superimposed upon a constant

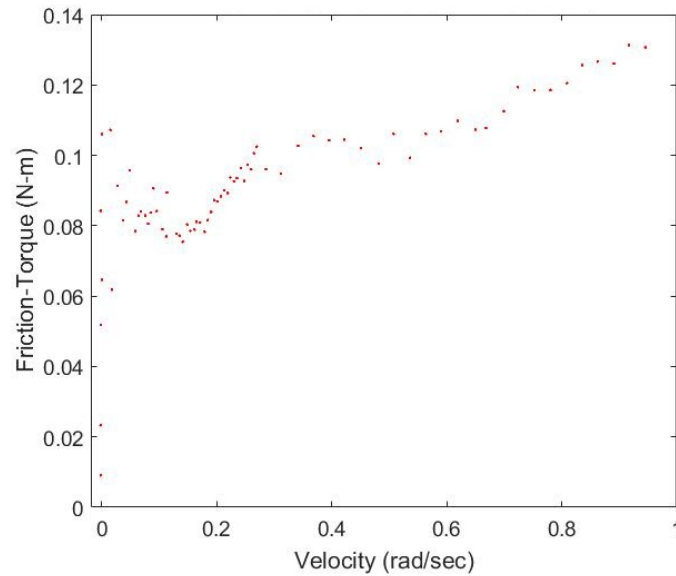


Fig. 4.4 The friction torque measured against velocity for the constant velocity friction experiments

positive signal whose value is greater than the amplitude of the sine sinusoidal signal. This is to ensure adequate capture of low velocity variations as a function of time without the signal swinging between positive and negative values. To achieve this a sinusoidal velocity signal of the form was used

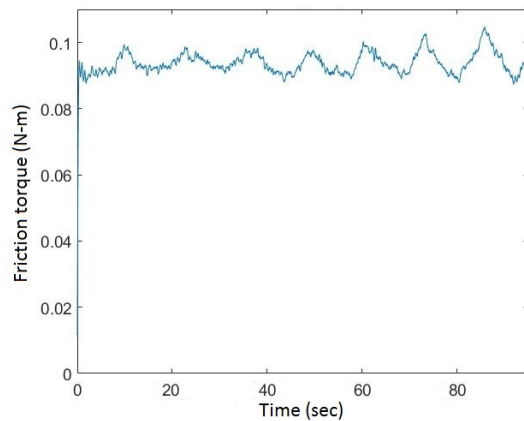
$$v(t) = A + B \sin(\omega t) \quad (4.13)$$

where A is a positive bias velocity signal chosen in such a way as to ensure the velocity is always unidirectional ie B is less than A . the values of omega are: 1, 2, and 5 rad/sec.

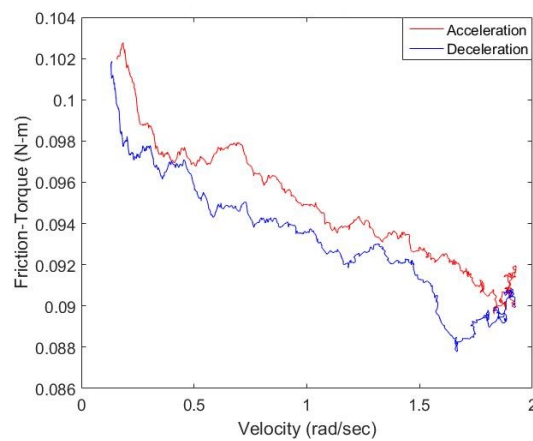
Constraint: The variables B and A have to be chosen so as to make the total velocity fall in the range so as to capture the Stribeck slope as suggested in the experiment 1. A was chosen to ensure positiveness of the time varying velocity at all times. So $B = 1$, and $A = 0.95$ and as such the periodic velocity becomes:

$$v(t) = 1 - 0.95 \sin(\omega t) \quad (4.14)$$

The choice of these values were such that true sliding is ensured avoiding periods of sticking and zero or reversal velocities. For each run of the experiment, the corresponding values of the friction-torque and velocity were obtained for the acceleration and deceleration regimes. The experiments were performed as in experiment 1 above and the average of the measured friction-torque and velocity recorded. Various frequencies of $\omega = 2, 5$ and 10 rad/sec, were used to run the experiment and the data sets recorded. Identification and validation data sets



(a)



(b)

Fig. 4.5 The Frictional-Lag experiment: **(a)** Torque output against-time, and **(b)** The lag plot average showing friction torque variations the acceleration and deceleration velocity regimes of the unidirectional signal

were collected from two separate experiments to be used in the next section. The data set for the validation was based on a system with frequency of 5 rad/sec while the identification data was based on a chirp signal (10 rad/sec). The same block diagram scheme as in the constant-velocity experiments was used to perform the frictional-lag experiments. The results so obtained is shown as figure 4.5b.

4.5.3 Experiment 3

Pre-sliding hysteresis characteristics

Objective: To determine the hysteretic relationship between the friction-torque and pre-

sliding displacement

Background: As stated previously, the pre-sliding hysteresis with non-local memory has been established as against the non-memory based behaviour earlier believed to govern the pre-sliding regime. This characteristic is independent of the velocity of the bodies in contact indicative of the pre-dominance of the elastic deformation characterizing the bristles behaviour. A simple position controller was designed to be used to carry out the experiments as shown in the figure below to ensure appropriate regulation.

Procedure: The experiment to determine this relationship friction has with displacement was performed in two stages as follows;

Stage 1: A ramp torque signal was injected into the system slowly incrementing it till the time gross-sliding was initiated and the surfaces moving relative to each other. This process was repeated several times and the average friction torque and the corresponding torque input were recorded thus giving us a range of values for which the system is in the pre-slide condition and that beyond which a relative motion was observed. This breakaway friction-torque is generally called the Stiction torque. The value of the pre-sliding displacement was also obtained to determine a range of values for the pre-sliding displacement before breakaway. By this the breakaway friction torque, and the corresponding breakaway displacement were obtained. In the same way, a negative signal was used to determine the range for the negative breakaway torque and the corresponding breakaway displacement.

Stage 2: A special input displacement signal shown as figure 4.6a was then used to ensure the Stiction torque range as earlier determined in stage 1 above was never exceeded both in the negative and positive going reference signal inputs. The measured friction torque from the experiments is shown in figure 4.6b. This experiment was done in same manner as in experiment stage1 and their average values for friction-torque shown in figure.

4.5.4 Experiment 4

Breakaway friction characteristics

Objective: Determination of the breakaway (Stiction) torque and varying breakaway friction characterization.

Background: Upon external torque exertion (say a ramp signal), a stationary system does not immediately go into sliding until the input torque becomes large enough to break the forces of adhesion between the surfaces after which relative motion is initiated. As stated previously this value of friction-torque for which the gross-sliding is initiated is called the breakaway torque or simply the Stiction-torque. The experiment for the determination of this friction feature was thus designed with the input being a ramp signal. The breakaway

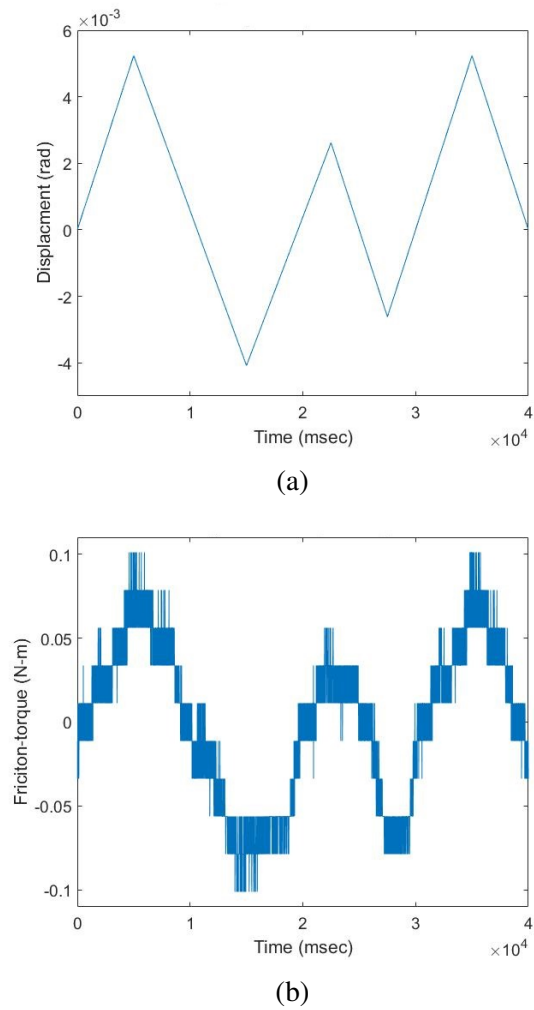


Fig. 4.6 The Pre-sliding Hysteresis with non-local memory **(a)** Reference input signal, and **(b)** Measured hysteretic friction-torque output showing quantisation

friction-torque has also been variously reported to vary in response to variations in the rate at which the input force is varied.

To investigate these features namely; the breakaway torque and its variations in response to variations in the input, two different experiments were performed. They are the Stiction experiment and the varying breakaway experiment.

Stiction experiment

Similar to the stage 1 in experiment 3, a slowly incrementing input ramp signal was introduced into the system and the output velocity and friction-torque observed and recorded. The signal lasted till there is an observed sliding of the surfaces showing transition from stick-to-slip regime of friction. At this point the friction-torque was observed to sharply fall and settle to a lower (kinetic friction torque) level before gradually rising again as the signal continued to rise. A series of runs were performed and the average obtained and recorded to improve accuracy and repeatability.

Varying Breakaway experiment

Some time-varying input torque signals were introduced into the test-bed with their properties such as amplitude being the same. These conditions are quite similar to that of experiment 2 for the frictional-lag behaviour and hence suffices to illustrate this relationships since the torque input is proportional to velocity input, though our interest is on what happened in the pre-sliding to just after the gross-sliding was initiated. As such the various frequencies represent the varying rates of input signal application. The rates investigated are; 1 rad/sec, 5 rad/sec and 10 rad/sec, and the relationships shown in figure 4.7. From this figure it is clearly shown that the greater the rate of change of the input torque the larger the breakaway (Stiction) torque and also the larger the breakaway displacement.

4.5.5 Analysis of results of characterisation experiments

Here an analysis of the various results obtained from the experimental test-bed designed to study friction behaviour in the laboratory is presented. The presentation is structured similar to the previous section for the various characterisation experiments.

Constant-velocity characterisation results

During the run of the experiments it was observed that as the velocity is incremented from zero with a step of 0.03 rad/sec the rig showed no relative motion, the offset error due to the tachometer was corrected. Increasing the input signal the torque output was observed to increase, though the output velocity remained zero indicating static friction build up. From a velocity value of 0.1 rad/sec, the system was noted to begin to show momentary motions

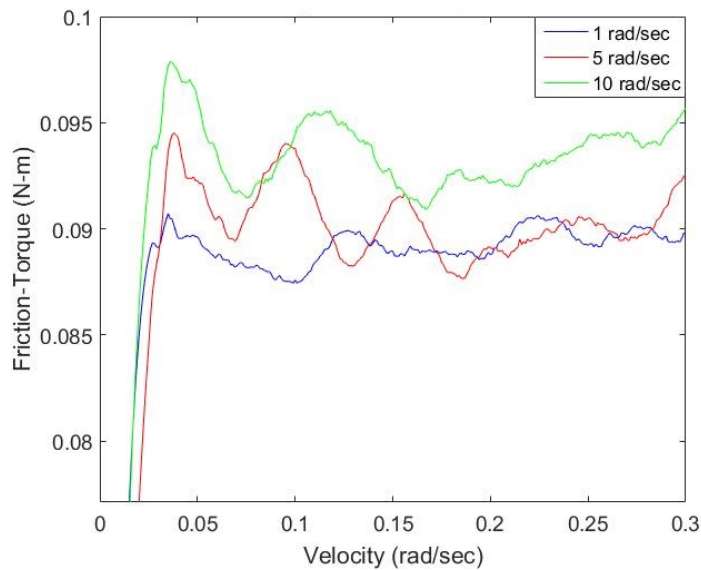


Fig. 4.7 Friction torque against velocity showing friction dependence on the rate of application of force

marked with periods of elongated slip followed by small stick. This region was characterized with moments of slip and stick motions. Suggesting the exhibition of stick-slip motion discussed in chapter 2. The system continued with this motion pattern with increasing slip moment and decreasing stick moments. Basically this marked the transition range from sticking regime to the gross-sliding regime was shown to be a range of values rather than single valued. Also the moment the disc began to exhibit increased slip the torque sensor reading indicated a fall in the values of the measured torque between the surfaces after which it tends to be more constant. This behaviour is indicative of the fact that for the system the stiction (static) friction is greater than the coulomb (kinetic) friction. This torque at the point of slip is the stiction or the breakaway torque and the friction at constant motion the coulomb-viscous friction. From the plot of the friction-torque versus velocity shown in figure 4.4, it is obvious that at low velocities (between 0 and 0.2 rad/sec) the friction-torque generally decreases as the velocity increased typical of the Stribeck effect of friction at low velocities. Research findings support this important feature of friction as earlier highlighted in the literature review. From the figure, in the region of low velocities one notes that the friction velocity measurements are rather erratic with much variation but generally showing a negative slope in an exponential manner. This relative high degree of variation in the low velocity underscores the fact that friction is very difficult to effectively capture and model in this range of velocities. This could be due to forces of adhesion, and non-uniform asperity deformations, whether the net bristle distributions are in trough (valley) or on mountain contact scenario.

Other factors contributing to this large variations are system noise in the measuring devices like the torque sensor and environmental factors such as temperature and lubrication. From the graph of figure 4.4, the medium to high velocity range (from 0.2 and above) there seemed to be a more linear relationship between the friction-torque and the velocity as the measured torque steadily increased as velocity increased. This behaviour is also evidently supported by many research findings. In this medium to high velocities range, the friction torque could easily be modelled using classical models of the coulomb-viscous model with minimal errors. This behaviour of the friction phenomenon as a function of increasing velocities from zero is thus called the Stribeck effect and the graph of the relationship the Stribeck curve.

Varying velocity characterisation results

Close examination of the frictional-lag features of figure 4.5b suggests some erratic behaviours (for velocities much lower than the Stribeck velocity) whereby the friction torque at a particular velocity instant is seen to be lower in the acceleration regime than the deceleration regime contrary to the general known friction behaviour. Generally, results of figure 4.5b for the varying velocity characterisation experiment showed a correspondence with research findings, [20], [34]. In the experiment it was observed that the friction torque corresponding to a given velocity does not happen instantaneously but after some lag in time and as such the torques for acceleration periods were higher than those for deceleration. The width of the lag was seen to widen as the reference input velocity rate increased. In other to relate this inputs rates were varied as 2 rad/sec, 5 rad/sec, and 10 rad/sec. The results of these effect was rather made more pronounced using the proposed model as illustrated in the friction lag identification of next section and agreed with other research findings of chapter 2.

Pre-sliding hysteresis characterisation results

The graph for the pre-sliding experiment showed the non-local memory characteristic of this regime as explained in chapter 2. This dynamic behaviour suggests friction to be displacement dependent in the pre-slide regime and independent of velocity of motion between the surfaces. From the results of the pre-sliding experiments performed figure 4.6b, the following observations could be made

1. The asymmetric nature of friction such that the negative velocity regime and the positive velocity regime each give rise to different parameter values like Stiction, Coulomb force etc.

2. That friction is mostly non-linear near zero velocities and at zero velocities.
3. That friction is proportional to displacement in the pre-sliding regime and may not necessarily be zero at zero displacement.

As a result of the foregoing it is not easy to capture the rich dynamics of the pre-sliding regime of the friction phenomenon.

Worthy of note is the observation that the friction torque as measured by the torque sensor appear quantised. This is primarily due to the measured torque values being very small (in the pre-sliding regime) in comparison to the capacity of the torque sensor which is about $23\text{ N} - m$.

Breakaway characterisation results

From the Stiction experiment results one observes that the friction-displacement relationship suggests the friction torque rises with the displacement up until a certain range of values beyond which the torque experiences a fall. This fall is of short duration and then the friction-displacement relation afterward becomes constant. The maximum displacement beyond which the friction falls is thus called the breakaway displacement and the associated friction the Stiction torque. From the various experiments the value of the Stiction-torque (breakaway friction-torque) was found to be in the range of $0.095\text{-}0.12\text{ N-m}$ and the breakaway displacement to be $0.0048\text{-}0.0063\text{ rads}$. Varying the rate of torque application to the test-bed resulted in the varying-Breakaway features of figure 4.7. From the figure it was noted that the friction torque for the breakaway was highest for the highest rate of torque input and least for the least rate of torque input. In fact the friction torque level was seen to be raised a bit higher for the high torque rate than for the low torque rate.

4.6 Parameter estimation of friction models

In this section, model parameters estimation and model validation were performed with the aim of identifying the parameter values for the different friction models capable of replicating the different friction features such as the frictional-lag, pre-sliding hysteresis with non-local memory, and the constant-velocity features. These parameter values were validated and a parsimonious system structure selected. For performance and comparison purposes four different friction models namely the; proposed, LuGre, GMS and Xiong models were investigated.

System identification has often been used for the modelling of non-linear systems, mainly due to the complex nature of the phenomenon and the involved nature of the physics behind

friction. Adequate understanding of the friction features between two surfaces in contact subject to relative motion is imperative for the realisation of an adequate model of friction capable of reproducing relevant features of friction. A set of experiments fit for use in identification of friction were designed and performed to acquire input-output data sets with which to work as described in the previous section. Different data-sets capturing relevant friction phenomena were thus obtained. The determination of the parameters of the various model structures as chosen earlier to capture these features of friction is the focus of this section. The data sets collected were prepared and a few outliers removed.

The model parameter identification problem can by proper formulation be transformed to an Optimisation of a cost function. The optimization of the cost functions obtained using various friction models to determine accurate model parameters for each of those models to replicate accurately the observed relationships and predict future values given certain inputs was carried out. Different optimisation techniques were adopted for the different phenomena of friction, and were thus grouped in relation to the various experiments performed in the previous section.

4.6.1 Parameter estimation under constant velocity

The constant-velocity characterisation experimental result was used for the static parameter estimation. The concept behind the estimation of the static friction parameters is fitting the model into the constant-velocity experimental data set obtained in experiment 1 above. The static parameters to be determined are;

1. F_c , the coulomb friction parameter
2. F_s , the stiction friction parameter
3. f_v , the viscous friction coefficient parameter
4. v_s , the parameter representing the Stribeck velocity

The proposed model structure:

In the steady state the proposed friction model is given as, recall eqn. 3.18

$$F_f = \gamma + f_v v \quad (4.15)$$

that is

$$F_f = F_c + (F_s - F_c)e^{-(\frac{v}{v_s})^2} + f_v v \quad (4.16)$$

This therefore reduces the proposed model to the Stribeck model structure see equation 2.11 given the exponential nature of the data points as observed from the constant velocity experiment. If the torque output data set is $Y(t)$, and the velocity input data set $U(t)$, then the input-output data set is given as

$$\theta(t) = [U(t), Y(t)]^T \quad (4.17)$$

$$U(t)^T = [u(t), u(t-1), u(t-2), \dots, u(t-n)] \quad (4.18)$$

$$Y(t)^T = [y(t), y(t-1), y(t-2), \dots, y(t-n)] \quad (4.19)$$

where $\theta(t)$ is a vector of the input and output data set, $U(t)$ is the vector input data ($U \in \mathbb{R}^n$), and $Y(t-1) \in \mathbb{R}$ with $i = 1, \dots, n$ the scalar output data. Therefore we want to obtain estimates for the mathematical relationship between the input-output data sets so as to enable the prediction of future values from these past observations. This relationship is thus defined as

$$y(t+1) = g(\theta(t), \phi) + e(t+1) \quad (4.20)$$

with $y(t+1)$ as the future friction-torque output known, $g(\cdot)$ a non-linear function defining the model structure (such as eqn.(4.16)), is the regression vector, ϕ is the parameter vector to be identified, $e(t+1)$ being the error term added to account for the fact that the next output is no perfect function of the past input-output data set. The goal is to ensure the contribution of the error term is infinitesimal so as to reasonably say that for a given past data set the future output $y(t+1)$ is accurately predicted by the model structure so chosen, that is

$$g(\theta(t), \phi) = F_c + (F_s - F_c)e^{-\left(\frac{v}{v_s}\right)^\delta} + f_v v \quad (4.21)$$

the function $g(\cdot)$ can be parameterized with a finite dimensional vector (which is often an approximation), thus yielding $g(t)$, v is the input velocity represented as $U(t)$.

Fortunately the LuGre, E-P, models are of the same structure as the proposed model in the constant velocity (steady state) and were modelled using the Stribeck model structure as given above.

The Xiong model structure:

The Xiong and GMS models are similar in structure being multi-element based (2.28), so they have same structure in the steady state with a structure of the form

$$g(\theta(t), \phi) = F_{ci} + (F_{si} - F_{ci})e^{-\left(\frac{v}{v_{si}}\right)^\delta} + f_v v \quad (4.22)$$

similar to the proposed and LuGre models where $i = 1, 2, \dots, N_e$ with i as the i th bristle element of the system and N_e the number of bristle elements used for the modelling.

Various approaches have been adopted for the estimation of the static parameters, [117], [118], [119], [120]. This kind of identification problem usually gives rise to a non-linear regression between the chosen model and the data-set as shown below.

$$C = \sum_{t=1}^{N_p} \|y(t+1) - g(\theta(t), \phi)\|^2 \quad (4.23)$$

with N_p being the number of data-points in the data-set, C the cost function, and every other term as previously defined. The optimization problem for this system reduces to a curve-fitting problem of finding the minimal error in a least squares sense between the measured output friction-torque and input velocity data sets and a chosen model structure representation. Various model structures (proposed, LuGre, Xiong, and GMS models) were examined.

Substituting eqns. 4.21 and 4.20 for the proposed model and eqns. 4.22 and 4.20 for the Xiong model into the cost function equation 4.23 is therefore a quadratic curve-fitting problem of the data set in a least squares sense using a non-linear optimization tool. In this case an *lscurvefit* optimization tool was used and the parameter values obtained for the system was shown in table with the mse value.

The *lscurvefit* tool found in the Matlab optimization tool box is often used for solving non-linear data-fitting problems. It uses the the large-scale or medium scale optimization algorithms with the former as a default. Thus given a set of input data $U(t)$ with the observed data set $Y(t)$, the objective is to find coefficients of ϕ that gives the mathematical model $g(\theta(t), \phi)$ a best-fit. This thus leads to the minimization of

$$\frac{1}{2} \|g(\theta(t), \phi) - U(t)\|_2^2 = \frac{1}{2} \sum_i (g(\theta(t)_i, \phi) - U(t)_i)^2$$

For more details of the use of *lscurvefit* in this research and associated codes see appendix B. The graph of the measured torque against velocity and the modelled torque against velocity is shown as figure 4.8a for the proposed and LuGre models and figure 4.9a for the GMS and Xiong models. The graphs of the optimization results show the general behaviour of friction capturing the Stribeck effect and the linear viscous plus coulomb friction. To obtain a parsimonious friction model which best models the friction-velocity relationship at steady state velocities a validation of the various model structures representative of friction in the regime would be done. At relatively high velocities the friction can effectively be approximated or modelled by the viscous friction model of equation 2.6 while the low

Table 4.2 Estimated static parameters for constant-velocity motion using the proposed/LuGre models

Model Parameter	Estimated value	$\text{msex}10^{-5}$
F_s	0.0994	
F_c	0.0929	
v_s	0.1407	
f_v	0.0603	
Estimation		3.7316
Validation		5.4988

Table 4.3 Predicted (static) parameters for constant-velocity using the GMS/Xiong models

Model Parameter	Estimated value	$\text{msex}10^{-5}$
F_s	0.1035	
F_c	0.0921	
v_s	0.1	
f_v	0.0584	
λ_1	0.2841	
λ_2	0.2341	
λ_3	0.2341	
λ_4	0.2341	
Identification		4.1394
Validation		6.8605

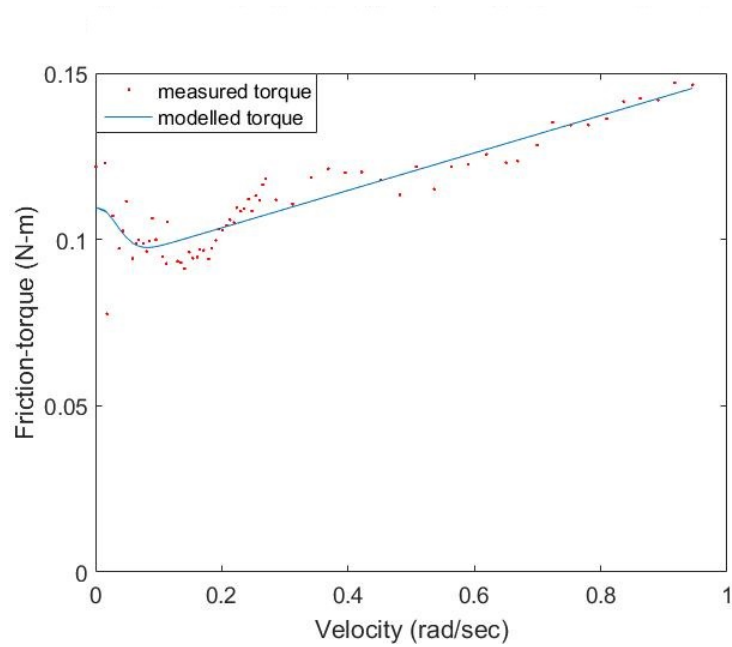
velocities are quite non-linear but decreasing exponentially before increasing with a minimum friction value (Coulomb) at the Stribeck velocity.

4.6.2 Parameter estimation under pre-sliding

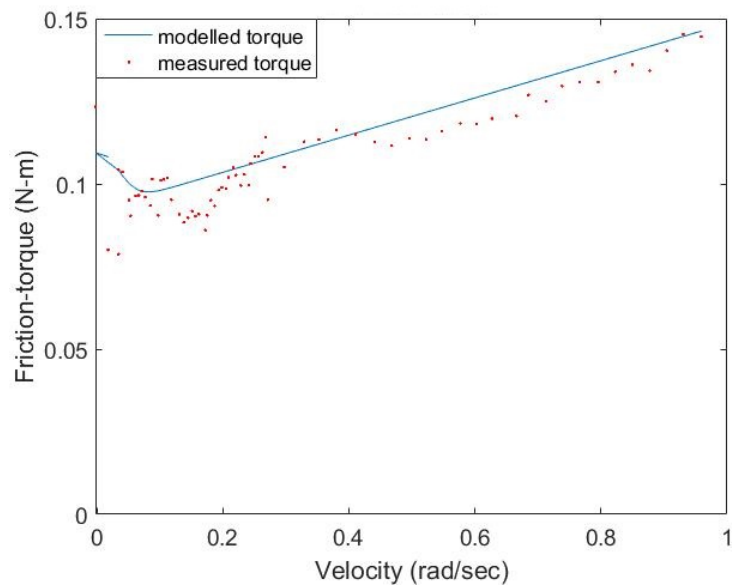
From figure 4.6 it is clearly illustrated the hysteretic features of friction in the pre-sliding regime of motion. An attempt is made here to capture this feature and identify model parameters capable of depicting such feature of friction for the different friction models. The model equations are modified for the individual model structures whose parameters are to be identified.

The proposed model structure:

In the pre-slide regime the parameters of interest for the proposed model are the Stiction torque F_s and the breakaway displacement Z_b . However, the stiction torque identified in the constant velocity identification was used to provide bounds to for the identification. The

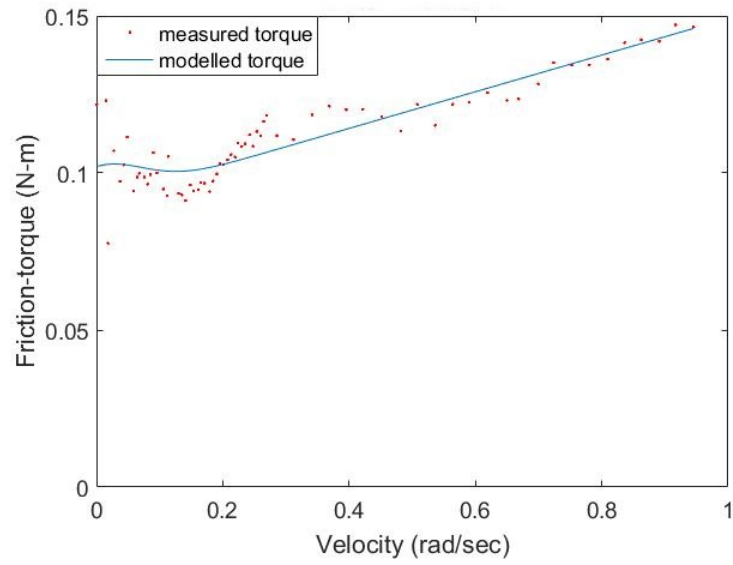


(a)

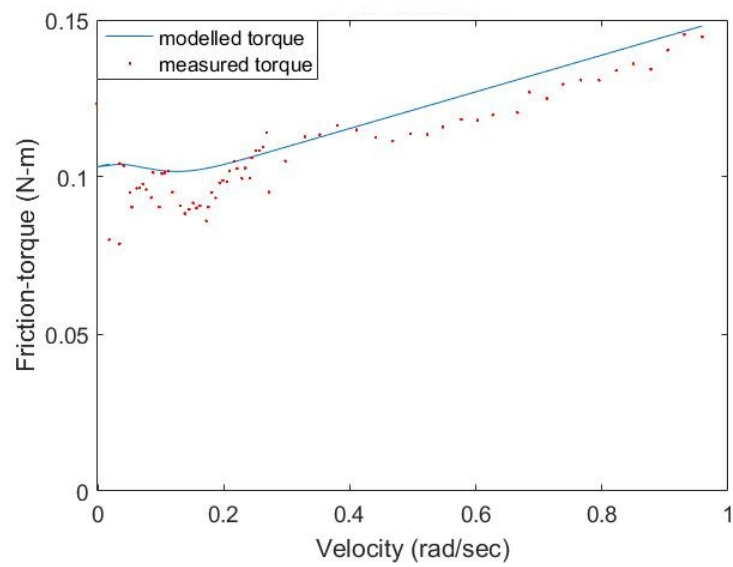


(b)

Fig. 4.8 The modelling of constant-velocity friction-torque relationship with the proposed model (a) Estimation result, and (b) Validation result



(a)



(b)

Fig. 4.9 The modelling of constant-velocity friction-torque relationship with the Xiong model
(a) Estimation result, and (b) Validation result

proposed model equation for the pre-sliding friction regime is

$$F_f = F_{hyst}(z) + \sigma \dot{z} \quad (4.24)$$

and

$$\dot{z} = v \quad (4.25)$$

z average bristle deflection, and σ the micro-damping parameter, and

$$F_{hyst}(z) = \left(\sin \left(\frac{z - z_r}{|z_t - z_r|} \frac{\pi}{2} \right) \right) |f_t - f_r| + f_r$$

being the pre-sliding friction function. Using a slowly varying input signal makes it possible to neglect the dynamics; the macro and micro damping effects [34]. Re-formulating the optimisation as in equation (4.23) with

$$g(\theta(t), \phi) = \left(\sin \left(\frac{z - z_r}{|z_t - z_r|} \frac{\pi}{2} \right) \right) |f_t - f_r| + f_r \quad (4.26)$$

Thus the identifiable parameters are 2; the breakaway displacement Z_b and the breakaway friction torque F_s , of the hysteresis with non-local memory. The identification reduces to the minimisation of the cost function

$$C = \sum_{t=1}^{N_p} \|y(t+1) - g(\theta(t), \phi)\|^2 \quad (4.27)$$

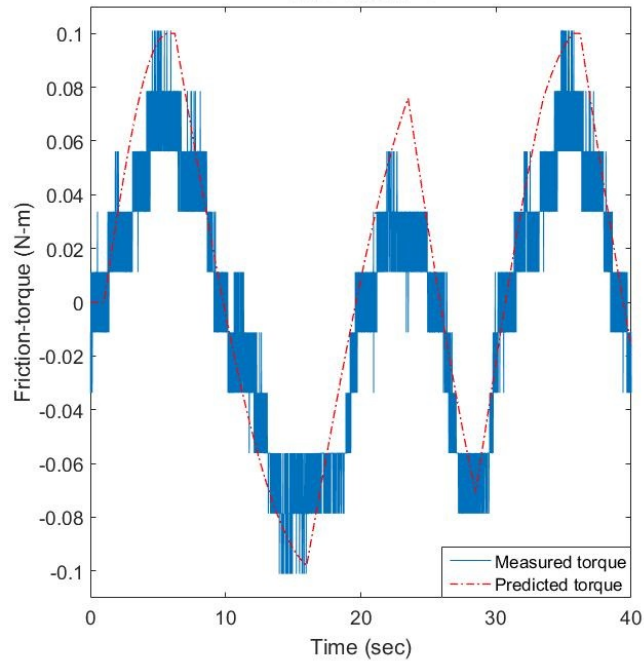
The identified parameters F_s and Z_b , and the mse values are given in the table 4.4, while the predicted friction-torque features as against the true hysteretic friction is shown in figure 4.10a. Figure 4.10b shows the friction-torque against the displacement with non-local memory hysteretic feature.

The LuGre model structure:

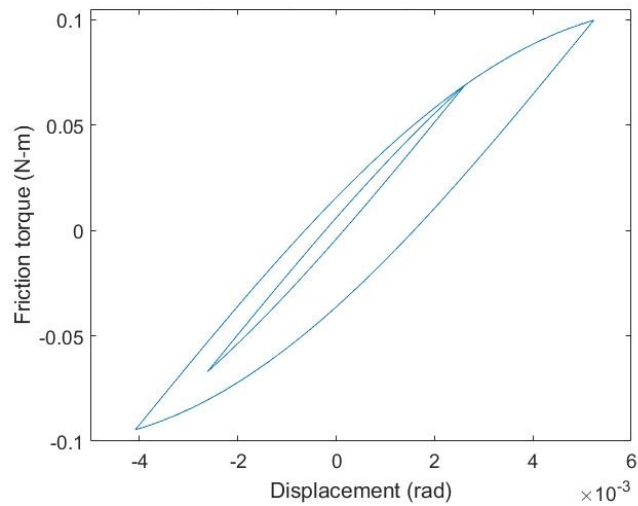
Table 4.4 Estimated parameters under pre-sliding for the proposed model

Model Parameter	Estimated value	mse $\times 10^{-4}$
F_s	0.0980	
Z_b	0.0060	
Estimation		3.6074
Validation		8.9796

For the LuGre model an approach as illustrated in [121], [122], was adopted bearing in mind that this model utilises the same set of equations both for the pre-sliding and gross-sliding

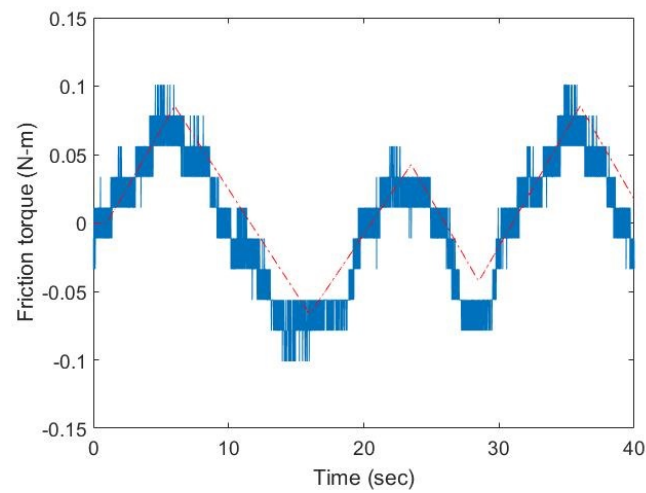


(a)

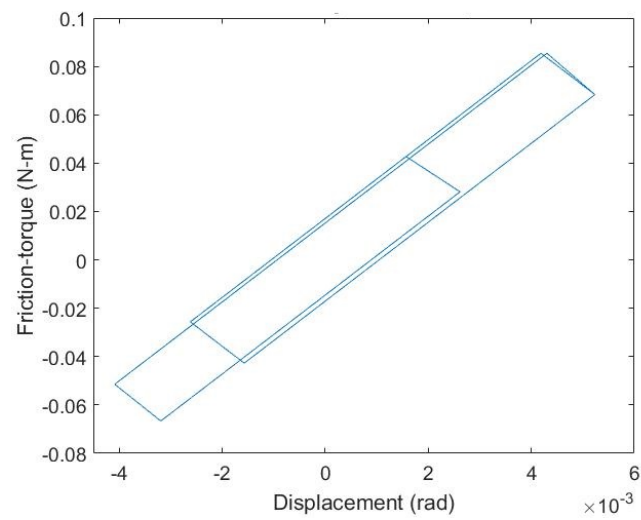


(b)

Fig. 4.10 The modelling of pre-sliding hysteresis friction-torque displacement relationship with the proposed model (a) Estimation result, and (b) Torque-displacement result



(a)



(b)

Fig. 4.11 The modelling of pre-sliding hysteresis friction-torque displacement relationship with the LuGre model (a) Estimation result, and (b) Torque-displacement result

Table 4.5 Predicted parameters for friction hysteresis with LuGre model

Model Parameter	Predicted value	mse $\times 10^{-4}$
σ_0	16.4690	
Identification		3.8059
Validation		9.6759

friction regimes unlike the proposed, GMS and Xiong models. The model structure of the LuGre eqn. 2.18 was used for the identification with the notion that the slowly varying parameter renders \dot{z} to be approximately equal to zero. The parameter to be identified is the σ (bristle stiffness). The friction-torque is therefore

$$F_f = \sigma_0 z \quad (4.28)$$

With this formulation an estimate of the stiffness parameter σ_0 of the LuGre model was obtained by solving the optimisation problem. Formulating the identification problem with this equation and performing the resulting minimisation of the cost function with a non-linear optimisation algorithm yields the result in figure 4.11 and the parameter and mse values are as presented in table 4.5.

The GMS model structure:

Using the GMS model parameters for pre-sliding hysteresis identification; Recall the GMS model equations 2.27, 2.28 and 2.28, and the number of bristle elements used for the identification is $N_e = 4$. During pre-sliding

$$\dot{z}_i = v \quad (4.29)$$

and

$$F_f = \sum_{i=1}^{N_e} \sigma_{oi} z_i \quad (4.30)$$

Formulation of the optimisation problem (minimization of the cost function C) and using non-linear optimisation algorithm, the parameter values estimated and the mse value are as in table 4.6 and the predicted and measured friction torque versus velocity plotted in figure 4.12.

The Xiong model structure:

For the Xiong model parameter prediction; the model equations for the identification of the friction feature are equations 2.30, 2.31 and 2.32. Similar to the GMS model the pre-sliding

equations for a four element model are

$$\dot{z}_i = v \quad (4.31)$$

and

$$F_f = \sum_{i=1}^{N_e} K_i z_i \quad (4.32)$$

Thus the identification of Xiong model parameters is similar to that of the GMS as represented in figure 4.13. Table 4.7 contains the predicted model parameters with the error metric.

Table 4.6 Estimated parameters under pre-sliding for th GMS model

Model Parameter	Estimated value	mse $\times 10^{-4}$
σ_{01}	7.9605	
σ_{02}	4.8757	
σ_{03}	2.6039	
σ_{04}	1.0290	
Estimation		3.8059
Validation		9.7548

Table 4.7 Estimated parameters under pre-sliding for the Xiong model

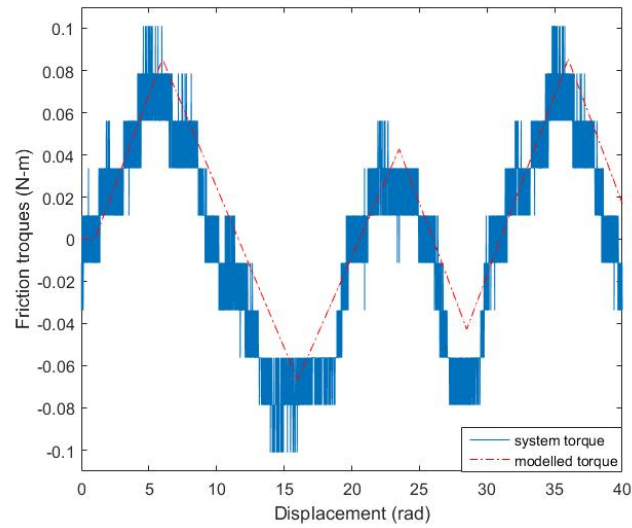
Model Parameter	Estimated value	mse $\times 10^{-4}$
K_{01}	10.9915	
K_{02}	2.7836	
K_{03}	1.9866	
K_{04}	0.7792	
Estimation		3.8062
Validation		9.7153

4.6.3 Computation of the micro-damping parameters

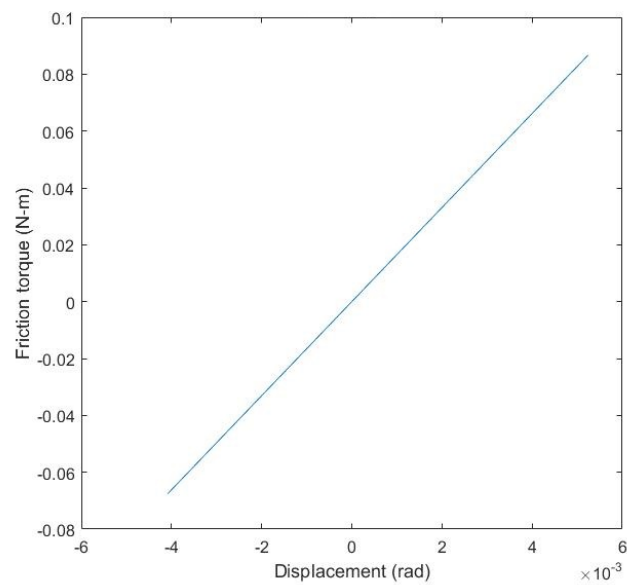
From previous identification approaches we have been able to estimate most of the parameters of the proposed friction model with the exception of the micro-damping parameter σ and the lag parameter τ . There has been no straight forward manner for the determination (estimation) of the parameter, however many approaches have been adopted for its computation from experimental results, [121], [119] and similar approach was adopted here also.

Proposed new model

In this thesis the σ parameter was computed with the assumption of a linear model of the

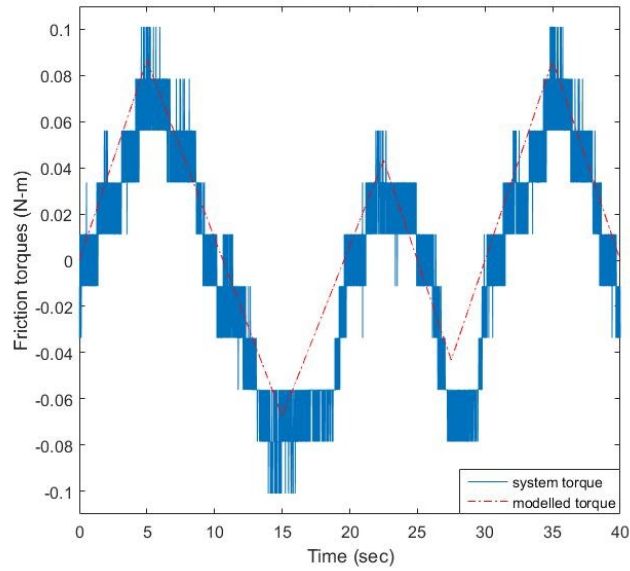


(a)

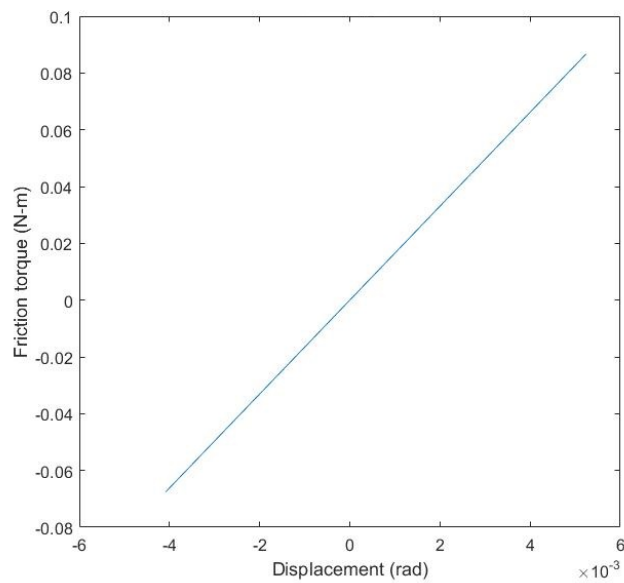


(b)

Fig. 4.12 The modelling of pre-sliding hysteresis friction-torque displacement relationship with the GMS model (a) Estimation result, and (b) Torque-displacement result



(a)



(b)

Fig. 4.13 The modelling of pre-sliding hysteresis friction-torque displacement relationship with the Xiong model (a) Estimation result, and (b) Torque-displacement result

pre-sliding hysteresis function, the experiment was constrained only for the pre-slide regime of friction with a slowly varying ramp input signal, [121]. Thus a linearised version of the pre-sliding function eqn. 3.1 and 3.2 is

$$f_{hyst}(z) = \left(\frac{z - z_r}{|z_t - z_r|} \frac{\pi}{2} \right) |f_t - f_r| + f_r \quad (4.33)$$

with $f_r = z_r = 0$ for a motion starting from rest, $z_t = Z_b$ and $f_t = F_s$, see section 3.2.1.

Then

$$f_{hyst}(z) = \frac{F_s \pi}{2Z_b} z \quad (4.34)$$

For the system (experimental test-bed), a second order representation

$$Js^2 z = u - F_f$$

with u as the control input, F_f being the proposed new model of friction equation 3.5, with

$$f_{hyst}(z) = \frac{F_s \pi}{2Z_b} z$$

Substituting this value gives the transfer function

$$G(s) = \frac{1}{Js^2 + (\sigma + f_v)s + \frac{F_s \pi}{2Z_b}} \quad (4.35)$$

Assuming a damping ζ such that $0.5 \leq \zeta \leq 1$, to ensure adequate damping of the system is chosen, here a value of $\zeta = 0.7$ was chosen. Comparing equation 4.35 with the standard second order transfer function, the micro-damping parameter could be determined. Thus from equation 4.35 above

$$\sigma + f_v = 2\zeta\omega_n \quad (4.36)$$

with $\omega_n^2 = \frac{F_s \pi}{2Z_b}$ and substituting to obtain

$$\sigma = 2\zeta J \sqrt{\frac{F_s \pi}{2Z_b}} - f_v \quad (4.37)$$

given that F_s , Z_b , f_v , are as previously obtained in the previous estimation as 0.0980, 0.0060, and 0.0403 respectively. Then $\sigma \approx 0.3213$.

From the values of the static friction F_s and breakaway displacement Z_b parameters of the proposed new model, one can easily compute the approximate bristle stiffness parameter σ_0

of the LuGre model given that

$$\sigma_0 = \frac{F_s}{Z_b} \quad (4.38)$$

thus $\sigma_0 \approx 16.3333$ which is in close agreement with predicted values in the parameters identification of the LuGre model table 4.5.

LuGre model

Adopting the same line of argument the micro-damping parameter of the LuGre model is also obtained considering the transfer function equation of the form

$$G(s) = \frac{1}{Js^2 + (\sigma_1 + f_v)s + \sigma_0} \quad (4.39)$$

with σ_1 as the micro-damping parameter, σ_0 the stiffness parameter and f_v the viscous friction coefficient. so that

$$\sigma_1 = 2\zeta J \sqrt{\frac{\sigma_0}{J}} - f_v \quad (4.40)$$

given that σ_0, f_v , are as previously obtained in the previous estimation (LuGre) as 16.4690, and 0.0403 respectively. Then $\sigma_1 \approx 0.2494$.

GMS model

For the multi-element GMS model which comprises of many LuGre model structure in parallel, thus the LuGre model was used for the determination of the 4 micro-damping parameters since the number of elements used $N = 4$. Using eqns.4.39 and 4.40 with the values of σ_{oi}, f_v for $i = 1, 2, 3, 4$ as in table 4.6 the following values were obtained for the micro-damping parameter $\sigma_{11} = 0.1611, \sigma_{12} = 0.1173, \sigma_{13} = 0.0749, \sigma_{14} = 0.0321$.

Xiong model

The Xiong and GMS friction models are similar in the pre-sliding motion regime so following the same reasoning and referring to table 4.6, the micro-damping parameters are $\sigma_1 = 0.1964, \sigma_2 = 0.0788, \sigma_3 = 0.0603, \sigma_4 = 0.0227$.

4.6.4 Parameter estimation under frictional-lag

At low to medium unidirectional velocities, there is a lag between the friction torque and the corresponding velocity and this is called frictional-lag. The friction model structures for the gross-sliding regime are used for the parameter estimation purposes.

The proposed new model structure:

For the proposed model, the following model structure is used for the quadratic function

formulation from the model equations of (4.15) and (4.16)

$$F_t = \gamma + f_v v \quad (4.41)$$

with

$$\dot{\gamma} = \frac{g(v) - \gamma}{\tau} \quad (4.42)$$

From this equations it is obvious that the static parameters appear here as well as in the constant velocity identification so the estimates earlier obtained from the steady velocity identification serve as guides for the present estimation. As such the major concern is the identification of the lag parameter τ . Interior-point-large scale optimization algorithm was used for the estimation of the model parameters. The predicted and measured frictional-lag features are shown in figure 4.14a, while the parameters values and the mse are recorded in table 4.8. The width of the frictional lag has earlier been shown to widen or shrink as the velocity rate increases or decreases respectively. This phenomenon is also called friction-velocity hysteresis see section 3.5. The friction-torque against velocity for the various unidirectional velocities was plotted using the identified parameters of the proposed model is shown in figure 4.18. This clearly illustrates that the lag feature widens as the frequency increases as the suggested by the figure for the following frequencies; 2 rad/sec, 5 rad/sec and 10 rad/sec.

The LuGre model structure:

For this model, the friction force and the state equations as in equations 2.18 and 2.19 as shown. Notice from the equations that all the model parameters are represented, with the static parameters earlier identified in the constant velocity process as guides for their respective estimates in this process. Coarse and fine optimisations were performed with non-linear optimisation algorithms and the estimated parameters results recorded in table 4.9, along with the mse value and maximum error. Model prediction and the frictional lag measured are plotted against time in figure 4.15a.

The GMS model structure:

The GMS model structure is shown as equations 2.28 and 2.29 with that the result of the optimisation process performed using non-linear algorithm and the predicted values and mse in table 4.10, while figure 4.16a captures the measured and predicted frictional lag. The main parameter of interest is C_i parameter estimation With the same line of reasoning for the LuGre process above we analyse the Xiong model.

The Xiong model structure:

For the Xiong model the predicted static model are used to provide bounds for this process while the parameter of interest is τ . The parameter estimates and the mse value is recorded

in table 4.11 and the measured and predicted frictional-lag were plotted in figure 4.17a.

The figures also show the deviations of the various experimental runs in terms of the quartiles, and how the predicted curves closely follow the mean experimental data.

Table 4.8 Estimated parameters under frictional lag for the proposed model

Model Parameter	Estimated value	mse $\times 10^{-6}$
F_s	0.0986	
F_c	0.0925	
v_s	0.1526	
f_v	0.0403	
τ	0.0111	
Estimation		8.3762
Validation		9.5132

Table 4.9 Estimated parameters under frictional lag for the LuGre model

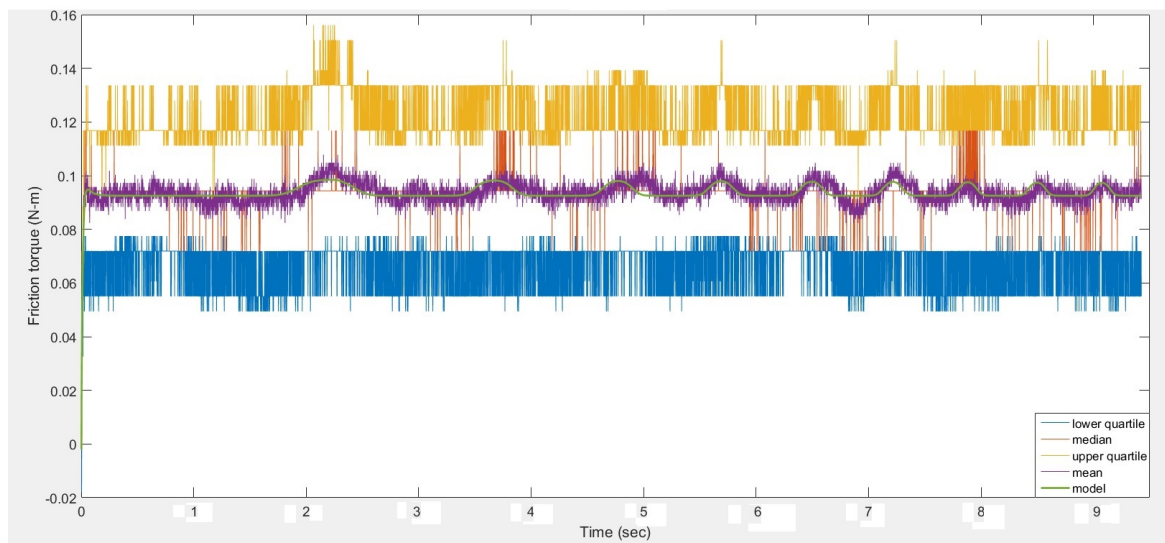
Model Parameter	Estimated value	mse $\times 10^{-6}$
F_s	0.0994	
F_c	0.0929	
σ_0	15	
σ_1	0.1307	
v_s	0.1468	
f	0.0603	
Estimation		8.6065
Validation		10.091

4.6.5 Friction model validation

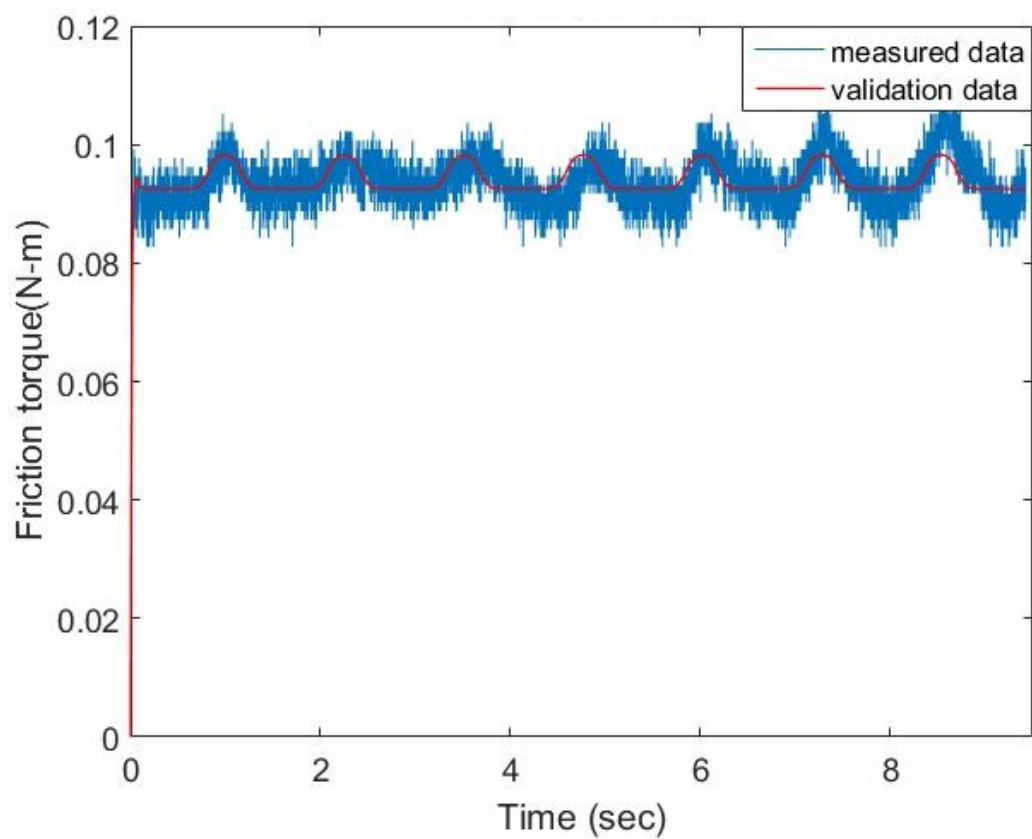
A set of unused data was used for the validation of the various model structures and their values as identified in the previous section. For simplicity, the approach adopted closely resembled the optimisation approach of splitting the validation process into the constant-velocity, pre-sliding hysteresis, and the frictional-lag procedures.

Constant velocity;

The various models were validated against the set of constant velocity friction data different from the one used for the identification and the performance of the various models were illustrated. From the various figures, the proposed model figure 4.8b (same for the LuGre model) performance showed stronger correlation with the validation data than the GMS and Xiong models of figure 4.9b. The mse for the proposed new model is 5.4988×10^{-5} and

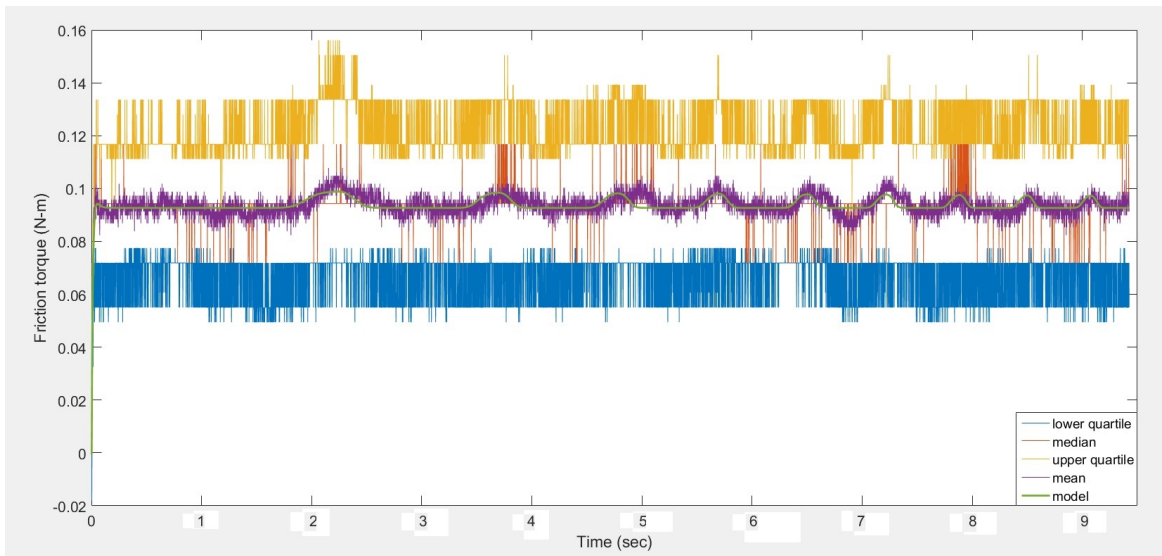


(a)

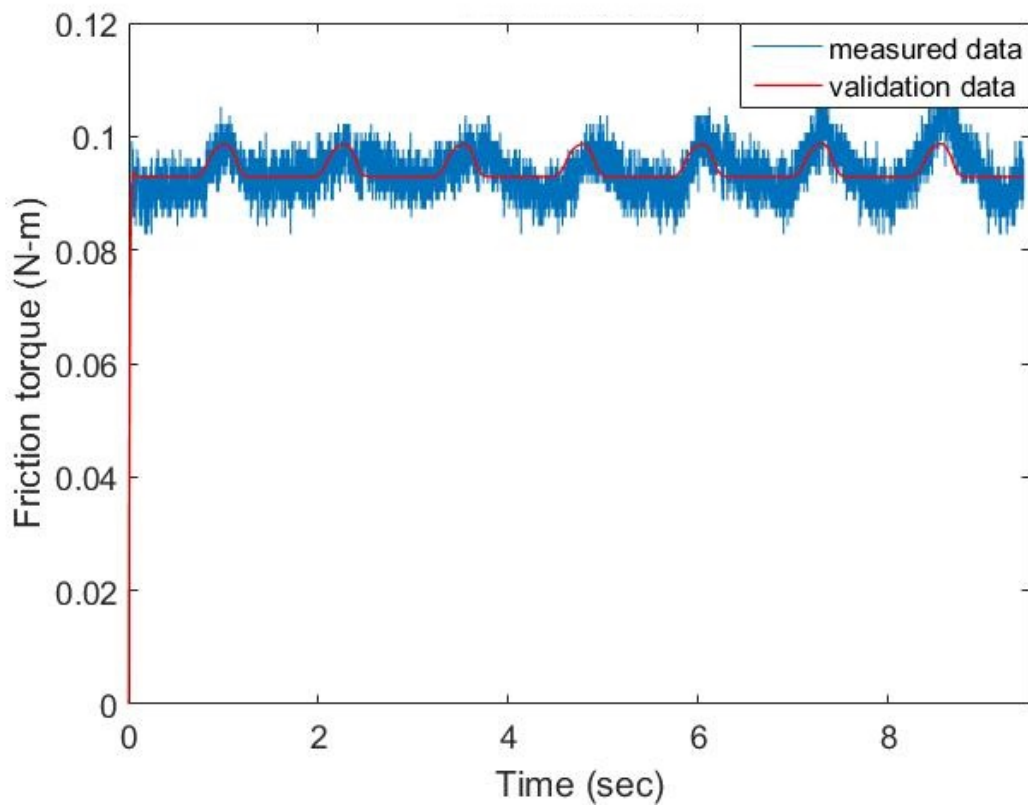


(b)

Fig. 4.14 The modelling of frictional-lag with the proposed model (a) estimation result, and (b) validation result, for unidirectional motion

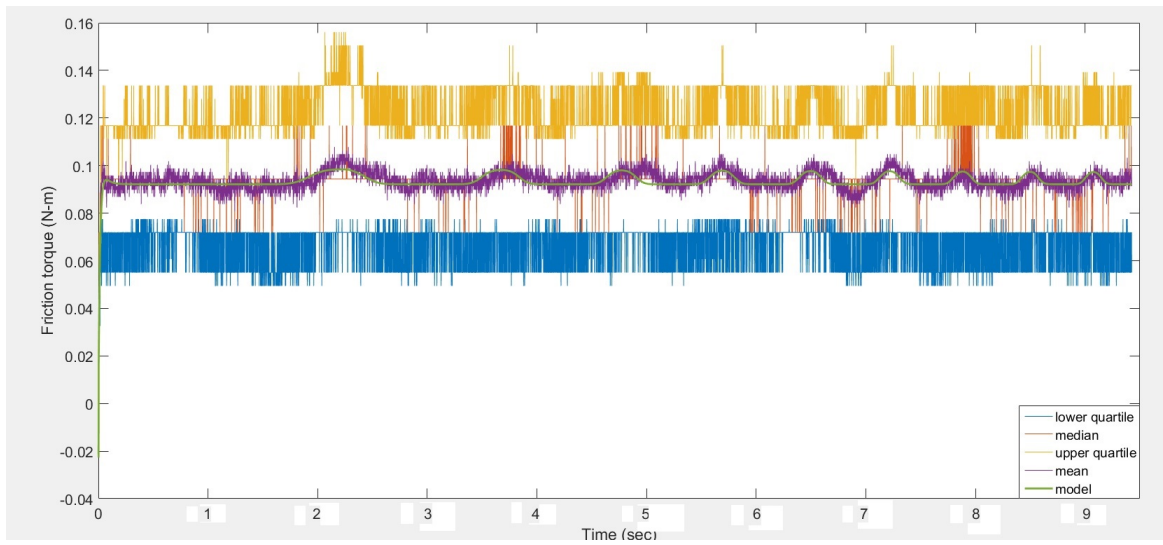


(a)

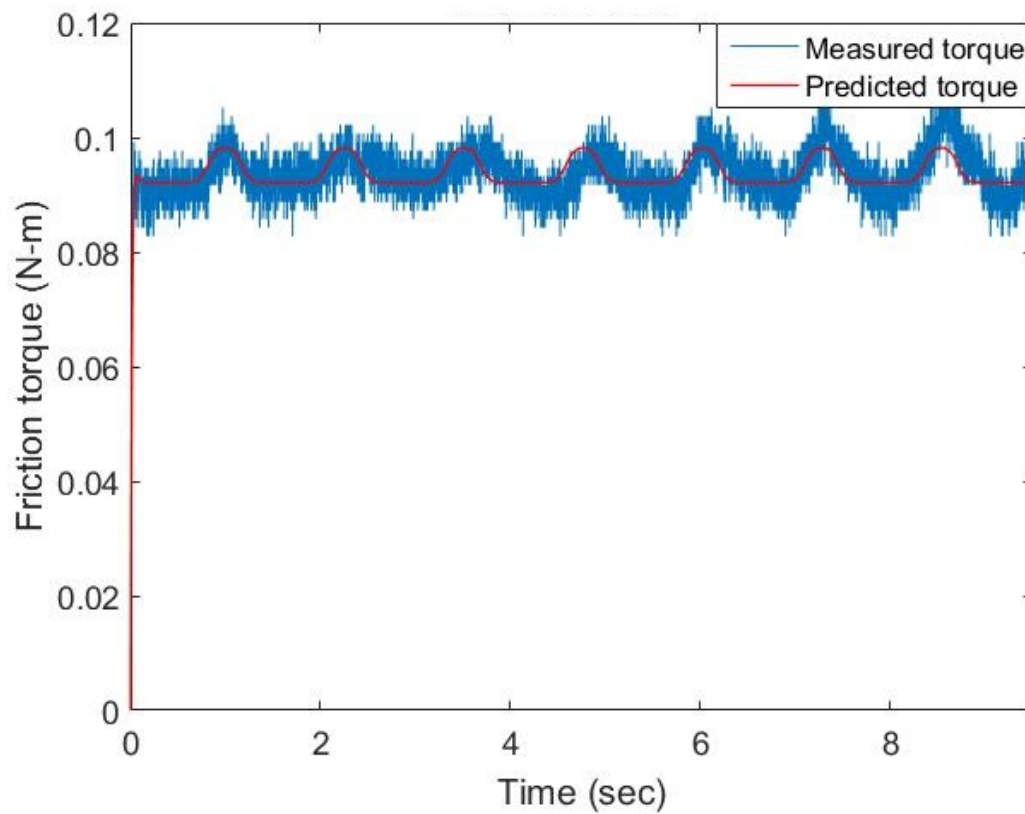


(b)

Fig. 4.15 The modelling of frictional-lag with the LuGre model (a) estimation result, and (b) validation result, for unidirectional motion

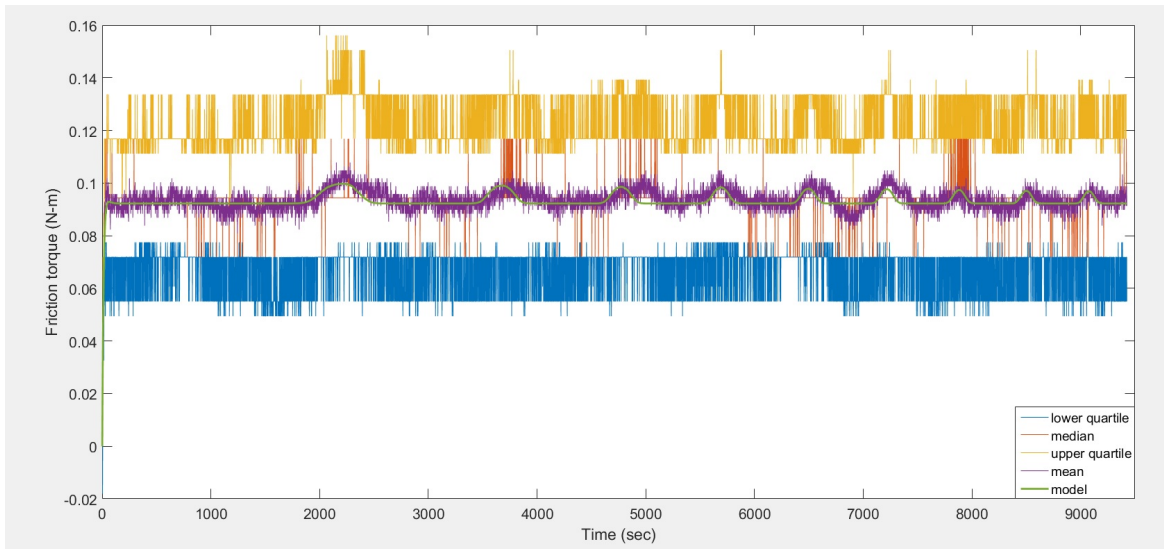


(a)

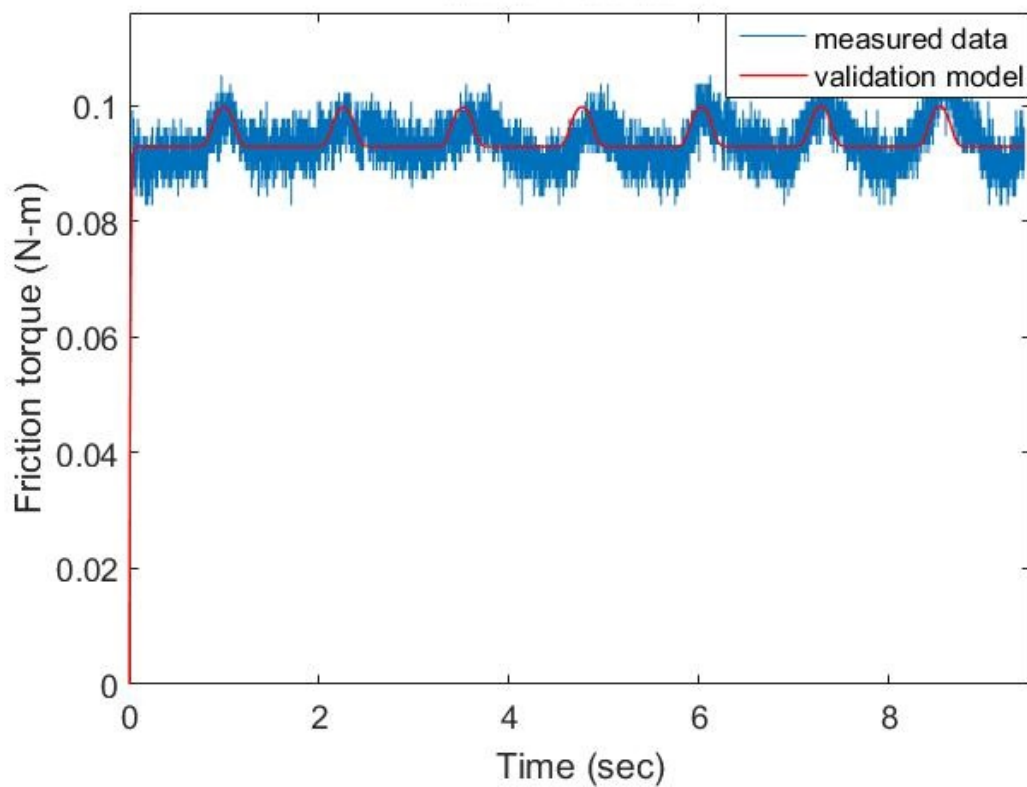


(b)

Fig. 4.16 The modelling of frictional-lag with the GMS model (a) estimation result, and (b) validation result, for unidirectional motion



(a)



(b)

Fig. 4.17 The modelling of frictional-lag with the Xiong model (a) Estimation result, and (b) Torque-displacement result, for unidirectional motion

Table 4.10 Estimated parameters under frictional lag for the GMS model

Model Parameter	Estimated value	mse $\times 10^{-6}$
F_s	0.1647	
F_c	0.1540	
σ_{o1}	15	
σ_{o2}	15	
σ_{o3}	15	
σ_{o4}	15	
σ_{11}	0.0686	
σ_{12}	0.0686	
σ_{13}	0.0686	
σ_{14}	0.0686	
α_1	0.1500	
α_2	0.1500	
α_3	0.1500	
α_4	0.1500	
v_s	0.1536	
C	0.6539	
Estimation		8.6428
Validation		9.3469

6.8605×10^{-5} for the GMS model.

Pre-sliding hysteresis;

The behaviour of the various friction models in the pre-sliding regime against a sinusoidal test signal used for validation, figures 4.19 and 4.20 showed that the proposed model performance with mse of 8.9796×10^{-4} exhibited improvement over the others; LuGre model with mse of 9.6759×10^{-4} , the GMS model with mse of 9.7548×10^{-4} , and the Xiong model with mse of 9.7153×10^{-4} . This fact underscores the in-ability of the LuGre model to capture non-local features of the pre-sliding friction-displacement relationship efficiently. The results of this suggests that modelling the pre-sliding hysteretic function with the GMS or Xiong models might require many elements (more than the 4 elements used here). This poses more complexity for system identification and thus use of these multi-element models. More complex and computationally involving methods have been used by some authors for the estimation of the parameters of the GMS model. On the other hand the proposed model was able to capture the non-local hysteresis feature without any complications as a result of the pre-sliding hysteresis function integrated into the new model.

Frictional lag;

Using the obtained parameter values for the various friction models with the validation data

Table 4.11 Estimated parameters under frictional lag for the Xiong model

Model Parameter	Estimated value	mse $\times 10^{-6}$
F_s	1.0057	
F_c	0.09237	
λ_1	0.2998	
λ_2	0.2998	
λ_3	0.2998	
λ_4	0.1005	
v_s	0.13121	
τ	0.0124	
Estimation		8.5868
Validation		10.087

set generated from a 5 rad/sec unidirectional velocity input, the models performance against the test data was captured in the different figures for the various models. The GMS model figure 4.16b with mse 9.3469×10^{-6} , showed strongest correlation with the data set. This was closely followed by the proposed new model of figure 4.14b with mse of 9.5132×10^{-6} , Xiong figure 4.17b and mse 10.087×10^{-6} and the LuGre figure 4.15b and an mse of 10.091×10^{-6} models in the order.

4.6.6 Analysis of parameter estimates

Steady state identified parameters:

From the estimation and validation results under constant velocity parameter estimation, it was observed that despite the fact that the mse for both the GMS (Xiong) and the proposed (LuGre) models were very closely tied as shown in tables 4.2 and 4.3 and their respective figures above, there was high deviation of the predicted coulomb torque using the GMS (Xiong) models from the expected value as seen in the tables also. Also the validation tests of the proposed model was seen to be much in agreement with obtained data with less mean square error than the GMS model.

Pre-sliding hysteresis identification results:

From the simplified approach adopted for the models parameter identification for the pre-sliding friction hysteresis, the various performance indicators and predicted parameter values, the proposed model seemed to predict this friction feature more adequately than the LuGre model. Also the predicted parameters agree with the values expected as in the Stiction experiment. *Frictional lag identification results:*

Generally, the various friction models capture the frictional lag phenomenon differently since

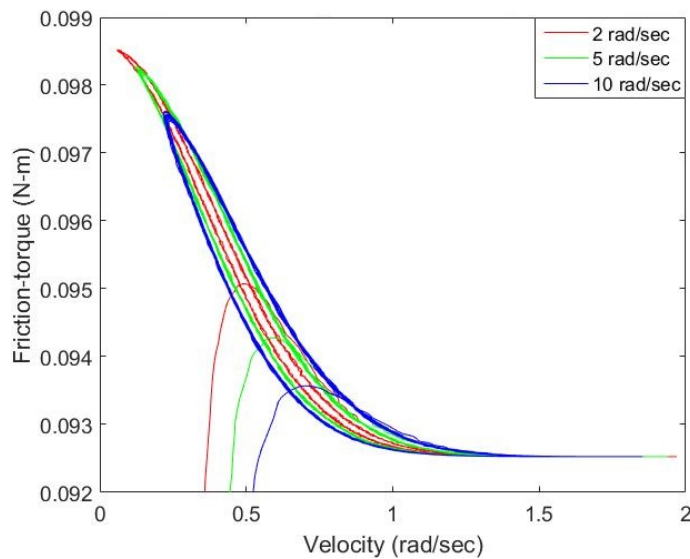
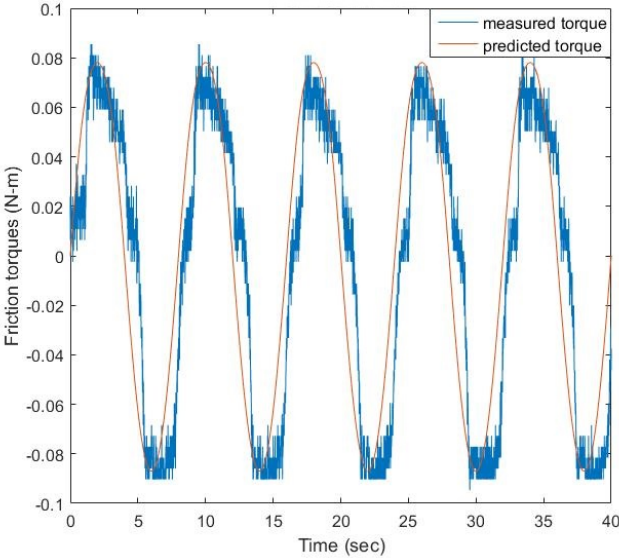


Fig. 4.18 The frictional-lag: obtained by plotting the predicted friction torque for varying velocities against velocity

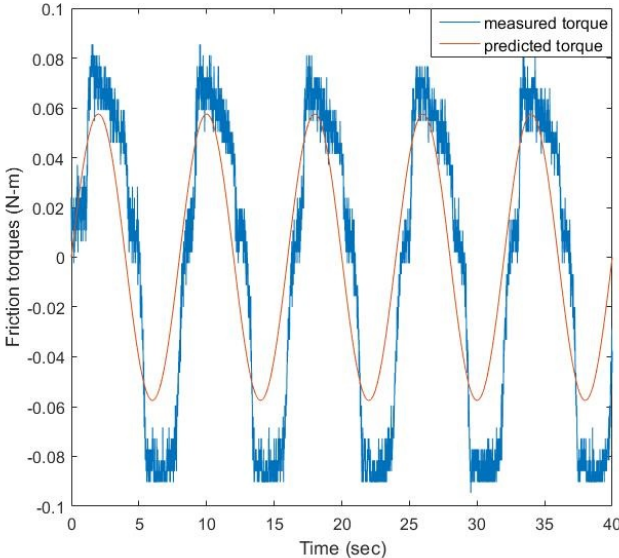
they involve almost all their model parameters pertaining to gross sliding regime thus the different models were analysed independently. From the graphical plots of the measured and identified lag data, the order of performance and model agreement with validation data was the GMS and proposed, Xiong, and LuGre models respectively with the proposed model showing a stronger relationship and capability in predicting friction torque- varying velocity relationship. This observation is the result of due considerations of the predicted values agreement with measured values and the individual model and validation errors.

Thus from the performance indices the following was shown

1. The LuGre model was able to achieve good modelling correlations of the identification and validation data. Being simple with unified pre-sliding and gross-sliding equations it lacked the needed flexibility to capture adequately the non-local hysteretic features of friction. This inadequacy motivated the integration of the pre-sliding hysteresis function in the proposed new model, and also the positional drift it suffers from.
2. Strong performance correlation of the proposed model in modelling the frictional feature obtained from the experimental laboratory friction test-bed. This low parameter dynamic model of friction with non-local pre-sliding features is easy to implement for identification purposes. It demonstrated robustness to parameter variations during the identification process unlike the other models of the LuGre and GMS models. This made parameter adjustments much faster.

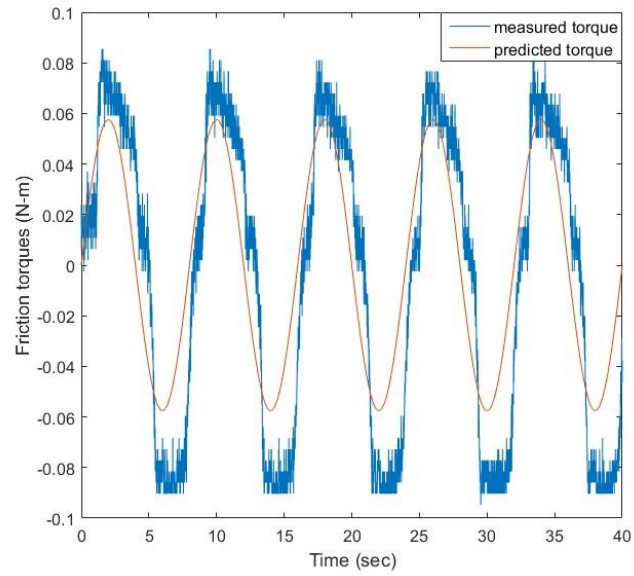


(a)

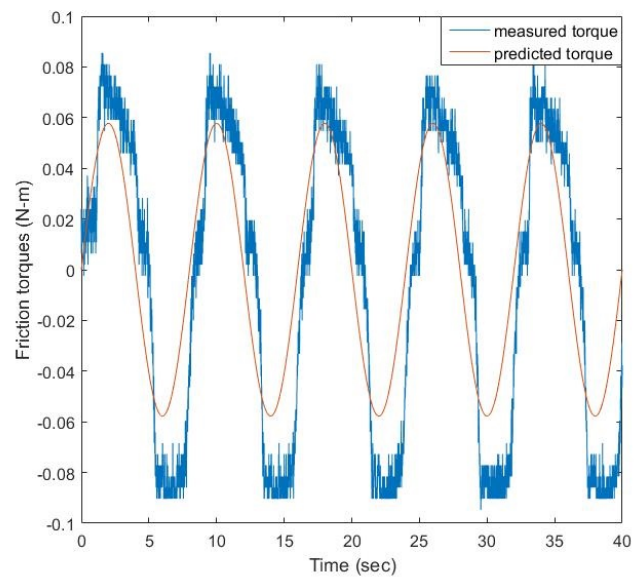


(b)

Fig. 4.19 Pre-sliding hysteresis validation results for: (a) The proposed model, and (b) The LuGre model



(a)



(b)

Fig. 4.20 Pre-sliding hysteresis validation results for: (a) The GMS model, and (b) The Xiong model

3. Capturing the lag effect using the proposed model was possible due to the extra state introduced specifically for the purpose. This two state model structure with pre-sliding hysteresis demonstrated strong correspondence with measured pre-slide data and also the validation data set unlike the other models.
4. The proposed model can be seen as a modified LuGre in that it has an extra function to capture pre-slide hysteretic features of friction.
5. The Xiong model being a multi-element model has great flexibility to model frictional characteristics with little error as the GMS. However the model is complex and computationally demanding because of the large number of parameters needed for identification of the pre-sliding and gross-sliding friction features. Moreover, the Xiong model has no recorded documentation of its applicability to identification and control of real systems with friction.
6. The GMS model's ability to capture the pre-sliding hysteretic features lies in its multi element nature using many 'LuGre frictional elements' and a switching function for changing from pre-slide to the gross-slide regime. These make the use of this model for identification and control purposes difficult as was pointed out in the literature review. This computational complexity thus limits its usage for control purposes.

The table 4.12 presents the different identification method adopted for the parameter estimation for the various friction models. The estimated parameter values for each friction model as tabulated in their respective tables above are harmonised with respect to the estimated parameters of interest in each identification process. These are captured in the tables 4.13, 4.14, 4.15 and 4.16 for the proposed, LuGre, GMS and Xiong models respectively.

4.7 Chapter summary

In this chapter an experimental test-bed was designed for the characterisation of the friction phenomena and a model structure for the experimental test-bed used for friction characterisation experiment was derived. A careful design of a set of experiments were carried out and the experiments performed so as to acquire relevant data for the determination of the various friction characteristics as enumerated in chapter 2 section 2.2 of this thesis. Results of the various experiments illustrated the rich friction dynamics and generally in agreement with most experimentally observed friction phenomena. The system under test was derived providing background for the series of friction identification measurements which follow subsequently. From the different friction features and the characterization data, model parameter

Table 4.12 Predicted parameters for frictional lag using the Xiong model

Model	Parameters	No. of parameters	Identification method
LuGre	$F_s, F_c, v_s, \sigma_0, \sigma_1, f_v$	6	$(F_s, F_c, v_s, f_v) \rightarrow$ pecv $\sigma_0 \rightarrow$ peps $\sigma_1 \rightarrow$ computed
Proposed	$F_s, F_c, v_s, \sigma, f_v$	7	$(F_s, F_c, v_s, f_v) \rightarrow$ pecv $Z_b \rightarrow$ peps $\sigma \rightarrow$ computed $\tau \rightarrow$ pefl
GMS	$F_s, F_c, v_s, \sigma_{oi}, \sigma_{li}, f_v, C_i, \alpha_i$	20 (N=4)	$(F_s, F_c, v_s, f_v, \alpha_i) \rightarrow$ pecv $\sigma_{oi} \rightarrow$ peps $\sigma_{li} \rightarrow$ computed $C_i \rightarrow$ pefl
Xiong	$F_s, F_c, v_s, K_i, \sigma_i, f_v, \lambda_i$	17 (N=4)	$(F_s, F_c, v_s, f_v, \lambda_i) \rightarrow$ cvi $K_i \rightarrow$ psi $\sigma_i \rightarrow$ computed $\tau \rightarrow$ fli

where $N \Rightarrow$ number of bristle elements

pecv \Rightarrow parameter estimation under constant velocity

peps \Rightarrow parameter estimation under pre-sliding

pefl \Rightarrow parameter estimation under frictional lag

and computed \Rightarrow computed by means of calculation

estimation was performed using some of the different models of friction reviewed in chapter 2 to emphasis the capabilities and limitations of these models in the light of the proposed model of friction in chapter 3. From the validation tests the performance of the proposed friction model was seen to exhibit stronger correspondence with the various features of the friction non-linearity among those models under test and for the set of experiments carried out. Thus the proposed friction model being simple both in structure and implementation demonstrates adequate capability for friction modelling in systems with friction. This proposed model and its estimated parameters thus form the basis of the set of control simulations and experiments to be carried out on the experimental test-bed.

Table 4.13 Harmonised parameter values for the proposed friction model

Model Parameter	Estimated value
F_s	0.0994
F_c	0.0925
v_s	0.1407
σ	0.2998
f_v	0.0403
τ	0.0011
Z_b	0.006

Table 4.14 Harmonised parameter values for the LuGre friction model

Model Parameter	Estimated value
F_s	0.0994
F_c	0.0929
σ_0	16.4690
σ_1	0.3213
v_s	0.1407
f_v	0.0403

Table 4.15 Harmonised parameter values for the GMS friction model

Model Parameter	Estimated value
F_s	0.1035
F_c	0.0921
v_s	0.1
f_v	0.0584
α_i	(0.2841, 0.2341, 0.2341, 0.2341)
σ_{oi}	(7.9605, 4.8757, 2.6039, 1.0290)
σ_{1i}	(0.1611, 0.1173, 0.0749, 0.0321)
C_i	(0.2998, 0.2998, 0.2998, 0.2998)

Table 4.16 Harmonised parameter values for the Xiong friction model

Model Parameter	Estimated value
F_s	1.0057
F_c	0.0924
f_v	0.1005
v_s	0.13121
τ	0.0124
λ_i	(0.2998, 0.2998, 0.2998, 0.2005)
σ_i	(0.1964, 0.0788, 0.0603, 0.0227)
K_i	(10.9915, 2.7836, 1.9866, 0.7792)

Chapter 5

Friction Compensation and Control

5.1 Introduction

Simulation analysis and control is a huge motivation for the modelling and identification of system models. The previous chapter centred on the friction characterisation and identification on the laboratory experimental test-bed designed for that purpose. Model parameters of the proposed friction model were identified along side the parameters of some other models considered, namely the LuGre, GMS and Xiong friction models. In this chapter attention is given to the compensation and control of systems influenced by friction non-linearity. In chapter 2, it was clear that linear controllers of the PID type are not very efficient when non-linearities are part of the system under control and thus the need for model-based compensation technique also reviewed in chapter 2, to compensate for the non-linear friction. This inefficiency of PID controllers for friction control becomes more obvious in the pre-slide regime and velocity reversals. As such the design of a model-based friction compensation scheme adequate for simulation analysis and control of the test-bed is desired if adequate control of the test-bed is to be ensured.

In model-based friction compensation design, two important steps necessary for optimal results are the design of a linear (PID) controller to reduce system error, disturbance and help improve system stability, and the design of a model-based friction observer for the estimation of the system friction. The purpose of the estimated friction is to use it to modify the control law in such a manner that it is able to cancel friction effects emanating from the system. For this approach to be effective, it's implementation is such that there is little or no dynamics between the control effort point of application and the point of friction activity. It therefore becomes relevant the new friction model accurately models the system friction in the various velocity ranges and reversal points.

The chapter layout is as follows: Section 5.2 deals with the design of the linear part

of the compensator called the feedback controller, section 5.3 with the design the friction observer for velocity and position control purposes. In section 5.4, the implementation of the velocity and position observer-based compensators is performed, while analysis of the results of simulations are discussed in section 5.5. The chapter ends with summary section 5.6.

5.2 Linear controller design for the experimental test-bed

Stated earlier in sec.2.4, Proportional, Integral, Derivative controllers or their combinations are often effective for linear systems control as they help achieve stability, eliminate error and ensure reductions in transients. However integration of this type of controllers with friction observer (for the estimation of the system friction) has been shown to be an effective means for the control of systems with friction. In this section the focus is on the design of adequate controllers for position and velocity control of the laboratory test-bed of chapter 4. The design closely follows the set of velocity and position control design experiments used in the school of systems engineering, University of Reading with some modifications to adapt it for the present requirement. For many practical PID controller implementations, the derivative action is often reduced to a minimum if not zero or where possible a modified approach is sought to deal with potential challenges with the derivative action. The challenges of the derivative action on the traditional layout of the derivative are two fold namely

1. Larger values due to sharp transitions (at corners) in the reference signals for example a square wave, which give rise to unreasonably high control inputs.
2. The presence of noise in the measured signal usually of high frequency leading to large values of the input signal to the plant.

Possible solution to 1, is to assume that the derivative of the reference is zero in the steady state (true for many industrial processes) and then take the derivative of only the output signal. And for the second problem the need to introduce a first order filter and tune the poles to remove the chattering due to noise.

5.2.1 Design of a lag compensator for velocity control

A PI based controller has often been used rather than the regular PID controller for velocity control of systems. However, the similarities between the PI and Lag compensator is exploited and thus the design of proportional + lag compensator was pursued. The lag was preferred as it was shown to provide better filtering of properties though with the result that the steady state error would not be zero as would have been for a PI controller. To design a linear

controller for the test-bed an assumption of a friction-free system is made to obtain a linear model of the test-bed since friction is non-linear. So for the model of the experimental test-bed given as equation 4.9 with $B_{eq} = 0$ then the model equation reduces to

$$\frac{\omega_l(s)}{E_a(s)} = \frac{AK_m}{R_a J_{eq} s + (AK_m)^2} \quad (5.1)$$

then

$$\frac{\omega_l(s)}{E_a(s)} = K \frac{1}{Ts + 1} \quad (5.2)$$

where

$$K = \frac{1}{AK_m}$$

and

$$T = \frac{R_a J_{eq}}{(AK_m)^2}$$

are the system gain and time constant respectively. Equation 5.2 is the open loop transfer function of the test-bed model without friction consideration with angular velocity as output and voltage as input. For the objective of keeping the error to 1% and a cross over frequency of about 110 rad/sec, therefore the transfer function $A(s)$ of the controller for the velocity control of the laboratory test-bed is

$$A(s) = K_p \frac{T_i s + 1}{T_i s + \gamma} \quad (5.3)$$

with $K_p = 1.5136$ as the proportional gain of the controller, $T_i = 0.0909$ time constant, and $\gamma = 0.0285$. Detail of the controller design is in Appendix A.

5.2.2 Design of a PID controller for position control

For position control experiments and simulations a PID controller was designed to achieve zero error at steady state, overshoot of less than 15%, and fast response time. From the position model of equation 4.10, assuming no friction i.e $B_{eq} = 0$ then the model reduces to 4.12. this equation can also be re-written as

$$\frac{\theta_l(s)}{E_a(s)} = \frac{K}{s(Ts + 1)} \quad (5.4)$$

where

$$K = \frac{1}{AK_m}$$

and

$$T = \frac{R_a J_{eq}}{(AK_m)^2}$$

Equation 5.4 is the open loop transfer function of the experimental test-bed model without friction consideration and output as position and input as voltage.

The PID controller for the test-bed was designed with specification and details as shown in Appendix A. The transfer function of the PID controller is

$$A(s) = \frac{K_p s + K_i + K_d s^2}{s} \quad (5.5)$$

where $K_p = 5.7517$ is the proportional gain, $K_i = 10$ the integral gain, $K_d = -0.0768$ the derivative gain.

5.3 Friction observer design

With both the velocity and position controller design completed, this section is focused with the design of the friction observer for compensation of the friction non-linearities

5.3.1 Design concept

Consider a simple servo driven system represented as

$$Js^2 Y_0(s) = u - F_f \quad (5.6)$$

with J being the equivalent inertia of the system, F_f is the system friction, and u the control signal, $Y_0(s)$ is the output of the servo-system.

For the particular case the output is angular position then $Y_0(s) = \theta_o$ radians, or if the output is angular velocity then $Y_0(s) = \frac{\omega_o}{s}$ rad/sec. Generally, representation of the friction force could be with any of the friction model structures reviewed in chapter 2 or the new proposed model presented in chapter 3. However, for the design of the observer the proposed new model is used with known parameters as identified in chapter 4.

thus

$$Js\omega_0(s) = u - F_f \quad (5.7)$$

for velocity systems and

$$Js^2\theta_o(s) = u - F_f \quad (5.8)$$

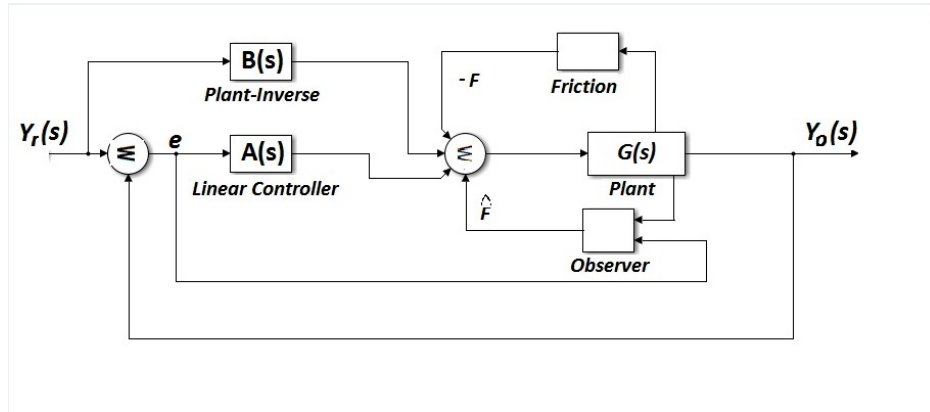


Fig. 5.1 The general structure for feedback model-based observer for friction control experiments

for position systems.

The design objective is the elimination of the unwanted system friction represented as F_f . One simple way of accomplishing this is to modify the control law by introducing an estimation of the system friction in the control law such that

$$u_{mod} = u + \hat{F}_f \quad (5.9)$$

where \hat{F}_f is the estimated friction from an observer and u_{mod} the modified control law. So equation (5.6) becomes

$$Js^2Y_0(s) = u_{mod} - F_f \quad (5.10)$$

substituting (5.9)

$$Js^2Y_0(s) = u - \tilde{F} \quad (5.11)$$

with

$$\tilde{F} = F_f - \hat{F}_f$$

where \tilde{F} is the estimation error, the error between the true system friction F_f and the estimated friction \hat{F}_f .

Since it is usually not possible to measure the internal state (z) of the system needed to evaluate the friction, an estimate of this is thus sought via an observer and this is used to obtain an estimation of the friction \hat{F}_f present in the system. A friction observer is therefore designed for the estimation of the internal state and subsequently friction in the system. The general structure of the observer based friction compensation scheme, using a feedback model-based compensation technique is shown in figure 5.1. Similar to the proposed friction

model, governing equations for the non-linear friction observer are given as

$$\dot{\hat{\gamma}} = \frac{g(v) - \hat{\gamma}}{\tau} - ke \quad (5.12)$$

$$\dot{\hat{z}} = \frac{1}{\sigma} (\text{sat}(\hat{\gamma}, F_{hyst}(\hat{z})) - F_{hyst}(\hat{z})) - ke \quad (5.13)$$

for the state variables γ and z estimates, and

$$\hat{F}_f = F_{hyst}(\hat{z}) + \sigma \dot{\hat{z}} + fv \quad (5.14)$$

for the estimated friction. Recall that the proposed friction model presented in chapter 3, equations 3.3, 3.4, and 3.5 with state equations

$$\dot{\gamma} = \frac{g(v) - \gamma}{\tau} \quad (5.15)$$

and

$$\dot{z} = \frac{1}{\sigma} (\text{sat}(\gamma, F_{hyst}(z)) + \sigma v - F_{hyst}(z)) \quad (5.16)$$

and the equation for friction force

$$F_f = F_{hyst}(z) + \sigma \dot{z} + fv \quad (5.17)$$

Therefore, the differences between the observer equations and the model equations are

$$\dot{\tilde{z}} = \dot{z} - \dot{\hat{z}} \quad (5.18)$$

$$\dot{\tilde{\gamma}} = \dot{\gamma} - \dot{\hat{\gamma}} \quad (5.19)$$

$$\tilde{F} = F_f - \hat{F}_f \quad (5.20)$$

yielding respectively

$$\dot{\tilde{z}} = \frac{1}{\sigma} (\text{sat}(\tilde{\gamma}, F_{hyst}(\tilde{z})) - F_{hyst}(\tilde{z})) + ke \quad (5.21)$$

$$\dot{\tilde{\gamma}} = \frac{\tilde{\gamma}}{\tau} + ke \quad (5.22)$$

$$\tilde{F} = F_{hyst}(\tilde{z}) + \sigma \dot{\tilde{z}} \quad (5.23)$$

Hence equations 5.21, 5.22 and 5.23 are known as the equations of the observer error.

Dissipativity of the observer error:

The dissipative properties of the proposed friction model structure equations 3.3, 3.4, and 3.5

was established in chapter 3. The dissipativity properties of the designed observer with e as input and \tilde{F} as output; both in it's states and the output friction torque is now established. This is necessary for establishing system stability since the system would then be considered as operators which map the input to the output. First the dissipativity of the map between the control error e and the observer error \tilde{F} is established.

Property 1

The map $\vartheta : e \mapsto \tilde{F}$ is dissipative with respect to a Lyapunov function defined as $V = \int_0^{\tilde{z}} F_{hyst}(\tau) d\tau$ with a derivative in the state's trajectory as $\dot{V} = F_{hyst}(\tilde{z})\dot{\tilde{z}}$.

Proof

From equations 5.21, 5.22, and 5.23

$$\tilde{F}e = (F_{hyst}(\tilde{z}) + \sigma\dot{\tilde{z}})e \quad (5.24)$$

from equation 5.21

$$e = \frac{1}{k}(\dot{\tilde{z}} - \frac{1}{\sigma}(\text{sat}(\tilde{\gamma}, F_{hyst}(\tilde{z})) - F_{hyst}(\tilde{z}))) \quad (5.25)$$

thus

$$\tilde{F}e = (F_{hyst}(\tilde{z}) + \sigma\dot{\tilde{z}})\frac{1}{k}(\dot{\tilde{z}} - \frac{1}{\sigma}(\text{sat}(\tilde{\gamma}, F_{hyst}(\tilde{z})) - F_{hyst}(\tilde{z}))) \quad (5.26)$$

leading to

$$\tilde{F}e = \frac{1}{k}[\sigma\dot{\tilde{z}}^2 + F_{hyst}(\tilde{z})\dot{\tilde{z}}] \quad (5.27)$$

for the stick regime,

and

$$\tilde{F}e = \frac{1}{\sigma k}[2\sigma F_{hyst}(\tilde{z})\dot{\tilde{z}} + (\sigma\dot{\tilde{z}} - \tilde{\gamma})\sigma\dot{\tilde{z}} + F_{hyst}(\tilde{z})(F_{hyst}(\tilde{z}) - \tilde{\gamma})] \quad (5.28)$$

for the slip regime.

Given that the second and third terms of eqn.5.28 are each ≥ 0

therefore,

$$\tilde{F}e \geq \dot{V} \quad (5.29)$$

for both regimes.

Next we investigate the dissipativity of the states \tilde{z} and $\tilde{\gamma}$ as follows;

Property 2

Given the map $\theta : e \mapsto \tilde{\gamma}$, the objective is to show that the input-state ($\tilde{\gamma}$) is dissipative with respect to a certain positive definite Lyapunov function $V = \frac{1}{2k}\tilde{\gamma}^2$ whose derivative in the state's trajectory is $\dot{V} = \frac{1}{k}\tilde{\gamma}\dot{\tilde{\gamma}}$.

Proof

with

$$\dot{\tilde{\gamma}} = \frac{\tilde{\gamma}}{\tau} + ke \quad (5.30)$$

then

$$\tilde{\gamma}e = \tilde{\gamma} \left(\dot{\tilde{\gamma}} - \frac{\tilde{\gamma}}{\tau} \right) \frac{1}{k} \quad (5.31)$$

yielding

$$\tilde{\gamma}e = \frac{1}{k\tau} (\dot{\tilde{\gamma}}\tilde{\gamma}\tau + \tilde{\gamma}^2) \quad (5.32)$$

that is

$$\tilde{\gamma}e = \frac{1}{k} \dot{\tilde{\gamma}}\tilde{\gamma} + \frac{1}{k\tau} \tilde{\gamma}^2 \quad (5.33)$$

such that

$$\tilde{\gamma}e \geq \dot{V} \quad (5.34)$$

Since $\tilde{\gamma}^2 \geq 0 \forall k, \tau \geq 0$.

Property 3

The map $\theta : e \mapsto \tilde{z}$ is also dissipative with respect to the Lyapunov function $V = \frac{1}{2k} \tilde{z}^2$, whose derivative in the state's trajectory is $\dot{V} = \frac{1}{k} \tilde{z} \dot{\tilde{z}}$.

Proof

We evaluate

$$\tilde{z}e = \frac{1}{k} \left(\dot{\tilde{z}} - \frac{1}{\sigma} (\text{sat}(\tilde{\gamma}, F_{hyst}(\tilde{z})) - F_{hyst}(\tilde{z})) \right) \tilde{z} \quad (5.35)$$

to yield

$$\tilde{z}e = \frac{1}{k\sigma} (\text{sat}(\tilde{\gamma}, F_{hyst}(\tilde{z})) - F_{hyst}(\tilde{z})) \tilde{z} + \frac{\dot{\tilde{z}}\tilde{z}}{k} \quad (5.36)$$

thus

$$\tilde{z}e = \frac{\dot{\tilde{z}}\tilde{z}}{k} \geq \dot{V} \quad (5.37)$$

for the stick regime, and

$$\tilde{z}e = \frac{1}{k\sigma} (F_{hyst}(\tilde{z})\tilde{z} - \tilde{\gamma}\tilde{z}) + \frac{\dot{\tilde{z}}\tilde{z}}{k} \quad (5.38)$$

for the slip regime.

But during slip

$$\sigma \dot{\tilde{z}} = \tilde{\gamma} - F_{hyst}(\tilde{z})$$

therefore

$$\tilde{z}e = \frac{2}{k} \dot{\tilde{z}}\tilde{z} \geq \dot{V} \quad (5.39)$$

Hence

$$\tilde{z}e \geq \dot{V}$$

for both regimes.

From the foregoing, the dissipativity properties of the observer has been demonstrated, this property of the observer is important as will be seen shortly in stability analysis and design of adequate control system.

5.3.2 Observer design for velocity control

In this section a friction observer was designed for the estimation of system friction. This friction observer is based on the proposed friction model of chapter 3 and also the linear plant (experimental test-bed) model. Defining the control signal u for the system of equation 5.6, to be of the form

$$u = -A(s)E(s) + B(s)\omega_r(s) \quad (5.40)$$

Then a modified control law for the system becomes as in 5.9

$$u_{mod} = -A(s)E(s) + B(s)\omega_r(s) + \hat{F}_f(s) \quad (5.41)$$

with $A(s)$ the transfer function of a linear controller, $E(s)$ is the error, the reference velocity ω_r is assumed to be differentiable, output velocity ω_o , $B(s)$ is the reciprocal of the input-output transfer function of the linear model of the process. Thus $B(s)$ is Js for velocity output.

Therefore u is a parallel combination of two linear controllers with $B(s)$ pre-determined from the given process dynamics and $A(s)$ chosen to meet certain design criteria outlined earlier. It should however be pointed out that the function $B(s)$ was put to increase error rejection as explained in section 2.3 and the system could also achieve specified performance index in the absence of $B(s)$. The structure adopted for the observer based compensation is as shown in figure 5.2. The error signal is taken as

$$E(s) = \omega_o - \omega_r$$

Putting equation 5.41 into 5.10 leads to

$$Js\omega_o(s) = -A(s)E(s) + B(s)\omega_r(s) - \tilde{F}(s) \quad (5.42)$$

with $B(s)\omega_r(s) = Js\omega_r(s)$

therefore

$$Js\omega_o(s) - Js\omega_r(s) = -A(s)E(s) - \tilde{F}(s) \quad (5.43)$$

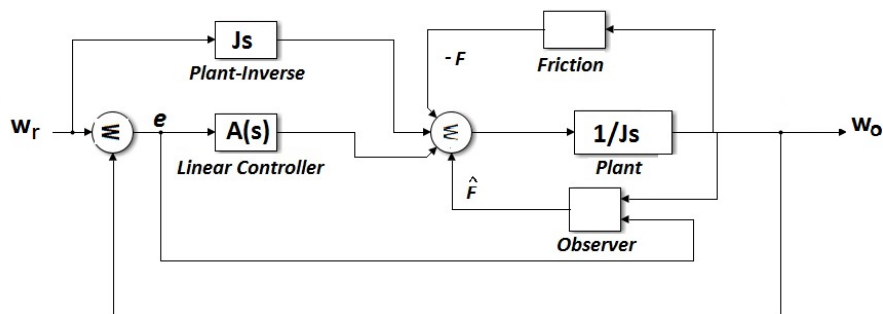


Fig. 5.2 The structure of an observer based friction compensation for velocity control simulations

$$JsE(s) + A(s)E(s) = -\tilde{F}(s) \quad (5.44)$$

Hence

$$E(s) = \frac{1}{Js + A(s)}(-\tilde{F}(s)) \quad (5.45)$$

and defining

$$G(s) = \frac{1}{Js + A(s)} \quad (5.46)$$

then

$$E(s) = -G(s)\tilde{F}(s) \quad (5.47)$$

Substituting equation 5.3 into equation 5.46 yields

$$G(s) = \frac{T_i s + \gamma}{Js(T_i s + \gamma) + K_p(T_i s + 1)} \quad (5.48)$$

the order difference of eqn. 5.48 is clearly 1 and on further testing it was shown to exhibit the strictly positive real (SPR) characteristics listed below. This implies that the transfer function $G(s)$ (5.48) is Strictly Positive Real (SPR). A system, such as $G(s)$ is SPR if the following conditions are satisfied [111];

1. $G(s)$ is Hurwitz
2. $G(j\omega) + G^T(-j\omega) > 0, \forall \omega \in \Re$
3. $G(\infty) + G^T(\infty) > 0$

THEOREM 5.1

Given the simple servo system of 5.7, with $G(s)$ SPR, with the friction model equations 5.15,

5.16 and 5.17, the observer equations 5.12, 5.13, and 5.14 together with the control law 5.41, the observation error \tilde{F} and the control error $E(s)$ will each asymptotically tend to zero, with bounded states. Such a system is said to be globally asymptotically stable as the control error converges to zero as well as the estimation error.

Proof:

Consider a state space representation of the single input single output system $G(s)$ as

$$\dot{\varepsilon} = A\varepsilon + B(-\tilde{F}) \quad (5.49)$$

$$e = C\varepsilon \quad (5.50)$$

where ε is the state, \tilde{F} the input (friction), and e is the output (error). Given that $G(s)$ is Strictly Positive Real (SPR) then from *Kalman-Yakubovich's Lemma* [111], there exists a set of matrices P and Q with the following properties $P = P^T > 0$ and $Q = Q^T > 0$ such that

$$A^T P + PA = -Q \quad (5.51)$$

$$PB = C^T \quad (5.52)$$

Following a similar argument in [109], a Lyapunov function V that is radially unbounded in the states ε and \tilde{z} is chosen such that

$$V = \varepsilon^T P \varepsilon + \frac{4}{k} \int_0^{\tilde{z}} F_{hyst}(\tilde{\tau}) d\tau \quad (5.53)$$

then the derivative is

$$\dot{V} = \varepsilon^T (P + P^T) \dot{\varepsilon} + \frac{4}{k} F_{hyst}(\tilde{z}) \dot{\tilde{z}} \quad (5.54)$$

Re-arranging leads to

$$\dot{V} = \varepsilon^T P \dot{\varepsilon} + \varepsilon^T P^T \dot{\varepsilon} + \frac{4}{k} F_{hyst}(\tilde{z}) \dot{\tilde{z}} \quad (5.55)$$

substituting eqn. 5.49 yields

$$\dot{V} = \varepsilon^T P (A\varepsilon - B(\tilde{F})) + \varepsilon^T P^T (A\varepsilon - B(\tilde{F})) + \frac{4}{k} F_{hyst}(\tilde{z}) \dot{\tilde{z}} \quad (5.56)$$

on expanding

$$\dot{V} = \varepsilon^T P A \varepsilon - \varepsilon^T P B(\tilde{F}) + \varepsilon^T P^T A \varepsilon - \varepsilon^T P^T B(\tilde{F}) + \frac{4}{k} F_{hyst}(\tilde{z}) \dot{\tilde{z}} \quad (5.57)$$

Factorizing the above gives

$$\dot{V} = \varepsilon^T (PA + P^T A) \varepsilon - \varepsilon^T (PB + P^T B) \tilde{F} + \frac{4}{k} F_{hyst}(\tilde{z}) \dot{\tilde{z}} \quad (5.58)$$

From eqns. 5.51 and 5.52,
 $PA + P^T A = Q$ and $PB = C^T$
 thus

$$\dot{V} = -\varepsilon^T Q \varepsilon - 2e \tilde{F} + \frac{4}{k} F_{hyst}(\tilde{z}) \dot{\tilde{z}} \quad (5.59)$$

Recall that $e \tilde{F}$ was earlier obtained in eqn. 5.28,
 therefore,

$$\dot{V} = -\varepsilon^T Q \varepsilon - \frac{2}{\sigma k} (F_{hyst}(\tilde{z})(F_{hyst}(\tilde{z}) - \tilde{\gamma}) + \sigma \dot{\tilde{z}}(\tilde{z} - \tilde{\gamma})) \quad (5.60)$$

Since the terms in the parenthesis are positive then equation 5.60 clearly shows a non-increasing function (i.e the negative semi-definiteness of the derivative of the Lyapunov function V). This with the earlier condition that V is radially unbounded ensures the states are bounded also. From observation it is easily seen that this is an interconnection of a linear SPR function ($G(s)$) and a dissipative function whose output is \tilde{F} . Such systems are known to exhibit asymptotic stability. Thus the condition that the transfer function $G(s)$ is SPR and the passivity of the observer ensures the convergence of the control error $e \rightarrow 0$ and the estimation error $\tilde{F} \rightarrow 0$.

5.3.3 Observer design for position control

Next, the design of the position observer is discussed.

Consider a control signal u for the position control of the system of equation 5.6 of the form

$$u = -A(s)E(s) \quad (5.61)$$

Then the modified control signal eqn. 5.9 for the system becomes

$$u_{mod} = -A(s)E(s) + \hat{F}_f(s) \quad (5.62)$$

with $A(s)$ the transfer function of a linear controller often of the PID type, $E(s)$ is the error between the desired reference signal θ_r , assumed to be twice differentiable and the actual output signal $\theta_0(s)$. Thus $E(s) = \theta_o - \theta_r$. $B(s)$ is the reciprocal of the input output transfer function of the linear model of the process. Thus $B(s)$ is $J s^2$ for the position output. For the

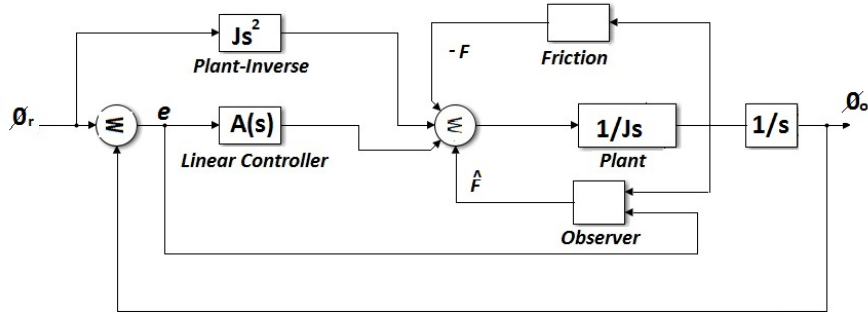


Fig. 5.3 The structure of an observer based friction compensation for position control simulations where F and \hat{F} are torque variables that depend on the angular velocity of the plant

design of the position observer the figure 5.3 is adopted for some reasons to be explained later. Putting equation 5.62 into 5.10

$$Js\theta_o(s) = -A(s)E(s) + B(s)\theta_r(s) - \tilde{F}(s) \quad (5.63)$$

with $B(s) = Js^2\theta_r(s)$

therefore

$$Js^2\theta_o(s) - Js\theta_r(s) = -A(s)E(s) - \tilde{F}(s) \quad (5.64)$$

$$-Js^2E(s) + A(s)E(s) = -\tilde{F}(s) \quad (5.65)$$

Hence

$$E(s) = \frac{1}{Js^2 + A(s)}(-\tilde{F}(s)) \quad (5.66)$$

and define

$$G(s) = \frac{1}{Js^2 + A(s)} \quad (5.67)$$

then

$$E(s) = -G(s)\tilde{F}(s) \quad (5.68)$$

From the above equation it is not feasible to find a transfer function $A(s)$ such that $G(s)$ is Strictly Positive Real (SPR). This is because the difference in the order of denominator and numerator must be 0 or 1, but in this case it is 2.

However, it is possible to find some functions of $A(s)$ such that the function $G(s)$ is asymptotically stable in the neighbourhood of the equilibrium. For this we seek $A(s)$ such that $G(s)$ is; positive real (PR), has no poles on the imaginary axis and $Re[G(i\omega)] > 0$. For such a

system, the error $E(s) \rightarrow 0$ and all other states remain bounded. Such PR functions allow the use of pure integrators as $A(s)$.

THEOREM 5.2

Assuming the system given as equation 5.8 with the friction force of equations 5.15, 5.16 and 5.17, the observer equations 5.12, 5.13, and 5.14 together with the control law 5.63, if the closed loop transfer function $G(s)$ equation 5.67 is PR, has no poles on the imaginary axis and $Re(G(i\omega)) > 0$ for $\omega > 0$, then such system is said to be globally asymptotically stable so that the error $e \rightarrow 0$ and the states are bounded.

Proof

If we chose a State Space representation of $G(s)$ as

$$\dot{\varepsilon} = A\varepsilon + B(-\tilde{F}) \quad (5.69)$$

$$e = C\varepsilon \quad (5.70)$$

There exists a set of matrices P, L and W with the following properties

$$P = P^T > 0$$

$$A^T P + PA = -L^T L$$

$$PB = C^T - L^T W$$

and

$$W^T W = D + D^T$$

Therefore introducing a Lyapunov function V that is radially unbounded in the states ε and \tilde{z} such that

$$V = \varepsilon^T P \varepsilon + \frac{4}{k} \int_0^{\tilde{z}} F_{hyst}(\tilde{\tau}) d\tau \quad (5.71)$$

then the derivative is

$$\dot{V} = \varepsilon^T (A^T P + PA) \varepsilon - 2\varepsilon^T P B \tilde{F} + \frac{4}{k} F_{hyst}(\tilde{z}) \dot{\tilde{z}} \quad (5.72)$$

$$\dot{V} = -\varepsilon^T L^T L \varepsilon - 2\varepsilon^T C^T \tilde{F} + \frac{4}{k} F_{hyst}(\tilde{z}) \dot{\tilde{z}} \quad (5.73)$$

then

$$\dot{V} = -\varepsilon^T L^T L \varepsilon - 2e\tilde{F} + \frac{4}{k} F_{hyst}(\tilde{z}) \dot{\tilde{z}} \quad (5.74)$$

substituting $e\tilde{F}$, equation 5.28 into 5.74 yields

$$\dot{V} = -\varepsilon^T L^T L \varepsilon - \frac{2}{\sigma k} [F_{hyst}(\tilde{z})(F_{hyst}(\tilde{z}) - \tilde{\gamma}) + \sigma \dot{\tilde{z}}(\tilde{z} - \tilde{\gamma})] \quad (5.75)$$

therefore

$$\dot{V} \leq 0 \quad (5.76)$$

holds true since the terms in the parenthesis are always positive then equation 5.75 clearly shows a non-increasing function (i.e the negative semi-definiteness of the derivative of the Lyapunov function V). This with the earlier condition that V is radially unbounded ensures the states are bounded also. However, the asymptotic stability could not be ascertained. La Salle's theorem is now applied to proof this and also the convergence of the control error to zero ($e \rightarrow 0$) and the estimation error to zero ($\tilde{F} \rightarrow 0$). The condition that equation 5.75 is zero, that is

$$\dot{V} = 0$$

is possible only if the following are satisfied

1. $L\varepsilon = 0$
2. $F_{hyst}(\tilde{z})(F_{hyst}(\tilde{z}) - \tilde{\gamma}) = 0$, and
3. $\sigma \dot{\tilde{z}}(\tilde{z} - \tilde{\gamma}) = 0$

Thus when $\tilde{z} = 0$ then from 5.22 the estimation error $\tilde{F} = 0$ and the control error $E(s) = 0$ from eqn. 5.68 implying that $G(s)$ is asymptotically stable.

The design of the PID controller $A(s)$ in section 5.2 is such that this condition of positive real is satisfied with

$$A(s) = \frac{K_p s + K_i + K_d s^2}{s}$$

5.4 Observer based friction compensation implementation

In this section the feedback model-based observer compensators designed in the previous section are used for the purposes of both velocity and position control of simple system subject to the friction influence. Some of the relevant friction model structures were used as well as the new model presented for the purposes of performance comparisons and analysis. This simulation analysis served as a test of the suitability of the compensator to perform within acceptable design specifications.

5.4.1 Velocity control example

To illustrate the ability of model-based friction compensation, consider the servo system given as

$$Js\omega_o = u - F_f$$

where J is the inertia of the system, ω_o the output velocity, u the control command and F_f system friction modelled by the proposed friction model. Given the absence of an input velocity (i.e $\omega_r = 0$), though the system is subjected to a disturbance velocity signal as shown in the figure 5.4. Thus the system output velocity is $\omega_o \neq 0$. Since the reference velocity is zero, the objective is to eliminate the error between input reference ω_r and the response ω_o so as to make $\omega_o \rightarrow 0$. The choice for the nature of the disturbance signal was informed by the fact that friction is most disturbing near-zero velocities and velocity reversals. As such the disturbance signal is chosen to be low enough with many reversal velocities. To capture the capability of the proposed, and other friction model structures to compensate friction effects in this region, a disturbance signal of the form shown in figure 5.4 was used as suggested in [109]. This disturbance signal was obtained by passing a white noise signal with zero mean and deviation of unity through a filter $H(s)$ of the form

$$H(s) = \frac{1}{40} \frac{s^2}{(s+0.2)^4} \quad (5.77)$$

For the control implementation of the observer based feedback control system shown as figure 5.5, the values of the linear controller are $P = 4$ and $I = 16$. The parameter values of the proposed model used for the simulation are; $F_s = 0.33$, $F_c = 0.28$, $v_s = 0.01$, $\sigma = 60$, $\tau = 0.002$, $Z_b = 0.001$, and $f_v = 0.0176$. First a PI-control implementation in the absence of friction was performed and the results illustrated in figure 5.6, while figure 5.7 captured the linear controller implementation in the presence of friction. From these two figures it is clear that friction effects on the system is more pronounced in the near zero and velocity reversals and this rendered the linear PI controller inadequate for high precision velocity systems control. The error measure was more pronounced around zero velocities as compared with the case of no friction. As a measure of the effectiveness of the control scheme, mean square error (mse) and the maximum error values were used. For all the velocity control schemes studied these two measures were obtained and presented in table 5.1.

Subsequently, the proposed model observer was introduced as shown in the figure 5.5 to provide added control for the non-linear friction and the results shown in figure 5.8, while the mse and maximum error values are in table 5.1. In the same token LuGre model-based observer, GMS model-based observer and Xiong model-based observer were

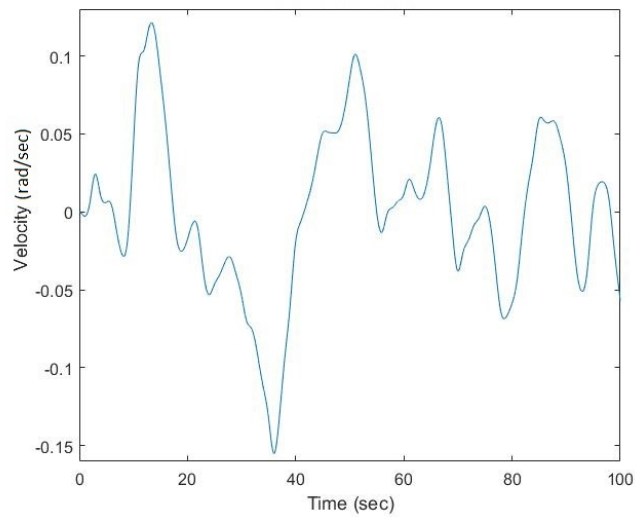


Fig. 5.4 A disturbance signal used for the velocity control simulations

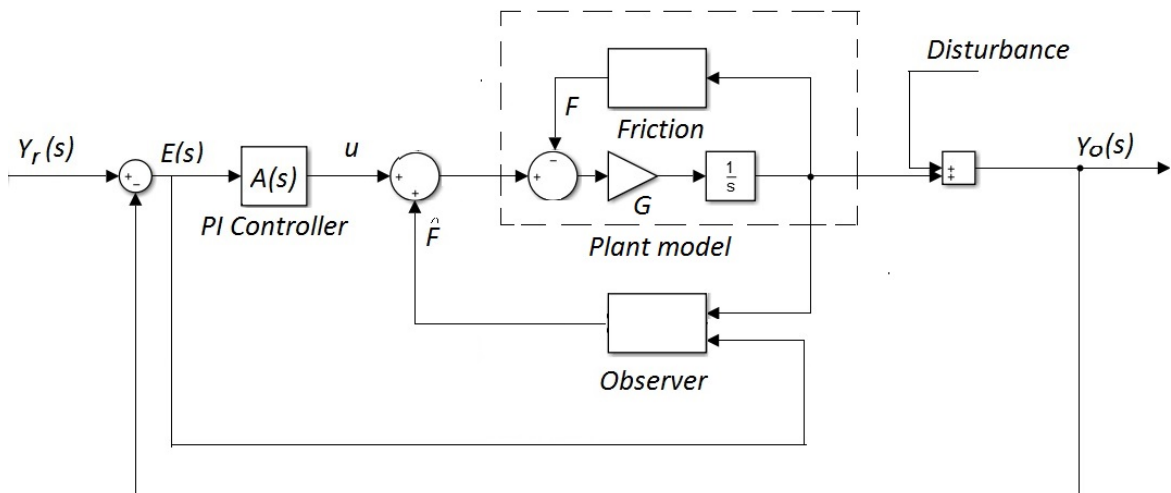


Fig. 5.5 Block diagram of the observer-based friction compensator for the velocity control simulation example

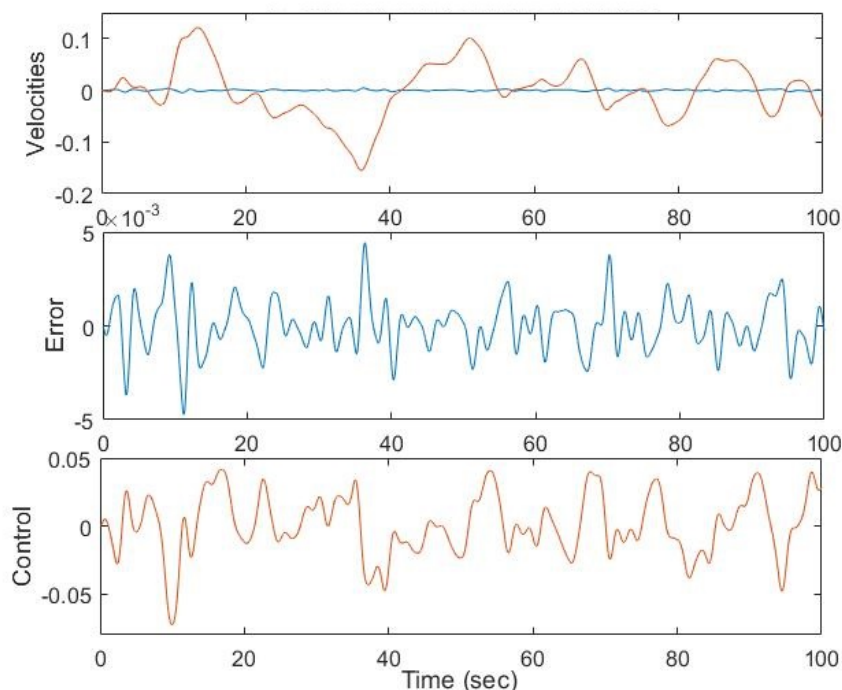


Fig. 5.6 Linear controller performance in the absence of friction: **top-** Disturbance (red), and output (blue) velocities, **middle-** The control error signal, and **bottom-** The PI control signal

implemented and the results of the various control schemes shown in figures 5.9, 5.10, and 5.11 respectively. Their respective mses' and maximum errors were presented in the table 5.1. The parameters for the LuGre model-based observer used for the simulation are: $F_s = 0.33$, $F_c = 0.28$, $v_s = 0.01$, $\sigma_1 = 20$, $\sigma_0 = 1000$, and $f_v = 0.0176$. For the GMS model-based observer using 4 slip elements: $F_s = 0.33$, $F_c = 0.28$, $v_s = 0.01$, $\sigma_{0i} = 25$, $\sigma_{1i} = 0.0015$, $C_i = 0.025$, $f_v = 0.0176$, and $\alpha_i = 0.25$. The parameters for the Xiong model-based observer with 4 slip elements are: $F_s = 0.33$, $F_c = 0.28$, $v_s = 0.01$, $K_i = 2.5$, $\sigma_i = 1.5$, $f_v = 0.0176$, and $\lambda_i = 0.25$, and $\tau = 0.002$. From the table 5.1 it is shown that with the proposed model,

Table 5.1 Performance indices for the various control schemes studied under velocity control

Controller type	mse ($\times 10^{-6}$)	Maximum error ($\times 10^{-4}$)
PI no Friction	1.7187	47
PI with Friction	101.42	543
proposed model observer	1.0855	25
LuGre model observer	1.3738	47
GMS model observer	1.6553	50
Xiong model observer	1.6322	48

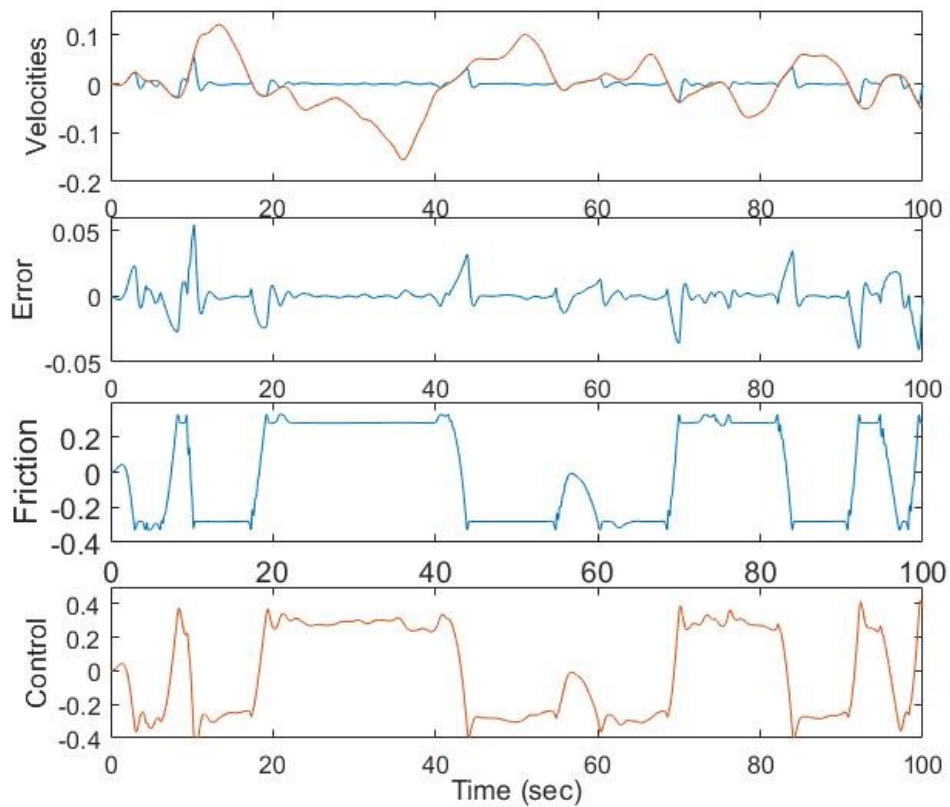


Fig. 5.7 Linear controller performance in the presence of friction: **top-** Disturbance (red), and output (blue) velocities, **mid-upper-** The error signal showing increased error due to friction, **mid-lower-** The system friction, and **bottom-** The PI control signal

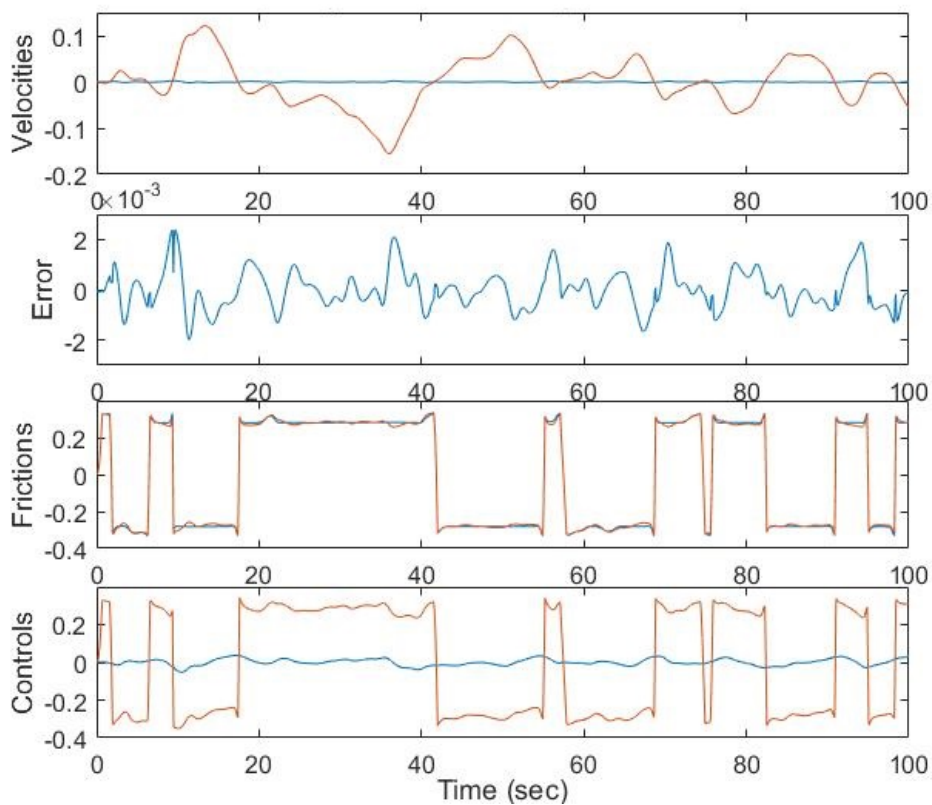


Fig. 5.8 Observer based velocity control of a system subject to friction using the proposed model: **top-** Disturbance 'red', and output 'blue' velocities, **mid-upper-** The error signal showing increased error due to friction, **mid-lower-** The system friction 'red' and estimate friction 'blue', and **bottom-** The linear control signal 'blue' and the modified control law 'red'

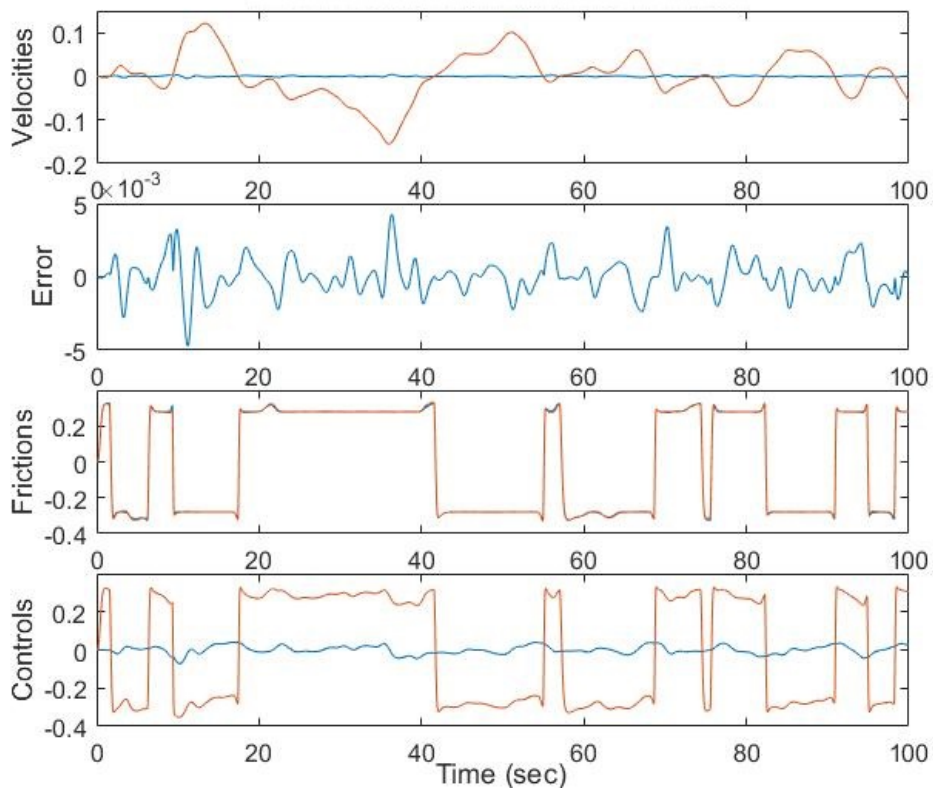


Fig. 5.9 Observer based velocity control of a system subject to friction using the LuGre model: **top-** Disturbance 'red', and output 'blue' velocities, **mid-upper-** The error signal showing increased error due to friction, **mid-lower-** The system friction 'red' and estimate friction 'blue', and **bottom-** The linear control signal 'blue' and the modified control law 'red'

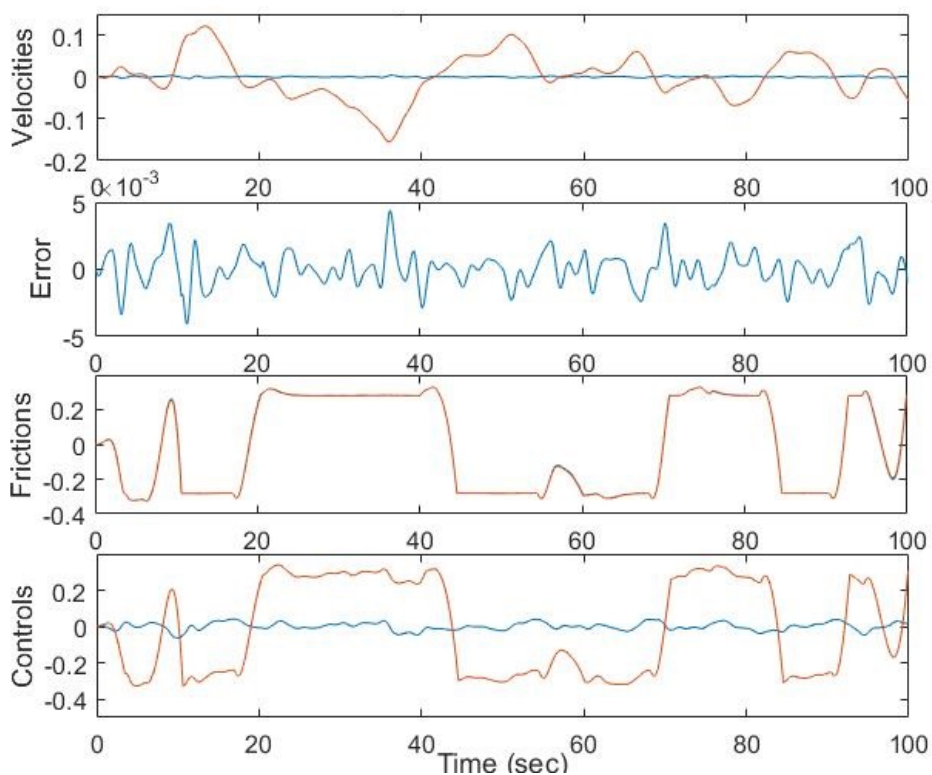


Fig. 5.10 Observer based velocity control of a system subject to friction using the GMS model: **top-** Disturbance 'red', and output 'blue' velocities, **mid-upper-** The error signal showing increased error due to friction, **mid-lower-** The system friction 'red' and estimate friction 'blue', and **bottom-** The linear control signal 'blue' and the modified control law 'red'

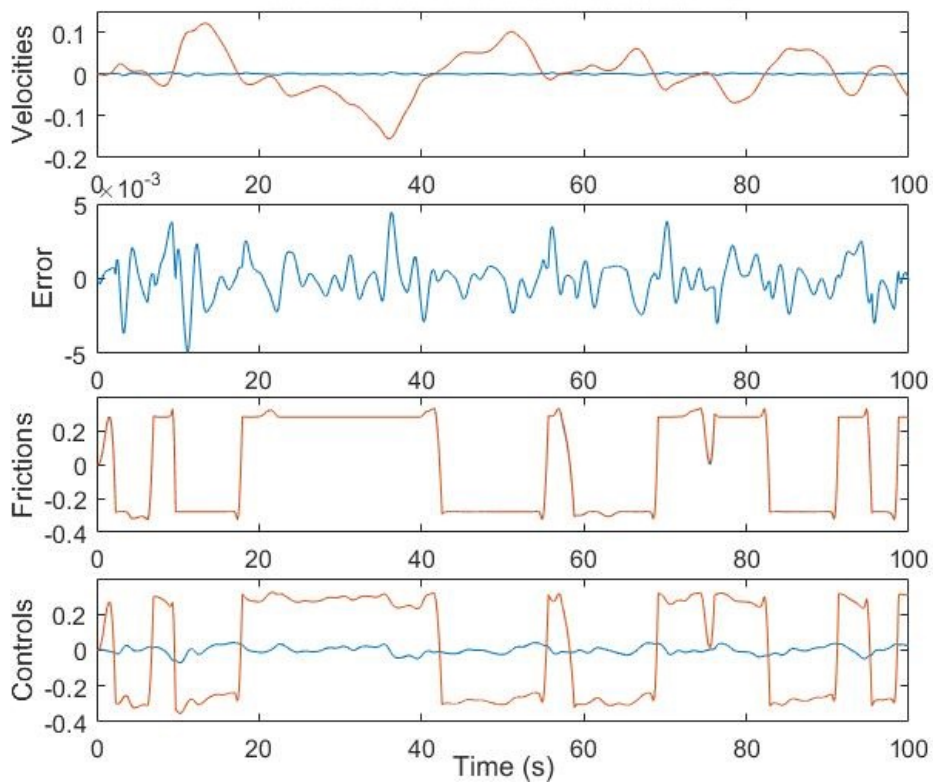


Fig. 5.11 Observer based velocity control of a system subject to friction using the Xiong model: **top-** Disturbance 'red', and output 'blue' velocities, **mid-upper-** The error signal showing increased error due to friction, **mid-lower-** The system friction 'red' and estimate friction 'blue', and **bottom-** The linear control signal 'blue' and the modified control law 'red'

the compensator scheme was able to reduce the error originating from frictional effects in the system as indicated by the lowest value of the maximum error recorded. As such the performance order of the model-based observers investigated here showed the proposed model performance for the chosen reference signal to be better. This closely followed by the LuGre, Xiong and GMS models in that order.

Next was a look at using the same concept for position control of a system under the influence of friction.

5.4.2 Position control example

The position control scheme example is shown in figure 5.12. Consider the simple system subjected to a step input position and the objective is to ensure the error $E(s)$ between output position θ_o and reference position θ_r is as small as possible. First a simple PID controller was implemented with the following parameter values: $P = 0.1$, $I = 0.4$, and $D = 0.05$ and the results obtained both for the cases of no friction and that with friction are shown in figures 5.13 and 5.14 respectively. The process friction was modelled using the proposed friction model. From these figures, position control was effectively accomplished with a simple PID feedback controller in the absence of friction, see figure 5.13. On the other-hand, introduction of friction into the system complicated and posed a challenge which the simple PID controller could not handle, see figures 5.14 effectively. In other to confront this an observer based position controller designed in the previous section was implemented for a step input reference (basic changes has to do with the PID parameters, but the structure remains the same). For the observer based schemes, the various models of friction (proposed, LuGre, GMS and Xiong) were used for the observer implementation as in the figure 5.12. The results of the position control as a result of the new observer based compensators with the proposed, LuGre, GMS, and the Xiong models respectively are shown as figures 5.15, 5.16, 5.17, and 5.18. The various mse and maximum errors presented also in table 5.2. The observer based compensators generally were shown to remarkably improve the system performance by reducing the friction induced error. All the systems under study showed better performance than the case of the simple linear controller, with the proposed model exhibiting the best compensatory qualities as regards to the friction phenomenon.

5.5 Analysis of simulation results

In this section an analysis of the simulation results is carried out with a view to understanding the general behaviour of the proposed model and some others as it relates to velocity and

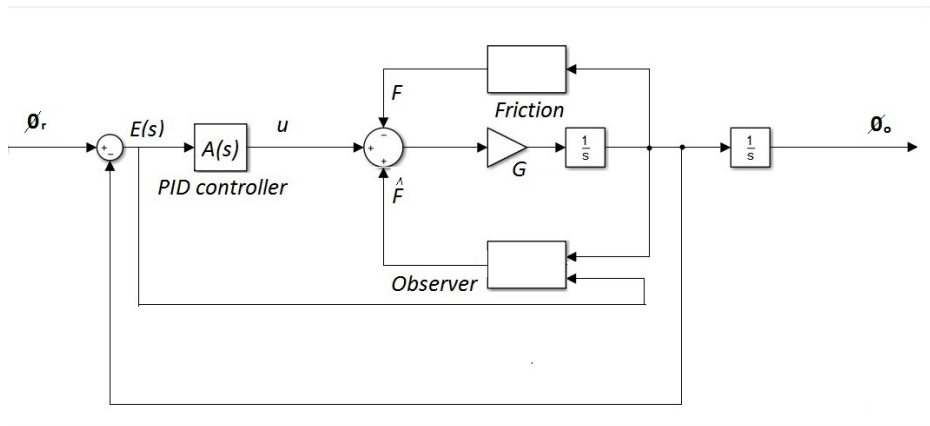


Fig. 5.12 Block diagram of the observer-based friction compensator for the position control simulation example

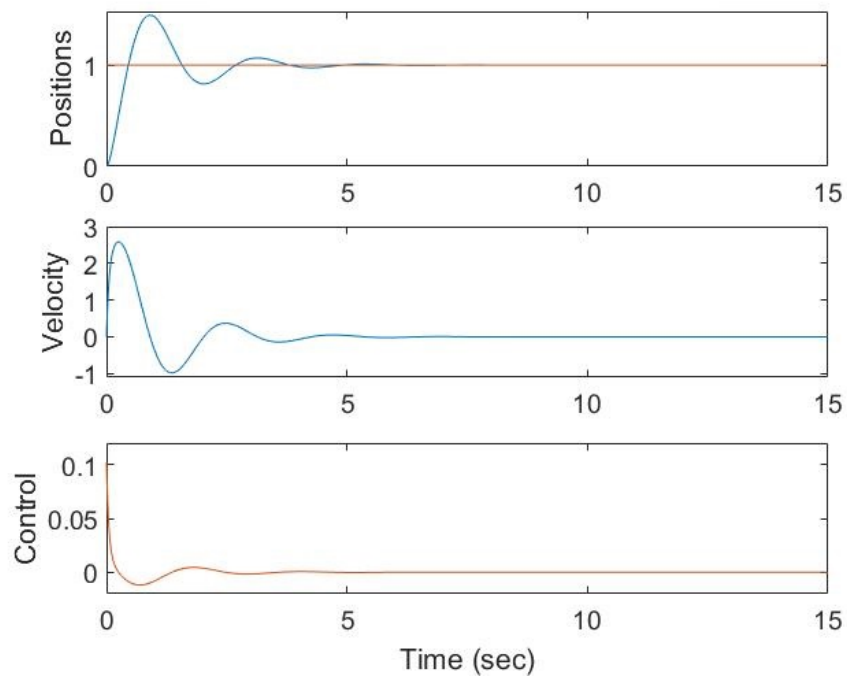


Fig. 5.13 Linear controller position control performance in the absence of friction: **top-** Reference input 'red', and output response 'blue' positions, **middle-** The velocity signal, and **bottom-** The PID control signal

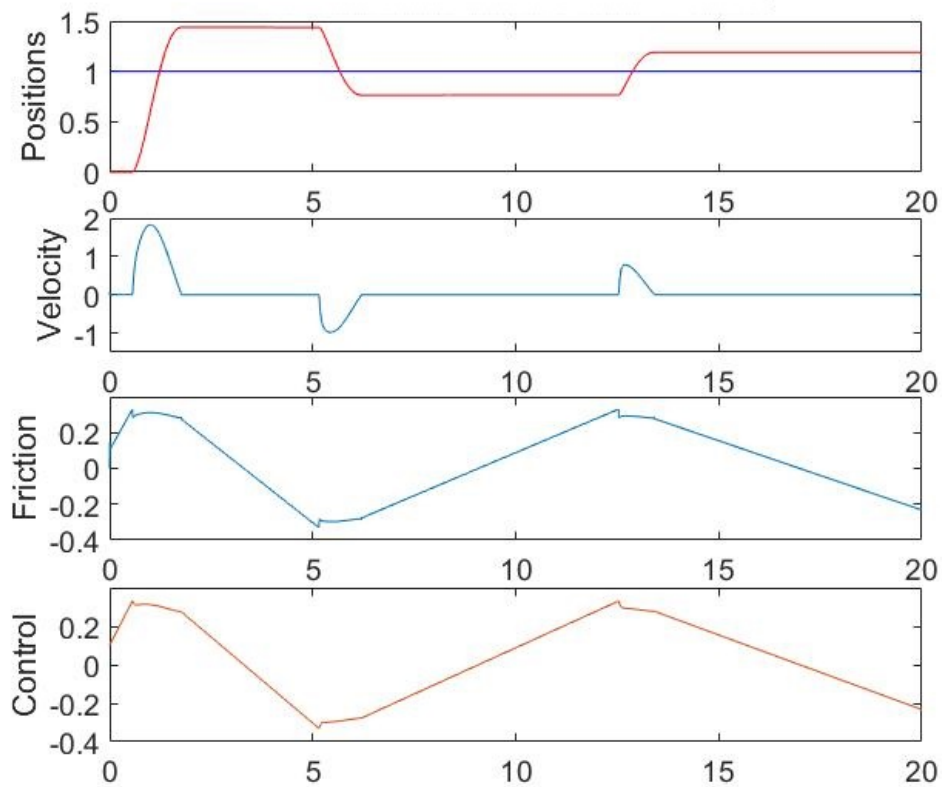


Fig. 5.14 Linear controller position control performance in the presence of friction: **top-** Reference input (green), and output response (red) positions, **mid-upper-** The velocity signal showing limit cycle prediction, **mid-lower-** The friction predicted and **bottom-** The PID control signal

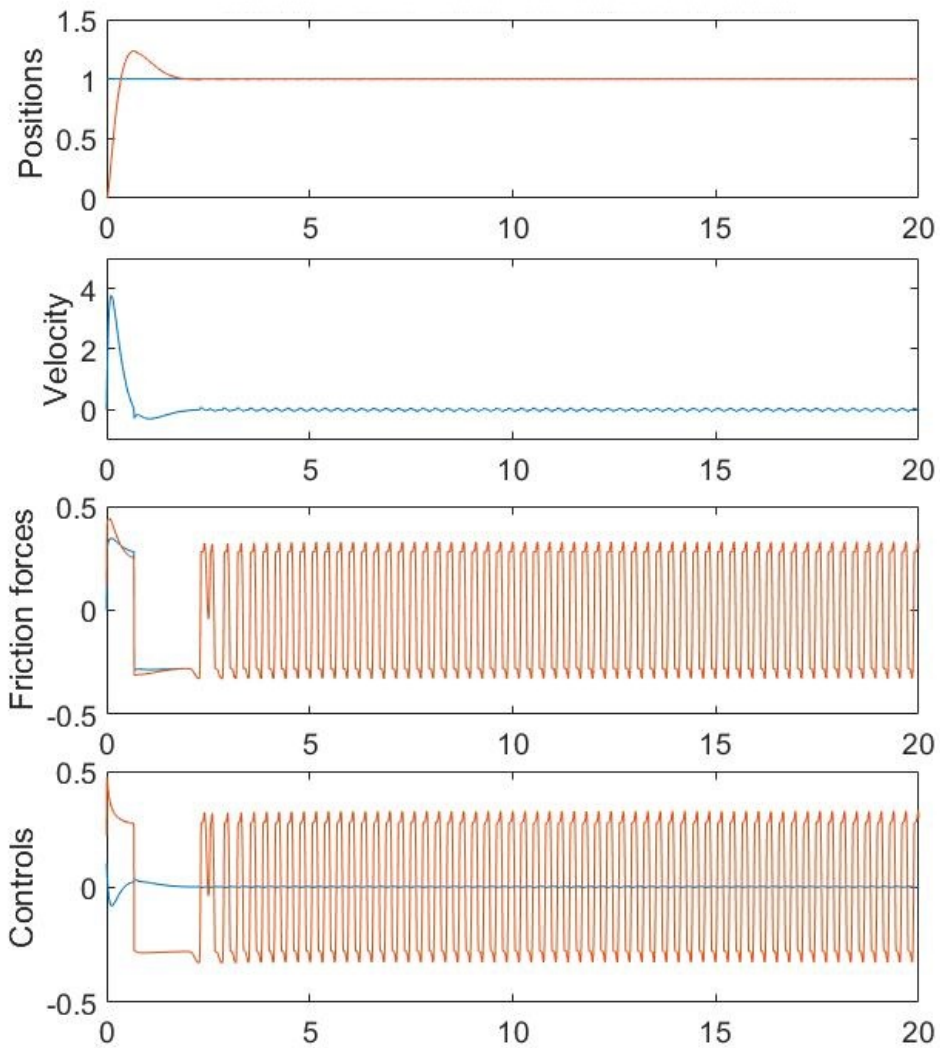


Fig. 5.15 Position control of a system subject to friction using the proposed model as observer: **top-** Reference input 'green', and output response 'red' positions, **mid-upper-** The velocity signal, **mid-lower-** The friction forces (both estimated and predicted and **bottom-** The PID 'blue' and modified 'red' control signals

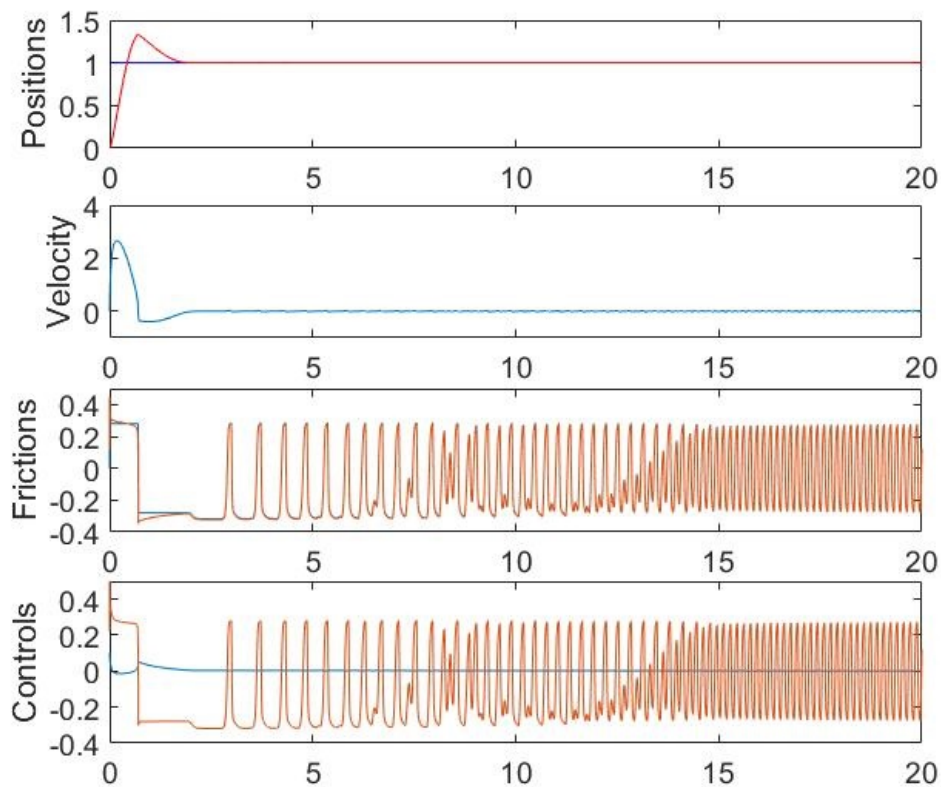


Fig. 5.16 Position control of a system subject to friction using the LuGre model as observer: **top-** Reference input 'green', and output response 'red' positions, **mid-upper-** The velocity signal, **mid-lower-** The friction forces (both estimated and predicted and **bottom-** The PID 'blue' and modified 'red' control signals

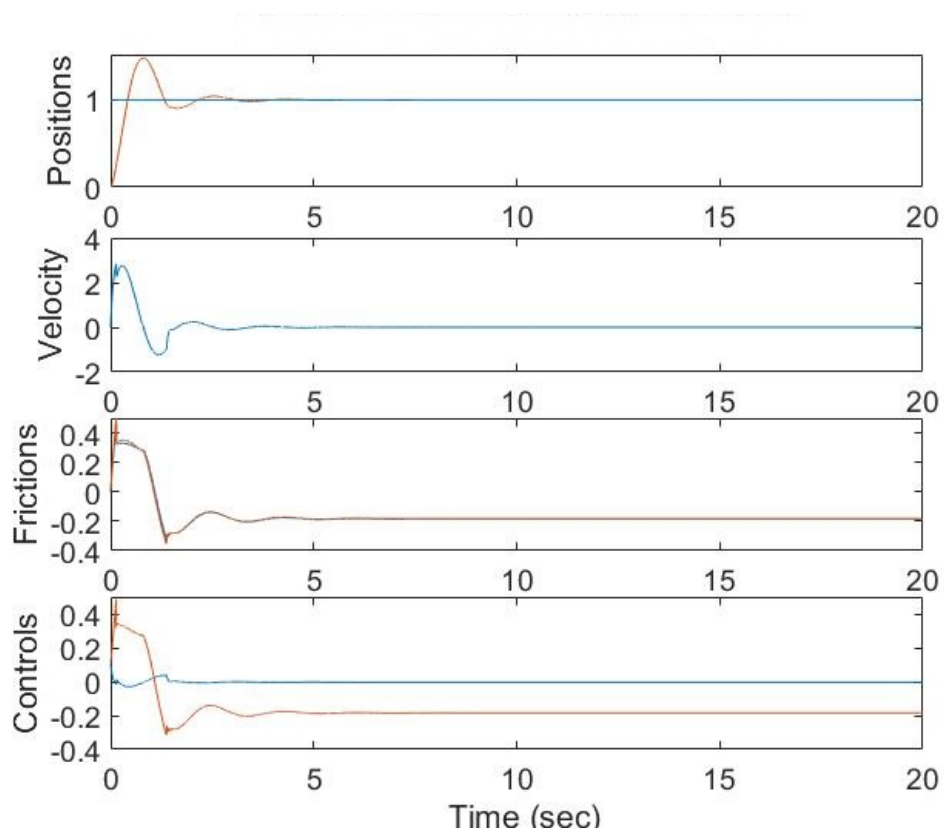


Fig. 5.17 Position control of a system subject to friction using the GMS model as observer: **top-** Reference input 'green', and output response 'red' positions, **mid-upper-** The velocity signal, **mid-lower-** The friction forces (both estimated and predicted and **bottom-** The PID 'blue' and modified 'red' control signals

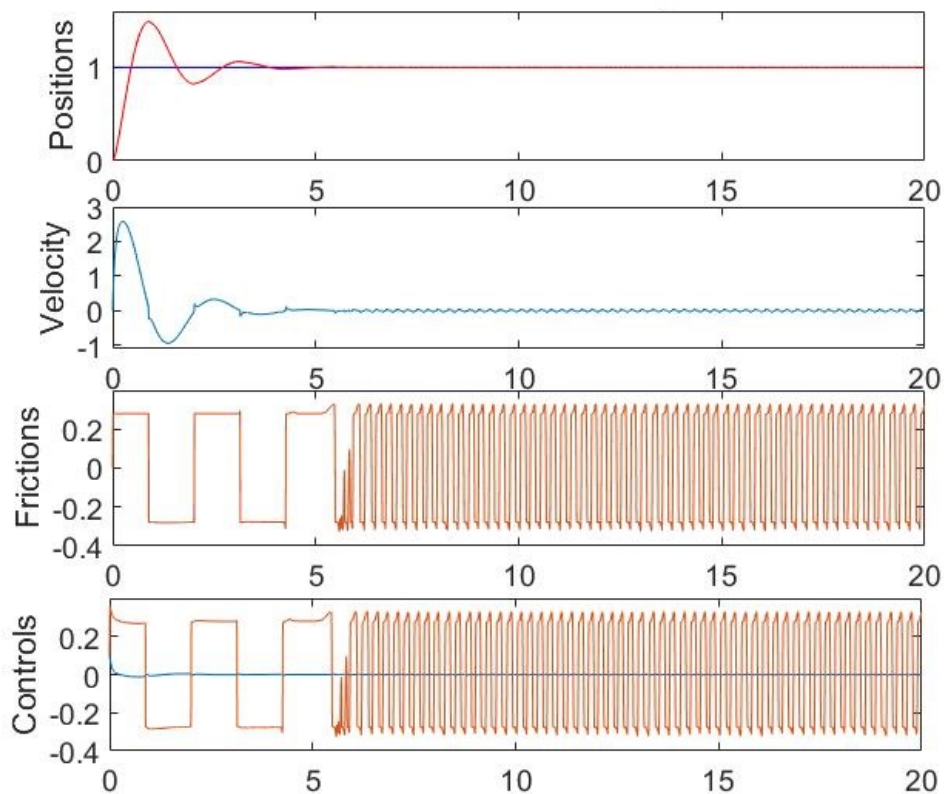


Fig. 5.18 Position control of a system subject to friction using the Xiong model as observer: **top-** Reference input 'green', and output response 'red' positions, **mid-upper-** The velocity signal, **mid-lower-** The friction forces (both estimated and predicted and **bottom-** The PID 'blue' and modified 'red' control signals

Table 5.2 Performance indices for the various control schemes studied under position control

Controller type	mse ($\times 10^{-4}$)
PI no Friction	67
PI with Friction	441
proposed model observer	30
LuGre model observer	41
GMS model observer	44
Xiong model observer	65

position control. The performance the observer in compensating the friction phenomena for the velocity and position control systems studied is also investigated hereunder.

5.5.1 Velocity control

A low velocity signal used for the simulation was necessary so as to capture the effects of friction non-linearity especially at low velocities and reversals. From the simulation results of figure 5.6, the linear controller implementation was effective for the system velocity control as the controlled error result showed. This is typical of linear control in the absence of friction. The control of systems with friction is most problematic in the low and reversal velocity regions and as such linear controllers are not effective when used as stand alone controllers for non-linear systems involving these velocity regions. This scenario was shown in figure 5.7 where the introduction of friction non-linearity to the system rendered the otherwise appropriate linear controller inefficient for velocity control. This deterioration in the control as measured by the mse and maximum error is of a unit order (10 times worse) than the case for no friction. The control law also was shown to increase by a factor of about 10 and the system friction as modelled by the proposed model is shown also. With a model-based friction observer to compensate friction non-linearities incorporated in the control loop of figure 5.5, improvements are easily observed. From the results of figure 5.8 the controlled error was seen to be well below the error obtained for the cases of no friction of figure 5.6 and simple linear controller in the presence of friction figure 5.7. The control signal needed to achieve this improved control is quite small also. The error reduction of the model-based observer compensation (with proposed model) was about 2 times better than the no friction compensated control and 20 times better than with friction. Using the LuGre model-based observer of figure 5.9 good performance of the control scheme is observed and the error improvement against the no friction control and no model observer compensation was about the same and 10 times respectively for both scenarios. The performance of the GMS and Xiong models observer compensations were of the same order as the LuGre

model and generally showed improvement over the conventional linear controller. It should be noted that the improvement of the model-based compensation strategy over the simple control even in the case of no friction suggests the capability of model-based compensators to improve linear system performance also. Low velocities and reversal point velocities control measures of the compensators from the various performance results of figures 5.6 to 5.11 indicate the ability of the observer based compensation approach to be superior to the velocity control schemes based only on the linear controller. A critical look at the error results in the relevant figures and tables also indicate that the performance improvement of the observer based compensation to be mostly in the low and reversal velocities where friction is mostly non-linear. Among the various model-based observers investigated namely the proposed, LuGre, GMS and Xiong models, index results suggests that better control performance (velocity regulation) was achieved with the proposed model observer than the others. This was followed closely by the LuGre, Xiong and GMS models in the order. These measures of performance of the various control schemes namely the mean square error (mse) and maximum error are published in table 5.1.

5.5.2 Position control

Position control simulation results for the system of figure 5.12 performed using the linear (PID) controller show good performance of the control approach given that the position error in the steady state is effectively reduce to zero as also indicated by the velocity and the control signal required for optimal system performance figure 5.13. This results suggests that linear controller are generally appropriate for control of systems without any non-linearities such as friction. On introduction of friction as modelled by the proposed model, the system performance of the control scheme, see figure 5.14 indicates the presence of limit cycle oscillations. This limit cycle oscillation is as a result of the integral action of linear controller. Thus the output position 'never' settles on the reference but rather oscillates around it in a periodic manner. With model-based friction observer integrated into the control loop as shown in the figure 5.12, performance improvements were obtained suggesting the elimination or reduction of the limit cycle oscillations. Performance of the observer compensation based on the proposed model is shown in figure 5.15, the output position tracks the reference position with zero error in the steady state, Settling time was also seen to have reduced as well as the maximum overshoot when compared with the performance of figure 5.13. The observer friction force and system friction appear the same and move between the positive and negative stiction values. The performance index of the proposed model suggests mse of 2 times better than the linear controller without friction and 15 times better than the case with friction.

Implementation of LuGre model-based friction observer compensation performance for the control of position is shown in figure 5.16. Close observation indicate similarities with the proposed model observer with position error of zero in the steady state, and the observer and system frictions being the same. The LuGre based approach showed improved performance of 1.5 times better than the case of ordinary linear controller without friction and 10 times the case with friction present. In the same manner GMS based observer performance of figure 5.17 shows an improvement in the range of the LuGre against the linear controller implementations, while the performance of the Xiong model-based friction observer has compatible results like the case of linear controller implementation in the absence of friction, see figure 5.17.

Therefore position control simulation results of a step reference position indicates that the observer based control to be superior to the stand alone linear (PID) controllers in handling position control of systems with possible frictional non-linearity. Among the various model-based observers investigated namely the proposed, LuGre, GMS and Xiong models, index results suggests better control performance was achieved with the proposed model observer than others. This was followed closely by the LuGre, GMS and Xiong models in the order. The index used as performance measure is the mse shown in table 5.2. The behaviour of the GMS model-based compensation was different qualitatively to the rest in that there is a presence of bias friction force (about -0.2 N-m) at zero error and no or zero velocity.

5.5.3 Comments on results

In general it is also worth noting that the capability of the model-based friction compensation approach is based on the assumption of a perfect knowledge of the system friction structure and parameters. However, deviations do exist between the real system friction and model, and also between real friction parameters and those of the model used for their compensation design. Discrepancies arising from these give rise to model structure uncertainties and parameter uncertainties respectively and often lead to deterioration of the performance of model-based observers for friction compensation and control. Over-compensation and under-compensation are possible problems that could arise due to this mis-match between the system friction parameters (F_s and F_c) and the modelled friction parameters (\hat{F}_s and \hat{F}_c) used for observer design. To overcome such problems associated with such errors adaptive friction compensation using models that easily update themselves on-line and use the updates to adapt to the system friction, see section 2.5.2 for more details. This is due to the fact that it is often difficult to perfectly identify these parameters, and also their variations in response to varying operating conditions. It would really be interesting to investigate the effects of the variations of other parameters of the proposed model structure (apart from the Coulomb and

static friction parameters) on the performance of the model-based observer compensation technique. For the proposed friction model, such parameters are; the micro-damping σ , the Stribeck velocity v_s , the pre-sliding breakaway displacement Z_b , and the viscous friction coefficient f_v .

5.6 Chapter summary

Compensation of friction in real systems is difficult to achieve due mainly to the nature of friction. A combination of the traditional PID based linear controller (for stability and error reduction), and a model-based friction observer (for the estimation of system friction) adopted for compensation and control is termed observer-based friction compensation scheme. The model-based friction compensation method used in this thesis is based on the general feedback principle. In this chapter an observer-based friction compensation and control strategy was designed and implemented. The design was a two part process: First, the linear controller design using the proportional + lag compensator for the velocity control, and a PID linear controller for position control meeting design specifications as highlighted was achieved to ensure appropriate controller performance. Second, a model-based friction observer utilising the proposed model for the estimation of the observed friction has been designed both for velocity and position control. The implementation of the observer based friction compensator designed for velocity and position control was performed and results obtained analysed. Performance of the observer based compensation using other models of friction was also obtained and analysed. From the analysis it was shown that performance improvements were guaranteed by the observer based compensation scheme against the traditional linear controllers. These linear controllers as a stand alone were also shown to have appropriate performance results in the absence of friction but deteriorates in the presence of friction.

The accuracy of model-based friction compensation techniques is strongly dependent on the choice of an adequate friction models and it's parameters as demonstrated by the simulations. Inaccuracies arising from mis-match in these parameters can lead to issues of over-compensation and under-compensation which are capable of rendering the behaviour of the observer based compensator inferior to the linear controllers. Based on the reference signals used and the results obtained, the proposed model showed strong improvement over the other models compared as indicated by used metrics.

Since parameter variations affecting friction requires that friction parameters adapt to these changes there is need for adaptation of the model and design and implementation of such adaptive controllers. In the next chapter these compensators would be incorporated into

the laboratory test-bed for the purposes of real time friction compensation control and their performance studied.

Chapter 6

Friction Compensation Experiments and Analysis

6.1 Introduction

In the preceding chapter a model-based friction observer (that uses the proposed friction model) was designed for the compensation and control of systems with friction with particular emphasis given to the laboratory test-bed earlier designed in chapter 4. Friction compensation and control is one core area of applications of system models. As such the new friction model presented in this research should be able to meet control objectives. Simulation analysis of the designed observer based friction compensator (using the new friction model presented) was performed in the previous chapter and was compared with some observer based compensators (using other models such as the LuGre, GMS, and Xiong friction models) and the results of the analysis demonstrated the effectiveness of the observer based compensator with the new friction model over the others especially in the pre-slide regime of friction.

In this chapter the focus is on the implementation of the model-based friction observer for the purposes of friction compensation and control of the laboratory test-bed. Both velocity and position control experiments would be carried out to demonstrate the effectiveness or otherwise of the new model-based friction observer for compensation and control. Tracking and regulation control experiments would be performed for both the velocity and position schemes. In the same vain experimental comparison of the performance of the other model-based observers as carried out for the simulation analysis of chapter 4 would also be implemented for the purposes of comparing the performance of the various compensators. Finally a simulation of the observer based compensation of the test-bed would be performed

and the results compared with actual experimental results so obtained. The layout of the chapter is as follows; In section 6.2 set-up of the experiment, model parameters used for the experimental implementation of friction compensation and control of the test-bed are discussed while velocity control experiments were performed on the test-bed and subsequent analysis of the experimental results in section 6.3. Position control experiments and result analysis were discussed separately in section 6.4. Section 6.5 presented velocity and position control simulations conducted on the test-bed. Analysis of both simulation and experimental results of velocity and position control were done in section 6.6. Chapter conclusions are contained in section 6.7.

6.2 Friction compensation implementation on the test-bed

In this section an explanation of the experimental set-up for the performance of the various friction compensation and control experiments on the test-bed is given. Model parameters used for the for friction estimation by the various friction observers are also explained.

6.2.1 Experimental set-up

The set-up of the laboratory friction test-bed is as shown in figure 4.1 of chapter 4, and it consists of an SRV-02 rotary servo in the high gear ratio driving a load through an external gear system. Friction occurs in the motor shaft, gear system, and the load-discs in the system, with the friction between load-discs being larger than the others. A data acquisition card is used as interface between the hardware (friction test-bed) and the MATLAB/SIMULINK software used to drive the system running on a PC with quarc software as an interface between the software and the hardware. The SIMULINK block diagram representation of the system with the hardware in the loop (the actual system) is represented in figure 6.1. The quadrature encoder reads the angular position of the load while the tachometer measures the motor angular speed. The SIMULINK provide a platform for command inputs and implementation of control strategies on the test-bed. A universal power supply module supplies dc power to drive the motor, while another dc source is used to power the torque sensor. During rotation the torque between the load-disc and the disc attached to the output shaft of the gear is measured by the sensor attached to the fixed load-disc.

Real time position and velocity control experiments were then carried out first using varying position and velocity inputs and also constant position and velocity inputs with the controllers and observers designed in the previous chapter. For the velocity and position control simulations, a model structure for the test-bed derived in chapter 4 with the friction

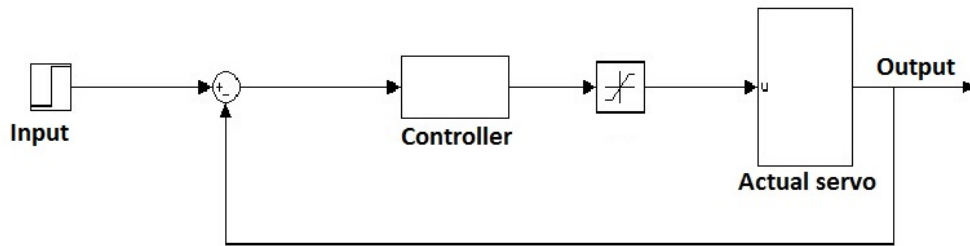


Fig. 6.1 The SIMULINK-hardware-in-the-loop of the friction test bed for real time control

modelled as a linear function of the velocity $B_{eq}v$ was used. This expression for friction would then be replaced by the non-linear friction model presented in chapter 3. Series of simulations for position and velocity control were carried out on the test-bed model structure using MATLAB/SIMULINK software.

Both tracking and regulation control tasks were investigated with the test-bed, the parameters of the friction models used are as obtained from the parameter identification in chapter 4. However after some series of experiments performed, the micro-damping parameter σ_1 estimated values seemed to negatively affect the results obtained. On adjusting to a lower value of this parameter and from experimental investigation a value different from the identified values was seen to yield better results and this value was adopted for the experiment. The viscous friction coefficient had the same effect and was later adjusted to fit experimental observations. The possible reasons for these deviations would be explained later in the chapter. So a harmonised model parameter values (for the micro-damping and viscous friction coefficient parameters) for the experimental investigations on the laboratory friction test-bed was used for the entire experiments in this chapter along-side the tables of parameter estimates for the various friction models in chapter 4 (tables 4.13, 4.14, 4.15 and 4.16). The adjusted parameter values are presented in table 6.1 below.

Table 6.1 The adjusted parameter values for the friction control experiments

Model Parameter	Value
f_v	0.00403
σ_{1i}	0.0375, 0.0375, 0.0375, 0.0375

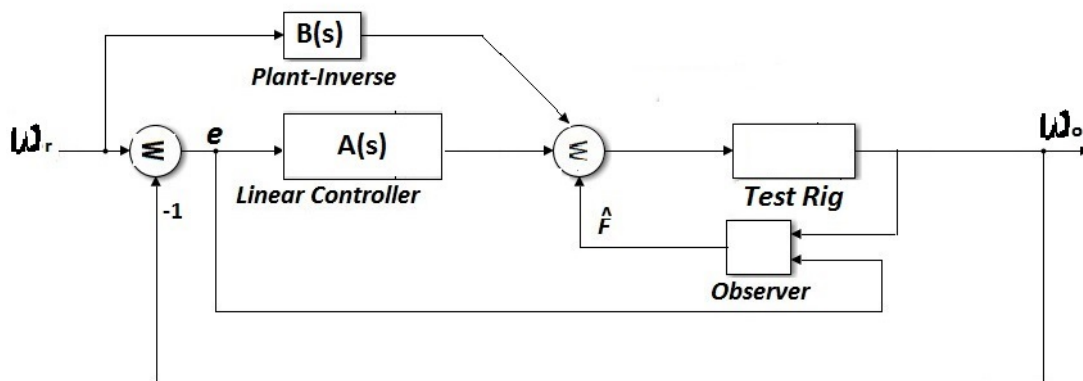


Fig. 6.2 Velocity control implementation experiments for the laboratory test-bed

6.3 Velocity control experiments

Velocity control of systems with friction especially in the low velocity range has been demonstrated to be more effective when a friction observer with adequate representation of the system friction is used for the elimination of the friction non-linearity inherent in the system. The experimental test-bed implementation of the observer based friction compensation is shown in figure 6.2. The parameter values of the linear controller with the transfer function $A(s)$ is

$$A(s) = K_p \frac{T_i s + 1}{T_i s + \gamma} \quad (6.1)$$

where $K_p = 1.5136$ is the proportional gain, and the second term the lag compensator with parameters $T_i = 0.0909$ and $\gamma = 0.0285$. The plant inverse $B(s) = 1/G(s)$ where $G(s)$ is given by eqn. 5.2. The condition for the plant inverse to be part of the control is for differentiable input reference. Thus for the constant velocity regulation case this branch will be removed since the differential of a constant is zero while for varying velocity the branch will be included as in the tracking experiment. For the control schemes first a linear controller only is implemented then a friction observer based on the proposed new model and finally friction observer based on some other models for comparison of their performance. Velocity tracking and regulation experiments performed would be discussed in the following subsections.

6.3.1 Tracking experiment

For the velocity tracking and control experiments, a low amplitude, slowly varying sinusoidal velocity reference signal was used on the system represented of figure 6.2. The aim of the experiment is to track a given velocity trajectory with minimal error in the presence of friction non-linearity. The observer design was based on the new friction model proposed in this thesis and subsequently other friction models were implemented for comparison. The metrics for comparing the effectiveness of the various model-based observers are the mean square error (mse) and the maximum error values.

First and experimental implementation of the linear controller without any form of friction compensation was performed and the result shown in figure 6.3. Second, the implementation of the tracking experiment using the friction observer based on the proposed new model is as shown in figure 6.4 and the other models namely the LuGre, GMS and Xiong models are as shown in figures 6.5, 6.6, and 6.7 respectively, while their mse and maximum error values are recorded in table 6.2. The friction torque in the system was measured by the torque sensor attached to the output load, the velocity also measured by the tachometer. The process was performed 5 times and the average measurements taken for each set of experiment. The results were also filtered to reduce the effect of sensor noise.

Table 6.2 Index for velocity tracking experiment

Friction model	mse value ($\times 10^{-5}$)	max. error ($\times 10^{-4}$)	Percent Improvement
PID only	1.8279	275	Reference
Proposed model	1.2806	239	13.1
LuGre model	1.3177	248	9.82
GMS model	1.4749	253	8
Xiong model	1.4384	249	9.45

6.3.2 Regulation experiment

The ability of the various model-based friction observers implemented for velocity regulation to a specified constant reference input value such as a step input was investigated similar to the tracking case. Since this involves a constant input signal velocity, the plant inverse block will be eliminated for the constant velocity control experiment. A step input velocity signal was used as reference with a magnitude of 1 rad/sec. The performance of the linear controller for velocity control is investigated followed by the various observer-based controllers. Similar to the tracking experiment 5 experimental runs were carried out for each control method implemented and their filtered average recorded. First the result of

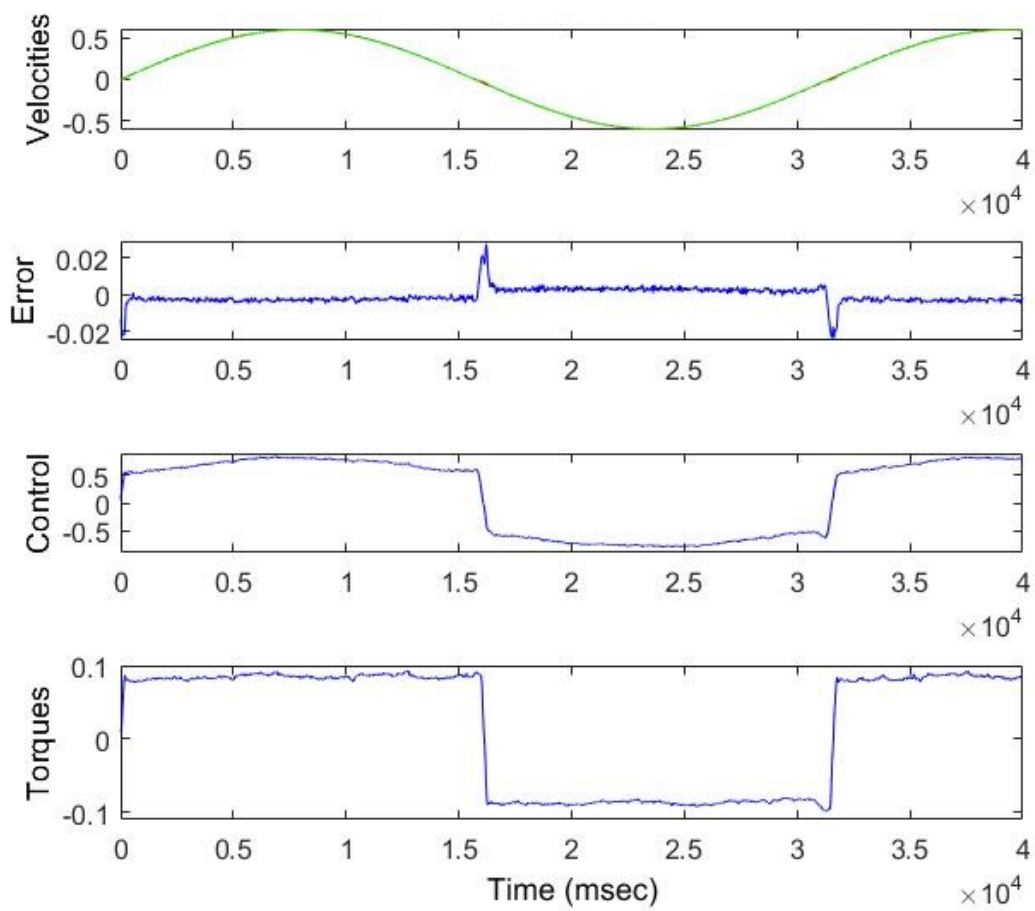


Fig. 6.3 A linear controller implementation result for velocity tracking of the test-bed showing: **top-** The input (red) and output (green) velocities in (rad/sec), **mid-upper-** The velocity error signal, **mid-lower-** The control signal input to the plant, and **bottom-** The friction torque in (N-m)

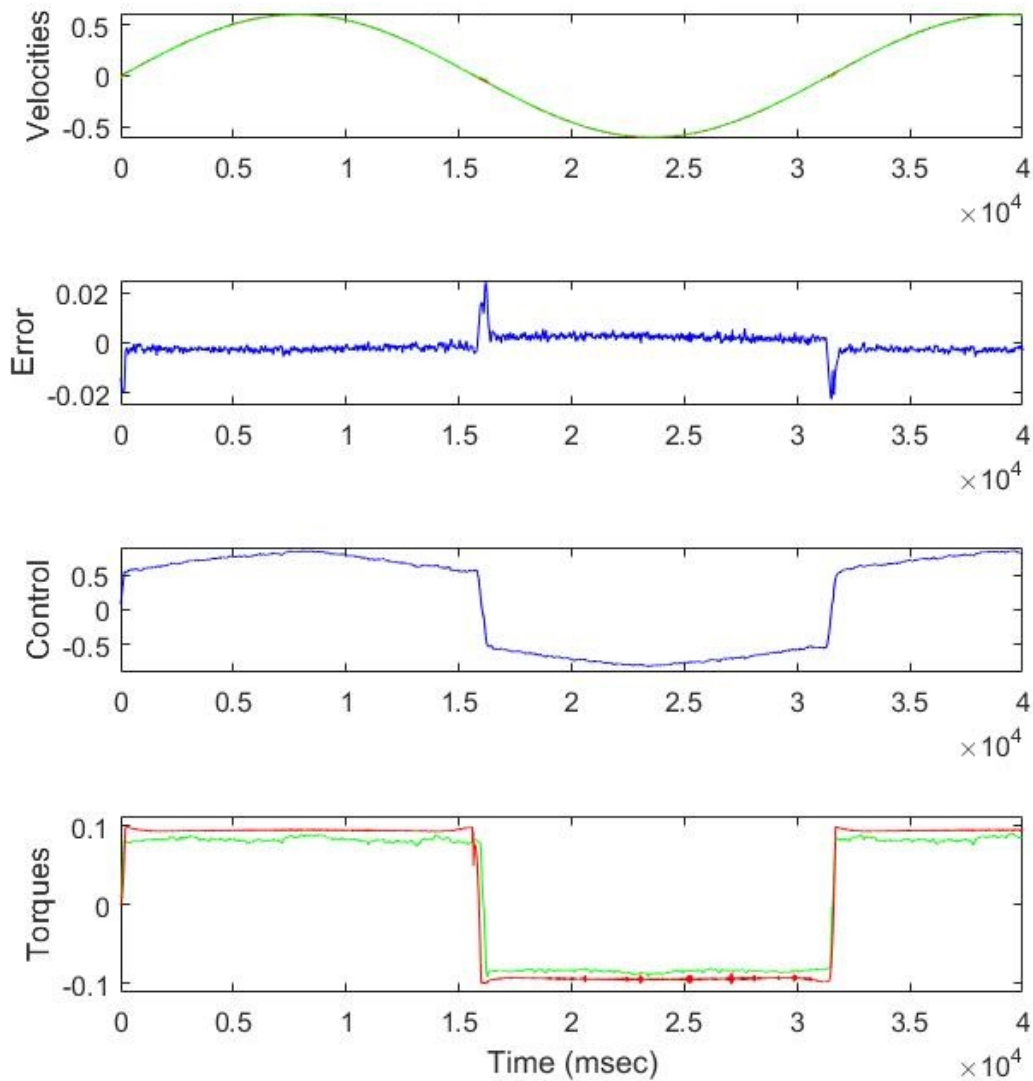


Fig. 6.4 A velocity tracking and control experiment with a model-based friction observer for the test-bed with: **top-** The output 'green' and reference 'red' velocities, **mid-upper-** The error signal, **mid-lower-** The control signal and **bottom-** The friction torques of the system rig 'green' and estimated by the observer 'red'

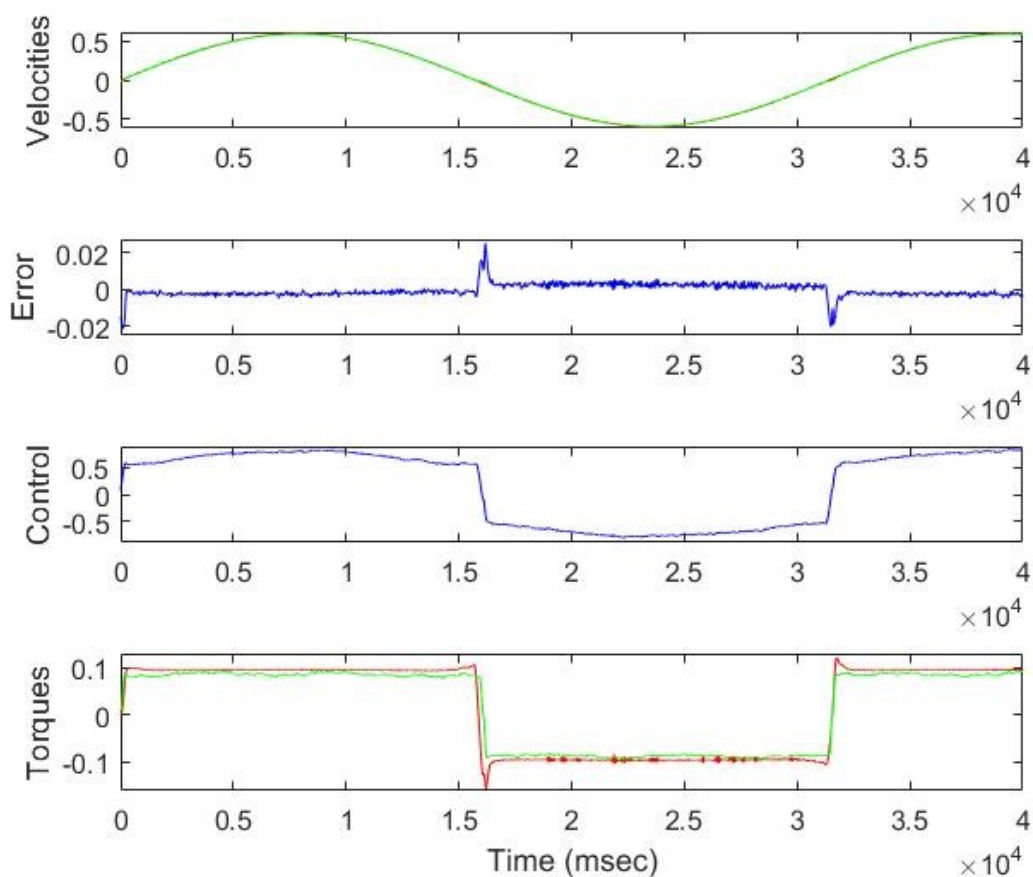


Fig. 6.5 A velocity tracking and control experiment with a model-based friction observer for the test-bed with: **top-** The output 'green' and reference 'red' velocities, **mid-upper-** The error signal, **mid-lower-** The control signal and **bottom-** The friction torques of the system 'green' and estimated by the observer 'red'

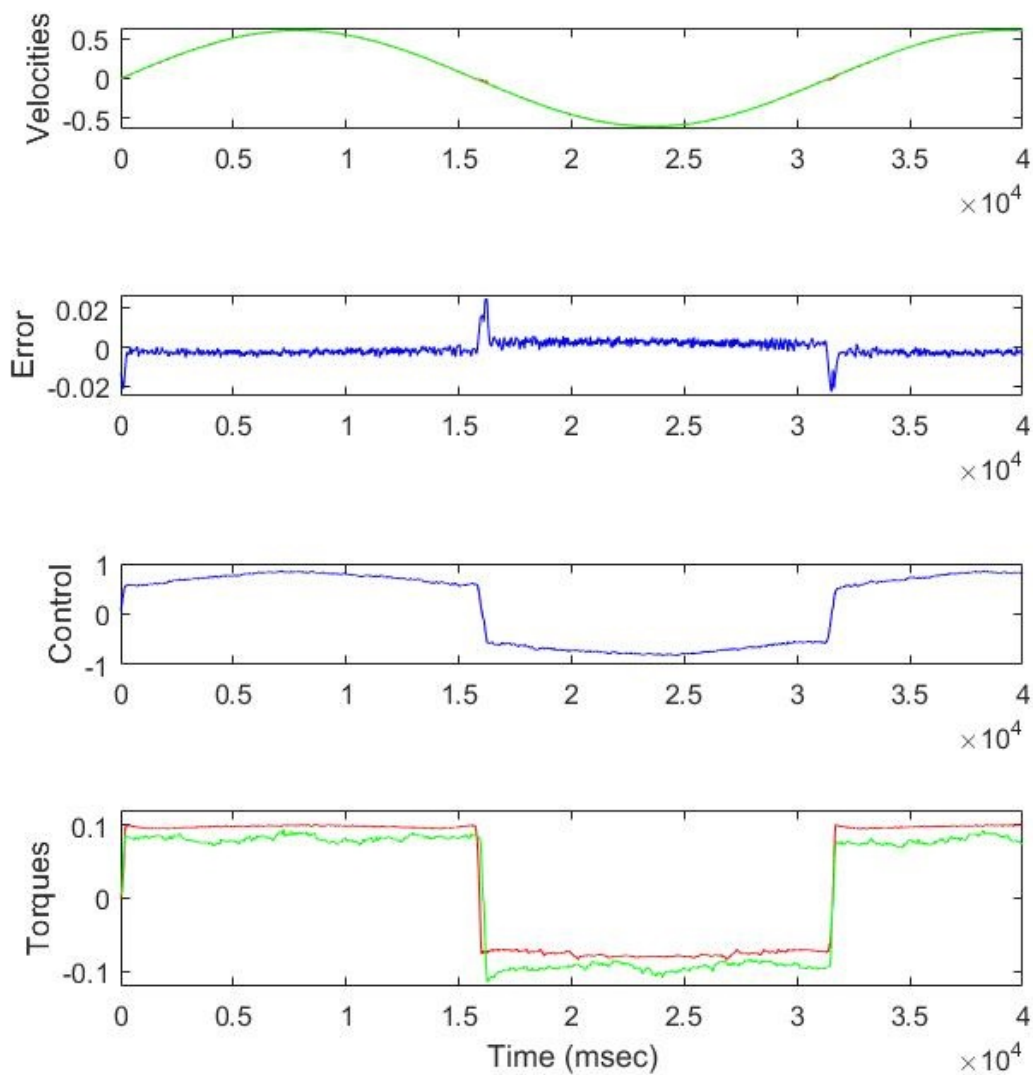


Fig. 6.6 A velocity tracking and control experiment with a model-based friction observer for the test-bed with: **top-** The output 'green' and reference 'red' velocities, **mid-upper-** The error signal, **mid-lower-** the control signal and **bottom-** The friction torques of the system 'red' and estimated by the observer 'green'

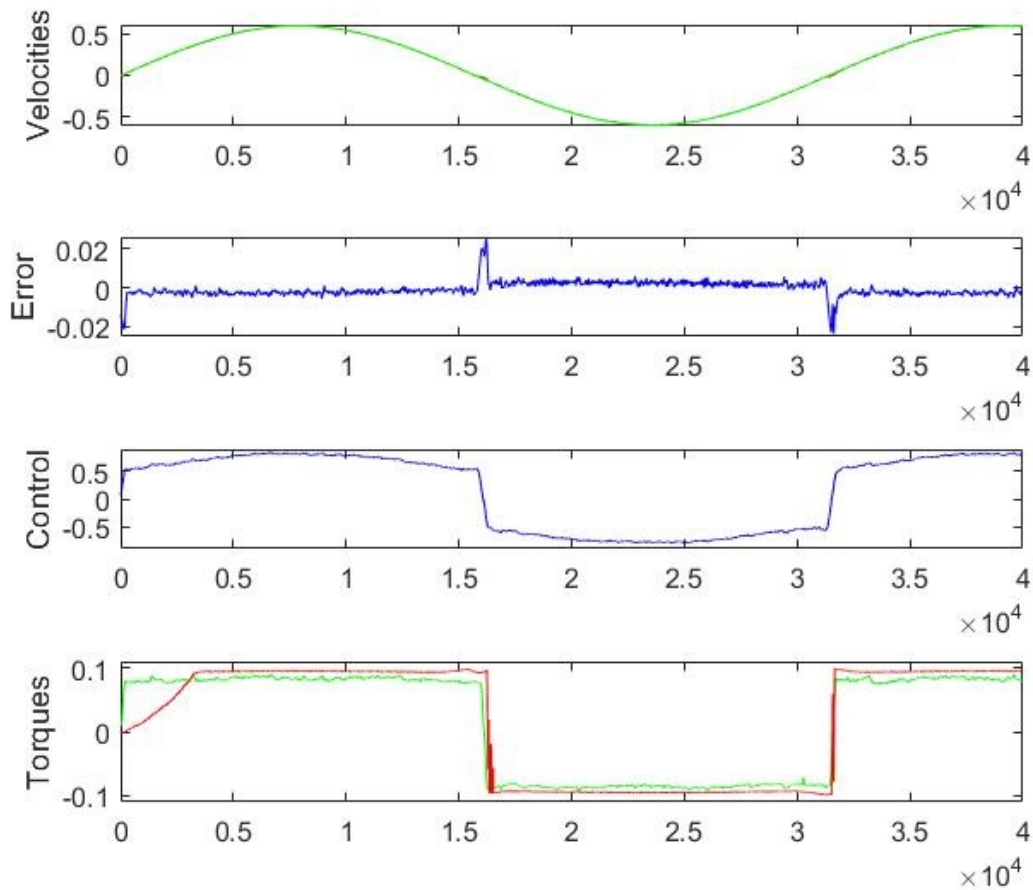


Fig. 6.7 A velocity tracking and control experiment with a model-based friction observer for the test-bed with: **top-** The output 'green' and reference 'red' velocities, **mid-upper-** The error signal, **mid-lower-** the control signal and **bottom-** The friction torques of the system 'green' and estimated by the observer 'red'

experimental implementation of the linear controller for velocity control without any form of friction compensation is presented in figure 6.8. Implementation of the velocity regulation experiment using the friction observer based on the proposed model is as shown in figure 6.9, and the other models namely the LuGre, GMS and Xiong models are as shown in figures 6.10, 6.11, and 6.12 respectively. Their respective error measures namely mse and maximum error values are recorded in table 6.3.

Table 6.3 Index for the velocity regulation experiment

Friction model	mse value ($\times 10^{-4}$)	max. error ($\times 10^{-4}$)	percent improvement
PID only	9.6548	5474	Reference
Proposed new model	9.4329	5432	0.77
LuGre model	9.4808	5438	0.66
GMS model	9.4554	5444	0.48
Xiong model	9.4757	5452	0.40

6.3.3 Analysis of results

The model-based friction compensation and control experiments performed on the test-bed showed strong improvement over the case of linear controller only implementation both for the tracking and regulation scenarios. Considering the friction models used for the friction estimation of the observer in comparison with the linear controller case, from table 6.2, the proposed new friction model-based observer showed good improvement over the linear controller in the maximum error and the mse error for velocity tracking experiment. The LuGre friction model performance against the linear controller in terms of the mse and maximum error also showed some improvement. In the same vain, the GMS and Xiong models performance improvement against the linear controller in terms of mse and maximum error were good.

For the velocity regulation, performance indices also showed good improvement over the linear controller in terms of mse and maximum error for the proposed new model observer, the LuGre model observer. The GMS observer and the Xiong model observer recorded improvement also over the linear controller table 6.3. These indices as captured in tables 6.2 and 6.3 showed that better regulation and tracking results for the specified low velocity regimes was achieved using an additional observer for friction compensation. From these tables also it is observed that the proposed new model showed superior performance in terms of the mean square error (mse) and maximum error measures than the other observer based control. The order of performance being; proposed new friction model, LuGre, GMS and Xiong were closely matched.

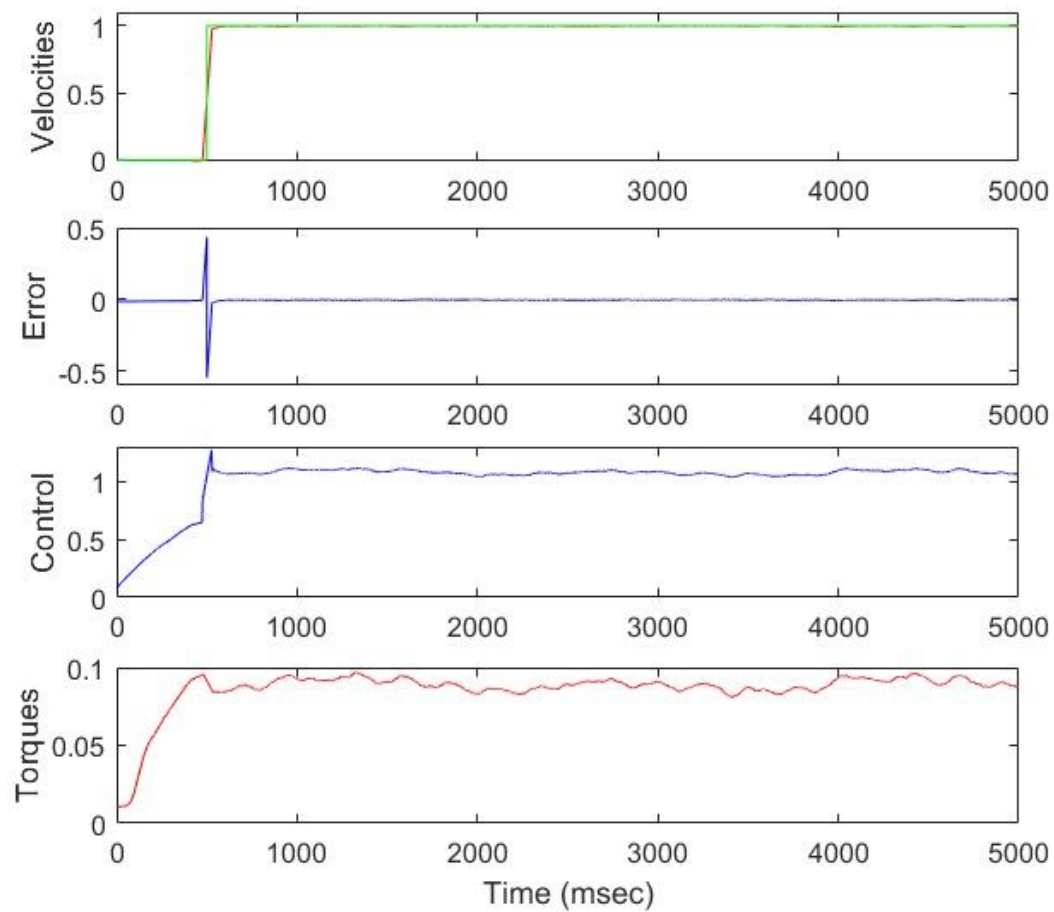


Fig. 6.8 A linear controller implementation result for velocity regulation of the test-bed showing: **top-** The input (red) and output (green) velocities in (rad/sec), **mid-upper-** The velocity error signal, **mid-lower-** The control signal input to the plant, and **bottom-** The friction torque in (N-m)

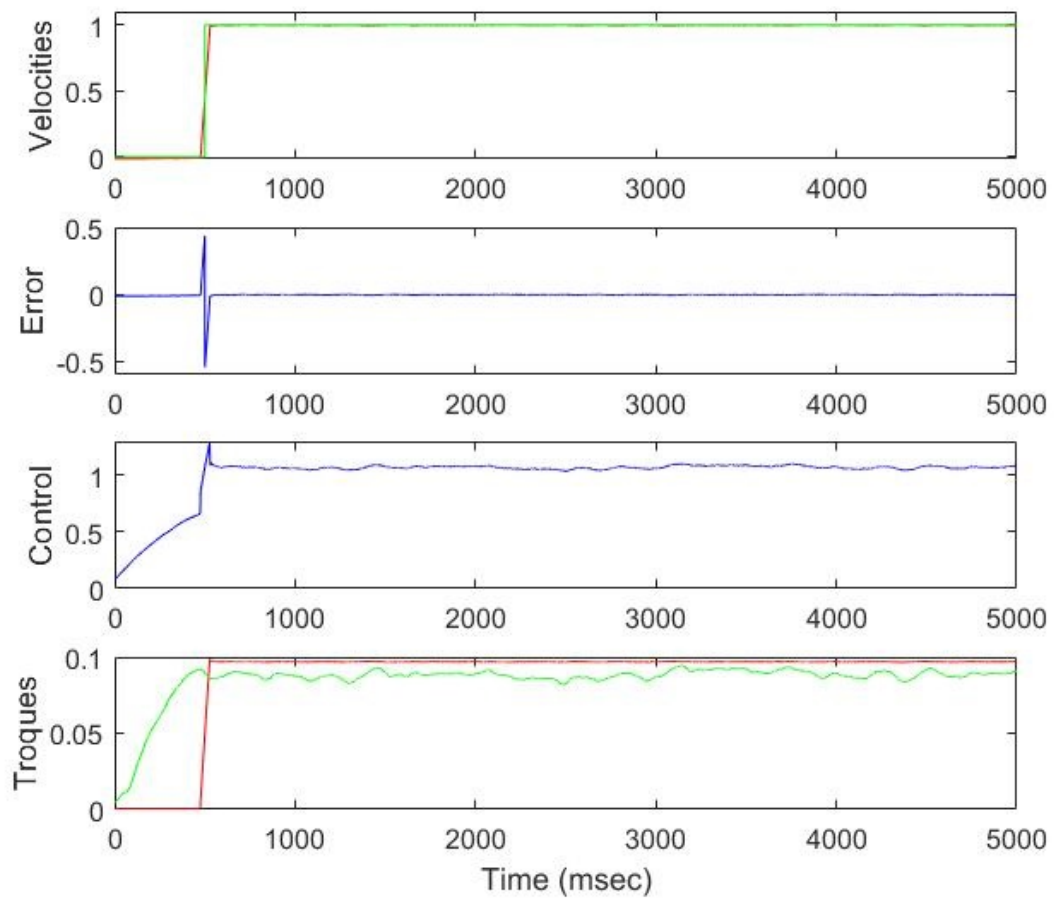


Fig. 6.9 A velocity regulation and control experiment with a model-based friction observer for the test-bed with: **top-** Output 'red', input 'green', **mid-upper-** Error, **mid-lower-** The control law and **bottom-** The friction torques; system 'green', observer 'red'

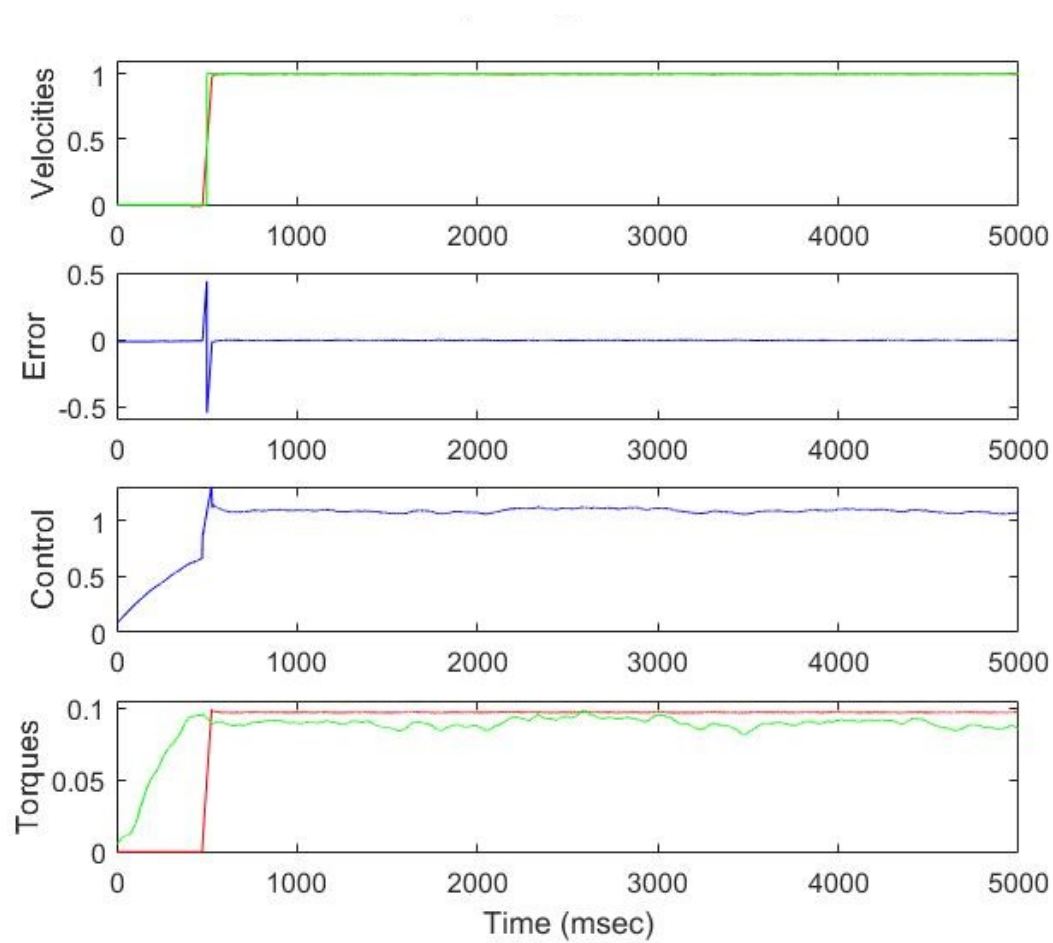


Fig. 6.10 A regulation tracking and control experiment with a model-based friction observer for the test-bed with: **top-** Output 'red', input 'green', **mid-upper-** Error, **mid-lower-** The control law and **bottom-** The friction torques; system 'green', observer 'red'

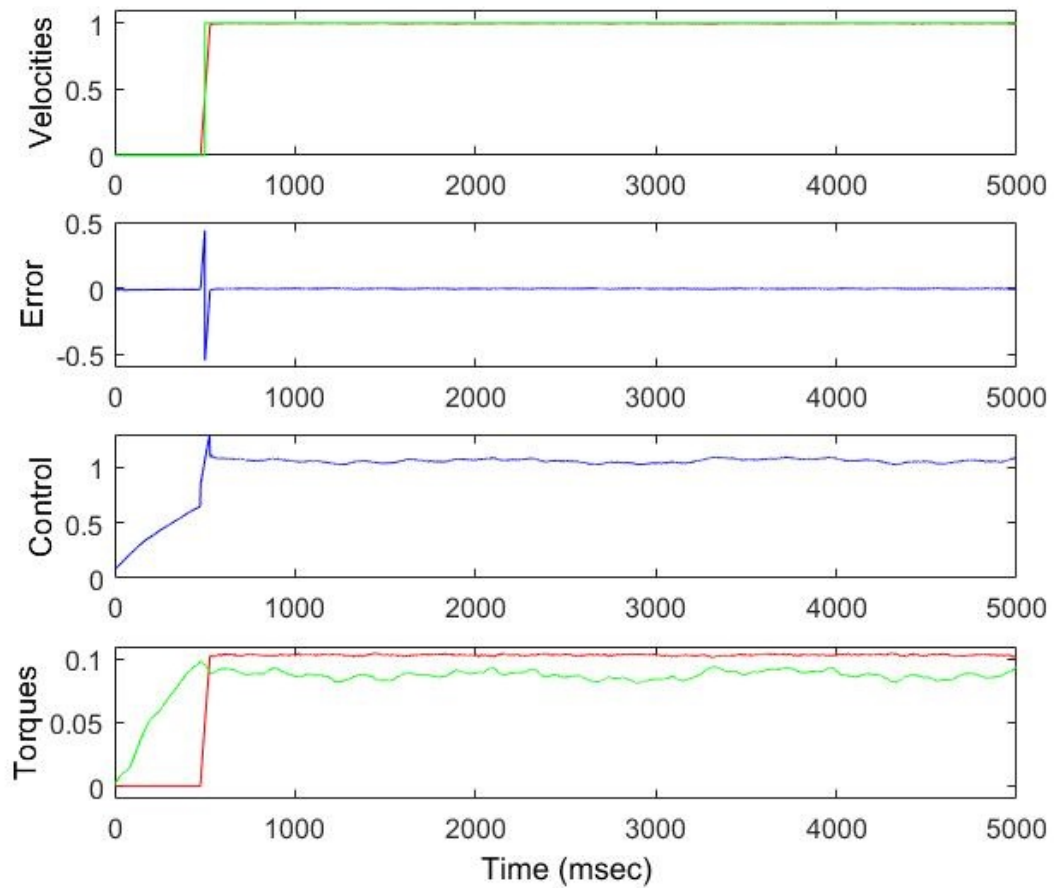


Fig. 6.11 A velocity regulation and control experiment with a model-based friction observer for the test-bed with: **top-** Output 'red', input 'green', **mid-upper-** Error, **mid-lower-** The control law and **bottom-** The friction torques; system 'green', observer 'red'

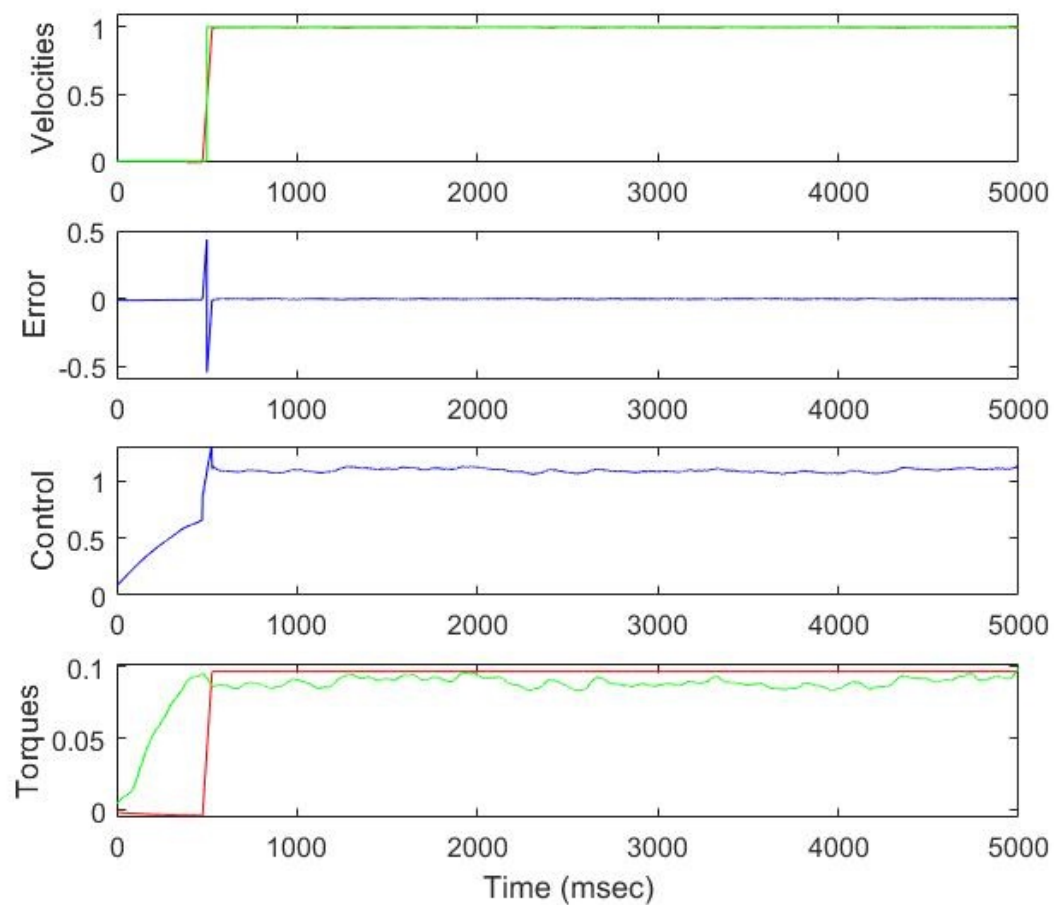


Fig. 6.12 A velocity regulation and control experiment with a model-based friction observer for the test-bed with: **top-** Output 'red', input 'green', **mid-upper-** Error, **mid-lower-** The control law and **bottom-** The friction torques; system 'green', observer 'red'

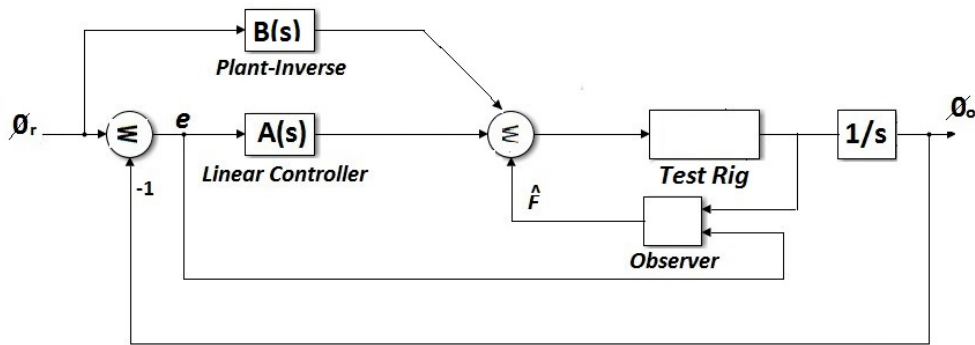


Fig. 6.13 Position control implementation experiment for the laboratory test-bed

6.4 Position control experiment

In this section position control experiments are conducted on the test-bed demonstrating the performance of the various control schemes developed in the previous chapter, namely the PID linear controller, and the various friction observers. The parameters of the linear PID controller used for the position control experiment are $K_p = 5.7517$, $K_i = 10$, and $K_d = -0.0768$, with K_p as the proportional gain of the controller, K_i the integral gain, and K_d the derivative gain.

Thus the transfer function of the linear controller is

$$A(s) = \frac{K_p s + K_i + K_d s^2}{s} \quad (6.2)$$

The transfer function of the plant inverse is $B(s) = 1/G(s)$ with $G(s)$ as described in equation 5.4. The parameter values of the various friction observers are as presented in the respective tables. The set-up for the implementation of the observer based friction compensation is shown in figure 6.13. As with the velocity control, the plant inverse block assumes the input position signal to be twice differentiable.

6.4.1 Tracking experiment

For the position tracking and control experiments, a slowly varying sinusoidal position reference signal was used. The aim of the experiment is to demonstrate the superior performance of the model-based friction compensation and control approach over the linear controller method to track a given position trajectory with minimal error in the presence of friction. The observer design was based on the friction model proposed in this thesis

and subsequently other friction models were implemented for comparison. The metrics for comparing the effectiveness of the various model-based observers are the mean square error and the maximum error values.

First the experimental implementation of the linear controller without any form of friction compensation was performed and the result shown in figure 6.14. Second, the implementation of the tracking experiment using the friction observer based on the proposed friction model is as shown in figure 6.15, and the other models namely the LuGre, GMS and Xiong models shown in figures 6.16, 6.17, and 6.18 respectively while their mse and maximum error values are recorded in table 6.4. The friction torque in the system was measured by the torque sensor attached to the output load, the velocity also measured by the tachometer and position obtained by integrating the velocity signal. The output of the encoder was recorded and used to compare its relation with the tachometer output. The process was performed 5 times and the average measurements taken for each set of experiment. The results were filtered to reduce the effect of sensor noise.

Table 6.4 Index for position tracking experiment

Friction model	mse value ($\times 10^{-4}$)	max. error ($\times 10^{-4}$)	Percent improvement
PID only	4.2465	1203	Reference
Proposed new model	2.2029	899	25.27
LuGre model	2.1074	901	25.10
GMS model	2.7844	962	20.03
Xiong model	2.2430	903	24.94

6.4.2 Analysis of results

The model-based friction compensation and control experiments for position control performed on the test-bed showed strong improvement over the case of linear controller only implementation. The various friction models used for the friction estimation of the observer in comparison with the linear controller case showed varying degrees of improvement as seen from table 6.4. The proposed friction model-based observer showed 48.12% improvement over the linear controller case in the mean square error (mse) and 25.27% in maximum error while the LuGre friction model performance against the linear controller in terms of the mse and maximum error are 50.37% and 25.1% respectively. The GMS performance improvement against the linear controller was 34.43% for mse and 20.03% for maximum error. Likewise the Xiong performance was 47.18% for mse and 24.94% for the maximum error index. From this the LuGre model showed strong reduction in the overall means square error index. The error reduction at zero or low velocity and reversals is captured by the

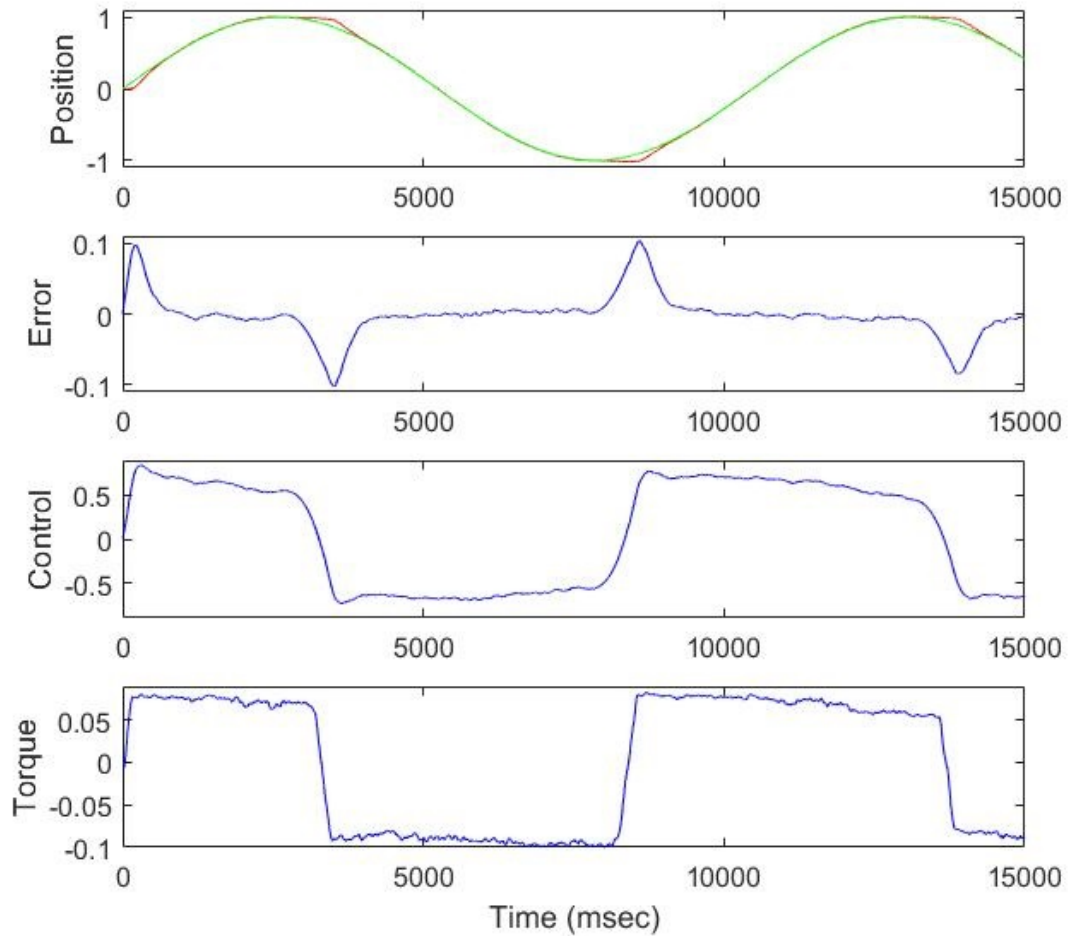


Fig. 6.14 A linear controller implementation result for position tracking of the test-bed showing: **top-** The input (green) and output (red) positions in (radians), **mid-upper-** The position error signal, **mid-lower-** The control signal input to the plant, and **bottom-** the friction torque in (N-m)

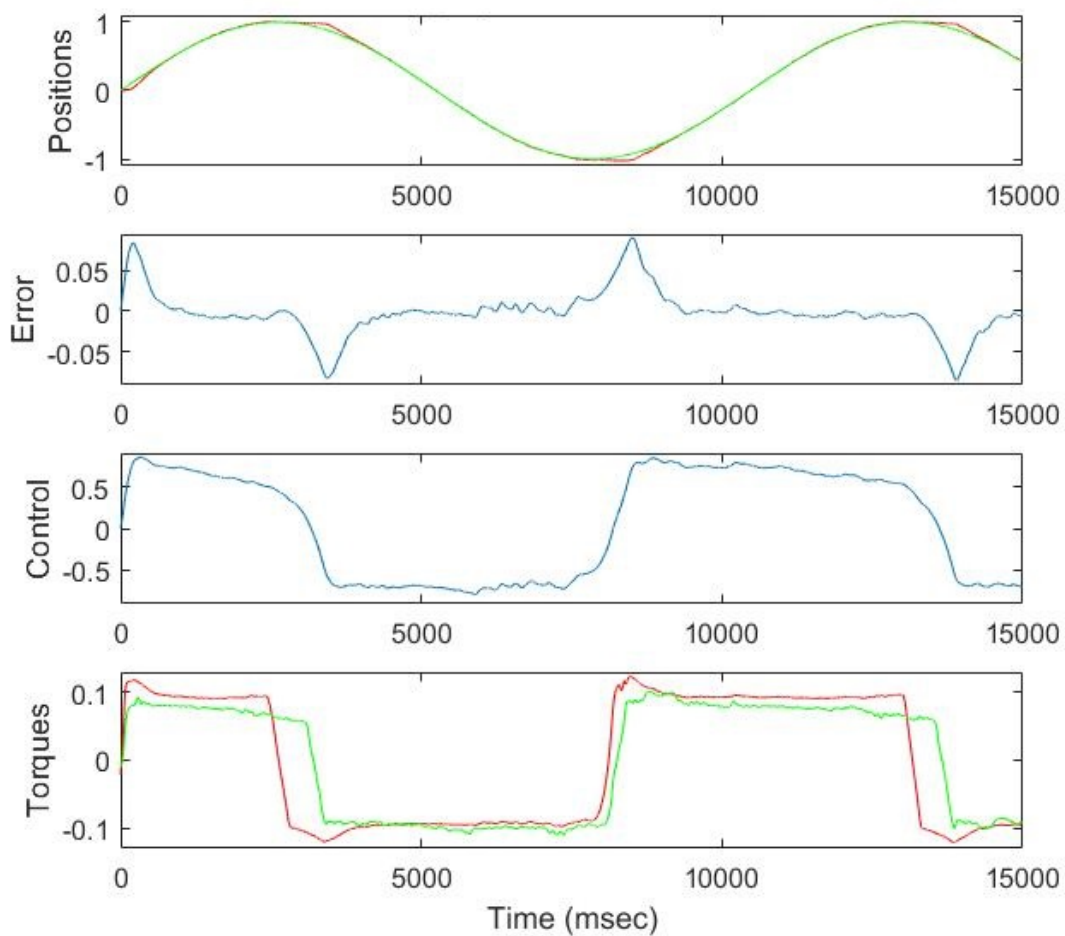


Fig. 6.15 A position tracking and control experiment with a model-based friction observer for the test-bed with: **top-** Output 'red' input 'green', **mid-upper-** Error, **mid-lower-** The control law and **bottom-** The friction torques; system 'green', observer 'red'

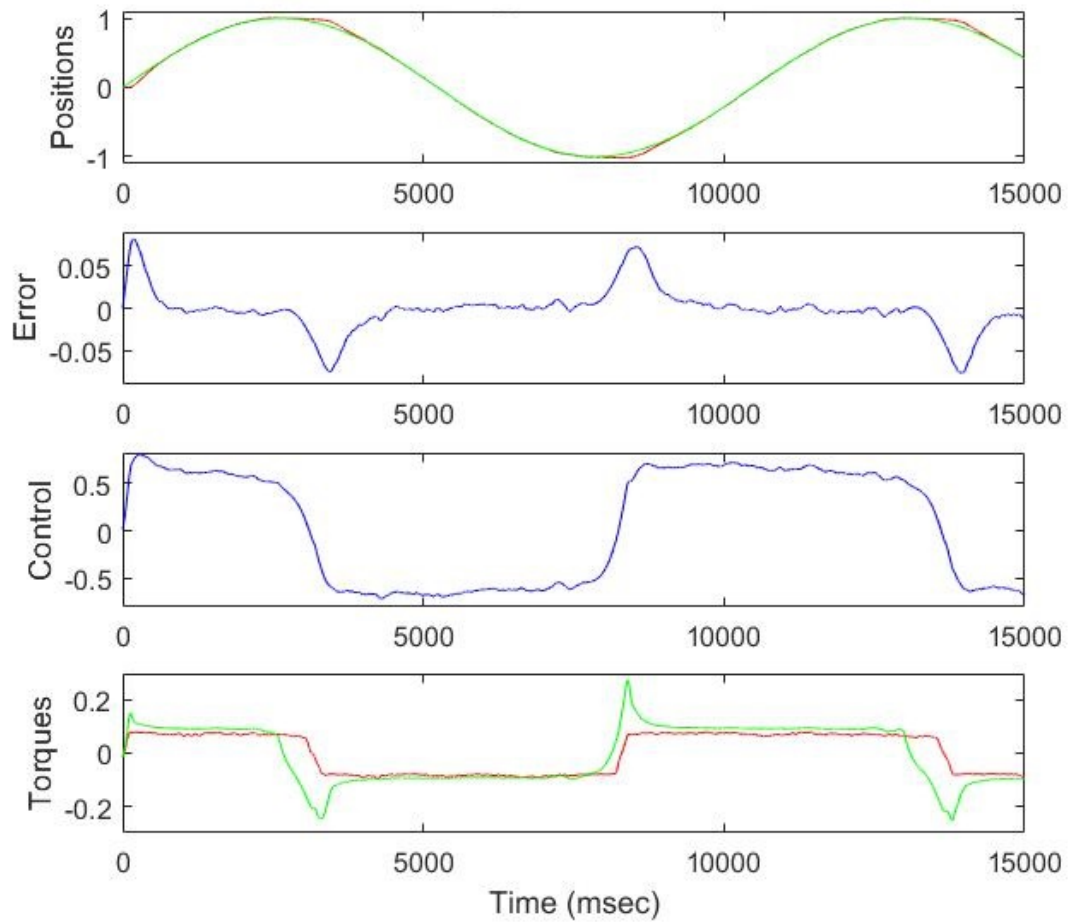


Fig. 6.16 A position tracking and control experiment with a model-based friction observer for the test-bed with: **top-** The output 'red' and reference 'green' velocities, **mid-upper-** The error signal, **mid-lower-** the control signal and **bottom-** The friction torques of the system 'red' and estimated by the observer 'green'

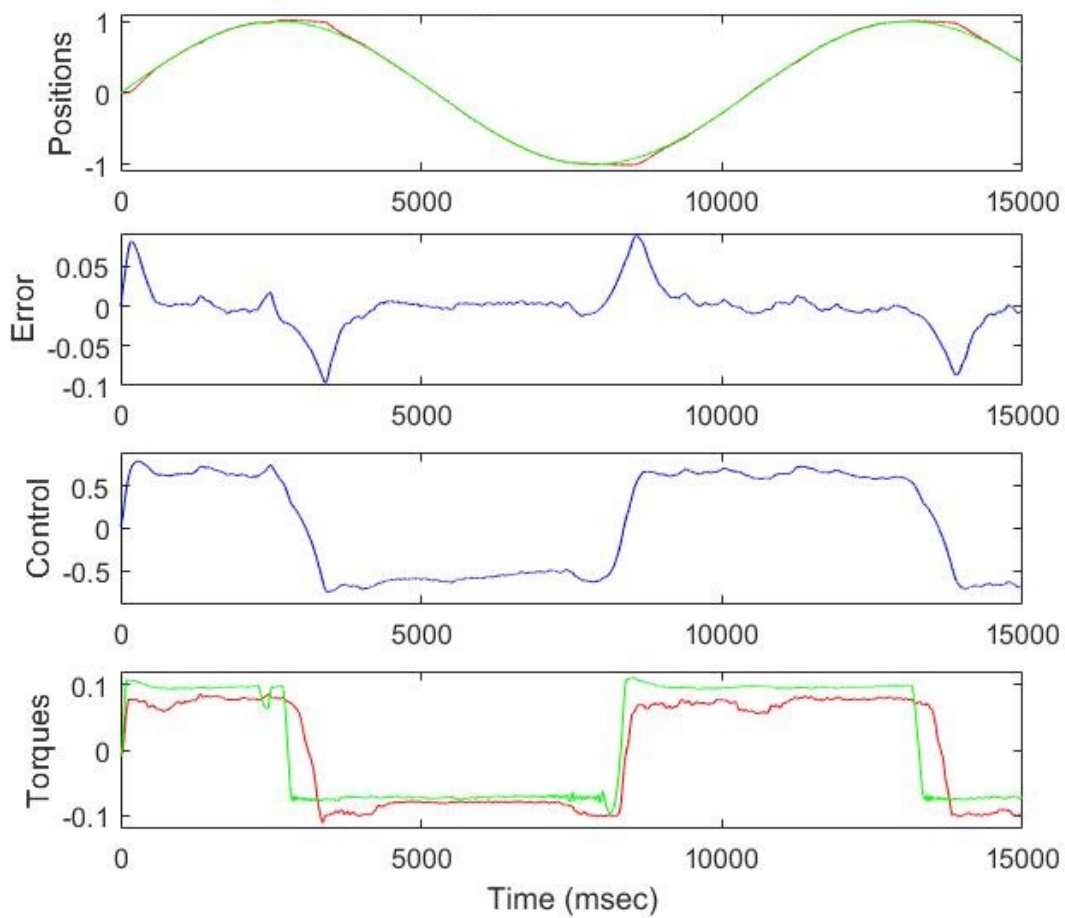


Fig. 6.17 A position tracking and control experiment with a model-based friction observer for the test-bed with: **top-** Output 'red' input 'green', **mid-upper-** Error, **mid-lower-** The control law and **bottom-** The friction torques; system 'green', observer 'red'

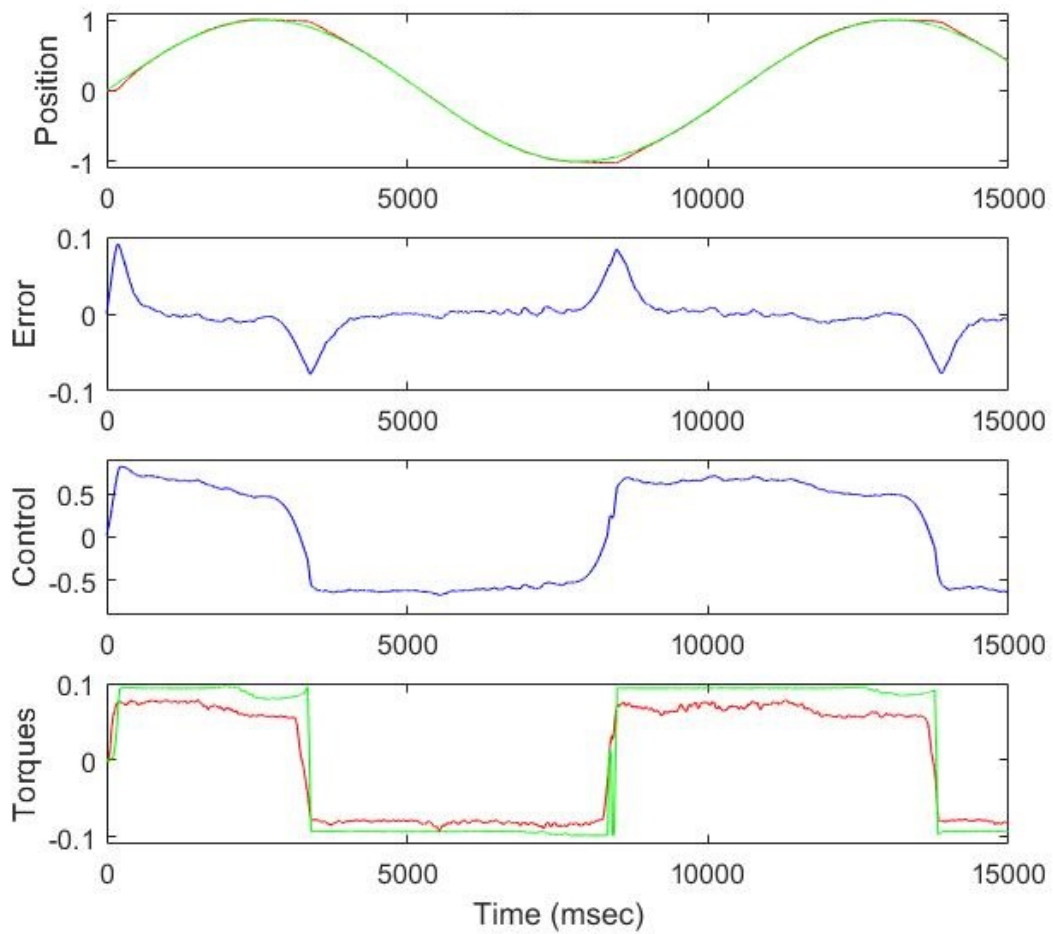


Fig. 6.18 A position tracking and control experiment with a model-based friction observer for the test-bed with: **top-** Output 'green', input 'red', **mid-upper-** Error, **mid-lower** The control signal and **bottom-** The friction torques; system 'green', observer 'red'

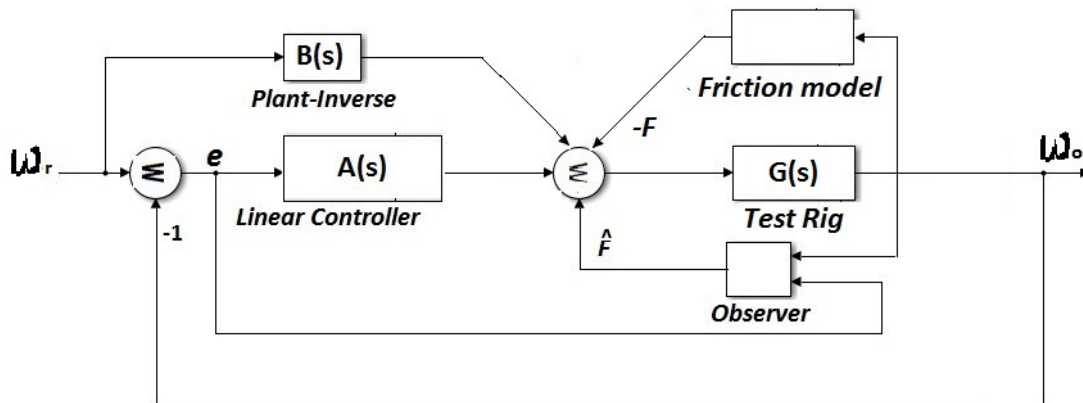


Fig. 6.19 Block diagram for velocity control simulations of the experimental test-bed

maximum error index which show that the proposed model performance was superior to that of the LuGre model. The Xiong model also had a better mean square error measure than the GMS model while the later show greater error reduction at reversal velocities. These are further discussed below.

6.5 Velocity and position control simulations

Velocity and position control simulations are further performed with the friction test-bed using the new friction model proposed in this thesis for the friction-observer design. The aim is to compare the performance of the simulation results against the real experimental results. Thus the linear part of the plant (test-bed) is represented by the transfer function $G(s)$ (see equations 5.2 or 5.4) and the frictional non-linear part modelled using the new friction model proposed earlier in chapter 3 equations 3.1, 3.2, 3.3, 3.4 and 3.5. For comparison purposes, the same signal inputs for the velocity tracking and regulation, and position regulation experiments in previous sections would be used for the simulation described below with a linear controller described by equation 6.1 for the velocity control simulations. The figure 6.19 shows the block implementation of the velocity control scheme while figure 6.20 shows the block implementation of the position control simulations and the linear controller is described by equation 6.2 for position simulations.

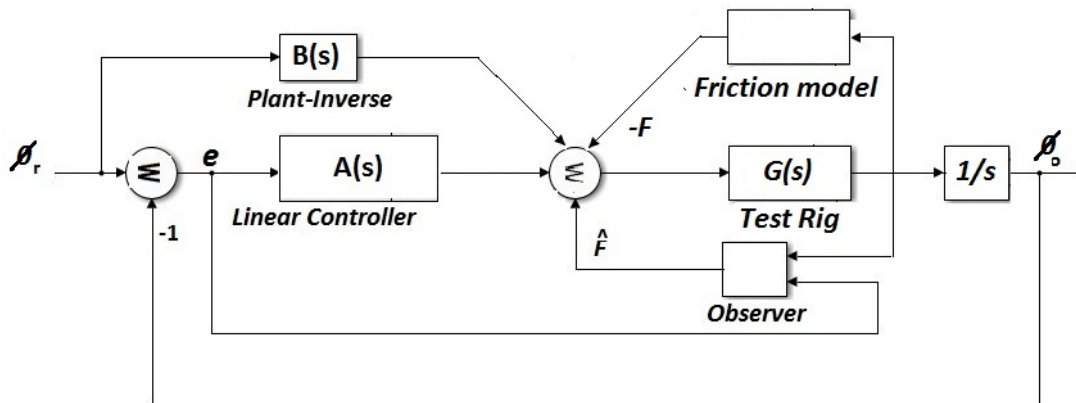


Fig. 6.20 Block diagram for position control simulations of the experimental test-bed

6.5.1 Velocity tracking simulation

Low amplitude, slowly varying sinusoidal velocity reference signal was used for the simulation as for the real experiment. The observer design was based on the new friction model proposed. The metrics for comparing the effectiveness of the various model-based observers are the mean square error (mse) and the maximum error values. The linear controller transfer function $A(s)$ is given as in (6.1) and the plant inverse $B(s) = 1/G(s)$. With the values specified in Appendix A, the transfer function $G(s)$ for the velocity model becomes

$$G(s) = \frac{1.863}{0.02388s + 1} \quad (6.3)$$

First and experimental implementation of the linear controller without any form of friction compensation is performed and the result shown in figure 6.21. Second, the implementation of the tracking experiment using the friction observer based on the proposed friction model is as shown in figure 6.22. The mean square error and maximum error metric for each control method was presented in table 6.5

Table 6.5 Index for velocity tracking simulation

Controller Type	mse ($\times 10^{-5}$)	max. error ($\times 10^{-4}$)	% Improvement
PID	1.2664	165	Reference
Proposed new mode observer	0.4994	36	78.2

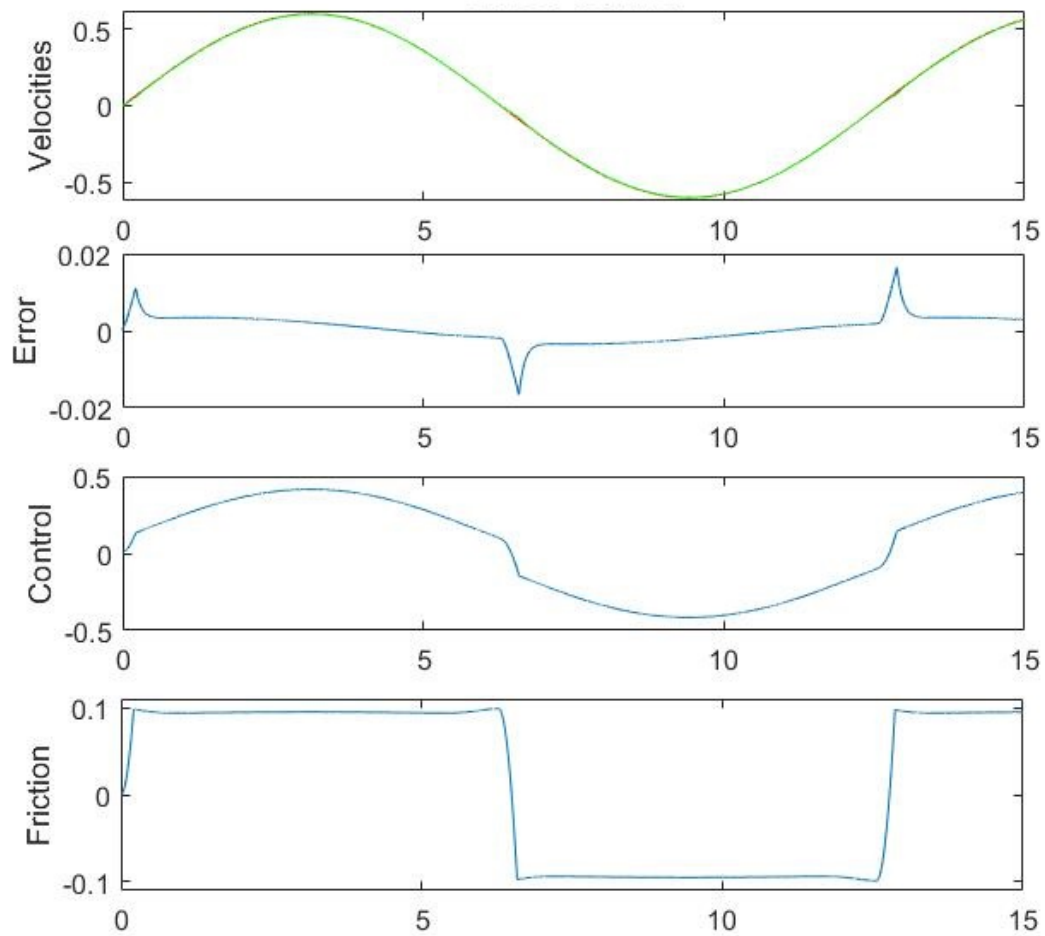


Fig. 6.21 Linear controller simulation result for velocity tracking of the test-bed showing: **top-** The input (green) and output (red) velocities in (rad/sec), **mid-upper-** The velocity error signal, **mid-lower-** The control signal input to the plant, and **bottom-** The friction torque in (N-m)

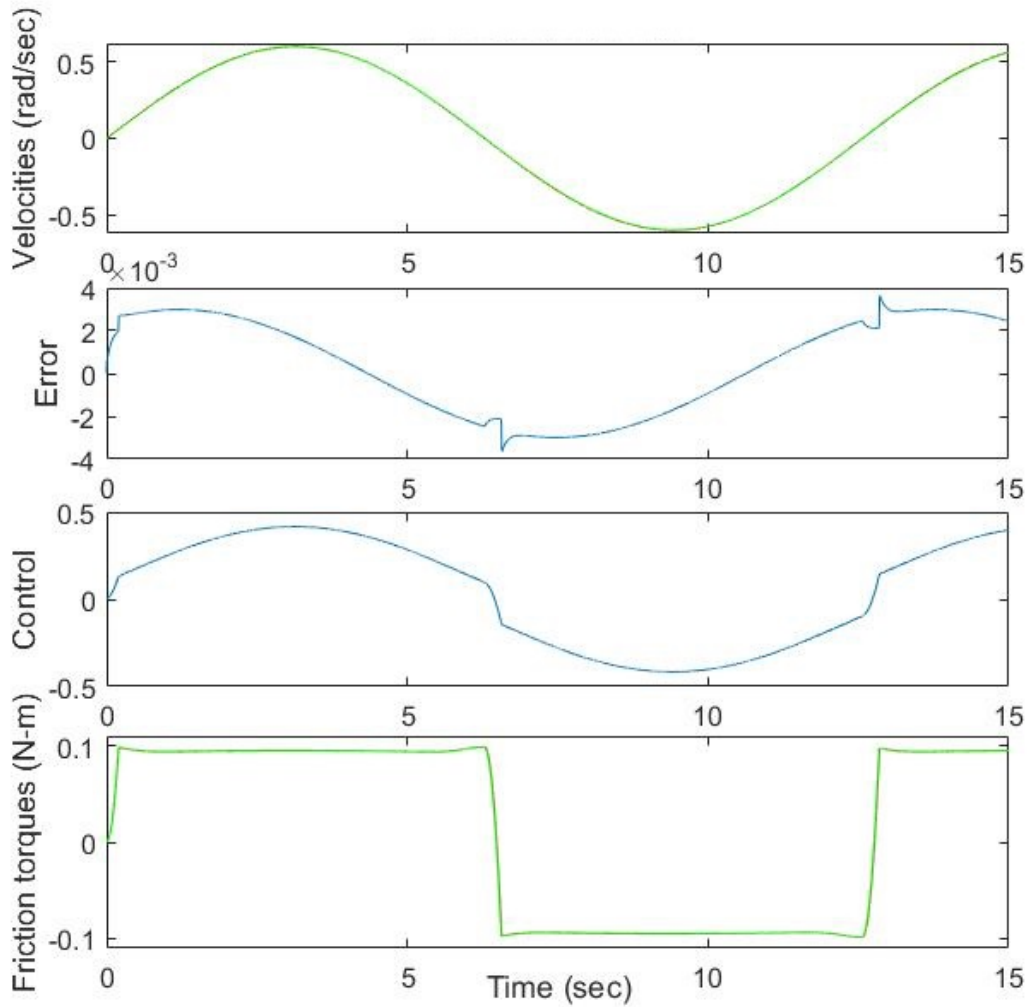


Fig. 6.22 A velocity tracking and control simulation with a model-based friction observer for the test-bed with: **top-** Output 'green', input 'red', **mid-upper-** Error, **mid-lower-** Control and **bottom-** The friction torques; system 'green', observer 'red'

6.5.2 Velocity regulation simulation

A step input velocity signal was used as reference with a magnitude of 1 rad/sec. The performance of the linear controller for velocity control is investigated followed by the friction observer-based controller. First the result of simulation implementation of the linear controller for velocity control without any form of friction compensation is presented in figure 6.23. Then the implementation of the velocity regulation experiment using the friction observer based on the proposed new model is as shown in figure 6.24. Their respective error measures namely mse and maximum error values are recorded in table 6.6.

Table 6.6 Index for velocity regulation simulation

Controller Type	mse value ($\times 10^{-4}$)	max. error	mse % improvement
Linear controller	1.1182	1	Reference
Proposed model observer	0.9434	1	15.6

6.5.3 Position control simulation

For the position tracking simulation, a slowly varying sinusoidal reference signal was used similar to the experimental implementation. The linear controller transfer function $A(s)$ is given as in (6.2) and the plant inverse $B(s) = 1/G_p(s)$. With the values specified in Appendix A, the transfer function $G_p(s)$ for the model becomes

$$G_p(s) = \frac{1.863}{s(0.02388s + 1)} = \frac{1}{s}G(s) \quad (6.4)$$

First the implementation of the linear controller without any form of friction compensation was performed and the result shown in figure 6.25. Second, the simulation of the tracking control using the friction observer based on the proposed new model is performed and the result as shown in figure 6.26. Their respective mse and maximum error values are recorded in table 6.7 as measure of performance.

Table 6.7 Index for position tracking and control simulation

Controller Type	mse value ($\times 10^{-4}$)	max. error ($\times 10^{-4}$)	Error % improvement
PID only	2.9779	567	Reference
Proposed model observer	1.4854	432	23.8

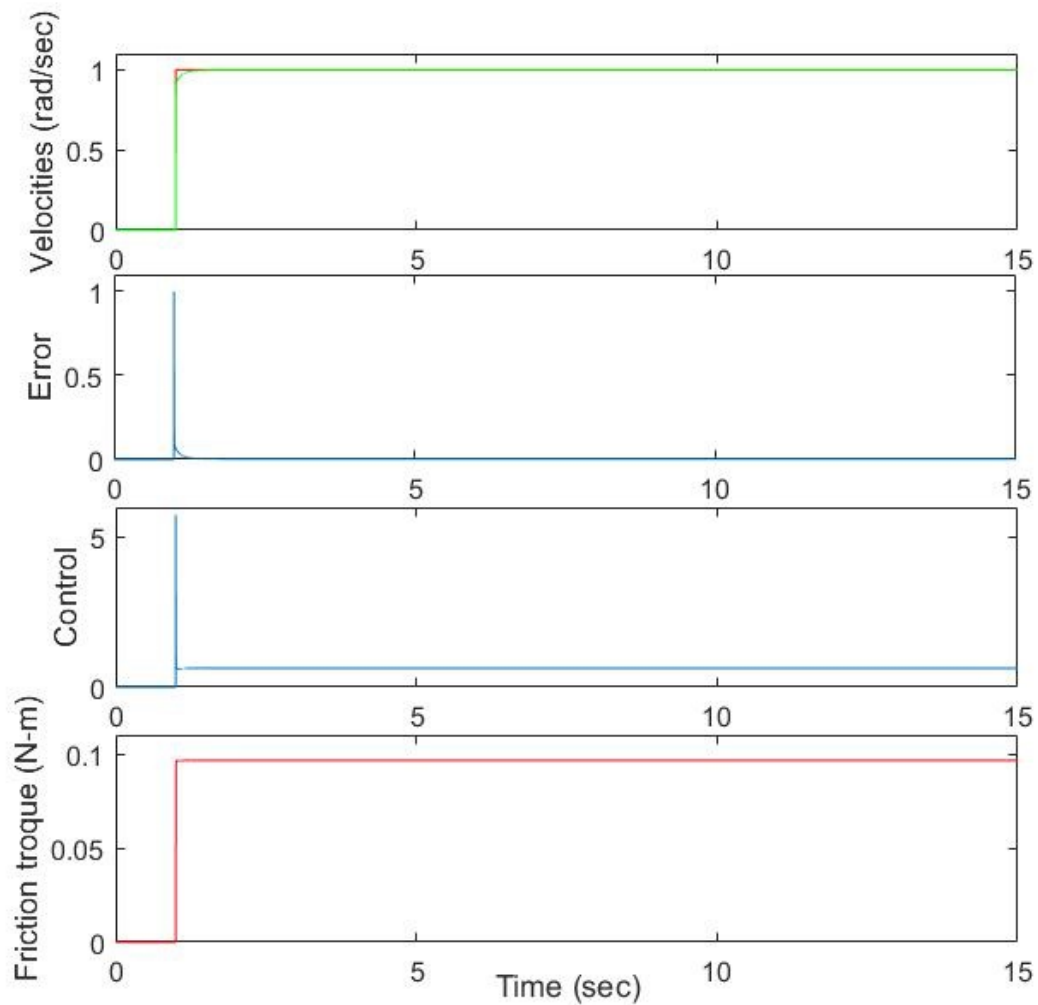


Fig. 6.23 Linear controller simulation result for velocity regulation of the test-bed showing: **top-** The input (red) and output (green) velocities in (rad/sec), **mid-upper-** The velocity error signal, **mid-lower-** The control signal input to the plant, and **bottom-** the friction torque in (N-m)

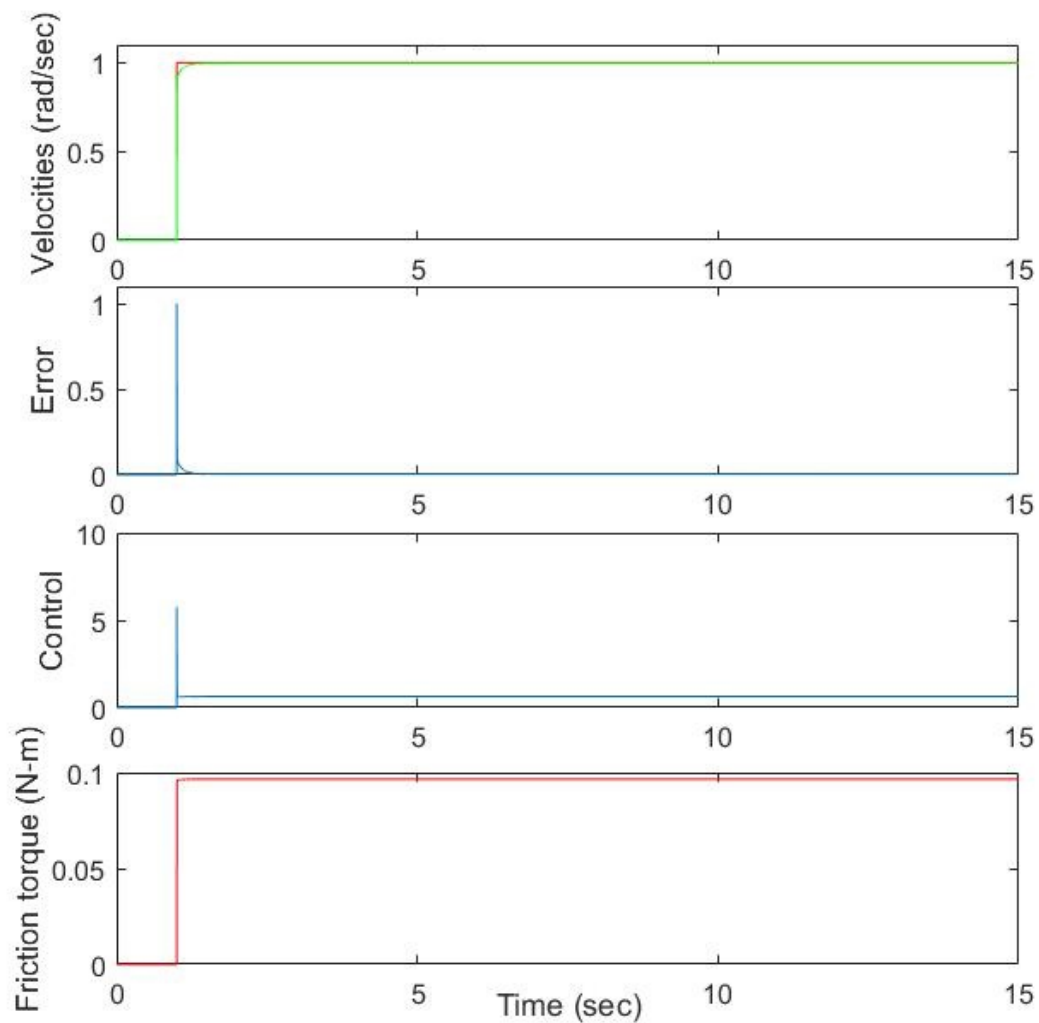


Fig. 6.24 A velocity regulation and control simulation with a model-based friction observer for the test-bed model with **top-** Output 'red', input 'green', **mid-upper-** Error, **mid-lower-** Control and **bottom** The friction torques; system 'green', observer 'red'

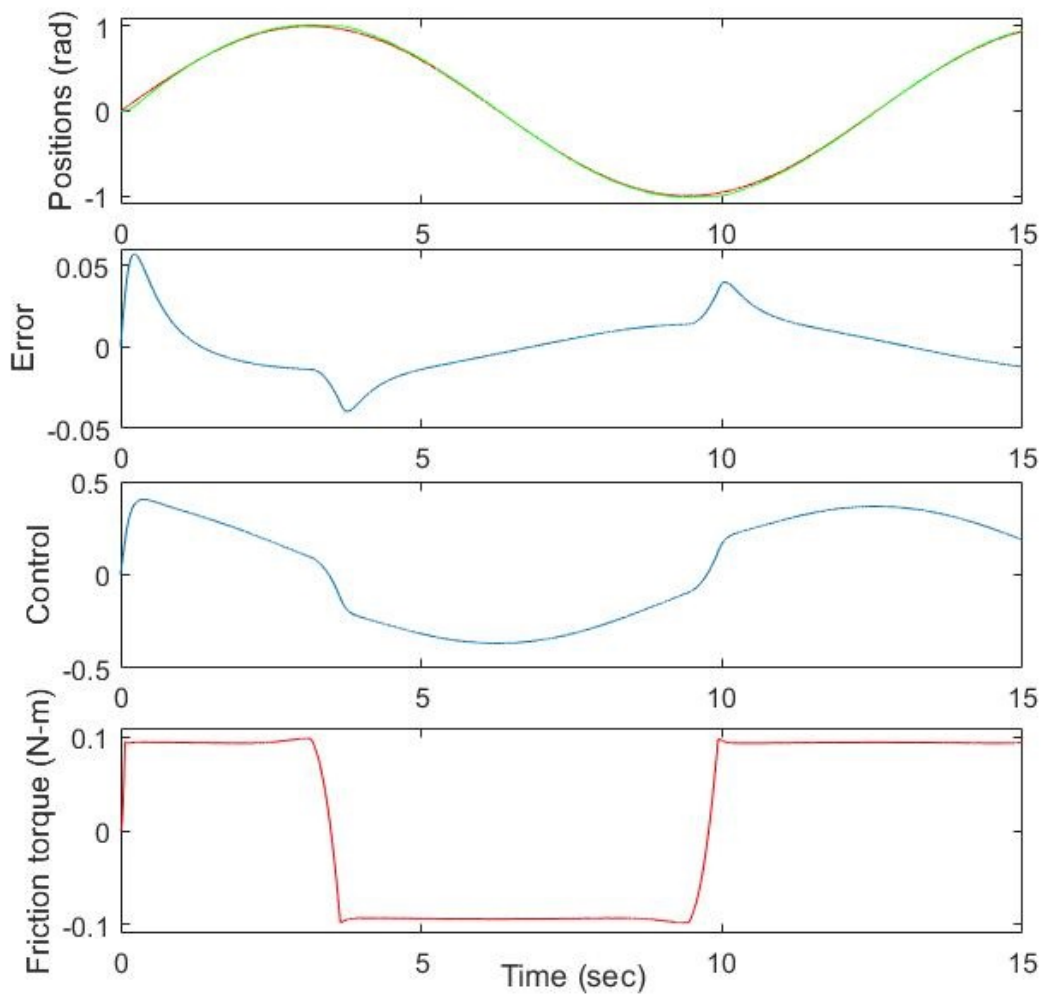


Fig. 6.25 A linear controller implementation for position tracking of the test-bed

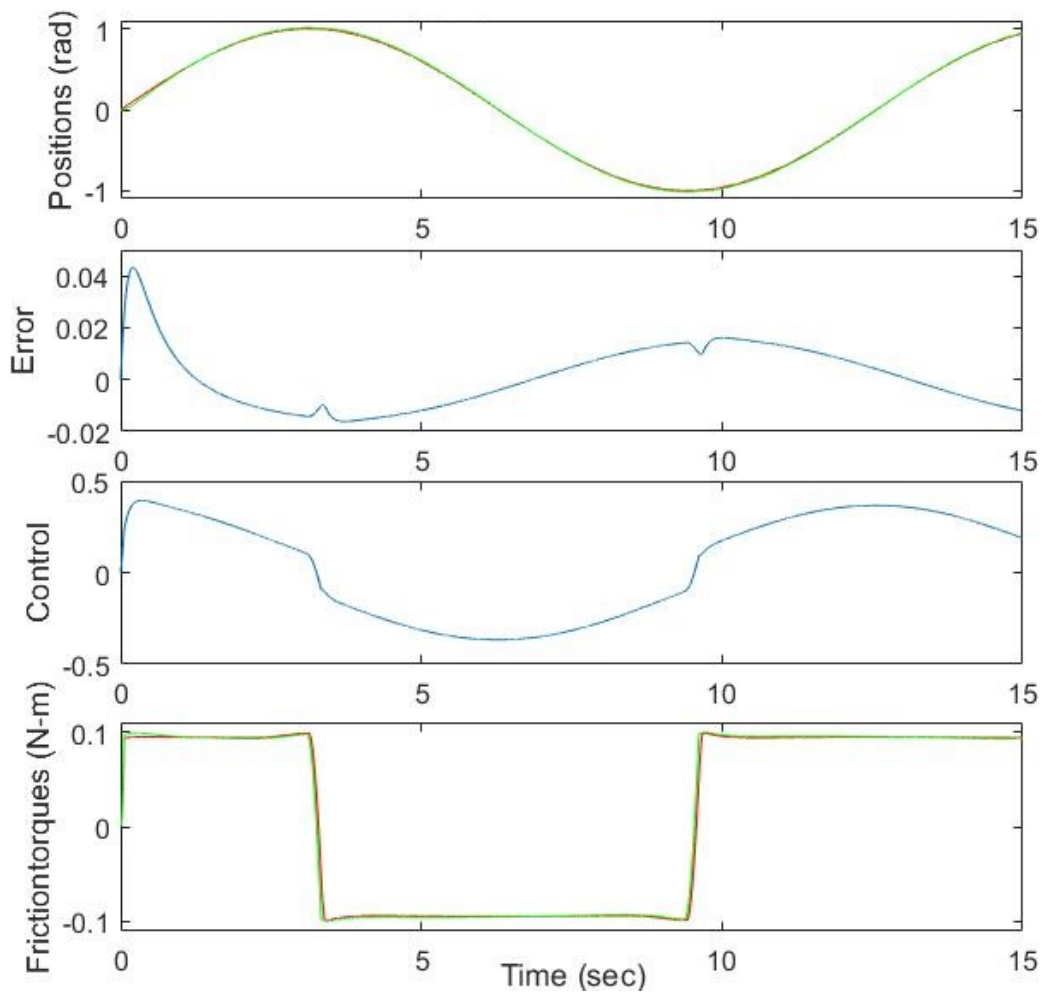


Fig. 6.26 A position tracking and control simulation with a model-based friction observer for the test-bed with **top-** Output 'red' input 'green', **mid-upper-** Error, **mid-lower-** Control and **bottom** The friction torques; system 'green', observer 'red'

6.6 Comparing the experimental and simulation results

The proposed friction model presented in this thesis was used for to perform a series of simulations with the derived model of the test-bed. The results obtained would then be compared with that of real experimental results obtained earlier.

Velocity Tracking and Regulation

The performance of the simulation example showed better improvement in velocity tracking for both the linear controller and the friction observer. This is attributed to the fact that the simulation assumed a noise free process where as in the real experiment, noise is inevitable to some degree and this affects results accuracy. Though the maximum error for the linear controller is less than twice that for the simulation case, the maximum error in the presence of observer changes greatly with a factor of almost 7. But generally the shapes of both simulation and experiment results are similar with the simulation showing how well the model is able to track velocity variations. The same trend is seen for the regulatory case where the tracking error is effectively reduce to near-zero in the steady both for simulation and experiment.

Position Tracking

Similar trend was observed for the position tracking simulation and experiment while the percent error improvement are 24% and 25% respectively with a general improvement in error and mean square error for the simulation against the experimental results due likely to a perfect matching of model parameters in the simulation, and a noiseless scenario contrary to the experiment in which error could not be 100% removed.

6.6.1 Discussion

During the experimental run it was observed that degradation in controller due to too high a value of the micro-damping and the viscous friction coefficient. The values used were as estimated however their performance was poor. Adjustment of these parameters were carried until adequate experimental response obtained. Therefore these values were changed as in table 6.2 above. The reason for this variation could be attributed to the established experimental fact that friction varies with operational conditions like temperature, humidity. This often leads to mis-match between the parameter values used for estimation and the values observed during such experiment. This is the reason adaptive control using online parameter identification technique to estimate friction parameters is desirable. One of the effects of this parameter mis-match is over-compensation and under-compensation as a result of using larger and lower parameter values respectively than the actual value at the time of the experiment. Both simulation and experimental results for velocity and position control show

that friction causes performance degradation in systems and linear controllers may not be effective in control experiments and simulations for such systems with friction. This is most obvious in the zero velocity regions as in figures 6.21 and 6.3. Compensation and control improvements in both velocity and position control are easily obtained with the introduction of friction observers as in figures 6.22 and 6.4. Friction compensation and control based on the observer based on the new friction model presented in this thesis from the result tables 6.2, 6.3 and 6.4, show superior improvement on the control of systems with friction non-linearity than the other models compared for the set of control experiments.

6.7 Chapter summary

A set of friction compensation and control experiment and simulation have been performed using first linear controllers only to investigate their effectiveness for control of systems subject to friction non-linearity. The result of such control underscores the need for a friction observer to be incorporated into the system to improve the overall control effort. Implementation of an observer-based friction compensator designed in the previous chapter was carried out for the velocity and position control of the experimental laboratory test-bed and strong improvements were recorded. Both velocity and position tracking and regulation were conducted. The different models investigated showed superior control performance against the linear controller as a stand alone implementation. Thus the non-linearity in the system due to friction posed greater control problem for the linear controller which was greatly minimised by the introduction of the friction observer. From the results of the various friction observers used for friction estimation namely the proposed friction model, LuGre model, GMS model and the Xiong model, the performance of the proposed new model for the set of experiments performed using the experimental friction test-bed indicates better improvement in the velocity and position control of systems subject to friction non-linearity, this was followed by the LuGre model, the GMS and Xiong models respectively.

Chapter 7

Conclusion and Recommendations

7.1 Introduction

Friction in physical systems generally results in performance degradations as a result of its non-linear nature and its attendant features such as stick-slip motion, Stribeck effect, pre-sliding hysteresis with non-local memory, and frictional lag. An experimental friction test-bed was designed in the laboratory for characterisation and identification of friction and also for control experiments. The new friction model presented in this thesis was used on the experimental test-bed for velocity and position control. An improved performance due to the integration of the pre-sliding function in the new model was shown.

In this chapter the following form the core of the discussion. Section 7.2 contains a summary drawn from the research report while the original contributions of the research to the general body of knowledge is discussed in section 7.3. The limitations and constraints encountered in the course of the research is discussed in section 7.4. Section 7.5 offering recommendations for future research in this area concludes the thesis report.

7.2 Summary

Investigation of the dynamics of friction using the laboratory test-bed designed showed the characteristic features of friction as supported by many other experimental studies and capture the underlying mechanisms of friction. A deeper understanding of the underlying friction dynamics characterizing friction was thereby established. From such it is evident that friction behaviour is most problematic in the pre-sliding, reversal and low velocity regimes. This is because of the rich dynamism characterizing friction in these regions. Due to this rich dynamism exhibited by systems with friction earlier model formulations to model friction

features for control purposes have either over-simplified the phenomenon (Coulomb model) with the effect of losing its dynamism or have become complex for implementation and simulation (GMS model). Many of such friction models and their relative complexities and ability to model adequately friction features were studied in chapter 2. Motivated by the need to formulate a friction model structure adequate for compensation and control, a new friction model structure simple enough for simulation, implementation and control purposes and yet rich enough to model observed friction dynamics was proposed in chapter 3. This new model of friction has a function which modelled the pre-sliding friction regime in which friction was seen to be pre-dominantly a function of the displacement rather than the velocity. This pre-sliding model captures the hysteresis features with non-local memory typical of friction unlike the more popular models such as the LuGre model. The proposed model properties such as stability, passivity, boundedness and dissipativity were established. Simulation analysis was performed to study the model behaviour especially in the pre-sliding and low velocities and the result of such simulations compared with the results of other models such as the LuGre, GMS, Elasto-Plastic, and Xiong friction models. Sensitivity analysis of the new model was also investigated against the other models and the model was shown to exhibit robustness to parameter variations. From the simulation studies it was established that the model is capable of modelling known friction dynamics. Model parameter identification and analysis to obtain estimates of the parameters of the new friction model and the parameters of the LuGre, GMS, and Xiong model for the representation of the friction in the laboratory test-bed was performed and the various parameters of interest used for system validation to obtain parsimonious models.

The performance indices from such identification experiments namely the mean square error and the maximum error metrics were used to compare the various models in terms of modelling identified friction features of the test-bed. Such results indicate the strong correlation between the identified friction features of the test-bed and that obtained from the proposed model. A model-based friction observer was therefore designed in chapter 5 using the new model presented for the estimation of the system friction for the laboratory test-bed. The design was based on the passivity of the friction model presented and a simulation example was used to demonstrate the observer performance with some other observers obtained using the LuGre, GMS, and Xiong friction models. The simulation results indicate improvement in both velocity and position control of systems with friction against the more popular LuGre and GMS models. In chapter 6, a control experiment was performed for the position and velocity control of the laboratory test-bed. The position and velocity control experiments were performed both for the cases where only a linear controller was used and for the case where a friction observer was integrated into the control loop. For

performance comparison purposes the friction observers were based on the proposed new model, LuGre model, GMS model and Xiong model. With mse and maximum error as performance indicators, it was observed that strong improvements were achieved for the cases where a friction observer was integrated into the control loop against the cases where the linear controller only was used. Considering the relative performance of the friction observers, the observer based on the proposed new friction model showed better performance as suggested by the error measures.

7.3 Original contributions to knowledge

In line with set research objectives the following are original contributions to the body of knowledge arising from this thesis:

1. A new friction model structure capable of modelling the friction phenomena especially in the low regimes of velocity, and velocity reversals has been developed. Rigorous sensitivity and robustness analysis of the new friction model were carried out and its performance compared other relevant friction models.
2. A describing functions based hysteretic equation originating from the new friction model for the prediction of the existence of limit cycles in systems with friction.
3. An experimental laboratory test-bed adequate for friction characterisation, parameter estimation, compensation and control related experiments was designed and constructed. A set of friction characterisation, compensation and control experiments performed.
4. Friction model parameter estimation for the proposed friction model and some other popular friction models and a comparative analysis of the estimation results of other friction models have been provided.
5. Design and analysis of a model based friction observer using the new friction model. Simulated and experimental comparison between the model-based friction observer using the the new friction model and other observers.

7.4 Limitations of the work

The research work conducted within the time frame has led to the development of a new friction model capable of modelling identified features of friction. The model integrates a

pre-sliding friction function to capture the non-local hysteretic friction as a function of bristle displacement. There have been however some challenges and limitations in the course of the research. Some of these limitations are therefore discussed below

1. The pre-sliding hysteretic function implementation in this research has assumed a simplified approach in its realisation. The implementation of the target values (z_t and f_t) using only a single value both for the negative and positive bristle movements. More accurate implementation would naturally consider the bristle direction and thus use corresponding value of the breakaway displacement (Z_b) and the static friction value (F_s).
2. The implementation of friction observers only considered the positive parameter values and thus the model accuracy and capability to model both friction in both directions was reduced.
3. An off-line friction parameter identification was adopted for simplicity neglecting possible parameter variations during system operation. Thus no parameter adaptation was conducted.

7.5 Recommendations for further research

The laboratory test-rig designed for this particular friction experiments could be re-engineered to increase the efficiency and accuracy of such friction experiments in the following specific areas given the time and resource availability;

- The capacity of the torque sensor used for the experiment is about 23 N-m while the actual system experimental torques captured for the various experiments are in the range of less than ± 0.2 N-m. Using a more sensitive sensor with range in the neighbourhood of the actual values would help in increasing the accuracy of the test-rig results.
- A more accurate axial alignment of the load (friction) discs with the axis of the gear and motor shaft to avoid uneven loading that may result due to axis mis-alignment. In this experiment a laboratory clamp was used to keep the load disc-torque sensor system horizontal and the axial alignment was done manually
- A structured rig providing more options in terms of motor type and capacity so that various friction systems could be studied.

Possible extension of application areas to include robot systems and mechanisms with multiple degrees of freedom would be an important research area to be pursued and many systems with rolling and sliding mechanisms. These extensions might as well lead to possible modifications of the proposed model structure to conform with application needs.

Model parameter changes are unavoidable since friction is dependent on the system operating conditions such as temperature, lubrication, time, humidity etc. Thus a given model might be more accurate at some operating conditions and inaccurate at others. This variation could be costly where high precision is required hence necessitating parametric models whose parameters change in accordance to changes in the system friction and operating conditions. Such systems are called adaptive control systems. Friction force parameters of the proposed friction model can be made adaptive to reflect parametric changes resulting in operational variations of the system. Online and offline parameters identification are often used for system identification and modelling. Offline approach adopted in this research usually leads to models of friction with static parameters while online approach yields adaptive models capable of tracking changes in model parameters as a result of changes in the system. These adaptive systems could be made robust to handle uncertainties in the modelling, [117], [105], [103], [37]. Design of such adaptive model-based friction compensators and subsequent implementation would yield more accurate results for velocity and position control of such systems under the influence of friction. In [56], a modified LuGre model was used for design of an adaptive robust friction compensator for linear motors. The implementation of such adaptive controllers would require the relaxation of the strictly positive real (SPR) property imposed on the system during the design of the friction observer (chapter 5), to a more simple version requiring the transfer function to be only positive real (SR).

A simplified linear version of the non-linear pre-sliding friction model structure could be adopted and analysis of such a model performed to test its ability to model friction features as it relates to the pre-sliding regime of friction. This could lead to a simpler model with the sine function removed. This approach could thus lead to a more simplified pre-sliding function for the purposes of analysis and stability studies.

Due to the non-linearity of the friction phenomenon and its asymmetric nature, it would be interesting to extend the new model to reflect different parameter values for the positive and negative friction regimes. Therefore further research would be on the impact of this parameter changes on the pre-sliding hysteretic function.

References

- [1] Wei Wu. DC Motor Parameter Identification Using Speed Step Responses. In *American Control Conference*, pages 1937–1941, Marriott Waterfront, Baltimore, MD, USA, 2010.
- [2] Ruijuan Guo, Juan Chen, and Xiaoxing Hao. Position Servo Control of a DC Electromotor Using a Hybrid Method Based on Model Reference Adaptive Control (MRAC). In *International Conference on Computer, Mechatronics, Control, and Electronic Engineering (CMCE)*, pages 534–537, 2010.
- [3] Mohammad A. Obeidat, Le Yi Wang, and Feng Lin. On-line parameter estimation of PMDC motors using binary-valued speed measurements. In *2012 IEEE Power and Energy Conference at Illinois*, pages 1–5. Ieee, Feb 2012.
- [4] Mohammad Kia, Kaveh Razzaghi Rezayieh, and Reza Taherkhani. A novel method for measuring rotational speed of BLDC motors using voltage feedback. In *The 2nd International Conference on Control, Instrumentation and Automation*, pages 791–794. Ieee, Dec 2011.
- [5] Lőrinc Márton and Béla Lantos. Modeling , Identification , and Compensation of Stick-Slip Friction. *IEEE transactions on industrial electronics*, 54(1):511–521, 2007.
- [6] T. Piatkowski. Dahl and LuGre dynamic friction models — The analysis of selected properties. *Mechanism and Machine Theory*, 73:91–100, Mar 2014.
- [7] Lőrinc Márton, Szabolcs Fodor, and Nariman Sepehri. A practical method for friction identification in hydraulic actuators. *Mechatronics*, 21(1):350–356, Feb 2011.
- [8] Zhang Tao, Lu Changhou, and Xi Zhuyan. Modeling and Simulation of Nonlinear Friction in XY AC Servo Table. *2006 International Conference on Mechatronics and Automation*, pages 618–622, Jun 2006.
- [9] Kok Kiong Tan, T H Lee, Sunan N Huang, Xi Jiang, and Student Member. Friction Modeling and Adaptive Compensation Using a Relay Feedback Approach. *IEEE transactions on industrial electronics*, 48(1):169–176, 2001.
- [10] I.B. Tijani and Rini Akmeliawati. Support vector regression based friction modeling and compensation in motion control system. *Engineering Applications of Artificial Intelligence*, 25(5):1043–1052, Aug 2012.
- [11] J. Awrejcewicz and P. Olejnik. Analysis of Dynamic Systems With Various Friction Laws. *Applied Mechanics Reviews*, 58(6):389–411, 2005.

- [12] C.T. Johnson and R.D. Lorenz. Experimental identification of friction and its compensation in precise, position controlled mechanisms. *Conference Record of the 1991 IEEE Industry Applications Society Annual Meeting*, pages 1400–1406, 1991.
- [13] Kemao Peng, Ben M Chen, Senior Member, Guoyang Cheng, Student Member, and Tong H Lee. Modeling and Compensation of Nonlinearities and Friction in a Micro Hard Disk Drive Servo System With Nonlinear Feedback Control. *IEEE TRANSACTIONS ON CONTROL SYSTEMS TECHNOLOGY*, 13(5):708–721, 2005.
- [14] D.D. Rizos and S.D. Fassois. Friction Identification Based Upon the LuGre and Maxwell Slip Models. *IEEE Transactions on Control Systems Technology*, 17(1):153–160, 2009.
- [15] Steffen Buechner, Stephan Zschaecck, Arvid Amthor, Christoph Ament, and Mike Eichhorn. Dynamic friction modeling and identification for high precision mechatronic systems. In *IECON 2012 - 38th Annual Conference on IEEE Industrial Electronics Society*, pages 2263–2268. Ieee, Oct 2012.
- [16] Chen Hsieh and Y.-C. Pan. Dynamic behavior and modelling of the pre-sliding static friction. *Wear*, 242(1-2):1–17, Jul 2000.
- [17] R. Stribeck. Die wesentlichen eigenshaften der gleit-und rollenlager- The Key Qualities of sliding and roller bearings. *VDI-Zeitschrift Seutscher Ingenieure*, 46:38(39):1341–1348, 1902.
- [18] Rached Dhaouadi and Fathi Ghorbel. MODELLING AND ANALYSIS OF NON-LINEAR STIFFNESS, HYSTERESIS AND FRICTION IN HARMONIC DRIVES GEARS. *International Journal of Modelling and Simulation*, 28(3):329–336, 2008.
- [19] D. P. Hess and A. Soom. Friction at a Lubricated Line Contact Operating at Oscillating Sliding Velocities. *Journal of Tribology*, 112(1):147, 1990.
- [20] E Rabinowicz. The Intrinsic Variables affecting the Stick-Slip Process. In *Proceedings of the Physical Society of London*, volume 71, pages 668–675, 1958.
- [21] Chih-jer Lin, Her-terng Yau, and Yun-cheng Tian. Identification and Compensation of Nonlinear Friction Characteristics and Precision Control for a Linear Motor Stage. In *IEEE Transactions on Mechatronics*, volume 18, pages 1385–1396, 2013.
- [22] Ej Berger. Friction modeling for dynamic system simulation. *Applied Mechanics Reviews*, 55(6):535, 2002.
- [23] Tolgay Kara and İlyas Eker. Nonlinear modeling and identification of a DC motor for bidirectional operation with real time experiments. *Energy Conversion and Management*, 45(7-8):1087–1106, May 2004.
- [24] Farid Al-Bender, Vincent Lampaert, and Jan Swevers. Modeling of dry sliding friction dynamics: From heuristic models to physically motivated models and back. *Chaos: American Institute of Physics Inc.*, 14(2):446–460, Jun 2004.

- [25] Shuang Cong, Guodong Li, and Xianyong Feng. Parameters Identification of Nonlinear DC Motor Model Using Compound Evolution Algorithms. In *Proceedings of the World Congress on Engineering*, volume I, 2010.
- [26] D.B. Miracle and S. L. Donaldson. *ASM Handbook: Friction, Lubrication and Wear Technology*, volume 18. ASM International., 2001.
- [27] Dean Karnopp. Computer Simulation of Stick-Slip Friction in Mechanical Dynamic Systems. *Journal of Dynamic Systems, Measurement, and Control*, 107(1):100–103, 1985.
- [28] C. Makkar, G. Hu, W.G. Sawyer, and W.E. Dixon. Lyapunov-Based Tracking Control in the Presence of Uncertain Nonlinear Parameterizable Friction. *IEEE Transactions on Automatic Control*, 52(10):1988–1994, Oct 2007.
- [29] Bojana Drincic. *Mechanical Models of Friction That Exhibit Hysteresis , Stick-Slip , and the Stribeck Effect*. PhD thesis, The University of Michigan, 2012.
- [30] P R Dahl. Solid Friction Model. Technical report, The Aerospace Corporation, El Segundo, Calif., 90245, USA, 1968.
- [31] Leonid Freidovich, Anders Robertsson, Anton Shiriaev, and Rolf Johansson. LuGre-Model-Based Friction Compensation. *IEEE Transactions on Control Systems Technology*, 18(1):194–200, Jan 2010.
- [32] C Canudas De Wit, H Olsson, Student Member, K J, and P Lischinsky. A New Model for Control of Systems with Friction. *IEEE Transactions on Automatic Control*, 40(3):419–425, 1995.
- [33] D. A. Haessig and B. Friedland. On the Modeling and Simulation of Friction. *Journal of Dynamic Systems, Measurement, and Control*, 113(3):354, 1991.
- [34] Jan Swevers, Farid Al-bender, Chris G Ganseman, and Tutuko Prajogo. An Integrated Friction Model Structure with Improved Presliding Behavior for Accurate Friction Compensation. 45(4):675–686, 2000.
- [35] V. Lampaert, J. Swevers, and F. Al-Bender. Modification of the Leuven integrated friction model structure. *IEEE Transactions on Automatic Control*, 47(4):683–687, Apr 2002.
- [36] Bashir M Y Nouri. Friction identification in mechatronic systems. *ISA transactions*, 43(2):205–216, Apr 2004.
- [37] Denis Garagić and Krishnaswamy Srinivasan. Adaptive friction compensation for precision machine tool drive. *Control Engineering Practice*, 12(11):1451–1464, Nov 2004.
- [38] Brian Armstrong-Helouvry, Pierre Dupont, and Carlos Canudas De Wit. A Survey of Models, Analysis Tools and Compensation Methods for the Control of Machines with Friction. *Automatica*, 30(7):1083–1138, 1994.

- [39] Lőrinc Márton and Béla Lantos. Control of mechanical systems with Stribeck friction and backlash. *Systems & Control Letters*, 58(2):141–147, Feb 2009.
- [40] Yu.A. Karpenko and Adnan Akay. A numerical model of friction between rough surfaces. *Tribology International*, 34(8):531–545, Aug 2001.
- [41] Bharat Bhushan, Jacob N Israelachvili, and Uzi Landman. Nanotribology: friction, wear and lubrication at the atomic scale. *Nature*, 374(6523):607–616, Apr 1995.
- [42] A.J. McMillan. A NON-LINEAR FRICTION MODEL FOR SELF-EXCITED VIBRATIONS. *Journal of Sound and Vibration*, 205(3):323–335, Aug 1997.
- [43] V. I Johanness, M. A. Green, and C. A Brockley. The Role of the Rate of Application of the Tangential Force in Determining the Static Friction Coefficient. *Wear*, 24:381–385, 1973.
- [44] F Al-Bender and K De Moerlooze. Characterization and modeling of friction and wear: an overview. *Sustainable Construction and Design*, pages 19–28, 2011.
- [45] Osborne Reynolds. Theory of Lubrication and its Application to Mr . Beauchamp Tower’s Experiments, Including an Experimental Determination of the Viscosity of Olive Oil. In *Philosophical transactions of The Royal Society of London*, volume 177, pages 157–234. The Royal Society, 1886.
- [46] H. Olsson, K.J. Åström, C. Canudas de Wit, M. Gäfvert, and P. Lischinsky. Friction Models and Friction Compensation. *European Journal of Control*, 4(3):176–195, Jan 1998.
- [47] Sergio Sánchez-Mazuca and Ricardo Campa. An Improvement Proposal to the Static Friction Model. *Mathematical Problems in Engineering*, 2013:1–8, 2013.
- [48] Johan Paduart, Lieve Lauwers, Jan Swevers, Kris Smolders, Johan Schoukens, and Rik Pintelon. Identification of nonlinear systems using Polynomial Nonlinear State Space models. *Automatica*, 46(4):647–656, Apr 2010.
- [49] Tijani Ismaila B, Rini Akmeliawati, and Momoh Jimoh E Salami. Artificial Intelligent Based Friction Modelling and Compensation in Motion Control System. In Prof. Horacio Martinez-Alfaro, editor, *Advances in Mechatronics*, chapter 3, pages 43–68. InTech, 2011.
- [50] Chow Yin Lai, Frank L Lewis, Venkatakrishnan Venkataramanan, Xuemei Ren, Shuzhi Sam Ge, and Thomas Liew. Disturbance and Friction Compensations in Hard Disk Drives Using Neural Networks. *IEEE transactions on industrial electronics*, 57(2):784–792, 2010.
- [51] V Van Geffen. A study of friction models and friction compensation. Technical report, Department of Mechanical Engineering, Technische Universiteit, Eindhoven, 2009.
- [52] Javier Moreno, Rafael Kelly, and Ricardo Campa. On Velocity Control Using Friction Compensation’. In *41st IEEE Conference on Decision and Control*, pages 95–100, 2002.

- [53] Danielle Chou. *Dahl Friction Modeling*. PhD thesis, Massachusetts Institute of Technology, 2004.
- [54] Raul Guenther, Eduardo A. Perondi, Edson R. DePieri, and Antônio C. Valdiero. Cascade controlled pneumatic positioning system with LuGre model based friction compensation. *Journal of the Brazilian Society of Mechanical Sciences and Engineering*, 28(1):48–57, Mar 2006.
- [55] Karim Khayati, Pascal Bigras, and Louis-A. Dessaint. LuGre model-based friction compensation and positioning control for a pneumatic actuator using multi-objective output-feedback control via LMI optimization. *Mechatronics*, 19(4):535–547, Jun 2009.
- [56] Lu Lu, Bin Yao, Qingfeng Wang, and Zheng Chen. Adaptive robust control of linear motors with dynamic friction compensation using modified LuGre model. *Automatica*, 45(12):2890–2896, Dec 2009.
- [57] Friedhelm Altpeter. *Friction Modeling, Identification and Compensation*. PhD thesis, ECOLE POLYTECHNIQUE FED ERALE DE LAUSANNE, 1999.
- [58] F. Al-Bender, V. Lampaert, and J. Swevers. The generalized Maxwell-slip model: a novel model for friction Simulation and compensation. *IEEE Transactions on Automatic Control*, 50(11):1883–1887, Nov 2005.
- [59] Pierre Dupont, Brian Armstrong, and Vincent Hayward. Elasto-plastic friction model: contact compliance and stiction. In *Proceedings of the 2000 American Control Conference. ACC (IEEE Cat. No.00CH36334)*, pages 1072–1077 vol.2. IEEE, 2000.
- [60] S. Sobczyk, E. Perondi, and M. A Cunha. A continuous approximation of the lugre friction model. In *ABCMSymposium Series in Mechatronics*, volume 4, pages 218–228. ABCM, 2010.
- [61] Mario R. Sobczyk, Eduardo A. Perondi, and Mauro A. B. Cunha. A continuous extension of the LuGre friction model with application to the control of a pneumatic servo positioner. In *2012 IEEE 51st IEEE Conference on Decision and Control (CDC)*, pages 3544–3550. IEEE, Dec 2012.
- [62] P. Dupont, V. Hayward, B. Armstrong, and F. Altpeter. Single state elastoplastic friction models. *IEEE Transactions on Automatic Control*, 47(5):787–792, May 2002.
- [63] V. Lampaert, F. Al-Bender, and J. Swevers. A generalized Maxwell-slip friction model appropriate for control purposes. In *2003 IEEE International Workshop on Workload Characterization (IEEE Cat. No.03EX775)*, volume 4, pages 1170–1177. IEEE, 2003.
- [64] Michael Ruderman and Torsten Bertram. Modified Maxwell-slip Model of Presliding Friction. In *18th IFAC World Congress*, pages 10764–10769, Milano, Italy, 2011.
- [65] Brian Armstrong and Qunyi Chen. The Z-properties chart. *IEEE Control Systems Magazine*, 28(5):79–89, Oct 2008.

- [66] A.K. Padthe, JinHyoung Oh, and D.S. Bernstein. On the LuGre model and friction-induced hysteresis. In *2006 American Control Conference*, number 5, pages 3247–3252. IEEE, 2006.
- [67] Max Boegli, Tinne De Laet, Joris De Schutter, and Jan Swevers. A Smoothed GMS Friction Model Suited for Gradient-Based Friction State and Parameter Estimation. *IEEE/ASME Transactions on Mechatronics*, 19(5):1593–1602, Oct 2014.
- [68] Max Boegli, Tinne De Laet, Joris De Schutter, and Jan Swevers. A smoothed GMS friction model for Moving Horizon friction state and parameter estimation. *International Workshop on Advanced Motion Control, AMC*, pages 1–6, 2012.
- [69] X Xiong, R Kikuuwe, and M Yamamoto. A differential algebraic method to approximate nonsmooth mechanical systems by ordinary differential equations. *Journal of Applied Mathematics*, 2013, 2013.
- [70] Xiaogang Xiong, Ryo Kikuuwe, and Motoji Yamamoto. A Differential-Algebraic Multistate Friction Model. In *Lecture Notes in Computer Science (including subseries Lecture Notes in Artificial Intelligence and Lecture Notes in Bioinformatics)*, volume 7628 LNAI, pages 77–88, 2012.
- [71] M.T. Bengisu and A. Akay. Stability of Friction-Induced Vibrations in Multi-Degree-of-Freedom Systems. *Journal of Sound and Vibration*, 171(4):557–570, Apr 1994.
- [72] J. Wojewoda, A. Stefanski, M. Wiercigroch, and T. Kapitaniak. Hysteretic effects of dry friction: modelling and experimental studies. *Philosophical Transactions of the Royal Society A: Mathematical, Physical and Engineering Sciences*, 366(1866):747–765, Mar 2008.
- [73] Pierre-Alexandre Bliman and Michel Sorine. A system-theoretic approach of systems with hysteresis: application to friction modeling and compensation. *Proceedings of the second European control conference*, pages 1844–1849, 1993.
- [74] Pierre-Alexandre Bliman and Michel Sorine. Easy-to-use realistic dry friction models for automatic control. *Proceedings of the 3rd European Control Conference*, pages 267–272, 1995.
- [75] Oliver Nelles. *Nonlinear System Identification*. Springer, Berlin, Heidelberg, 2001.
- [76] R. Grino, G. Cembrano, and C. Torras. Nonlinear system identification using additive dynamic neural networks—two on-line approaches. *IEEE Transactions on Circuits and Systems I: Fundamental Theory and Applications*, 47(2):150–165, 2000.
- [77] Lennart Ljung. Perspectives on system identification. *Annual Reviews in Control*, 34(1):1–12, Apr 2010.
- [78] R.K. Pearson. Selecting nonlinear model structures for computer control. *Journal of Process Control*, 13(1):1–26, Feb 2003.
- [79] Anatoli Juditsky, Håkan Hjalmarsson, Albert Benveniste, Bernard Delyon, Lennart Ljung, Jonas Sjöberg, and Qinghua Zhang. Nonlinear black-box models in system identification: Mathematical foundations. *Automatica*, 31(12):1725–1750, Dec 1995.

- [80] Lennart Ljung. Identification of Nonlinear Systems. Technical report, Division of Automatic Control, Linköpings Universitet, Linköpings, Sweden, 2007.
- [81] Ronald K Pearson and Martin Pottmann. Gray-box identification of block-oriented nonlinear models. *Journal of Process Control*, 10(4):301–315, Aug 2000.
- [82] Alain Y. Kibangou, Gérard Favier, and Moha M. Hassani. Selection of generalized orthonormal bases for second-order Volterra filters. *Signal Processing*, 85(12):2371–2385, Dec 2005.
- [83] Alain Y Kibangou, Gérard Favier, Moha M Hassani, Route Lucioles, and Sophia Antipolis. ADAPTIVE LAGUERRE-VOLTERRA FILTERS OPTIMIZATION BASED ON LAGUERRE SPECTRA. *EURASIP Journal on Advances in Signal Processing*, (17):2874–2887, 2005.
- [84] Juan C. Gómez and Enrique Baeyens. Identification of block-oriented nonlinear systems using orthonormal bases. *Journal of Process Control*, 14(6):685–697, Sep 2004.
- [85] Jonas Sjöberg, Qinghua Zhang, Lennart Ljung, Albert Benveniste, and Bernard Delyon. Nonlinear Black-box Modeling in System Identification : Unified Overview . *Automatica*, 31(12):1691–1724, 1995.
- [86] J.A.C. Martins, J.T. Oden, and F.M.F. Simões. A study of static and kinetic friction. *International Journal of Engineering Science*, 28(1):29–92, Jan 1990.
- [87] Elena Teidelt, Jasminka Starcevic, and Valentin L. Popov. Influence of Ultrasonic Oscillation on Static and Sliding Friction. *Tribology Letters*, 48(1):51–62, Oct 2012.
- [88] B. Armstrong. Friction: experimental determination, modeling and compensation. In *Proceedings. 1988 IEEE International Conference on Robotics and Automation*, pages 1422–1427. IEEE Comput. Soc. Press, 1988.
- [89] Brian Armstrong and Bimal Amin. PID control in the presence of static friction: A comparison of algebraic and describing function analysis. *Automatica*, 32(5):679–692, May 1996.
- [90] P.E. Dupont. Avoiding stick-slip through PD control. *IEEE Transactions on Automatic Control*, 39(5):1094–1097, May 1994.
- [91] Pierre E Dupont and Eric P Dunlap. Friction Modeling and PD Compensation at Very Low Velocities. *Journal of Dynamic Systems, Measurement, and Control*, 117(1):8–14, 1995.
- [92] N.E. Leonard and P.S. Krishnaprasad. Adaptive friction compensation for bi-directional low-velocity position tracking. In *Proceedings of the 31st IEEE Conference on Decision and Control*, pages 267–273. IEEE, 1992.
- [93] J.D. Han, Y.C. Wang, D.L. Tan, and W.L. Xu. Acceleration feedback control for direct-drive motor system. In *IEEE/RSJ International Conference on Intelligent Robots and Systems (IROS 2000) (Cat. No.00CH37113)*, volume 2, pages 1068–1074. IEEE, 2000.

- [94] Karl-petter W Lindegaard. *Acceleration Feedback in Dynamic Positioning*. PhD thesis, Norwegian University of Science and Technology, 2003.
- [95] K. Kiguchi, H. Henrichfreise, and K.-P. Hessler. Friction compensation of the electromechanical drive systems using neural networks. In *30th Annual Conference of IEEE Industrial Electronics Society*, volume 2, pages 1758–1762. IEEE, 2004.
- [96] M. Kemal Cılız and Masayoshi Tomizuka. Friction modelling and compensation for motion control using hybrid neural network models. *Engineering Applications of Artificial Intelligence*, 20(7):898–911, Oct 2007.
- [97] Timothee Basson and Julien Lescot. *Model-Based Friction Compensation*. PhD thesis, Lund University, Sweden, 2009.
- [98] Lőrinc Márton and Béla Lantos. Identification and Model-based Compensation of Striebeck Friction. *Acta Polytechnica Hungarica*, 3(3):45–58, Feb 2006.
- [99] Tegoeh Tjahjowidodo, Farid Al-Bender, Hendrik Van Brussel, and Wim Symens. Friction characterization and compensation in electro-mechanical systems. *Journal of Sound and Vibration*, 308(3-5):632–646, Dec 2007.
- [100] C.T. Johnson and R.D. Lorenz. Experimental identification of friction and its compensation in precise, position controlled mechanisms. *IEEE Transactions on Industry Applications*, 28(6):1392–1398, 1992.
- [101] V. Lampaert, J. Swevers, and F. Al-Bender. Comparison of model and non-model based friction compensation techniques in the neighbourhood of pre-sliding friction. *Proceedings of the 2004 American Control Conference*, 2, 2004.
- [102] Chao-Yun Chen and Ming-Yang Cheng. Adaptive disturbance compensation and load torque estimation for speed control of a servomechanism. *International Journal of Machine Tools and Manufacture*, 59:6–15, Aug 2012.
- [103] Tong Heng Lee, Kok Kiong Tan, and Sunan Huang. Adaptive Friction Compensation With a Dynamical Friction Model. *IEEE/ASME Transactions on Mechatronics*, 16(1):133–140, Feb 2011.
- [104] Wen-fang Xie. Sliding-Mode-Observer-Based Adaptive Control for Servo Actuator With Friction. *IEEE Transactions on Industrial Electronics*, 54(3):1517–1527, Jun 2007.
- [105] C Canudas, K. J. Astrom, and K. Braun. Adaptive Friction Compensation in DC-Motor Drives. *IEEE Journal of Robotics and Automation*, RA-3(6):681–685, 1987.
- [106] G L Wang, Y F Li, Senior Member, and D X Bi. Support Vector Networks in Adaptive Friction Compensation. *IEEE Transactions on Neural Networks*, 18(4):1209–1219, 2007.
- [107] Han Me Kim, Soo Hong Park, and Seong Ik Han. Precise friction control for the nonlinear friction system using the friction state observer and sliding mode control with recurrent fuzzy neural networks. *Mechatronics*, 19(6):805–815, Sep 2009.

- [108] S. Suraneni, I.N. Kar, O.V. Ramana Murthy, and R.K.P. Bhatt. Adaptive stick–slip friction and backlash compensation using dynamic fuzzy logic system. *Applied Soft Computing*, 6(1):26–37, Nov 2005.
- [109] Henrik Olsson. *Control Systems with Friction*. PhD thesis, Lund Institute of Technology, Jun 1996.
- [110] G Nicolis. Dissipative systems. *Reports on Progress in Physics*, 49(8):873–949, Aug 1986.
- [111] Jean-Jacques E. Slotine and Weiping Li. *Applied Nonlinear Control*. Prentice-Hall International, Inc, Englewood Cliffs, New Jersey 07632, 1991.
- [112] Filipe Marques, Paulo Flores, J. C. Pimenta Claro, and Hamid M. Lankarani. A survey and comparison of several friction force models for dynamic analysis of multibody mechanical systems. *Nonlinear Dynamics*, 86(3):1407–1443, Nov 2016.
- [113] Farid Al-bender. Fundamentals of friction modeling. In *ASPE Spring Topical Meeting on Control of Precision Systems, MIT, April 11-13*, pages 117–122. ASPE-The American Society of precision Engineering, Nov 2010.
- [114] V. Lampaert, F. Al-Bender, and J. Swevers. A generalized Maxwell-slip friction model appropriate for control purposes. In *2003 IEEE International Workshop on Workload Characterization (IEEE Cat. No.03EX775)*, volume 4, pages 1170–1177. IEEE.
- [115] Corrado Guarino, Lo Bianco, and Aurelio Piazzì. A servo control system design using dynamic inversion. *Control Engineering Practice*, 10:847–855, 2002.
- [116] Si-lu Chen, Student Member, Kok Kiong Tan, and Sunan Huang. Friction Modeling and Compensation of Servomechanical Systems With Dual-Relay Feedback Approach. *IEEE Transactions on Control Systems Technology*, 17(6):1295–1305, 2009.
- [117] C. Canudas de Wit and P. Lischinsky. Adaptive friction compensation with partially known dynamic friction model. *International Journal of Adaptive Control and Signal Processing*, 11(1):65–80, Feb 1997.
- [118] Hussain N Al-duwaish. Parameterization and Compensation of Friction Forces Using Genetic Algorithms. *Dynamical Systems*, 00(c):653–655, 1999.
- [119] Hongbiao Xiang, Zurong Qiu, and Xingfei Li. Simulation and experimental research of non-linear friction compensation for high-precision ball screw drive system. In *2009 9th International Conference on Electronic Measurement & Instruments*, pages 3–604–3–609. IEEE, Aug 2009.
- [120] E. W. Bai. Parametrization and adaptive compensation of friction forces.pdf. *International Journal of Adaptive Control and Signal Processing*, 11:21–31, 1997.
- [121] F.J.T. Vargas, E.R. De Fieri, and E.B. Castelan. Identification and friction compensation for an industrial robot using two degrees of freedom controllers. *ICARCV 2004 8th Control, Automation, Robotics and Vision Conference.*, 2:1146–1151, 2004.
- [122] Vries Prof. *Model based friction compensation for an electromechanical Stewart platform actuator Name* :. PhD thesis, Delft University of Technology, 2011.

Appendix A

Linear Controller Design

Overview

A description of the design approach adopted for the design of linear controllers for the friction test-bed in this research is similar to that for speed and position experiments performed as part of the non-linear systems and control course module at the school of system engineering, university of Reading. Here the process is explained step-by-step starting with the lag compensator design for velocity control experiments and then the PID controller for position control experiments.

Lag Compensator Design

Considering the model structure of the friction test-bed given as

$$\frac{\omega_l(s)}{E_a(s)} = \frac{AK_m}{J_{eq}R_a s + (AK_m)^2} \quad (\text{A.1})$$

this equation can further be reduced to

$$\frac{\omega_l(s)}{E_a(s)} = \frac{1}{\frac{J_{eq}R_a s}{A+K_m} + AK_m} \quad (\text{A.2})$$

Given

$$K = \frac{1}{AK_m}$$

and

$$T = \frac{R_a J_{eq}}{(AK_m)^2}$$

then

$$G(s) = \frac{\omega_l}{E_a(s)} = \frac{K}{Ts + 1} \quad (\text{A.3})$$

which is the open loop transfer function of the linear frictionless model structure of the test-bed with the output as the velocity and input as the armature voltage. The objective is to design a velocity controller for this system to meet certain criteria such as steady state error of 0.01 to a step input signal, and a cross-over frequency of about 110 rad/sec Procedure

A lag compensator structure is chosen for this task of velocity control over the PI controller because it reduces the influence of high frequency noise signals on the overall control scheme. The parameters of the friction test-bed that are of interest as contained in the manufacturer's data sheet are shown in table A.1. First a check to ascertain if the original system meet design

Table A.1 Parameters of the friction test-bed

Parameter	Description	Value	Unit
K_m	Motor torque constant	0.00767	N-m/A
A	Gear box transmission ratio	70:1	-
J_l	Moment of inertia of load	2.6583×10^{-5}	kgm^2
J_m	Moment of inertia of the motor armature	3.87×10^{-7}	kgm^2
K_b	Back emf constant	0.00767	N-m/A
R_a	Armature resistance	2.6	ω

specification without any modifications is carried out as follows: For a Bode plot of the of the open loop transfer function $G(s)$ in figure A.1b it is observed that the cross-over frequency criterion is not met since it's cross-over frequency is 65.8 rad/sec. The closed loop response of the system to a step input signal as presented in figure A.1a shows the steady state error 0.35 to be much greater than specified. Introducing a lag compensator network

$$C_{lag} = K_p \frac{T_i s + 1}{T_i s + \gamma} \quad (\text{A.4})$$

with K_p being the proportional gain, T_i time constant, and γ .

First design for the gain parameter: Since $G(s)$ is a first order type 0 system, the steady state error e_{ss} to a reference step is

$$e_{ss} = \frac{1}{1 + K_n} \quad (\text{A.5})$$

where $K_n = KK_p$ is the loop gain for the entire system which ensures the error criterion is satisfied. Substituting values yields $K_n = 99$ and from there

$$K_p = \frac{K_n}{K} = 53.1401$$

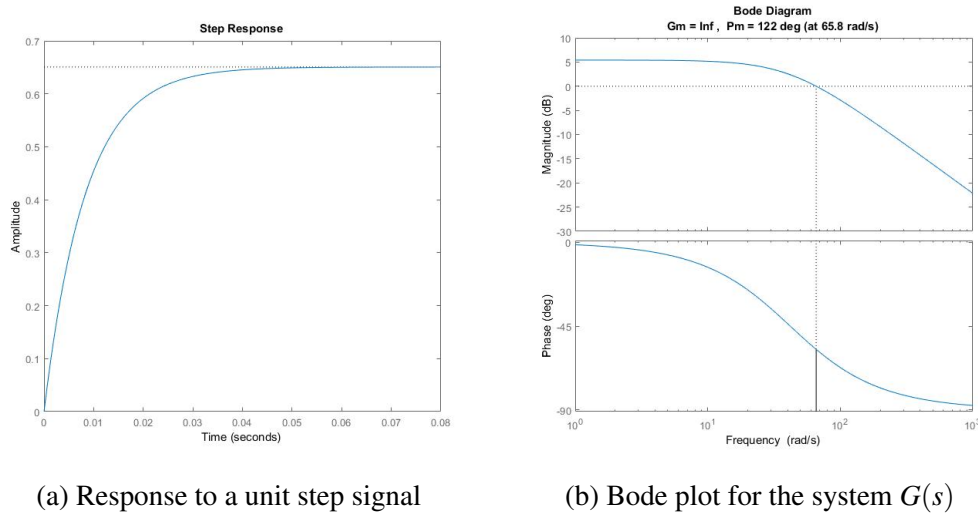


Fig. A.1 Test-rig response and Bode diagram of the open loop transfer function

Therefore the loop gain is modified to $K_p G(s)$, plots for the open loop Bode plot and the closed loop response to a step input are then obtained and compared with specifications. From the closed loop response figure A.2a, the error requirement of 0.01 is now satisfied. However, from the Bode plot of figure A.2b the cross-over frequency of 4.15×10^3 rad/sec has become too high. From the open loop Bode plot of figure A.1b, it is observed that a magnitude shift of 3.6dB will meet the cross-over frequency criterion. This adjustment thus alters the system gain also. This alteration in the error would be corrected via the lag network. Having met the cross-over frequency requirement of 110 rad/sec as shown in figure A.3b, a plot of the closed loop step response is obtained and it shows some deviation at steady state from expected, figure A.3a. The parameters of the lag network are then computed as.

$$\gamma = \frac{K_p K e_{ss}}{1 - e_{ss}} = 0.0285$$

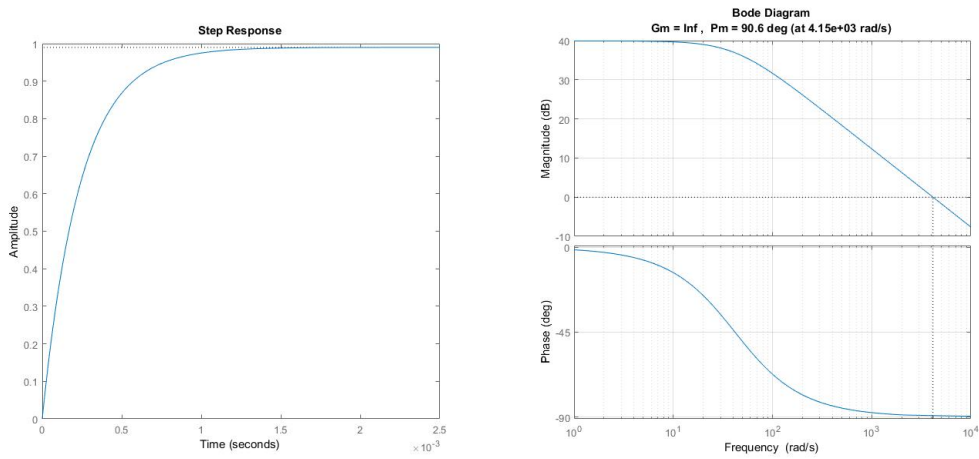
and

$$T_i = \frac{10}{\omega_c} = 0.0909$$

where ω_c is the specified cross-over frequency. Hence the parameters of the lag compensator for the control of the system are $K_p = 1.5136$, $\gamma = 0.0285$ and $T_i = 0.0909$ and equation A.4 becomes

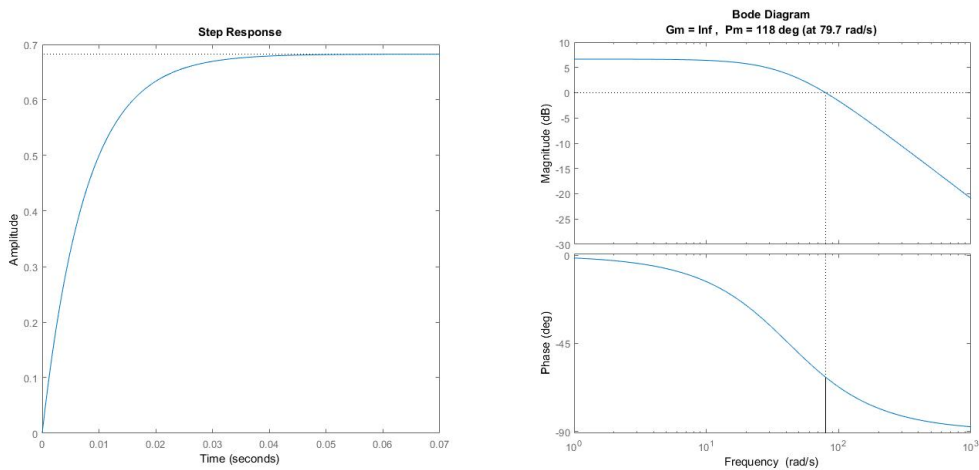
$$C_{lag} = 1.5136 \frac{0.0909s + 1}{0.0909s + 0.0285} \quad (\text{A.6})$$

This equation was used for the velocity control experiments of chapter 6



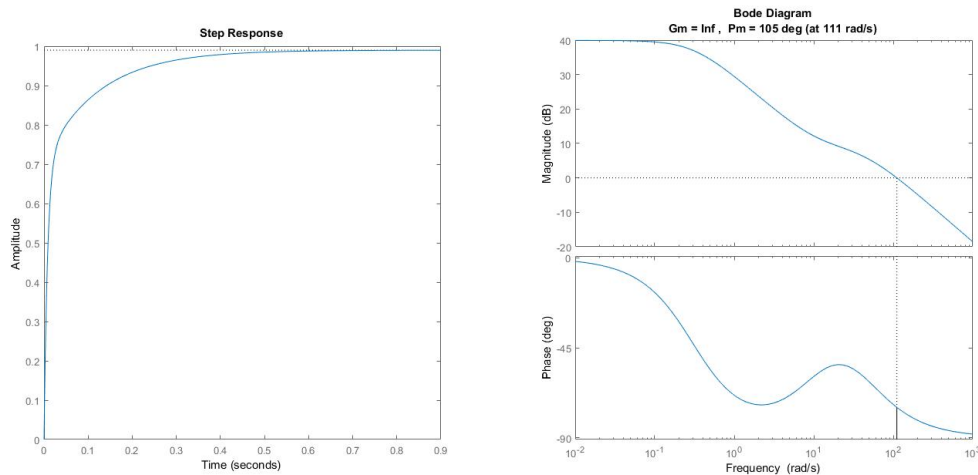
(a) Response to step input meeting error re-quirement (b) Bode plot for the system $K_p G(s)$ with too high cross-over frequency

Fig. A.2 Test-rig response and open loop Bode diagram of the transfer function showing too high cross-over frequency



(a) Response to step input with error for the new system $K_p G(s)$ (b) Bode plot for the system meeting cross-over frequency requirement

Fig. A.3 Test-rig response to input step, and Bode diagram showing error difference



(a) Response meeting required steady state error (b) Bode plot meeting required cross-over frequency

Fig. A.4 Integrating the compensator network to improve system performance

PID controller Design

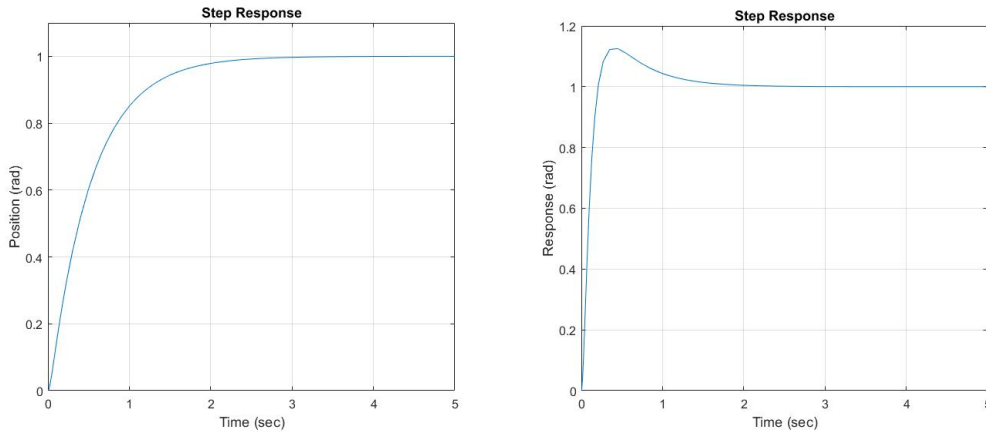
The Proportional+Integral+Derivative controller for position control exhibits efficient control dynamics such as fast response, elimination of steady state errors and oscillations and improves system stability. However the design of such controller to meet certain specifications sometimes are not straight forward and could involve a series of trial and error approach. The first thing is to set the required performance specifications for the controller to be designed. For the experimental friction test-bed designed for the characterisation of the friction phenomenon, the following features were specified.

1. A settling time of not more than 1 second
2. Maximum overshoot of 15%
3. A zero steady state error to a unit step signal
4. A rise time of 0.2 seconds

The individual contributions of the various controllers (P,I,D) to the overall control dynamics of the entire control system and how they effect other aspects of the control system could vary greatly. The table A.2 shows the effects of introducing the Proportional K_p , Integral K_i and Derivative K_d parameters to a given linear closed loop control system. From these the objective is to derive the right combinations of these controllers to give specified performance

Table A.2 Parameters effect on the closed loop response

Parameter	Rise time	Overshoot	Settling time	Steady state error
K_p	Decreases	Increases	Little effect	Decreases
K_i	Decreases	Increases	Increases	Eliminates
K_d	Little effect	Decreases	Decreases	No effect



(a) Step response of the friction test-bed in the absence of PID controller
 (b) Step response of the friction test-bed with PID controller

Fig. A.5 PID controller design

index. Recall the position control equation of the experimental test-bed for a friction free scenario is given as

$$\frac{\theta_l(s)}{E_a(s)} = \frac{AK_m}{s((J_{eq}s + B_{eq})R_a + (AK_m)^2)} \quad (\text{A.7})$$

then

$$G(s) = \frac{\theta_l(s)}{E_a(s)} = \frac{K}{s(Ts + 1)} \quad (\text{A.8})$$

with K and T as previously defined and the θ_l being the load position. In the absence of any form of control the closed loop step response of the system function $G(s)$ is presented in figure A.5a with no steady state error due to the system being of type 1. However, the settling time and the rise time are respectively 1.72 seconds and 1.22 seconds much more than the specified requirement. By a series of trial and error approach (though other methods like auto-tuning could be adopted) a PID controller with parameters; $K_p = 5.7517$, $K_i = 10$, and $K_d = 0.0768$ was obtained satisfying the control requirements. The settling time of the closed loop step response is 1 second, rise time of 0.17 seconds and an overshoot of 12.5% all within the required specifications. the step response of the PID controlled friction test-bed is presented in figure A.5b.

Appendix B

Simulations, Simulink diagrams and Matlab codes

B.1 Introduction

A more detailed description of the various approaches adopted in both the experimental investigations of the test-bed and its model simulations as well as the respective Matlab codes and Simulink diagrams used are provided. To accomplish this and make it easy for the reader, a chapter by chapter structure and explanations is given to explain the underpinning procedures starting with chapter 3 to chapter 6 which form the core of the research report.

B.2 In chapter 3

This section a description of the realisation of the proposed non-drift dynamic friction model and the associated Matlab codes and the Simulink diagram is given. In the same manner also provided is the Simulink diagram for the Stick-slip phenomenon and the sensitivity analysis.

B.2.1 The proposed non-drift friction model algorithm and Matlab codes

The model equations as given in chapter 3 are; equations (3.1, 3.2, 3.3, 3.4, and 3.5). The Simulink model for the proposed friction model structure is given in figure B.1.

Relevant Matlab codes for the individual blocks are as given below

Listing B.1 Friction force block

```
1 function Friction = fcn(v, Fhyst, gamma)
```

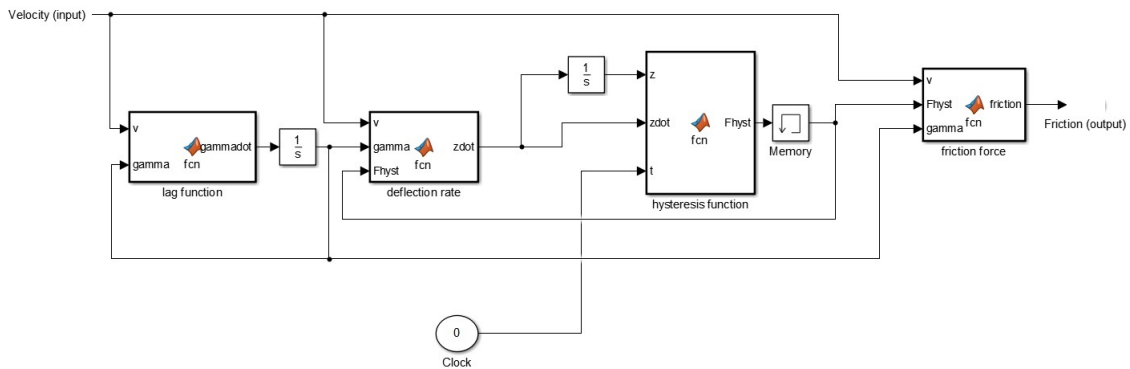


Fig. B.1 Proposed non-drift dynamic friction model structure representation with Simulink block diagram

```

2 % Code to determine the friction force value
3 sigma = sqrt(100000);
4 % F_f = sat(gamma, Fhyst(z) + sigma*v) + f_v*v : Friction
   force equation
5     saturated = Fhyst + sigma*v;
6     if abs(saturated) >= abs(gamma)
7         saturated = gamma;
8     end
9     Friction = saturated + f_v*v;
10
11 end

```

Listing B.2 Hysteresis function block

```

1 function Fhyst = fcn(z,zdot,t,x)
2 % Code to implement the hysteresis function:
3 % F_hyst=sin((z-z_r)*pi/(2*|Z_b-z_r|))*|f_t-f_r| + f_r
4 % Author: Anthony Nnaji
5 % Date: 20/07/2016
6 clear all;
7 %% persistent variables for calculations
8 persistent lastF lastZ pz pzdot direction %J
9
10 if isempty(direction)% detect the direction of signal
   positive or negative
11     direction = 0;

```

```
12 end
13 if isempty(lastF)    % detect the value of force at velocity
    change
14     lastF = zeros(1,1000000);
15 end
16 if isempty(lastZ)    % detect the value of displacement at
    velocity change
17     lastZ = zeros(1,1000000);
18 end
19 %% beginning of my code
20 if isempty(pzdot)
21     pzdot = zeros(1,1000000);
22 end
23 if isempty(pz)
24     pz=zeros(1,1000000);
25 end
26 time = round(t*1e3);
27
28 if time >=1
29
30     pz(time)= z;
31     pzdot(time)=zdot;
32
33     i=time;
34
35     if pzdot(i)==1
36         direction = direction+1;
37     end
38 hyst=0; ff=0;
39     % Here we need to choose the values of the maximum
    deflection Zb (break
40     % away) and
41     % the maximum friction force before gross sliding Fs (
    stiction) to
42     % integrated in the codes and not to change everything
    when they
```

```
43     % change .
44     Fs      = x(1);
45     Fc      = x(2);
46     vs      = x(3);
47     tau     = x(4);
48     sigma   = x(5);
49     Zb      = x(6);
50     zt=Zb;ft=Fs;Z=0;
51
52     %% defining the outer loop which the hysteresis
        function must not exceed
53     if i>1
54         if direction==0
55             if pz(i)>=pz(i-1)
56                 zt=Zb;ft=Fs;
57             else
58                 zt=-Zb;ft=-Fs;
59             end
60             if pz(i)>Zb
61                 Z=Zb ;
62             elseif pz(i)< -Zb
63                 Z=-Zb;
64             else
65                 Z= pz(i);
66             end
67             ff = (Z-lastZ(1))/abs(zt-lastZ(1));
68             hyst = ff*abs(ft-lastF(1))+lastF(1);
69             lastF(2) = hyst;
70             lastZ(2) = Z;
71         end
72     if direction==1
73         if pz(i)<=pz(i-1)
74             if pz(i)>Zb
75                 Z=Zb;
76             elseif pz(i)< -Zb
77                 Z=-Zb;
```

```

78         else
79             Z=pz(i);
80         end
81         if lastZ(2)<Zb
82             zt=-2*Zb+lastZ(2);
83             ft=-2*Fs+lastF(2);
84         elseif lastZ(2)==Zb
85             zt=-Zb;
86             ft=-Fs;
87             lastZ(2)=Zb;
88             lastF(2)=Fs;
89         end
90         ff = (Z-lastZ(2))/abs(zt-lastZ(2));
91         hyst = ff*abs(ft-lastF(2))+lastF(2);
92         lastF(3) = hyst;
93         lastZ(3) = Z;
94     end
95 end
96     if direction >1
97         j=direction;
98         if pz(i)>Zb
99             Z=Zb ;
100        elseif pz(i)< -Zb
101            Z=-Zb;
102        else
103            Z= pz(i);
104        end
105        if pz(i)<=pz(i-1)
106            if lastZ(j+1)<Zb
107                zt=-2*Zb+lastZ(j+1);
108                ft=-2*Fs+lastF(j+1);
109                if j>2
110                    ee = j-1;
111                    for k =1:2:ee-1;
112                        if pz(i)<= lastZ(j-k+1)
113                            zt=-2*Zb+lastZ(j-k);

```

```

114             ft=-2*Fs+lastF(j-k);
115             lastZ(j+1)=lastZ(j-k);
116             lastF(j+1)=lastF(j-k);
117         end
118     end
119     end
120     elseif lastZ(j+1)==Zb
121         zt=-Zb;
122         ft=-Fs;
123     end
124 end
125 if pz(i)>=pz(i-1)
126     if lastZ(j+1)>-Zb
127         if j==2
128             zt=2*Zb+lastZ(j+1);
129             ft=2*Fs+lastF(j+1);
130
131             if pz(i)>=lastZ(j)
132                 zt=Zb;
133                 ft=Fs;
134                 lastZ(j+1)=lastZ(j-1);
135                 lastF(j+1)=lastF(j-1);
136             end
137         end
138         if j>2
139             ee = j-1;
140             for k =1:2:ee-1;
141                 zt=2*Zb+lastZ(j+1);
142                 ft=2*Fs+lastF(j+1);
143                 if pz(i)>= lastZ(j-k+1)
144                     zt=2*Zb+lastZ(j-k);
145                     ft=2*Fs+lastF(j-k);
146                     lastZ(j+1)=lastZ(j-k);
147                     lastF(j+1)=lastF(j-k);
148                 end
149                 if pz(i)>=lastZ(2)

```

```

150             zt=Zb;
151             ft=Fs;
152             lastZ(j+1)=lastZ(1);
153             lastF(j+1)=lastF(1);
154         end
155     end
156     end
157     elseif lastZ(j+1)==-Zb
158         zt=Zb;
159         ft=Fs;
160         lastZ(j+1)=-Zb;
161         lastF(j+1)=-Fs;
162     end
163     end
164     ff = (Z-lastZ(j+1))/abs(zt-lastZ(j+1));
165     hyst = ff*abs(ft-lastF(j+1))+lastF(j+1);
166     lastF(j+2) = hyst;
167     lastZ(j+2) = Z;
168     end
169     end
170 else
171     hyst=0;
172     ff=0;
173 end
174
175 Fhyst = hyst;
176 end

```

Listing B.3 Deflection rate block

```

1 function zdot = fcn(v,gamma,Fhyst,x)
2 %Code to implement the rate of deflection
3 % Author: Anthony Nnaji
4 % Date: 20/07/2016
5 Fs = x(1);
6 Fc = x(2);
7 vs = x(3);

```

```

8 tau      = x(4);
9 sigma    = x(5);
10 Zb      = x(6);
11
12 % zdot = sat(gamma, Fhyst(z) + sigma*v) - Fhyst)/sigma;
13     saturated = Fhyst + sigma*v;
14     if abs(saturated) > abs(gamma)
15         change = sign(v)*gamma;           % slip regime
16     else
17         change = saturated; % stick regime
18     end
19     zdot = (change - Fhyst)/sigma;
20 end

```

Listing B.4 Lag-function block

```

1 function gammadot = fcn(v,gamma,x)
2 % Code to implement the friction force state: gammadot = (G
   -gamma)/tau;
3 % Author: Anthony Nnaji
4 % Date: 20/07/2016
5 Fs      = x(1);
6 Fc      = x(2);
7 vs      = x(3);
8 tau     = x(4);
9 G = (Fc + (Fs - Fc)*exp(-(v/vs)^2));
10
11 gammadot = (G-gamma)/tau;
12 end

```

B.2.2 The stick-slip effect

The stick slip motion was captured for a simple system of figure 3.7 and the Simulink block diagram model, using the proposed non-drift dynamic model to capture the system friction is shown as figure B.2. The solver type for the simulation results published in chapter 3 of the research report is the ode4 (Runge-Kutta) with a fixed step size of 1×10^{-5} .

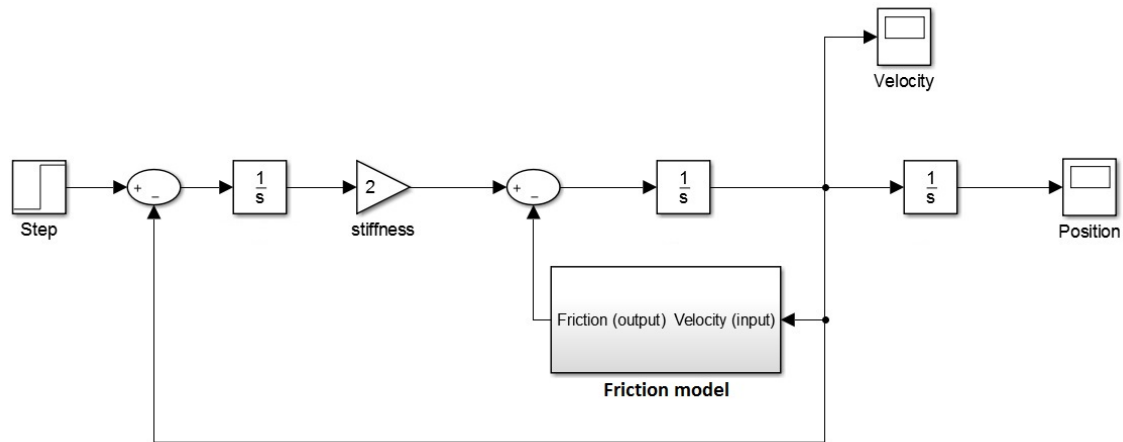


Fig. B.2 Block diagram for the simulation of stick-slip effect of friction using the proposed friction model

B.3 In chapter 4

The relevant Simulink models for the friction characterisation experiments and system identification are shown in the respective figures below.

For the characterisation experiments the block diagram is depicted in figure B.3.

For the system identification and parameter estimation, the block diagram is as shown in figure B.4

The data-fitting code was implemented using the *lscurvefit* algorithm in Matlab for the parameter estimation under the constant velocity regime. The code is as listed in B5.

Listing B.5 Code for data fitting and estimation of static friction parameters using the *lscurvefit* algorithm

```

1 % A script to run the curvefitting of the friction-torque
   and velocity
2 % data acquired from experiments using.
3 % Date:24.03.2016
4 % Author: Anthony Nnaji
5 %% system identification section
6 load xdata;% this is the measured velocity data
7 load ydata;% this is the measured torque data
8
9 %% % the data fitting (Identification)
10      % Proposed model structure

```

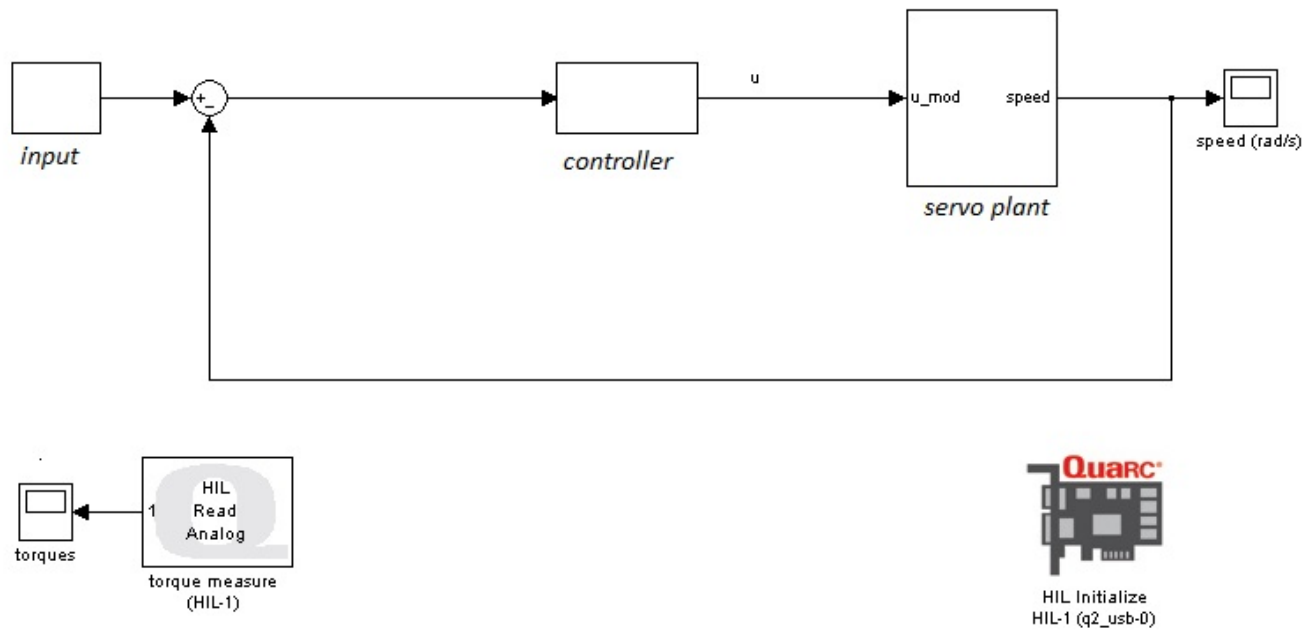


Fig. B.3 Simulink block diagram for the friction characterisation experiments using the test-bed

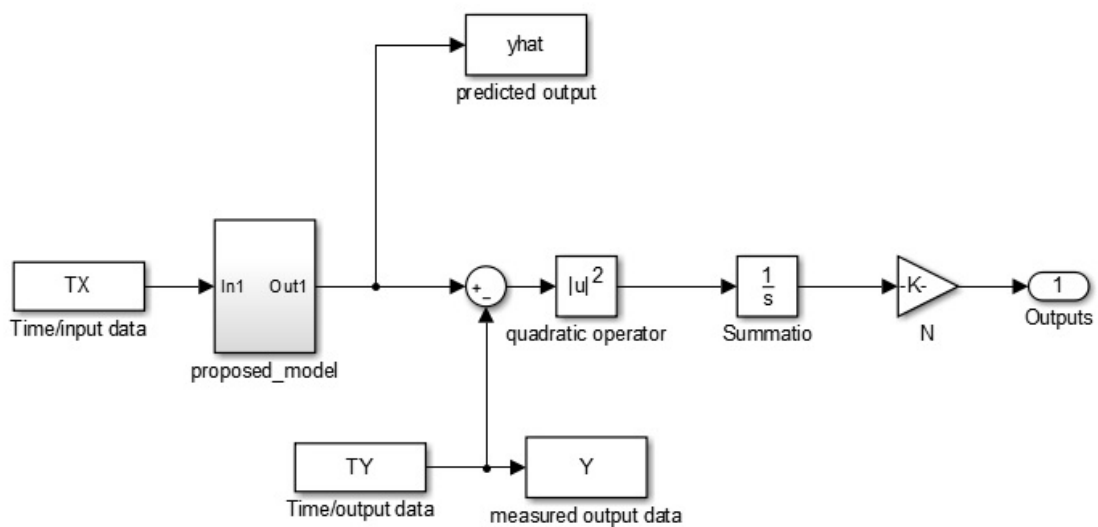


Fig. B.4 Simulink block diagram for the estimation of parameters of the proposed friction model

```
11     fun = @(x,xdata)(x(1)+ (x(2)- x(1))*exp(-(xdata/x(3))
        .^2) + x(4)*xdata);
12     x0 =[0.085,0.091,0.091,0.03];
13     [x,resnorm,residual,exitflag,output] = lsqcurvefit(
        fun,x0,xdata,ydata,[0.08 0.09 0.01 0.01],[0.92
        0.12 0.5150 0.7]);
14     %% Identification plots
15     figure;
16     plot(xdata,ydata,'r. ');
17     hold on;
18     plot(xdata,fun(x,xdata));
19     meansquareerror = sum((fun(x,xdata) - ydata).^2)/76;
20     hold off
21     %% Validation section
22     %%enter the velocity and friction values for validation
23     load validationvelocity;
24     load validationtorque;
25     xdata = validationvelocity;
26     ydata = validationtorque;
27
28     %%validation code
29     % Proposed model structure
30     x=[x(1) x(2) x(3) x(4)];
31     %     x(1) =0.085; x(2)=0.1064; x(3)=0.0813; x(4)=0.0690; %
        Put in the
32     %     values obtained from identification
33     F = x(1) + (x(2) - x(1))* exp(-(xdata/x(3)).^2) + x(4)
        *xdata;
34     % Validation plots
35     figure
36     plot(xdata, F);
37     hold on;
38     plot(xdata,ydata,'r. ');
39     hold off
40     meansquareerror2 = sum((F - ydata).^2)/76;
```

For the parameter estimation using the `fmincon` optimisation tool under frictional-lag the Matlab main and objective function scripts are respectively listed as B6 and B7.

Listing B.6 Main function for the estimation of friction parameters under frictional-lag

```

1 % A script to run the estimation of parameters under
   frictional-lag
2 % utilisising the fmincon optimisation tool
3 % Date 20/03/2016
4 % Author Anthony Nnaji
5 clear all;
6 load chirpdata.mat;
7
8 Tfinal = 9.424;
9 h = 0.001;
10 x0 = [0.1,0.08,0.2,0.02,1,0.001]';
11 A = [0,0,1,-1,0];
12 B = 0;
13 LB = [1,0,0.065,0.085,0.03];
14 UB = [5,inf,0.095,0.12,0.7];
15 options = optimset('LargeScale','off','Display','iter','
   TolX',0.0000001,'TolFun',0.0000001,'HessUpdate','bfgs','
   MaxIter',30);
16 % [x,fval,output] = fminunc('MAIN_obj', x0, options, h,
   Tfinal, TY, TX);
17 [x,fval,output] = fmincon('MAIN_obj', x0, A, B, [], [], LB,
   UB, [], options, h, Tfinal, TY, TX );
18
19 Fs      = x(1);
20 Fc      = x(2);
21 vs      = x(3);
22 tau     = x(4);
23 sigma   = x(5);
24 Zb      = x(6);
25
26 opt = simset('solver','ode5','SrcWorkspace','Current','
   FixedStep',h);
27 [tout,xout,yout] = sim('MAIN',[0 Tfinal],opt);

```

```

28 plot(tout , ydata , tout , yhat , '-.r');
29 figure;
30 plot(xdata , yhat);

```

Listing B.7 Objective function for the estimation of friction parameters under frictional-lag

```

1 function f = MAIN_obj(x,h,Tfinal, TY, TX)
2 %% The objective function for the frictional-lag script
3 Fs      = x(1);
4 Fc      = x(2);
5 vs      = x(3);
6 tau     = x(4);
7 sigma   = x(5);
8 Zb      = x(6);
9 opt = simset('solver','ode5','SrcWorkspace','Current','
             FixedStep',h);
10 [tout,xout,yout] = sim('MAIN',[0 Tfinal],opt);
11 f = yout(length(yout));

```

B.4 In chapter 5 and 6

Most of the simulation block diagrams used in chapters 5 and 6 appear in the relevant areas, so here some of the Simulink diagrams for the friction control simulation and experiments are further explained as they were used in the real experiments and simulations. For the position control simulations, figure B.5 depicts the structure of the simulink diagram used with the plant pictured as the dashed block containing the friction, gain and the integrator blocks.

In the same vein, the velocity control experiments performed on the test-bed using the proposed friction model to compensate for system friction is shown in block form in figure B.6.

Below B.1 is the table of parameter symbols used in the thesis alongside their descriptions and SI units

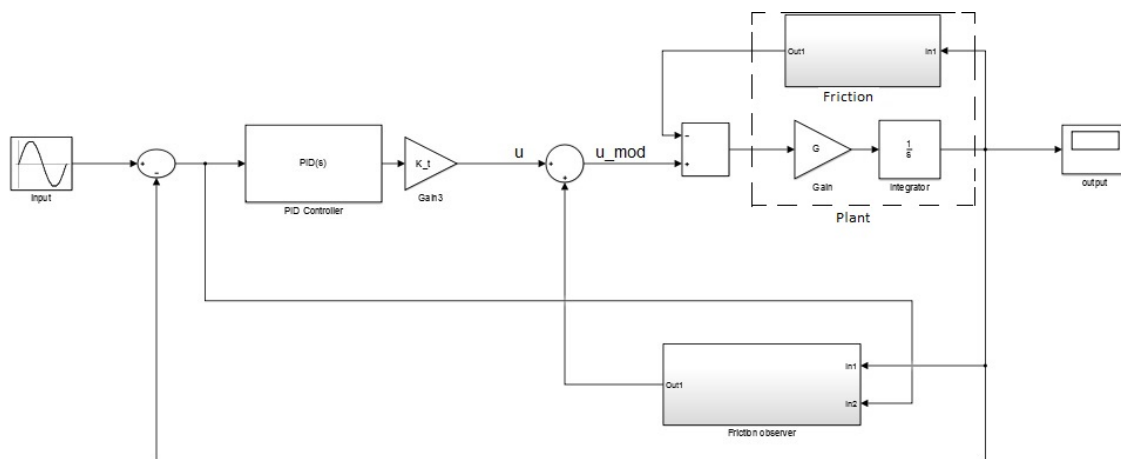


Fig. B.5 Block diagram for the position control simulations of the test-bed using the proposed friction model

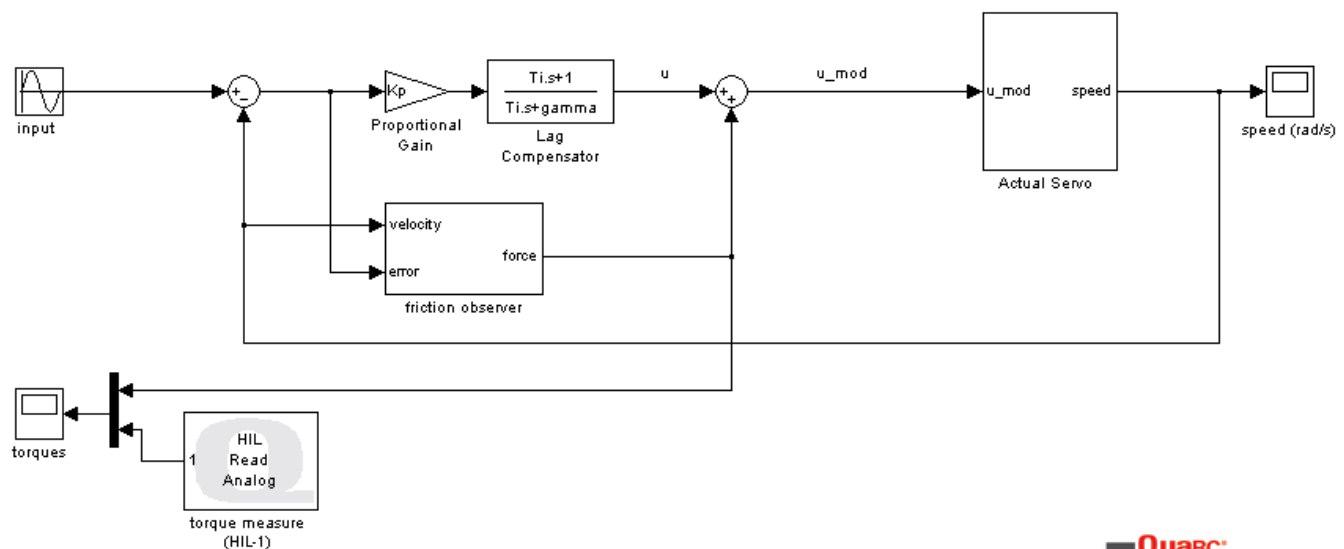


Fig. B.6 Block diagram for the velocity control experiments on the test-bed using the proposed friction model

Table B.1 Description of symbols used in the thesis with their SI units

parameter symbol	Description	SI unit
F	Force	[N]
F_f	Friction force	[N]
F_c	Static friction force	[N]
F_s	Kinetic friction force	[N]
$\sigma_0, (\sigma), K$	Stiffness	[N/m]
σ_1	Micro-damping	[Ns/m]
f_v	Coefficient of viscosity	[Ns/m]
v_s	Stribeck velocity	[m/s]
τ	Time constant	[s]
γ	Friction force state	[N]
λ	Friction force scale factor	[–]
J	Inertia	[kgm ²]
v	Velocity	[m/s]
z	Bristle deflection	[m]
Z_b	Breakaway displacement	[m]
K_p	Proportional gain	[N/m]
K_d	Derivative gain	[s]
K_i	Integral gain	[1/s]
δ	Shape parameter	[–]
ω_o	Angular velocity	[rad/s]
θ_o	Angular displacement	[rads]

